1989

An Inverse Finite Element Method For The Study Of Steady State Terrestrial Heat Flow Problems

Kelin Wang

NOTICE

The quality of this microform is heavily dependent upon the quality of the original thesis submitted for microfilming. Every effort has been made to ensure the highest quality of reproduction possible.

If pages are missing, contact the university which granted the degree.

Some pages may have indistinct print especially if the original pages were typed with a poor typewriter ribbon or if the university sent us an inferior photocopy.

Reproduction in full or in part of this microform is governed by the Canadian Copyright Act, R.S.C. 1970, c. C-30, and subsequent amendments.

AVIS

La qualité de cette microforme dépend grandement de la qualité de la thèse soumise au microfilmage. Nous avons tout fait pour assurer une qualité supérieure de reproduction.

S'il manque des pages, veuillez communiquer avec l'université qui a conféré le grade.

La qualité d'impression de certaines pages peut laisser à désirer, surtout si les pages originales ont été dactylographiées à l'aide d'un ruban usé ou si l'université nous a fait parvenir une photocopie de qualité inférieure.

La reproduction, même partielle, de cette microforme est soumise à la Loi canadienne sur le droit d'auteur, SRC 1970, c. C-30, et ses amendements subséquents.

AN INVERSE FINITE ELEMENT METHOD FOR THE STUDY OF STEADY STATE TERRESTRIAL HEAT FLOW PROBLEMS

by

Kelin Wang

Department of Geophysics

Submitted in partial fulfillment

of the requirements for the degree of

Doctor of Philosophy

Faculty of Graduate Studies

The University of Western Ontario

London, Canada

April, 1989

ISBN 0-315-49305 4

Canada

ABSTRACT

In solving terrestrial heat flow problems, the complexity of the earth medium and boundary conditions calls for frequent use of numerical modeling techniques. The ill–posedness of the problems due to lack of perfect knowledge of the material properties and the boundary conditions requires that inverse theories be applied. Methods that incorporate both numerical techniques and inverse theories have therefore been gaining attentions in heat flow research.

In this study, an inverse finite element method is developed to solve 2–D steady state heat flow problems involving uncertain material properties and boundary conditions. The problems are first parameterized using an isoparametric finite element model, in which the field variables, the material properties and the boundary conditions are formulated as discrete parameters. Information on the parameters is described in the form of Gaussian probabilities. A nonlinear parameter estimation method of Bayesian type is then used to update our knowledge of the parameters. For computational efficiency, a gradient method is used in the parameter estimation procedure, and the gradients are derived analytically at the elemental level.

The method is applied to two types of conductive heat flow problems, namely the topographic correction and the downward continuation of heat flow data, and to the problem of coupled thermal and hydrological regimes of sedimentary basin scale. Numerical examples have shown that the method provides a rigorous treatment of uncertainties in these problems. In the case of the coupled problem, however, the power of the method is limited by the strong nonlinearity, and better a priori information is needed to constrain the solution.

ACKNOWLEDGEMENTS

I wish to express my sincere thanks and appreciation to the following persons and institutions:

Dr. A.E. Beck, the supervisor, for his supervision and encouragement during the course of the study.

Dr. P.Y. Shen, for originally suggesting the project, and providing many valuable ideas.

Dr. S.B. Nielsen, for many inspiring discussions on various subjects relating to this research, before and after his graduation from this department.

Dr. L. Mansinha (Department of Geophysics) and Dr. H. Rasmussen (Department of Applied Mathematics), both on my supervisory committee, for helps and instructions.

Dr. H.N. Pollack (University of Michigan) and Dr. C. Clauser (Niedersächsisches Landesamt für Bodenforschung), for providing data and helpful comments on the research.

Dr. A. Woodbury (McGill University), Dr. S. Bachu (Alberta Research Council), Dr. S. Willett (University of Utah), Dr. L. Smith (University of British Columbia), among other scientists in the fields of terrestrial heat flow and groundwater hydrology, for providing, on various occasions, valuable suggestions and criticisms for this research.

Dr. R. Wang, Mr. Y. Cai and Mr. H. Zhang (all at Peking University), for drawing my attention to numerical methods and sharing their experience in finite element programming.

Mr. B. Dun..., for helps on computer matters.

The Education Ministry of China, for providing an overseas scholarship; the University of Western Ontario, for a foreign student bursary; the government of the province of Ontario, for an Ontario Graduate Scholarship.

The National Science and Engineering Research Council of Canada and the Imperial Oil Ltd., for research grants.

Finally, I wish to express my thanks to Zhen Lin, my wife, for her patience, kindness and help at all times.

TABLE OF CONTENTS

LIST OF TABLES

LIST OF FIGURES

LIST OF SYMBOLS

C, $\hat{C}$	a priori and a posteriori covariance matrices
C_{ee}	covariance matrix of e
C_{ff}, $\hat{C}_{ff}$	a priori and a posteriori covariance matrices of f
C_{pp}, $\hat{C}_{pp}$	a priori and a posteriori covariance matrices of p
C_{qq}, $\hat{C}_{qq}$	a priori and a posteriori covariance matrices of q
D	coefficient of thermal diffusion
D^{th}	coefficient of mechanical thermal dispersion
e	a random error vector
e	superscript, to denote elemental quantities
$F = F(P)$	vectorial functional relation of P components
F'	gradient matrix of F(P)
f, f^e	global and elemental flux–equivalent nodal flow vectors
G, G^e	global and elemental gradient matrix of g(p)
$g = g(p)$	non–linear part of F(P)
g	absolute value of gravitational acceleration
$H = H(r)$	shape functions for 2–D isoparametric finite elements
HFD	abbreviation for heat flow density
h, h	reference hydraulic head and its nodal value vector
h	superscript, to denote heat
I	identity matrix
i, j	superscripts and subscripts, to denote coordinate directions
K, K^e	global and elemental conductivity matrices
k, l, m, n	subscripts, to denote entries of matrices and components of vectors
k	subscript, to denote iteration steps

L	auto–correlation length of boundary fluxes
N_e	number of nodal points in a finite element
N_g	total number of nodal points in a finite element mesh
N_h	number of measured head values
N_p	number of aquifer parameters
P	global parameter vector
P_e	Peclet number
P_f	fluid pressure
$\mathcal{P}$	probability density function
p, p_o	non–linear part of P and its a priori value
q, q_o	linear part of P and its a priori value
q^h, $\mathbf{q}^h$	heat flow density (heat flux) and its nodal value vector
q^w, $\mathbf{q}^w$	Darcian velocity (specific discharge) and its nodal value vector
R	a positive definite matrix
RTV	abbreviation for Rodgers, Tarantola and Valette
r	position vector in the natural coordinate system of an element
S_{lk}	distance between boundary nodes l and k
STD	abbreviation for standard deviation
T	temperature
T_o	a reference temperture (= 30 °C)
t	superscript, to denote matrix transpose
U, $\mathbf{U}$	temperature–head vector and the vector of its nodal values
V, V^e	global and elemental boundary flux transformation matrix
W	source–equivalent nodal flow vector
x	position vector in the cartesian coordinate system
Y, $\mathbf{Y}$	transmissivity and the vector of its measured values
z, z_o	vector of log transmissivity–head values and its mean

ϑ	slope of the linear relation of ρ and T for water
$\gamma = \log\lambda$	logarithmic thermal conductivity
δ	Kronecker delta function
$\epsilon = \log\aleph$	logarithmic heat production rate
η	slope of the linear relation of μ^{-1} and T for water
θ	vector of parameters in the trend and covariance function of Y
κ	permeability
λ	thermal conductivity of a fluid–solid mixture
λ^s	thermal conductivity of a solid
μ, μ_0	dynamic viscosity of water and its value at T_0
$\aleph$	rock heat production rate
Π	objective function to be optimized
ρ, ρ_0	density of water and its value at T_0
ρ_r	relative density of water (dimensionless)
ρc	specific thermal capacity of water
σ, $\hat{\sigma}$	a priori and a posteriori standard deviation
σ^2, $\hat{\sigma}^2$	a priori and a posteriori variance
σ^2_{lk}	covariance between boundary flux values at nodes l and k
ϕ	porosity
$\psi = \log\kappa$	logarithmic permeability
Ω, Ω^e	area, and the area of a finite element

CHAPTER 1: INTRODUCTION

1.1 Preface

The study of terrestrial heat flow density (HFD) deals with the evaluation and interpretation of heat flow data measured in the upper few kilometers of the earth crust. In evaluating the quality of HFD data, the soundness of the methods of measurement, both in the field and in the laboratory, and corrections for various transient and steady state perturbing factors, such as climatic variations of surface temperature and groundwater flow, are considered. Having established the quality of the data we then make inferences about the thermal and tectonic state of the crust and the interior of the earth from the observed nearsurface HFD pattern to provide thermal constraints for a unified theory of tectonics and earth history.

Physical laws, such as Fourier's law of heat conduction and the laws of thermodynamics, govern the thermal processes in the earth at the macroscopic scale; partial differential equations, such as the equation of heat conduction, are common mathematical descriptions of these laws. Solving these equations under various conditions is a major task of the evaluation and interpretation of HFD data, and is the major concern of this study. The solutions to the equations can be classified as deterministic or probabilistic, forward or inverse, analytical or numerical, depending on the nature of the specific problem and the method used. Definitions for the terms used for the classifications will be given later in this chapter

The main objective of this research is to develop a numerical method that

incorporates inverse theories to solve steady state subsurface conductive and convective heat transfer problems.

Geophysics as a discipline is the study of inverse problems: data measured on or near the surface are used to infer the state of the deeper interior of the earth; it is natural, then, that inverse theories have been well developed in certain sub–disciplines of geophysics. Simultaneously, numerical methods based on those extensively employed in the engineering sciences are being developed in geophysics to solved problems in, e.g., solid and fluid mechanics and heat transfer. However, inverse methods incorporating numerical techniques have only recently begun to gain attention in geophysics, although they have been much used in engineering and groundwater research since mid 70's. A brief review is therefore given in the next two sections on the applications of forward and inverse methods to geophysical research in general and HFD work in particular. This review is followed by an outline of the work covered by this thesis.

In the following sections and the rest of the text, three terms will be frequently used for easy referencing physical quantities pertaining to the partial differential equations considered in this work. They are described as follows without strict mathematical and physical definitions.

Material properties. The physical quantities characteristic of the media that occupy the spatial domain of the problem considered, or their logarithmic transforms, are called material properties. The thermal conductivity of a rock is a material property; the heat production rate (or heat generation, heat production, heat productivity) of a rock is regarded as a material property in this work. In a heat transfer problem involving groundwater flow, the material properties of both the solid phase (rock matrix) and the liquid phase (pore water) that saturates the rock must be considered. The material properties of the solid phase include the thermal conductivity of the materials composing the matrix, the porosity and

intrinsic permeability of the porous medium. The material properties of the fluid include the density, viscosity, specific heat capacity, thermal conductivity, etc.. Very often, it is more convenient to consider the overall (or effective) material properties of the mixture of the solid and fluid phase, such as the bulk thermal conductivity and the hydraulic conductivity. Material properties are typically scalars or tensors of the second rank.

Field variables. The physical quantities distributed continuously in space and determined by the material properties and initial and boundary conditions are called the field variables. In the problems considered in this work, the field variables are scalars, such as the temperature and the hydraulic head, which will be defined in Chapter 2.

Boundary fluxes. The normal component of the aerial density of mass or energy flow across a point on a boundary of the spatial domain of the problem is a boundary flux at that point; examples are the boundary HFD and Darcian velocity. A flow density is a vector in general, but a boundary flux refers only to its component normal to the boundary and therefore can be treated as a scalar. In a forward solution to a partial differential equation, the specification of a boundary flux is referred to as a Neumann boundary condition.

1.2 Forward methods

When perfect knowledge, which may range from distinct numerical values to statistical moments, of the material properties and the initial and boundary conditions is given, solving a set of partial differential equations for the field variables is a forward problem. For example, given the thermal conductivity distribution of rock formations, the temperature distribution at ground surface and

the HFD distribution at other boundaries, solving the steady state heat conduction equation for the temperature distribution is such a forward problem.

Depending on the assumptions made about the intrinsic features of the physical quantities, a forward method can be either probabilistic or deterministic. The probabilistic approach becomes necessary when the spatial variability of the physical quantities is so complex that an exact description of the state of the quantities as functions of space and time is impossible. With this approach, the material properties and hence the field variables are regarded as realizations of spatial (or temporal) stochastic processes, or random fields. The quantities are described in terms of the statistical moments of the random fields, such as the mean and the auto– and cross–correlations. Principles of the probabilistic approach can be found in many text books (e.g., Strong, 1981), and examples of the applications of stochastic analysis to various geological problems can be found in Merriam (1976). In groundwater hydrology, stochastic analysis of groundwater flow has developed into a major discipline following the pioneer work by Freeze (1975). Representative work includes Bakr et al. (1978), Delhomme (1978), Smith and Freeze (1979), Dagan (1982) and Gelhar (1986). The approach was not formally introduced to the theoretical research of terrestrial HFD until 1987 when Nielsen applied a stochastic model to the steady state 3–D heat conduction problem in an attempt to interpret the empirical linear relationship between surface HFD and surface heat productivity of rock materials. For the mathematical foundation of this work, however, the deterministic methods are of more interest.

The deterministic forward techniques for solving partial differential equations fall into two categories: analytical and numerical methods. Most analytical solutions to the heat transfer equation under various initial and boundary conditions and domain configurations were derived decades ago, and can

be readily applied to terrestrial heat flow problems. Carslaw and Jaeger (1959), extensively referenced by both engineers and heat flow researchers, provided a respectable number of analytical solutions. The applications of some of these solutions to the evaluation of heat flow data were summarized by Jaeger (1965). An ensemble of solutions applicable to the evaluation and interpretation of heat flow data is also available in Cheremenski (1977).

Analytical solutions can be obtained only with simple and regular geometry and boundary conditions. To use the solutions in a more realistic situation, many simplifications have to be made to the particular problem. Some numerical techniques, such as the discrete Fourier transform, can extend the applicability of analytical solutions to a certain extent (Lindqvist, 1984; Clauser, 1984; Wang et al., 1986), but the flexibility is much limited. Although new analytical solutions with more complex problem setups can occasionally be seen in the heat flow literature (e.g., Nielsen and Balling, 1985; Shen and Beck, 1986), numerical methods for solving partial differential equations have become increasingly popular, for their flexibility in coping with irregular boundary conditions and complex material property structures. With the availability of high speed computers, numerical modeling is now widely regarded as an important technique in many fields of earth science. Commonly used numerical methods for solving partial differential equations are the finite difference method, the finite element method and the boundary element method.

The finite difference method has been developed for a long time and is widely used for its relative simplicity in computer programing. The general principles of the method are introduced in numerous text books (e.g., Smith, 1978). There are many applications of the the method to the evaluation and interpretation of heat flow data; examples are, Stromeyer (1984) and Cermak and Bodri (1986) for the problem of downward continuing heat flow data, Lewis and

Beck (1977) for illustrating the perturbations to the surface HFD value caused by water flow through an aquifer, Wang et al. (1985) for investigating the effects of variations of water bottom temperature and inhomogeneity of lake sediments on the probe measured temperature–depth profiles, Henry and Pollack (1985) for correcting heat flow data for the effects of topography and structure. More recently, Clauser (1988) used 2–D and 3–D finite difference techniques to model the interactions between the geothermal and the hydrological regimes.

The finite element method, which gained popularity in the 1970's, has matured rapidly in the past two decades. The finite element method is generally considered more convenient than the finite difference method in dealing with anisotropic media, complex material property structures and boundary conditions, and it is possible to set up very general finite element computer programs. It may also yield better accuracy and efficiency, compared to the finite difference method, in many problems. The general principles and technical details are well elucidated in many text books and treatises in engineering and mechanics (e.g., Zienkiewicz, 1972; Bathe and Wilson, 1976). In hydrology, where numerical modeling techniques are routinely used, there are a number of text books which specialize in the use of finite element methods to solve the problems of surface and subsurface flow, and solute and energy transport (Pinder and Gray, 1977; Huyakorn and Pinder, 1983). Since the mid–1970's, some examples of the use of the finite element method have appeared in terrestrial heat flow research, though not comparable in quantity to those in groundwater research. For example, Lee and Henyey (1974) and Finckh (1981, 1983) used the technique for topographic and structural corrections of measured HFD data. Zhang et al. (1982) and Xiong and Zhang (1984) used it to analyze subsurface temperature fields. Ballard and Pollack (1987) used a finite element model in the interpretation of heat flow data from Archean cratons and the surrounding younger terrains. 2–D or 3–D finite

element numerical modeling was made by Smith and Chapman (1983), Woodbury and Smith (1985), Willett and Chapman (1987), to investigate the thermal effects of groundwater flow. At least one text book is dedicated to the use of finite element methods in geothermal research (Zhang and Xiong, 1986).

The boundary element method (e.g., Ligget and Liu, 1983) is at present less favored in earth sciences than the finite difference and finite element methods, due mainly to its limited power in dealing with heterogeneous media. Applications of the method to heat transfer and geothermal problems can be seen in Pina (1984) and Powell et al. (1988), respectively.

Another important numerical method for solving partial differential equations is the Monte Carlo simulation based on random walks (Nakamura, 1977), which has long been applied to engineering heat conduction problems (e.g., Haji–Sheikh and Sparrow, 1967). Its application to the study of terrestrial heat flow has not been reported, but there is an example of its application to the study of lunar heat flow (Langseth et al., 1976). The concept of probability is essential in the random walk based Monte Carlo simulation, but when the material properties and the boundary and initial conditions are specified deterministically, the technique is essentially deterministic. The uncertainties in this type of Monte Carlo solution are due to the solution procedure itself, where the errors caused by finite sampling (Nakamura, 1977, p.334) are analogous to the discretization errors in the above three numerical methods, and not due to the intrinsic random nature of the physical quantities which are assumed in the probabilistic approach.

1.3 Inverse methods

An inverse problem always exists as the counterpart of a forward problem.

Both are specified by a mathematical model which is based on physical theories (that may involve simplifying assumptions) and which relate the field variables to the material properties, and both are subject to initial and boundary conditions. When the material properties and the initial and boundary conditions are perfectly known, and the mathematical model is used to determine the distribution of field variables that are entirely unknown, we are solving a typical forward problem. Conversely, if the field variables are perfectly known, and the objective is to determine the values of material properties or the initial or boundary conditions that are entirely unknown, we would be solving an inverse problem in the strictest sense. In practice, however, such idealized forward and inverse problems do not exist because none of the physical quantities would be known perfectly. Thus, a problem should be posed in a more general sense: to use the mathematical model and the available information on field variables, material properties and initial and/or boundary conditions to better our understanding of the physical system in question, i.e., to improve the state of our knowledge. Such a problem is called a generalized inverse problem, although it includes the forward problem as a special case. A common inverse problem, seen frequently in the literature of groundwater hydrology and engineering, is system identification where the values of material properties are determined, given a finite set of data on field variables and specified initial and boundary conditions. In terrestrial heat flow work, on the other hand, an inverse problem that is of considerable interest is the determination of a boundary flux, namely (the vertical component of) the HFD at a certain depth, given limited information on other physical quantities.

To define a problem as forward or inverse is in principle arbitrary. For example, there is no logical reason why we cannot exchange the positions of the field variables and the material properties in the above definitions of the forward and inverse problems. However, over time an implicit agreement appears to have

developed that an inverse problem can often be recognized by its ill–posedness, that is, nonuniqueness and instability. Without loss of generality, it is convenient to discuss the problem of ill–posedness by considering the particular type of inverse problem, system identification. In a typical system identification problem, parameters representing the material properties are to be estimated from data on the other physical quantities and two kinds of nonuniqueness in the determination of the parameters have to be recognized (Tarantola and Valette, 1982b). One is due simply to the paucity of data. The other, called nonidentifiability in hydrological inverse theories (Yeh, 1986; Carrera and Neuman, 1986a), is intrinsic to the structure of the mathematical and physical model, that is, the same set of data on the field variables and boundary conditions, no matter how redundant and accurate, could have been produced with more than one set of values of the material property parameters. For example, under the assumption of pure conduction and with a given HFD at a certain depth, identical ground surface temperature distributions can be produced by an infinite number of combinations of thermal conductivities and heat productivities of the rocks; therefore a unique determination of the subsurface distribution of thermal conductivity and heat production solely from ground surface temperature is impossible. To limit the second kind of nonuniqueness, some independent information on the parameters is needed. Instability is invariably due to the structure of the mathematical model of the inverse problem; an example is the comparison between upward continuation, which is stable, and downward continuation, which is unstable, of potential fields.

Solutions to an inverse problem can be found using a forward method with a trial and error approach. For example, given certain boundary conditions, we can find the thermal conductivity and heat source distributions by solving the heat conduction equation many times while adjusting the values of the two material properties each time, until the computed temperature values are close enough, by

certain criteria, to the measured temperature values at a given set of points (model fitting). This method, however, may not solve the problem of nonuniqueness. Studies to limit the problems arising from ill–posedness and to find unique and stable solutions to inverse problems have given rise to inverse methods that incorporate statistical principles. The solution obtained with such a method is called a formal inversion

Normally, an inverse method has two major steps: parameterization and parameter estimation. In parameterization, a finite number of parameters representing the physical quantities are found, and the forward model of the inverse problem is transformed into a parametric form such as an algebraic equation system. After parameterization (some inverse problems may already be defined in parametric forms), statistical parameter estimation methods are used to estimate the values of the parameters and to provide the degrees of uncertainties in the estimates. It should be noted that partial differential equations have been used above as the mathematical models of the inverse problems, which is a usual approach in hydrological inverse theories. In the literature of geophysical inverse theories, the forward models are often given in functional forms or as integral equations, most of which are solutions of, or alternative expressions of, partial differential equations (Oldenburg, 1984; Parker, 1977; Sabatier, 1977). Different forward mathematical models require different parameterization procedures, but do not usually influence the choice of a parameter estimation method.

There are a number of different philosophies of statistical parameter estimation, the two extreme cases being the methods based on sampling theory (or classical, non–Bayesian) statistics (Hoel, 1954) and the methods based on Bayesian statistics (Lindley, 1972, Box and Tiao, 1973). Although it would take a whole book to discuss adequately the various philosophies, a brief summary is necessary here because the fundamentally different philosophies have become

characteristic of the different schools of thought in geophysical and hydrological inverse methods.

Sampling theory statisticians believe in objectiveness. To them, the parameters are random variables, and probabilities are defined as the limit of the frequency of the occurrence of events in a sampling procedure. The parameter estimation methods based on this theory try to extract all information on the estimated parameters from objective data, using certain criteria such as minimum variance and unbiasedness. Methods in this category include the classical least squares method (Cooley, 1977) and the classical maximum likelihood method (Kitanidis and Lane, 1985).

Bayesian statisticians hold that probability is a formal way of stating our knowledge of the objective world (Jaynes, 1986); the parameters are not random, it is our imperfect knowledge that gives rise to the "randomness", that is, the uncertainty. Observed data are nothing but a component of this imperfect knowledge, save for the relatively smaller uncertainties; a priori information on the parameters, such as a researcher's personal belief, experience and judgment, is another indispensable component of this knowledge, often necessarily with larger uncertainties. Data provide a certain amount of information, and the inference should be left to the people who use the data. The basic principle of Bayesian statistics is the Bayes' rule. The a priori information enters the estimation procedure in terms of an a priori probability (or personal probability, subjective probability, intuitive probability); the objective data are used in the form of a likelihood function (Box and Tiao, 1973; Berger and Wolpert, 1984). The inference, i.e., the a posteriori probability, made by different researchers will generally be different because of the subjectiveness of the a priori probability distribution. Since our knowledge is imperfect, it is only natural that different people have somewhat different understandings of the parameters. Inverse

methods of Bayesian type are used by, e.g., Gavalas et al. (1976), Tarantola and Valette (1982b) and Jackson and Matsu'ura (1985).

Information is the key to limiting the ill–posedness of inverse problems (Tarantola and Valette, 1982a). No matter which technique is used to "constrain" or "regularize" the problem, some kind of prior information, explicit or implicit, objective or subjective, is inevitably introduced into the procedure. For this reason, methods based solely on sampling theory statistics are of very limited practical interest. However, many people find it hard to accept the extreme Bayesian philosophy. Compromise approaches can be found. One class of geophysical inverse methods is akin to the Bayesian type but contains elements of the sampling theory type, that is, the stochastic inversion (Franklin, 1970; Jackson, 1979). Stochastic inversion requires prior information, but uses the information formally as objective data, maintaining all the characteristics of the sampling theory type methods. Another compromise approach between the Bayesian and non–Bayesian philosophy is the "maximum likelihood method incorporating a priori information", known in probability theory and statistics as type II maximum likelihood method (Good, 1965; Berger and Wolpert, 1984), used frequently in hydrological inverse methods (Neuman and Yakowitz, 1979; Carrera and Neuman, 1986a) and occasionally in geophysical inverse methods (Menke, 1984). For linear inverse problems and to the same researcher, there is no practical difference between the stochastic inversion (or type II maximum likelihood method) and the Bayesian estimation (Backus, 1988); which method is used seems to depend mainly on one's personal preference, especially when the probability distributions are Gaussian. For nonlinear inverse problems, there is more fundamental difference in the calculation and interpretation of the results. This issue will be further examined in section 4.3.

Inverse methods are extensively used in many fields of geophysics; for

example, seismology (Wiggins, 1972; Cooke and Schneider, 1983; Gauthier et al., 1986, etc.), geomagnetism (Silva and Hohmann, 1983; Gubbins and Bloxham, 1985), atmospheric physics (Rodgers, 1976), geomechanical stress analysis (Angeliar et al., 1982), electromagnetic sounding (Constable et al., 1987), self–potential method (Fitterman and Corwin, 1982), etc.. In terrestrial heat flow studies, one well known application is the estimation of surface temperature history or simultaneous estimation of the surface temperature history and the local HFD using temperature or temperature gradient data measured in boreholes or in lacustrine and oceanic sediments (Cermak, 1971; Vasseur et al., 1983; Shen and Beck, 1983; Nielsen, 1986; Wang and Beck, 1987; Shen and Beck, 1988). Another application is the downward continuation of heat flow data (Huestis, 1978, 1980; Huestis and Parker, 1979; Stromeyer, 1984; Beck and Shen, 1989). Inverse approaches are also used in other cases of evaluation and interpretation of heat flow data, such as the estimation of HFD using scarce and noisy temperature data (Vasseur et al., 1986), topographic and structural correction of HFD data (Henry and Pollack, 1987) and analysis of bottom hole temperature data sets (Speece et al., 1985; Willett and Chapman, 1987; Deming and Chapman, 1988).

In groundwater studies, inverse methods have been used by many researchers to estimate aquifer parameters using measured hydraulic head data and other available information. In a sense, the term "inverse method" here is synonymous with "system identification". In addition to the use of a unique random field formulation (Kitanidis and Vomvoris, 1983; Hoeksema and Kitanidis, 1984), the inverse methods in groundwater hydrology as a whole are characterized by frequent incorporation of numerical methods for solving partial differential equations. There is an increasing number of publications in this field. Examples are: Cooley (1977, 1979), Neuman and Yakowitz (1979), Neuman et al. (1980), Yeh and Yoon (1981), Yeh et al. (1983), Dagan (1985), Sun and Yeh (1985),

Carrera and Neuman (1986a, b, c), Fradkin and Dokter (1987), Loaiciga and Marino (1987), Woodbury and Smith (1988), Lu et al. (1988). A review of three decades of work up to 1986 in this field was given by Yeh (1986).

1.4 Outline of the present work

The objective of the present research is to develop a method that incorporates a finite element numerical modeling technique and a geophysical inverse theory to solve 2–D steady state problems of heat conduction and of coupled hydrological and thermal regimes. For the problems considered in this research, we possess certain knowledge of all the three types of physical quantities, namely, the field variables, the material properties and the boundary fluxes, some of which are better known than others. The information on the quantities may be obtained through actual field measurements or provided intuitively by one's personal judgment and reasoning. The available information is then used to improve our knowledge of all components of the physical system. System identification is a special case in which the field variables and boundary fluxes are much better known than the material properties so that it is effectively the inversion of the former to yield estimates for the latter. The forward solution is another special case, where the state of the material properties and boundary conditions are assumed to be perfectly known and are used to determine the previously unknown field variables.

The solution procedure consists of the customary two major steps, parameterization and parameter estimation. The latter is performed in another two steps, nonlinear parameter estimation and boundary flux updating (linear parameter estimation). In the parameterization step, a finite number of

parameters are found to represent the spatially distributed material properties, field variables and the boundary fluxes, and a parametric relation between these parameters are established, by using a finite element model. The resultant parametric relation, which can be separated into a nonlinear and a linear part, is then used in a Bayesian parameter estimation procedure. The nonlinear parameter estimation procedure gives the estimates and the variances of the parameterized field variables and material properties. The subsequent linear parameter estimation updates our knowledge of the boundary fluxes.

Chapters 2, 3, 4 and 5 lay the theoretical foundations of the approach: the mathematical model in the form of partial differential equations (Chapter 2), the finite element parameterization of the problems (Chapter 3), the nonlinear parameter estimation procedure (Chapter 4), and the boundary flux updating techniques (Chapter 5). In the developments, the problem of heat conduction and the problem of coupled thermal and hydrological regimes are considered separately and in parallel, following the same basic ideas, although the second problem is technically by no means a simple extension of the first. The much simpler solution to the former will help explain the development of the more difficult solution to the latter.

In Chapter 6, the method is applied to two heat conduction problems, one is the topographic correction for HFD data and the other is the downward continuation of heat flow data. Field examples as well as synthetic data are used. In Chapter 7, the method is applied to the problem of basal HFD determination in the presence of basin scale groundwater flow. Synthetic examples are used to find the limitations of the method and to examine the general behavior of the solutions; the behavior of these solutions are much more complicated than that of the conduction problem, since the forward model consisting of two coupled partial differential equations is already nonlinear. Since a sufficient data set has so far not

been found in which the technique's power to predict hitherto unobserved features can be adequately tested, the potential of the method in solving field problems is illustrated by using synthetic data generated from a model based on a real sedimentary basin. The conclusions drawn in Chapter 8 include the advantages and disadvantages of the method and some observations on the performance of the method.

Three FORTRAN computer codes are developed and used in this research: FORCUP, to obtain forward numerical solutions to the 2–D steady state problem of heat conduction, isothermal groundwater flow, decoupled and coupled water flow and heat flow; INVCON and INVCUP, to obtain the inverse solution to the 2–D steady state problems of heat conduction and coupled water flow and heat flow, respectively. Aspects of the computer implementation of the inverse finite element method are discussed in the appendices.

CHAPTER 2: MATHEMATICAL MODELS

2.1 Preface

Two types of problems are considered in this work: heat conduction in solid earth media (briefly called the conduction problem) and coupled water flow and heat flow in permeable rock formations (briefly called the coupled problem). Both problems are assumed to be of steady state and 2–D. The mathematical models of the problems are given here in the form of partial differential equations, and will be transformed into parametric forms in Chapter 3 before the inverse solutions are sought.

The coordinate system will be Cartesian in a vertical 2–D plane (geological or geotectonical cross section) with the x_2 axis pointing upwards. As a convention, a letter with subscript(s) i, j, ..., n is used to denote the component of a vector or tensor unless otherwise specified; the subscripts i and j are reserved for $\mathbb{R}^2$, i.e., i,j = 1,2; for a vector, the same letter bold faced but without a subscript is used to denote the matrix form of the vector. In all equations, repeated subscripts and superscripts i through n (the default integer variables in FORTRAN computer language) imply summation.

2.2 Heat conduction problem

Fourier's law of heat conduction states that

$$q_i^h = -\lambda_{ij}^s \frac{\partial T}{\partial x_j} \tag{2.1}$$

where T is the temperature, q_i^h is the HFD and λ_{ij}^s is the tensor of thermal conductivity of the solid medium. The partial differential equation that governs the process of steady state heat conduction is given as (e.g., Carslaw and Jaeger, 1959)

$$\frac{\partial}{\partial x_i}(\lambda_{ij}^s \frac{\partial T}{\partial x_j}) + \aleph = 0 \tag{2.2}$$

where $\aleph$ is a heat source term, which, in terrestrial heat flow problems, is due mainly to the heat produced by the decay of natural radioactive isotopes in the earth's crust, and is referred to as the heat production rate. λ^s and $\aleph$ are regarded as material properties in this work.

Equation (2.2) is the mathematical model for our heat conduction problems. We make the assumption that λ^s is a function of x, not of T. This is valid when the values of temperature considered are not too high and the range is not too wide, as in the case of topographic corrections, where the depth range is generally no more than one or two km and the temperature ranges between approximately –20 °C and 40 °C. In such a case, equation (2.2) as a forward problem is linear. If a wider temperature range is considered, as in the case of downward continuation of heat flow data, where the temperature varies between a surface value of about 0 °C to Moho–boundary values of around 1000 °C, the temperature dependence of λ^s, and other forms of heat transfer, may become more significant (Cermak and Bodri, 1986). At temperatures higher than 400–600 °C, heat transfer by radiation begins to play more important roles and the radiative conductivity (Clauser, 1988) is a function of temperature. Nevertheless, in order to simplify the parameter estimation procedure in this inverse method, the material properties are not formulated as explicit functions of the field variables. The validity of this approximation for the problem of downward continuation of heat flow data will be discussed in section 6.4.3.

2.3 Coupled thermal and hydrological regimes

2.3.1 Governing equations

Our problem is confined to a low Reynolds number, slightly compressible, two dimensional Darcian flow of sedimentary basin scale. For non-isothermal subsurface flow problems, it is convenient and customary to define a quantity

$$h = \frac{P_f}{\rho_o g} + x_2 \tag{2.3}$$

where P_f = fluid pressure,

ρ_o = water density at a reference temperature T_o,

g = the absolute value of gravitational acceleration,

The quantity h was used by Hubbert (1940) and Bear (1972, p.654) to address the relative importance of buoyancy force versus gravity in the presence of variable fluid density. Frind (1980) used the same expression under the name equivalent freshwater hydraulic head. This usage was subsequently adopted by a number of authors (e.g., Smith and Chapman, 1983; Garven and Freeze, 1984a; Woodbury and Smith, 1985) in the numerical modeling of non-isothermal flow. However, when the variation of fluid density is due only to its temperature dependence, it is more appropriate to call h the reference hydraulic head (Clauser, 1988; Bachu, 1988, personal communication). Using the reference head, Darcy's law of fluid flow in porous media takes the form,

$$q_i^w = -\frac{\kappa_{ij}}{\mu} \rho_o g \left(\frac{\partial h}{\partial x_j} + \rho_r \delta_{2j}\right) \tag{2.4}$$

where q_i^w = specific discharge or Darcian velocity of water,

κ = permeability of the medium, a function of x_i,

μ = dynamic viscosity of water,

δ_{ij} = Kronecker delta,

ρ_r = the relative water density, defined as

$$\rho_r = \frac{\rho - \rho_o}{\rho_o} \tag{2.5}$$

with ρ being the water density at temperature T.

For a slightly compressible steady state Darcian flow, the following continuity equation is sufficiently accurate (e.g., Bear, 1972),

$$\rho_o g \frac{\partial}{\partial x_i}\left\{\frac{\kappa_{ij}}{\mu}\left(\frac{\partial h}{\partial x_j} + \rho_r \delta_{2j}\right)\right\} = 0 \tag{2.6}$$

where the constant $\rho_o g$ is left as a scaling factor to make finite element discretization (Chapter 3) more convenient.

In the existence of fluid flow, the steady state energy balance equation has an additional convective term as compared to equation 2.2,

$$\frac{\partial}{\partial x_i}\lambda_{ij}\frac{\partial T}{\partial x_j} - \rho c q_i^w \frac{\partial T}{\partial x_i} = 0 \tag{2.7}$$

where c is the specific heat capacity of water at constant pressure. It should be noticed that in equations 2.1 and 2.2, λ^s is the thermal conductivity of the solid medium, but in equation 2.7, λ represents the overall (or bulk) thermal conductivity of the fluid –saturated porous medium. Study of the mathematical representation for bulk conductivity of a multi–phase medium in terms of the structure and the constituent media is beyond the scope of this work; interested readers are referred to Brailsford and Major (1964), Jeffrey (1973) and Beck (1976). The heat source (cf. equation 2.2) has generally insignificant effects over the depth range of our problem (0–5 km) (Nielsen, 1986; Beck and Shen, 1989), and is not included in (2.7).

Equations (2.6) and (2.7), subject to appropriate boundary conditions, constitute the mathematical model of our problem. The two equations are coupled and the coupling is due to the temperature dependence of ρ and μ in (2.6) and the convective term in (2.7).

2.3.2 Temperature dependence of physical properties of water

The physical properties of water appearing in the governing equations include the density ρ, the specific heat capacity at constant pressure c and the dynamic viscosity μ. The thermal conductivity of water is not considered separately, because it is the formation thermal conductivity of the solid–fluid complex that is of interest in our problem.

The full expression for the steady state continuity equation is

$$\frac{\partial}{\partial x_i}(\rho q_i^w) = 0 \tag{2.8}$$

i.e.,

$$\frac{\partial q_i^w}{\partial x_i} + \frac{q_i^w}{\rho}\frac{\partial \rho}{\partial x_i} = 0 \tag{2.9}$$

If the overall variation in ρ over a characteristic length scale L' is $\Delta\rho$, the first left hand side term of (2.9) is of the order $\frac{q'}{L'}$, where q' is the characteristic value of the Darcian velocity. The order of magnitude of the second term is then $\frac{q'}{L'}\frac{\Delta\rho}{\rho_0}$. Since $\frac{\Delta\rho}{\rho_0} << 1$ in the problem under study, only the first term of (2.9) remains, which leads to (2.6).

In the cases of low topographic relief, however, the buoyancy term $\rho_r b_{2j}$ in equation (2.6) may not be negligible compared to the gravity term $\frac{\partial h}{\partial x_j}$ although in most cases it is indeed very insignificant. The thermal dependence of water density ρ is taken into account mainly because of the buoyancy term in this equation.

In the energy balance equation (2.7), the first and second term represent heat transfer by conduction and advection (forced convection), respectively. If the overall temperature variation over a certain length scale L' is ΔT, and the characteristic value of the thermal conductivity is λ', the orders of magnitude of the two terms in (2.7) are then $\frac{\Delta T}{L'^2}$ and $Pe\frac{\Delta T}{L'^2}$, respectively, where the dimensionless quantity

$$Pe = \frac{\rho c q' L'}{\lambda'} \qquad (2.10)$$

is the Peclet number. Pe is a measure of the relative importance of the conductive and advective heat transfer in a system or a local portion of a system; thus if Pe >> 1, advective heat transfer dominates.

For a given geometry and given thermal conductivity values, Pe is determined by ρ, c and q'. It is a common practice to consider ρc, the specific thermal capacity, as a single physical quantity, because the variations of ρ and c with changing temperature tend to offset each other for most materials (Beck, 1988). The ρc of water varies with temperature by only a few percent within the temperature range (0 – 120 °C) of the problem, as shown in Fig.2.1, therefore it is reasonable to take it as a constant. The Darcy velocity, and hence Pe, is inversely proportional to μ, the dynamic viscosity of water. Since μ varies by 400 to 500 % in the same temperature range (Fig.2.1). its thermal dependence must by taken into consideration.

A number of precise expressions for ρ and μ as functions of T exist in the literature (e.g., Mercer *et al.*, 1975; Straus and Schubert, 1977), but the following linear approximations illustrated in Fig.2.1, which have the merit of being convenient for analytical manipulation, are adopted in this work:

$$\rho = \rho_0 - \beta(T - T_0) \qquad (2.11)$$

$$\mu^{-1} = \mu_0^{-1} + \eta(T - T_0) \qquad (2.12)$$

where β and η are constants. It is easy to see that if better accuracy for ρ and μ, or if a wider temperature range is required, it is not difficult to replace (2.11) and (2.12) with multi–section linear forms. Parameter constants used in this study are listed in Table 2.1.

2.3.3 On the Peclet number Pe

The dimensionless number Pe is frequently used in the study of thermal

effects of groundwater flow or subsurface energy transport problems, sometimes with slight variations in its definition (e.g., Bachu, 1985; Woodbury et al., 1988). Equation (2.10) is the most general definition of the Peclet number. From (2.10), we have the following three observations:

1) For a 2–D or 3–D case, if the two vectors $\mathbf{q}^w$, the Darcian velocity, and ∇T, the temperature gradient, are nearly orthogonal to each other, no matter how large Pe is (but within the limit of laminar flow), the convective term in (2.7) is always negligible.

2) Using a single Peclet number (no matter how it is defined) to describe a whole system, as was done in Woodbury and Smith (1988), may be appropriate in some limited cases, but certainly not in all. For example, in a sedimentary basin where heat flow is essentially vertical, it is only in the regions of groundwater recharge and discharge, where the vertical component of water flow may be prominent, that the convective heat transfer can be significant; in regions where groundwater flow is largely horizontal, the transfer of heat (in the vertical direction) is mainly by conduction. Therefore, a Pe number can be applied meaningfully only in a local portion of the system to show the relative importance of the two mechanisms of heat transfer in that particular portion.

3) The Peclet number only gives an idea of the relative importance of the two types of heat transfer by orders of magnitude, as can be seen from the way it is defined; comparing two Peclet numbers with similar magnitudes (e.g., 2 and 3) is not very meaningful.

Based on the above observations, it can be concluded that the Peclet number, as one of the many ways of characterizing qualitatively the relative importance of convective to conductive heat transfer, is convenient to use in simple cases, especially 1–D cases, but may not be convenient in more complex cases.

2.3.4 On mechanical thermal dispersion

A simplification made in equation (2.7) worthy of remark is the neglect of mechanical thermal dispersion due to irregular motion of fluid particles in the void space of the porous medium (Bear, 1972). With the mechanical thermal dispersion taken into account, the HFD by conduction and dispersion at a point is given in a form resembling Fourier's law,

$$q_i^h = - D_{ij} \frac{\partial T}{\partial x_j} \tag{2.13}$$

where D_{ij} is the coefficient of thermal diffusion, given as (Bear, 1972; Sauty, 1982a; Garven and Freeze, 1984a),

$$D_{ij} = \lambda_{ij} + \phi \rho c D_{ij}^{th} \tag{2.14}$$

where ϕ is the porosity of the porous medium; D_{ij}^{th} is the coefficient of mechanical thermal dispersion, and was studied in detail by Scheidegger (1961).

Based on dimensional analysis, Bear (1972, p.651) concluded that for the range of Reynolds number (< 10), within which Darcy's law is valid, mechanical thermal dispersion is negligible. Even for large scale problems, numerical results show that the effects of mechanical thermal dispersion are often insignificant (Mercer et al., 1975; Woodbury and Smith, 1985). For these reasons, plus the fact that the mechanism of mechanical thermal dispersion is not fully understood and is controversial, it is reasonable to neglect the dispersion term in writing (2.7) for the inverse problem at the current stage of this study. This approximation can also be understood philosophically as lumping all effects into one coefficient (Mercer and Faust, 1980), and calling it the thermal conductivity, but keeping in mind that it may partially include the effects of mechanical dispersion, if the latter is not negligible.

Table 2.1. List of parameter constants in equations (2.6), (2.7), (2.11) and (2.12).

Constant	Value	Unit
T_o	30	°C
ρ_o	995.91	kg m^{-3}
β	0.53625	kg m^{-3} K^{-1}
μ_o^{-1}	1253.1	s m kg^{-1}
η	32.579	m s kg^{-1} K^{-1}
ρc	4.18 x 10^6	J m^{-3} K^{-1}
g	9.8	m s^{-2}

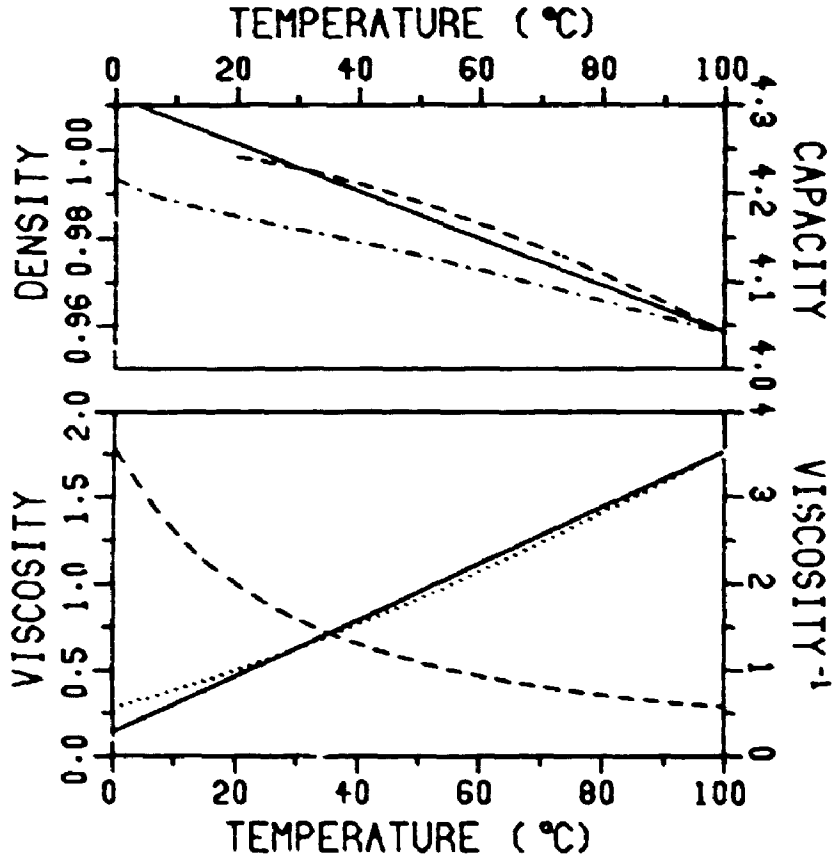

Fig.2.1. The specific thermal capacity ρc (J $cm^{-3}K^{-1}$), density ρ (g cm^{-3}) and dynamic viscosity μ (kg $s^{-1}m^{-1}$) of water as functions of temperature. The actual ρ and μ as given by Bejan (1984) are represented by dashed lines, and ρc by dot–dashed line; dotted line is μ^{-1}. The linear approximations of ρ and μ^{-1} (equations 2.11 and 2.12) are shown by solid lines.

CHAPTER 3: FINITE ELEMENT PARAMETERIZATION

3.1 Introduction

To use a discrete parameter estimation technique to estimate a spatially or temporally distributed physical quantity, a finite number of parameters that are sufficiently representative of the quantity must be found. This process, known as discretization or parameterization, is usually the first step of an inverse method. Since the dimensionality is reduced from an infinite to a finite number, assumptions and approximations are necessarily invoked. Superficially, the parameterization of a physical quantity can be performed in two different ways, corresponding to the probabilistic and deterministic forward methods mentioned in section 1.2.

From a probabilistic point of view, material properties and/or field variables are regarded as realizations of stochastic processes or random fields. With certain stationarity assumptions, these physical quantities can be described by statistical moments of the processes. The governing partial differential equations become stochastic partial differential equations.

The probabilistic approach based on statistical moments was used by Kitanidis and Vomvoris (1983) and Hoeksema and Kitanidis (1984, 1985b) in inverse problems of aquifer system identification. In their formulation, there are m point measurements of (logarithmic) transmissivity (Y) and n point measurements of hydraulic head (h) for an aquifer, from which the spatial distribution of the (log) transmissivity (Y) of the aquifer is to be estimated. The

actual h and Y are viewed as the realizations of random fields. The large scale spatial variability of Y, the trend in the mean, is described deterministically as a function of position x with a few unknown parameters, the small scale spatial variability is described statistically as a function of relative position Δx by a covariance function again with a few unknown parameters. Once the parameters in the trend and the covariance function are determined, the Y field is defined and the value at any point can be estimated (e.g., via kriging) with certain assumptions about stationarity of the random field. In the subsequent parameter estimation procedure, the measured values Y_i and h_j are combined into a single N ($N = m + n$) dimensional vector $\mathbf{z}$, which is assumed to have a jointly Gaussian probability density function

$$\mathcal{P}(\mathbf{z}|\boldsymbol{\theta}) = (2\pi)^{-N/2}|C|^{-1/2}\exp[-\frac{1}{2}(\mathbf{z}-\mathbf{z}_0)^t C^{-1}(\mathbf{z}-\mathbf{z}_0)]$$

where $\boldsymbol{\theta}$ is the vector of parameters in the trend and covariance function, and the expectation $\mathbf{z}_0$ and covariance matrix C are functions of $\boldsymbol{\theta}$. These functional relations are determined, as part of the parameterization procedure, by considering the first order perturbations to Y and h in the stochastic partial differential equation relating the two quantities. $\mathcal{P}(\mathbf{z}|\boldsymbol{\theta})$ can be maximized to give the maximum likelihood estimation of $\boldsymbol{\theta}$.

The vector $\mathbf{z}$ can be a certain transform of the measurement vector (Y_1, Y_2,...Y_m, h_1, h_2,...h_n. In that case C is correspondingly modified. A source term can be added to the partial differential equation; if this term is uncertain, it is also expressed as a function of unknown parameters. An apparent advantage of such a probabilistic approach is that a very small number of parameters are used while the arbitrary heterogeneity of the material property is still accounted for.

Any formal inversion is probabilistic. However, many parameterization methods need not invoke the concept of random fields, and the parameterization can be formally performed in a deterministic manner. A physical quantity can be

mapped onto a function space with a finite number of basis functions. Then the parameters to be estimated are usually the generalized coordinates of the bases. The simplest basis functions are step functions, and a generalized coordinate is the average value of the variable over the corresponding step length (or block, for more than one dimension) (Jackson, 1979). In the usual finite element formulation in hydrological inverse methods (Cooley, 1977; Neuman and Yokawitz, 1979; Sun and Yeh, 1985; Carrera and Neuman, 1986a,b,c; Woodbury and Smith, 1988), material properties are parameterized using step functions, that is, each element or a group of elements is assigned the same material property value (zonation); the field variables, on the other hand, are parameterized using the polynomial basis functions, with the generalized coordinates being the nodal values of the variables (interpolation). In some cases, the material properties are also parameterized by interpolation, using basis functions and nodal values (Yoon and Yeh, 1976; Yeh and Yoon, 1981). There are numerous other ways of deterministic parameterization; almost any numerical technique can be listed as an example.

Although conceptually very different, the two approaches are closely related in certain ways. If the generalized coordinates based on step–functions are viewed as random variables, they can be considered as approximations to a spatial stochastic process if the correlations between the steps are appropriately defined; the goodness of the approximation depends on the size of the steps (blocks). This fact permits the use of Monte Carlo methods in the analysis of the spatial variability of physical properties of subsurface porous media (Freeze, 1975; Smith and Freeze, 1979). Similarly, the discrete spectral representations of a time or space series in the inverse methods of Gavalas et al. (1976) and of Wang and Beck (1987) can be regarded as either probabilistic or deterministic. In fact, any deterministic parameterization method can have a probabilistic interpretation. For example, one may regard zonation as probabilistic, saying that the material

property is a stochastic process that has a perfect auto–correlation in each zone; one may also regard interpolation as probabilistic, maintaining that it is the first moment of the stochastic process that is interpolated. A comparison made by Kuiper (1986) shows that the deterministic approach based on finite elements, despite its simplicity, may perform as well as or better than the probabilistic approach based on statistical moments in 2–D inverse groundwater modeling problems.

In this work, the deterministic approach is chosen and the problems are parameterized with a 2–D finite element model. With this model, the spatial domain of the problem is first divided into a number of elements, each having a constant material property value. There are N_e nodal points in one element, and N_g in the global finite element mesh. The field variables are interpolated using their nodal values and polynomial basis (or shape, interpolation) functions $H_k(x)$, $k = 1, 2, ..., N_e$, in each element. The boundary fluxes are interpolated for each elemental boundary using the nodal values and the shape functions related to the nodes at the boundary.

The discretization of the conduction problem and of the coupled problem are performed separately in the following sections; some remarks on the 2–D isoparametric finite element model are made in the last section.

3.2 Parameterization of the heat conduction problem

The field variable, temperature T, at any point x in an element is interpolated from the nodal values T_k, $k = 1, 2, ..., N_e$, using the shape functions $H_k(x)$.

$$T = H_k T_k \tag{3.1}$$

Here the subscript k is understood as the elemental nodal number. Each elemental nodal number is associated with a global nodal number. When the elemental matrices and vectors with dimension N_e are written into global matrices and vectors of dimension N_g, the subscripts of the entries are correspondingly transformed into the global nodal numbers. Without creating ambiguity, the same notation for the subscripts are used to number the nodes in both the elemental and global dimensions. When the dimensions of the matrices and vectors are specified, the transformation between the elemental and global is self–evident.

If one of the boundaries of an element is also a part of the global boundary where the HFD is specified or to be estimated, the HFD on this boundary is interpolated in the same fashion as the temperature using the nodal HFD values,

$$q = H_k q_k \tag{3.2}$$

$k = 1, 2, ..., N_b$, where N_b is the number of nodes on the elemental boundary (normally three in this work). In 3.2), and the rest of the derivation for the conduction problem, the right superscript of q used to denote heat (i.e., the "h") is dropped; the superscript will be necessary in the coupled problem to distinguish between the HFD q^h and the Darcian velocity q^w. (3.2) differs from (3.1) in that the interpolation is performed over a line rather than an area, and only those shape functions H_k that are related to the boundary nodes are needed.

Applying the Galerkin weighted residual method (e.g., Zienkiewicz, 1972) to heat conduction equation (2.2), we have, for element e,

$$\int_{\Omega^e} H_l \left\{ \frac{\partial}{\partial x_i} \lambda^s_{ij} \frac{\partial T}{\partial x_j} + R \right\} d\Omega = 0 \tag{3.3}$$

$l = 1, 2, ..., N_e$; where the integration is performed over the whole element domain Ω^e. Using Gauss' theorem, or integrating by parts, we obtain

$$\int_{\Omega^e} \lambda^s_{ij} \frac{\partial H_l}{\partial x_i} \frac{\partial T}{\partial x_j} \, d\Omega = \int_{\Omega^e} H_l \, R \, d\Omega + \oint_{s^e} H_l \, \lambda^s_{ij} \frac{\partial T}{\partial x_i} n_j \, ds \tag{3.4}$$

where s^e is the boundary path of the element, n is a unit vector normal to s^e

pointing outwards from the element domain.

If we define heat flux going into the element as positive and that going out as negative, the heat flux input at an elemental boundary point is then

$$q = -q_j\, n_j = \lambda^e_{ij} \frac{\partial T}{\partial x_i} n_j \tag{3.5}$$

With (3.1), (3.2) and (3.5), (3.4) becomes

$$\int_{\Omega^e} \lambda^e_{ij} \frac{\partial H_l}{\partial x_i} \frac{\partial H_k}{\partial x_j}\, d\Omega \cdot T_k = \int_{\Omega^e} H_l\, d\Omega\, \aleph + \oint_{S^e} H_l H_k\, ds\, q_k \tag{3.6}$$

in matrix form, equation (3.6) is the following algebraic equation system

$$K^e \cdot T - W^e - V^e \cdot q = 0 \tag{3.7}$$

where K^e is the elemental conductivity matrix, with

$$K^e_{lk} = \int_{\Omega^e} \lambda^e_{ij} \frac{\partial H_l}{\partial x_i} \frac{\partial H_k}{\partial x_j}\, d\Omega \tag{3.8}$$

W^e is the elemental source–equivalent nodal flow vector, with

$$W^e_l = \int_{\Omega^e} H_l\, \aleph\, d\Omega \tag{3.9}$$

and the symmetric matrix V^e is the elemental boundary flux transformation matrix, defined as

$$V^e_{lk} = \oint_{S^e} H_l H_k\, ds \tag{3.10}$$

The use of the global vectors of nodal temperature T and nodal HFD q in (3.7) indicates that K^e, W^e and V^e are all of global dimension N_g, with the entries not relevant to the considered element being zeros. It should be noticed that the heat source term could be parameterized in exactly the same way as the boundary HFD, that is, using nodal value representation and shape function interpolation, and W^e would have an expression similar to the third term in (3.7). However, in this work, a constant heat source in each element is believed to be an adequate approximation to reality, considering our poor knowledge of the heat source distribution in the crust. Thus, a higher order parameterization is deemed unnecessary.

The global algebraic equation system of the problem,

$$\mathbf{K}\cdot\mathbf{T} - \mathbf{W} - \mathbf{V}\cdot\mathbf{q} = 0 \tag{3.11}$$

is the simple combination of the elemental systems (3.7) over all elements, with

$$\mathbf{K} = \sum_{e} \mathbf{K}^{e} \tag{3.12}$$

$$\mathbf{W} = \sum_{e} \mathbf{W}^{e} \tag{3.13}$$

$$\mathbf{V} = \sum_{e} \mathbf{V}^{e} \tag{3.14}$$

Equation (3.11) is the discretized form of the partial differential equation (2.2). This static algebraic system defines a parametric relation between the discretized temperatures, thermal conductivities, heat sources and boundary HFD. In a forward problem in which T is the only unknown quantity to be solved, (3.11) is a linear system. For an inverse problem, however, the thermal conductivities, heat sources and/or the boundary fluxes are to be estimated as well, and hence (3.11) is a nonlinear system. At the current stage, only isotropic media are considered, so that the thermal conductivity in the above derivations is reduced to a scalar.

In our problem, there is a "hard" constraint on the material property values, that is, they are never less than zero. This constraint can be conveniently implemented in the parameter estimation procedure by changing of variables using the following trivial mathematical equivalence,

$$\lambda^{\mathrm{s}} \equiv \exp(\gamma \ln 10) \tag{3.15a}$$

$$\aleph \equiv \exp(\epsilon \ln 10) \tag{3.15b}$$

where

$$\gamma = \log\lambda^{\mathrm{s}} \tag{3.16a}$$

$$\epsilon = \log\aleph \tag{3.16b}$$

are the parameters to be estimated. The logarithmic conductivity γ and heat source ϵ are invoked into the above equations simply by replacing λ and $\aleph$ by (3.15).

We define a parameter vector **P** that includes as its components all the nodal temperatures, the discretized γ and ϵ values and the nodal HFDs. Using the parameter vector **P**, we can write (3.11) as

$$\mathbf{F}(\mathbf{P}) = 0 \tag{3.17}$$

where

$$F_l(P) = K_{lk}(\lambda)\, T_k - W_l(\epsilon) - V_{lk}\, q_k \tag{3.18}$$

In equation (3.18), the third right–hand–side term is the multiplication of a constant matrix and the parameters that do not appear in other terms, and is called the linear part of **F**, denoted by **f**, which, for obvious reasons, is also called the flux–equivalent nodal flow vector:

$$f_l = V_{lk} q_k \tag{3.19}$$

The other two terms of (3.18) constitute the nonlinear part of **F**, denoted by **g**, i.e.,

$$g_l = K_{lk}(\lambda) T_k - W_l(\epsilon) \tag{3.20}$$

This separation has correspondingly divided the total parameter vector **P** into two parts,

$$\mathbf{P} = \begin{bmatrix} \mathbf{p} \\ \mathbf{q} \end{bmatrix} \tag{3.21}$$

where the nonlinear part **p** includes all the nodal temperatures and the discretized log conductivities, and the linear part **q** includes the nodal values of the boundary HFD. Therefore, (3.17) becomes

$$\mathbf{g}(\mathbf{p}) - \mathbf{f}(\mathbf{q}) = 0 \tag{3.22}$$

The advantages of separating the nonlinear and linear parts will be seen in Chapter 4 and 5.

3.3 Parameterization of the nonlinear coupled system

The field variables now are the temperature T and the reference hydraulic

head h, and the material properties are the thermal conductivity λ and the permeability κ. Similar to the discretization of the conduction problem, T and h at any point in an element are interpolated from their nodal values using the shape functions H_k,

$$T = H_k T_k \tag{3.23a}$$

$$h = H_k h_k \tag{3.23b}$$

$k = 1, 2, \ldots, N_e$; and the boundary HFD and Darcian velocity at any point at an elemental boundary are interpolated in the same way,

$$q^h = H_k q_k^h \tag{3.24a}$$

$$q^w = H_k q_k^w \tag{3.24b}$$

where q^h is the conductive heat flux defined by (2.1), with λ^* replaced by λ, and q^w is the water flux input at the elemental boundary. The total heat flux across a boundary also includes a convective term, $\rho c T q^w$, i.e., the heat transported by flowing water, but in this thesis, the term boundary heat flux (or boundary HFD) always implies the conductive component.

Applying the Galerkin weighted residual method to (2.7), we have, for element e,

$$\int_{\Omega^e} H_l \left\{ \frac{\partial}{\partial x_i} \lambda_{ij} \frac{\partial T}{\partial x_j} - \rho c q_i^w \frac{\partial T}{\partial x_i} \right\} d\Omega = 0 \tag{3.25}$$

Using Gauss' theorem leads to

$$\int_{\Omega^e} \left\{ \lambda_{ij} \frac{\partial H_l}{\partial x_i} \frac{\partial T}{\partial x_j} + H_l \rho c q_i^w \frac{\partial T}{\partial x_i} \right\} d\Omega = \oint_{s^e} H_l \lambda_{ij} \frac{\partial T}{\partial x_i} n_j \, ds \tag{3.26}$$

where Ω^e, s^e and n have the same meaning as in the conduction problem.

Substitution of (2.4), (3.5), (3.23) and (3.24a) into (3.26) yields

$$\int_{\Omega^e} \left\{ \lambda_{ij} \frac{\partial H_l}{\partial x_i} \frac{\partial H_k}{\partial x_j} - \rho c \frac{\kappa_{ij}}{\mu} \rho_o g \left(\frac{\partial H_m}{\partial x_j} h_m + \rho_r \delta_{2j} \right) H_l \frac{\partial H_k}{\partial x_i} \right\} d\Omega \cdot T_k = \oint_{s^e} H_l H_k \, ds \, q_k^h \tag{3.27}$$

Similarly, applying the Galerkin weighted residual method to (2.6), we have, after some manipulation,

$$\left[\int_{\Omega^e} \frac{\kappa_{ii}}{\mu}\rho_o g \frac{\partial H_l}{\partial x_i}\frac{\partial H_k}{\partial x_j}\,d\Omega\right]h_k - \left[\int_{\Omega^e} \delta_{2j}\frac{\kappa_{ii}}{\mu} g\beta \frac{\partial H_l}{\partial x_i} H_k\,d\Omega\right]T_k$$
$$= \oint_{S^e} H_l H_k\,ds\, q_k^w \tag{3.28}$$

again the inward going flux q^w to an element is defined as positive, i.e.,

$$q^w = -q_j^w n_j = \frac{\kappa_{ii}}{\mu}\rho_o g\left(\frac{\partial h}{\partial x_i} + \rho_r \delta_{2i}\right)n_j \tag{3.29}$$

The second term on the left hand side of (3.28) appears because ρ is a linear function of T as given by (2.11).

Defining a vector U in the (T, h) plane,

$$U = \begin{bmatrix} {}^1U \\ {}^2U \end{bmatrix} = \begin{bmatrix} T \\ h \end{bmatrix} \tag{3.30}$$

and correspondingly,

$$q = \begin{bmatrix} {}^1q \\ {}^2q \end{bmatrix} = \begin{bmatrix} q^h \\ q^w \end{bmatrix} \tag{3.31}$$

we can combine (3.27) and (3.28) into

$${}^{ij}K^e_{lk}{}^jU_k - {}^{ij}V^e_{lk}{}^jq_k = 0 \tag{3.32}$$

In (3.32) K^e is the elemental conductivity matrix, the (l,k)*th* entry of which being

$$K^e_{lk} = \begin{bmatrix} {}^{11}K^e_{lk} & {}^{12}K^e_{lk} \\ {}^{21}K^e_{lk} & {}^{22}K^e_{lk} \end{bmatrix} \tag{3.33}$$

with

$${}^{11}K^e_{lk} = \int_{\Omega^e}\left\{\lambda_{ij}\frac{\partial H_l}{\partial x_i}\frac{\partial H_k}{\partial x_j} - \rho c q_i^w H_l \frac{\partial_i I_k}{\partial x_i}\right\}d\Omega \tag{3.34a}$$

$${}^{12}K^e_{lk} = 0 \tag{3.34b}$$

$${}^{21}K^e_{lk} = -\int_{\Omega^e} \kappa_{ij}\mu^{-1} g\beta\delta_{2j}\frac{\partial H_l}{\partial x_i} H_k\,d\Omega \tag{3.34c}$$

$${}^{22}K_{lk} = \rho_o g\int_{\Omega^e} \kappa_{ij}\mu^{-1}\frac{\partial H_l}{\partial x_i}\frac{\partial H_k}{\partial x_j}\,d\Omega \tag{3.34d}$$

where q_i^w is defined by (2.4), and μ^{-1} by (2.12), with the T and h values interpolated using (3.23).

The boundary flux transformation matrix V^e is similar to that defined by (3.11), but each entry V^e_{lk} has four subentries,

$${}^{ij}V^e_{lk} = \oint_{S^e} {}^iH_l{}^jH_k\,ds \tag{3.35}$$

The above derivation is similar to that of Huyakorn and Pinder (1983, p.204).

From the elemental system (3.32), the global system is obtained

$$\mathbf{K}\cdot\mathbf{U} - \mathbf{V}\cdot\mathbf{q} = \mathbf{0} \tag{3.36}$$

The algebraic system (3.36) is the discretized form of the partial differential equations (2.6) and (2.7). Apart from the difference in physical meanings, there are two major mathematical differences between the static systems (3.11) and (3.36). The first difference is: the conductivity matrix K in (3.11) is a function of the material properties only which are independent of the field variables, but the K matrix in (3.36) is a function of the field variables as well because of the temperature dependence of ρ and μ, and the convection term in (2.7); therefore, for a forward problem where the field variables are the only unknowns, (3.11) is linear but (3.36) is nonlinear. The second difference is: in (3.11), K and V have the global dimension of N_g, the total number of nodal points, because each node has one degree of freedom; while in (3.36), each entry of K and V has four sub–entries and each entry of U and q has two sub–entries, and the global dimension is $2N_g$ instead of N_g, because each node has two degrees of freedom, T and h, rather like the two components of displacement in a 2 D mechanics problem.

For a forward finite element solution to the coupled problem described by equations (2.6) and (2.7), the above procedure is by no means the most efficient method. A better approach is a sequential solution procedure (Huyakorn and Pinder, 1983, p.198), in which the two equations are solved alternately, each time using the updated ρ and μ in (2.6) and $\mathbf{q}^w$ in (2.7) as functions of space, but not of temperature or head, thus making the equations linear, until both field variables, namely T and h, converge. Because the scheme has the nice property of using minimal computer memory and is easy to program, it was used almost exclusively

in the forward finite element numerical modeling of coupled systems (Andrews and Anderson, 1978, 1979; Sauty et al., 1982a, b; Garven and Freeze, 1984a, b; Smith and Chapman, 1983; Woodbury and Smith, 1985; Doligez et al., 1986; Burrus and Bessis, 1986). The scheme is also applicable to a nonlinear inverse problem, if gradient methods are not used in parameter estimation or if the gradients are obtained numerically. In order to use a computationally much more efficient analytical gradient method (see next chapter), the more suitable finite element coupled solution procedure as outlined above has been adopted for this work.

As in the conduction problem, we consider only isotropic media, and use the logarithmic transform of the material properties,

$$\gamma = \log \lambda \tag{3.37a}$$

$$\psi = \log \kappa \tag{3.37b}$$

A parameter vector P is defined that includes as its components all the discretized (after zonation) γ and ψ, defined by (3.37), all the nodal values of T and h, and all the nodal values of q^h and q^w, and (3.36) is written into the standard form to which a parameter estimation procedure is to be applied,

$$\mathbf{F(P)} = 0 \tag{3.38}$$

where

$${}^{i}F_{l}(P) = {}^{ij}K_{lk}(\gamma,\psi,U)^{j}U_{k} - {}^{ij}V_{lk}\,{}^{j}q_{k} \tag{3.39}$$

Similar to the conduction problem, the first and second right–hand–side term of (3.39) are the nonlinear and linear parts of the system F, respectively, with

$${}^{i}g_{l} = {}^{ij}K_{lk}(\gamma,\psi,U)^{j}U_{k} \tag{3.40}$$

$${}^{i}f_{l} = {}^{ij}V_{lk}\,{}^{j}q_{k} \tag{3.41}$$

and (3.38) can be formally written into the same form as (3.22),

$$\mathbf{g(p)} - \mathbf{f(q)} = 0 \tag{3.42}$$

where **q** contains the nodal flux values, and **p** contains the rest of the components of P

3.4 2–D isoparametric finite element model

The finite element discretization procedure developed in the previous two sections is general for any finite element model. In an actual forward implementation of a finite element model, some authors favor lower degrees of interpolation and hence fewer nodes in each element but correspondingly more nodes and elements in the whole mesh, while others prefer higher degrees of interpolation and hence more nodes in each element but fewer nodes and elements in the whole mesh. The extensively used linear triangular element model is an example of the former: it has the advantage that K^e and f^e can be readily obtained without performing numerical integration, but large numbers of nodes and elements are required to maintain a satisfactory accuracy of the discretization. In our inverse approach, all of the field variable nodal values are parameters, and hence it is expedient that we choose the latter to reduce the total number of parameters. In this work, a two–dimensional quadratic quadrilateral isoparametric finite element model is employed.

Lagrange and Serendipity are the names of the two families of isoparametric finite elements. A 2–D quadratic quadrilateral Lagrange element has nine nodes, with eight on the four sides and one in the middle of the element domain; the corresponding Serendipity element has only eight nodes on the four sides, with the middle point missing, therefore the polynomial interpolation is not complete (there are a total of nine possible monomials in a 2–D case). The Serendipity model is used in this work.

A typical quadrilateral Serendipity isoparametric finite element is shown in Fig.3.1. The middle node on each side can be omitted if necessary, making the construction of a finite element mesh very flexible, but with loss of degree of

interpolation. In such a quadrilateral element, a natural coordinate system (r_i) is established, with r_i ranging from −1 to +1. The coordinates in the x_i system are transformed into the natural system by a set of shape functions $H_k(r)$,

$$x_i(r) = H_k(r)x_{ik} \tag{3.43}$$

where the summation is over all the nodes in the element; x_{ik} denotes the x_i coordinates of node k. The H_k in (3.43) are exactly the same shape functions used to interpolate the field variables in equations (3.1), (3.2), (3.23) and (3.24) (and this is why the finite element was termed "isoparametric"). In other words, the nonlinear transformation maps the quadrilateral in the x_i space onto a square in the r_i space. The transformation defined by (3.43) is 1–1, i.e., the Jacobian of the transformation is nonsingular, or, there exists the inverse transform. The interpolation of the field variables is therefore actually performed in the x domain using $H_k[r(x)]$.

Since the coordinate transformation is performed for every element, all the elements become identical after the transformation. Therefore the efficient Gauss–Legendre numerical integration scheme (Appendix A) can be applied to all these elements to perform the integrations in computing K and V, and later in computing the gradient matrix required by the parameter estimation procedure (see section 4.3).

The shape functions $H_k(r)$ for four–to–eight–node elements, as well as other technical details of the Serendipity isoparametric finite element model, are given in Bathe and Wilson (1976). The efficiency of the isoparametric finite element method applied to groundwater research was demonstrated by Pinder and Frind as early as 1970. Further discussions on the advantages and disadvantages and recent improvements of the isoparametric finite element model can be found in Celia and Gray (1984).

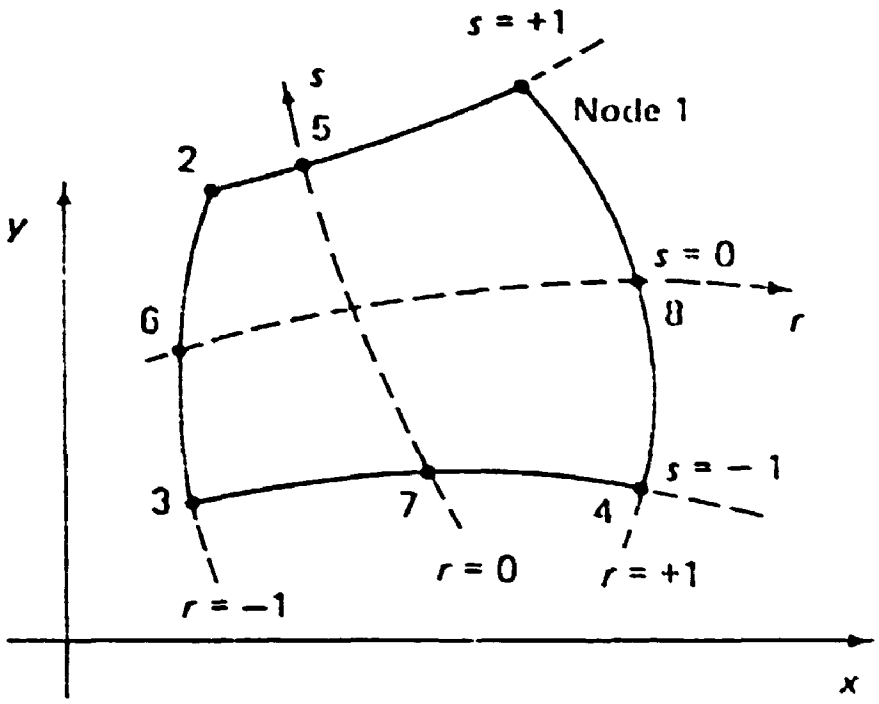

Fig.3.1. A typical 2–D quadratic Serendipity finite element. The element in the x coordinate system is mapped onto a square in the r coordinate system. In the figure, $y = x_2$, and $s = r_2$. After Bathe and Wilson (1976).

CHAPTER 4: PARAMETER ESTIMATION

4.1 Introduction to Bayesian estimation

4.1.1 Bayes' rule

In equations (3.17) and (3.38), the parameter vector **P** consists of the discretized values of the field variables, the material properties and the boundary fluxes. Very often we have some knowledge about every parameter, but we do not have complete knowledge about any parameter. For example, without any measurement, we know that the temperature at 1 km depth is unlikely to be below the freezing point at a latitude of 40°N; on the other hand, even with high precision instrument, a temperature measurement will still have uncertainties. In Bayesian statistical inference, this state of information is conveniently depicted by a probability distribution of **P**.

The physical theories may also not be exact, and the discretization leads to discretizing errors. To account for these uncertainties, an error term **e**, called model error, is added to the right–hand side of equation (3.17) and (3.38), so that

$$\mathbf{F}(\mathbf{P}) = \mathbf{e} \tag{4.1}$$

If the probability density function (PDF) of a vector **r** is denoted by $\mathcal{P}(\mathbf{r})$ and the conditional PDF of $\mathbf{r}_1$ given $\mathbf{r}_2$ by $\mathcal{P}(\mathbf{r}_1|\mathbf{r}_2)$, Bayes' rule states that

$$\mathcal{P}(\mathbf{P}|\mathbf{e}) = \frac{\mathcal{P}(\mathbf{e}|\mathbf{P})\ \mathcal{P}(\mathbf{P})}{\mathcal{P}(\mathbf{e})} \tag{4.2}$$

$\mathcal{P}(\mathbf{P})$, which tells us what is known about **P** without the knowledge of **e**, or in other words, without using the relation (4.1), is called the a priori PDF of **P**; $\mathcal{P}(\mathbf{P}|\mathbf{e})$, which tells us what is known about **P** given the knowledge of **e**, is called

the a posteriori PDF of P. $\mathcal{P}(\mathbf{P})$ is defined in an arbitrary manner using the available information on P based on observation, previous study or the personal experience and engineering judgment of the researcher. Here the word "arbitrary" is used to mean that physical laws such as equations (3.16) or (3.33) are not necessarily involved. On the other hand, by definition of conditional probability, $\mathcal{P}(\mathbf{e}|\mathbf{P})$, the PDF of e given P does involve the physical laws. If $\mathcal{P}(\mathbf{e}|\mathbf{P})$ is regarded as a function of P, not of e, it represents the likelihood for P given e, and is thus called the likelihood function for P.

The denominator $\mathcal{P}(\mathbf{e})$ in (4.2) can be shown to be a constant and of no importance in the estimation of P (Box and Tiao, 1973). Bayes' rule (4.2) provides a mathematical formulation of how knowledge from different sources can be combined to give new knowledge. The knowledge of e, in the form of $\mathcal{P}(\mathbf{e}|\mathbf{P})$, consists not only of the values (obviously, the conditional expectation of e given P is zero), but most importantly, also of the physical laws governing the relation between different components of P.

In this work we make the assumption that $\mathcal{P}(\mathbf{P})$ and $\mathcal{P}(\mathbf{e}|\mathbf{P})$ are Gaussian, with expectations $\mathbf{P}_0$ and $\mathbf{0}$, and covariance matrices C and C_{ee}, respectively. The a posteriori PDF defined by (4.2) is then,

$$\text{const}\cdot\exp-\frac{1}{2}\{[\mathbf{F}(\mathbf{P})]^t\, C_{ee}^{-1}\,[\mathbf{F}(\mathbf{P})] + [\mathbf{P}-\mathbf{P}_0]^t\, C^{-1}\,[\mathbf{P}-\mathbf{P}_0]\} \tag{4.3}$$

Support for the assumption of the probability of the logarithmic transforms of the thermal conductivity, heat production rate and permeability to be Gaussian includes evidence such as the well recognized log normal distribution of subsurface material permeability (Freeze, 1975) and the log normal–like shape of most of the thermal conductivity histograms compiled by Roy et al. (1981). Tarantola (1987, p.42) has also pointed out that the a priori information on this kind of positive quantities are best described by log–normal probabilities. When the STD of the

Gaussian PDF of the logarithmic transform of a parameter r is very small, for a given expectation $\log(r_o)$, the probability distributions of $\log(r)$ and of r become almost identical; this is often the case for thermal conductivity values.

With a typical Bayesian approach, the a priori information on the parameter vector P is purely intuitive. With a less typical Bayesian approach, the a priori information of P can be of objective as well as subjective origin, such as the information on the three types of physical quantities used in this method. For this reason, the parameter estimation procedure followed in this method is Bayesian in a broad sense.

4.1.2 The most probable point estimate

In Bayesian inference, only through a thorough study of the a posteriori PDF, can our updated knowledge of the parameters be sufficiently described (Box and Tiao, 1973). For a linear inverse problem based on Gaussian distribution, the a posteriori PDF is also Gaussian and can be completely characterized by its expectation and covariance matrix. In such a case, it is justified to speak of a point estimate. For a nonlinear inverse problem, a point estimate is generally not representative of the usually complex behavior of the non–Gaussian a posteriori PDF. However, for a large multivariate problem, the computation of the a posteriori PDF is usually an insurmountable task and the presentation of the results would also be difficult. For these reasons, to seek point estimates is still a common practice in Bayesian type nonlinear inversion (e.g., Gavalas et al., 1976; Jackson and Matsu'ura, 1985); in fact, the term "inverse method" in the most popular interpretation implies point estimates, but due to the complexity of the a posteriori PDF, the choice of a particular estimator is usually a matter of computational convenience, there being no general selection rule (Schweppe, 1973).

Schweppe (1973) summarized four types of point estimates for nonlinear

Bayesian problems, each revealing a different aspect of the a posteriori PDF, namely, the most probable, the conditional expectation, the median and the Min–max estimates (for definitions, refer to Schweppe, 1973, p.329). The most probable estimate, that is, the value of p that maximizes the a posteriori PDF (4.3), is also referred to as the maximum likelihood point (Menke, 1984; Tarantola, 1987), implying that the a posteriori PDF is regarded as the likelihood function. It is usually the easiest to compute, and gives the most physically meaningful point estimate if there has to be one. The validity of the most probable estimate depends inversely upon the nonlinearity of the problem; for a linear problem, the most probable estimate coincides with the a posteriori expectation; for a slightly nonlinear problem, the most probable estimate can be used to approximate the a posteriori expectation; for a very nonlinear problem, however, the most probable estimate may bear no relation to the expectation and caution should be taken in interpreting the results of point estimation.

In the above discussion, a key point is that the Bayesian interpretation of the inverse method always reminds us that the most probable estimate of a parameter is only one of the several possible point estimates, which have clear mathematical meanings. The most important reason for a Bayesian approach to be used is that intuitive information must necessarily be invoked in the inverse problems considered in this work. Strictly speaking, when some of the information used is intuitive, and hence the result depends on the researcher who makes the inference, it is very awkward to call the inverse method non–Bayesian. "One is *more or less* a Bayesian depending on the precision with which one is prepared to make intuitive probability estimates" (Good, 1965, p.10).

Adopting the most probable estimate, our problem becomes one of optimization with the objective function

$$\Pi = [\mathbf{F}(\mathbf{P})]^t \, C_{ee}^{-1} \, [\mathbf{F}(\mathbf{P})] + [\mathbf{P} - \mathbf{P}_0]^t \, C_{pp}^{-1} \, [\mathbf{P} - \mathbf{P}_0] \qquad (4.4)$$

We seek the point $\hat{P}$ at which Π reaches the global minimum. If the entries of C_{ee}^{-1} and C^{-1} are regarded as weighting coefficients, $\mathbf{0}$ and P_o are regarded as data, to minimize Π simply gives the weighted least squares solution of the inverse problem (Schweppe, 1973, p.339). It is well known that the least squares method, which minimizes the Euclidean distance between the estimates and the measured values (i.e., L_2 norm), is intrinsically not robust, in a sense that a few bad data points (outliers) may strongly influence the estimates. Introducing different weights to the least squares method may improve the robustness to a certain extent, but really robust methods are based on other, for example, L_1, norms (Menke, 1984).

4.1.3 Remarks on "zonation"

Zonation (see Chapter 3), as used in this work, is one way to reduce the total number of parameters. Besides saving on computational cost, the more valid reason for reducing the number of parameters is to constrain the problem and render it better determined. As mentioned in section 1.3, to constrain an inverse problem, further information is unexceptionally needed. Zonation utilizes the geological and geophysical information on, or the researcher's own understanding of, the structure of the subsurface medium by dividing the medium into a number of material property zones, each having distinct material property values. Therefore, even with a non–Bayesian method, a priori information would already have been used if zonation is performed, though not in an explicit way. The zonation, however, differs from other a priori information in that it implies hard constraints. Whereas some a priori information is given a probability distribution leading to updated values and variances, the zone boundaries are not adjustable in the inversion, and any errors incurred in the division of zones remain to be errors in the solutions. Here the term "error" is used instead of "uncertainty" because these errors may or may not be explicitly shown in the solutions by the variances.

Thus, it is expedient that caution be exercised in performing zonation.

The zonation errors can be reduced with a Bayesian approach as recommended by Lu et al. (1988). Since zonation is a step function approximation of the spatial distribution of the material properties, large number of small zones are needed to give a good approximation to a complex distribution. Instead of using very few large zones, one can constrain the problem by assigning a priori material property values and variances to a greater number of smaller zones. An extreme case is to treat every element as a material property zone.

It should be emphasized that from a probabilistic point of view, zonation is a poor representation of the spatial variability of the material properties. The constant material property value assigned to a zone should be interpreted as the mean value of the property over this zone.

4.2 RTV optimization scheme

4.2.1 General form

The objective function defined by (4.4) can be minimized using gradient methods which use the partial derivatives of Π with respect to the components of $\mathbf{p}$, and non–gradient methods which compute Π directly. The simplex technique (e.g., Beveridge and Schechter, 1965; Woodbury et al., 1988) is a classical non–gradient method. In addition to avoiding the computation of gradients and hence being easy to program, an obvious advantage of the simplex technique is that it can be readily applied to objective functions constructed with different norms. For example, it is much easier to adapt the simplex technique to L_1–norm minimization, a criterion which is much more robust than the L_2–norm minimization in the sense that a few bad data points (outliers) would not alter the

solution drastically (Woodbury et al., 1988). A disadvantage of the approach is that thousands of forward computations must be performed to solve the governing partial differential equations. If the forward model is linear, such as the conduction problem described by equation (2.2), a forward calculation can be done efficiently, and the simplex technique is therefore a practical approach. For example, Woodbury and Smith (1988), in the simultaneous inversion of thermal and hydrological data over a small depth range, regarded water density and viscosity as constants because the temperature range was small; as a result, they could use the simplex method because the heat transfer equation and the fluid flow equation are decoupled and linear, and need be solved only once for each forward calculation. However, for a nonlinear problem, such as the coupled problem described by equations (2.6) and (2.7), each forward computation requires, typically, 10 iterations for convergence, resulting in a 10–fold increase of computer time. For this reason, a gradient method that does not need numerous forward runs is preferred. Of course, a gradient method is a more efficient approach than a non–gradient method also for the linear conduction problem.

The commonly used gradient methods for optimization in the hydrological inverse theories are the conjugate gradient method (Neuman, 1980), Gauss–Newton method (Sun and Yeh, 1985), Newton–Raphson method (Neuman and Yakowitz, 1979), steepest descent method (Chavent et al., 1975), etc.. The following iteration scheme (briefly called the RTV scheme) for the optimization of the objective function II defined in equation (4.4) was derived by Rodgers (1976) and, independently, by Tarantola and Valette (1982), and later re–examined by Menke (1984, p.151), Wang and Beck (1987) and Tarantola (1987) from different perspectives.

$$\hat{\mathbf{P}}_{k+1} = \mathbf{P}_0 + \mathbf{C}\cdot\mathbf{F}_k^{t}\cdot(\mathbf{C}_{ee} + \mathbf{F}_k'\cdot\mathbf{C}\cdot\mathbf{F}_k^{t})^{-1}\cdot[\mathbf{F}_k'\cdot(\hat{\mathbf{P}}_k - \mathbf{P}_0) - \mathbf{F}(\hat{\mathbf{P}}_k)] \tag{4.5}$$

where bold faced subscript **k** is the iteration step number, and $\mathbf{F'_k}$ is the gradient matrix F' at the **k***th* iteration:

$$\mathbf{F'_k} = (\mathbf{F'_{lm}})_k = \left(\frac{\partial \mathbf{F}_l}{\partial \mathbf{P}_m}\right)\Big|_{\mathbf{P} = \dot{\mathbf{P}}_k} \tag{4.6}$$

The model error **e** is usually insignificant. If this term is ignored, as in the numerical examples used in this research, (4.5) becomes

$$\dot{\mathbf{P}}_{k+1} = \mathbf{P}_o + \mathbf{C}\cdot\mathbf{F'^t_k}\cdot(\mathbf{F'_k}\cdot\mathbf{C}\cdot\mathbf{F'^t_k})^{-1}\cdot[\mathbf{F'_k}\cdot(\dot{\mathbf{P}}_k - \mathbf{P}_o) - \mathbf{F}(\dot{\mathbf{P}}_k)] \tag{4.7}$$

It is important to notice that according to (4.7), an arbitrary scaling factor for the covariance matrix C will not affect the iteration. It is the relative magnitudes of the entries of C that are of importance to the iteration.

As shown by Rodgers (1976), Tarantola (1987) and Wang and Beck (1987), the scheme is asymptotically a Newton's iteration algorithm. Newton's iteration converges quadratically to a unique solution only when the problem is mildly nonlinear and when the initial parameter value is reasonably close to the solution value (Burden et al., 1981). Given the functional form of the objective function, the convergence behavior of the iteration scheme depends on the quality of the a priori information on **P**.

4.2.2 Separation of nonlinear and linear parts

In Chapter 3, the system **F** is separated into a nonlinear and a linear part,

$$\mathbf{F}(\mathbf{P}) = \mathbf{g}(\mathbf{p}) - \mathbf{V}\mathbf{q} = \mathbf{g}(\mathbf{p}) - \mathbf{f} \tag{4.8}$$

This is useful because, assuming no covariance between **p** and **q**, during iteration using the RTV scheme, the nonlinear part of **P**, **p**, is not influenced by any change in the linear part, **q**, therefore **p** and **q** can be estimated separately, which brings some computational convenience. To prove this point, we follow the example of Tarantola and Valette (1982b) and rewrite the gradient matrix F' using (4.8),

$$\mathbf{F'} = [\mathbf{G} \quad -\mathbf{V}] \tag{4.9}$$

where G is the gradient matrix of $\mathbf{g}$, defined as

$$G_{lm} = \left(\frac{\partial g_l}{\partial p_m}\right) \tag{4.10}$$

we also write the covariance matrix C into

$$C = \begin{bmatrix} C_{PP} & 0 \\ 0 & C_{qq} \end{bmatrix} \tag{4.11}$$

By substituting (4.10) and (4.11) into (4.7), we obtain,

$$\begin{bmatrix} \hat{p}_{k+1} \\ \hat{q}_{k+1} \end{bmatrix} = \begin{bmatrix} p_o \\ q_o \end{bmatrix} + \begin{bmatrix} C_{PP} & 0 \\ 0 & C_{qq} \end{bmatrix} \cdot \begin{bmatrix} G_k^t \\ -V \end{bmatrix} \cdot \left\{ [G_k \ -V] \cdot \begin{bmatrix} C_{PP} & 0 \\ 0 & C_{qq} \end{bmatrix} \cdot \begin{bmatrix} G_k^t \\ -V \end{bmatrix} \right\}^{-1}$$

$$\cdot \{ [G_k \ -V] \cdot \begin{bmatrix} \hat{p}_k - p_o \\ \hat{q}_k - q_o \end{bmatrix} - [g(\hat{p}_k) - V\hat{q}_k] \}$$

$$= \begin{bmatrix} p_o \\ q_o \end{bmatrix} + \begin{bmatrix} C_{PP} G_k^t \\ -C_{qq} V \end{bmatrix} \cdot \{ G_k C_{PP} G_k^t + V C_{qq} V \}^{-1} \cdot \{ G_k (\hat{p}_k - p_o) + V q_o - g(\hat{p}_k) \} \tag{4.12}$$

From (4.12), $\hat{p}_{k+1}$ is solved as

$$\hat{p}_{k+1} = p_o + C_{PP} G_k^t R_k^{-1} [f_o - g(\hat{p}_k) + G_k(\hat{p}_k - p_o)] \tag{4.13}$$

where

$$R_k = G_k C_{PP} G_k^t + C_{ff} \tag{4.14}$$

and

$$f_o = V q_o \tag{4.15}$$

$$C_{ff} = V \, C_{qq} \, V \tag{4.16}$$

The convergence of iteration algorithm (4.13) is defined as

$$\lim_{k \to \infty} \| p_{k+1} - p_k \| = 0 \tag{4.17}$$

where $\| \cdot \|$ represents the norm of a vector (for example, L_∞ norm).

The covariance matrix C_{PP} is always positive definite, C_{ff} is positive semi–definite, and G is of full rank. Therefore the symmetric matrix R is positive definite. It is important to notice that q_k does not appear in equation (4.13), which means that the linear part of P influences the iteration of the nonlinear part only through the a priori expectation q_o, not the updated values.

Now we examine the linear part of the system. From (4.12),

$$\hat{\mathbf{q}}_{k+1} = \mathbf{q}_0 - \mathbf{C}_{qq}\mathbf{V}\,\mathbf{R}_k^{-1}[\mathbf{f}_0 - \mathbf{g}(\hat{\mathbf{p}}_k) + \mathbf{G}_k(\hat{\mathbf{p}}_k - \mathbf{p}_0)] \tag{4.18}$$

Left–multiplying both sides of (4.18) by V, we obtain

$$\hat{\mathbf{f}}_{k+1} = \mathbf{f}_0 - \mathbf{C}_{ff}\mathbf{R}_k^{-1}[\mathbf{f}_0 - \mathbf{g}(\hat{\mathbf{p}}_k) + \mathbf{G}_k(\hat{\mathbf{p}}_k - \mathbf{p}_0)] \tag{4.19}$$

Note that

$$\mathbf{C}_{ff}\mathbf{R}_k^{-1} = (\mathbf{C}_{ff} + \mathbf{G}_k\mathbf{C}_{pp}\mathbf{G}_k^t - \mathbf{G}_k\mathbf{C}_{pp}\mathbf{G}_k^t)\,\mathbf{R}_k^{-1} = \mathbf{I} - \mathbf{G}_k\mathbf{C}_{pp}\mathbf{G}_k^t\,\mathbf{R}_k^{-1} \tag{4.20}$$

where I is the identity matrix. Substituting (4.20) into (4.19), and using (4.13), we have,

$$\hat{\mathbf{f}}_{k+1} = \mathbf{g}(\hat{\mathbf{p}}_k) + \mathbf{G}_k(\hat{\mathbf{p}}_{k+1} - \hat{\mathbf{p}}_k) \tag{4.21}$$

If (4.13) converges to $\hat{\mathbf{p}}$, (4.21) converges to (see equation 4.17)

$$\hat{\mathbf{f}} = \mathbf{g}(\hat{\mathbf{p}}) \tag{4.22}$$

and $\hat{\mathbf{q}}$, in turn, can be determined from $\hat{\mathbf{f}}$.

It has been demonstrated that the nonlinear and linear parts of the parameter vector P can be estimated separately. This separation 1) takes out the parameters that do not actively participate in the nonlinear iteration, and hence reduces the computational cost; 2) makes it convenient to formulate the a priori covariance matrices $\mathbf{C}_{pp}$ and $\mathbf{C}_{qq}$ in different ways (as will be seen later, $\mathbf{C}_{pp}$ is diagonal, and $\mathbf{C}_{qq}$ is generally a full matrix, in practical cases). The above derivation is made, for conciseness, using (4.7), where $\mathbf{C}_{ee} = 0$. It can be easily extended to the case where $\mathbf{C}_{ee} \neq 0$ by leaving $\mathbf{C}_{ee}$ in the R matrix. The rest of this chapter is devoted mainly to the nonlinear part of the problem; further discussions on the linear part, i.e., boundary flux updating, are left to Chapter 5.

4.2.3 A posteriori covariance matrices

The a posteriori covariance matrix of the total parameter vector P, C, is defined as

$$\hat{C} = E\{[P - E(P)]\cdot[P - E(P)]^t\} \tag{4.23}$$

where E(P) stands for the a posteriori expectation of P. For a linear problem

$$F(P) = F'\cdot P = e \tag{4.24}$$

where F' is a constant matrix; if the a priori PDF of P and of e are Gaussian, the a posteriori PDF $\mathcal{P}(P|e)$ is also Gaussian, and the most probable estimate is identical to the a posteriori expectation. In that case, the a posteriori $\hat{C}$ is given by (Schweppe, 1973; Rodgers, 1976; Tarantola and Valette, 1982):

$$\hat{C} = C - C\cdot F'^t\cdot(C_{ee} + F'\cdot C\cdot F'^t)^{-1}\cdot F'\cdot C \tag{4.25}$$

For the nonlinear systems (11) and (31), the a posteriori PDF is generally not Gaussian and it would be very difficult to develop $\hat{C}$. The usual practice is to linearize equation (4.6) in the neighborhood of the most probable estimate point $\hat{P}$, approximate the conditional expectation with $\hat{P}$, and use (4.25) as a linear approximation of the a posteriori covariance matrix (Jackson and Matsu'ura, 1985; Vasseur et al., 1986; Tarantola, 1987). In fact, Rodgers (1976) derived iteration scheme (4.6) by linearizing F(P) in the first place.

From (4.11) and (4.25), the a posteriori covariance matrices of p and q can be readily obtained as

$$\hat{C}_{pp} = C_{pp} - C_{pp}G^tR^{-1}\,G\,C_{pp} \tag{4.26}$$

$$\hat{C}_{qq} = C_{qq} - C_{qq}V\,R^{-1}\,V\,C_{qq} \tag{4.27}$$

where G and R are evaluated at point $\hat{p}$.

A parameter is said to be "well resolved" when the a posteriori variance, or its square root, the standard deviation (STD), is significantly smaller than the a priori one. A different concept of "resolution", commonly used in inverse methods that are not directly based on probability theories, was defined by Backus and Gilbert (1968) for the problem of continuous parameters and by, e.g., Menke (1984) for the discrete cases. Its relation to the resolution concept adopted in this work was discussed by Tarantola (1987).

4.3 Derivation of the gradient matrix

4.3.1 The elemental gradient matrices

For a gradient method of optimization to be efficient, one must have an efficient way of calculating the gradient matrix. In (isothermal) groundwater hydrology, the "gradients" are commonly the partial derivatives of head with respect to the aquifer transport parameters to be estimated, such as the transmissivities and storativities, and are called the sensitivity coefficients. The computation of sensitivity coefficients is usually a challenging task when numerical models are used in the parameterization of an inverse problem, especially for coupled problems such as the one given by the partial differential equation system (2.6) and (2.7).

In a comparative study, Li et al. (1986) summarized into three types the methods commonly used for computing sensitivity coefficients in isothermal hydrological inverse theories incorporating finite element methods: type 1, the influence coefficient method (or numerical differentiation), type 2, the sensitivity equation method (analytical differentiation) and type 3, the variational method; technical details of the methods are given in the quoted paper and Sun and Yeh (1985). As expected, errors are introduced when the differentiation is performed numerically, and hence the accuracy of the first method is the poorest among the three. If there are N_h head values and N_p parameter values, the first method requires N_p+1 (for backward or forward difference approximation) or $2N_p+1$ (for central difference approximation) forward simulation runs, the second and the third methods require N_p+1 and N_h+1 simulation runs, respectively (Li et al., 1986).

In this work, parameters are defined in a general sense (see section 3.2 and

3.3); the nonlinear part of the parameter vector P, p, includes the nodal values of the field variables as well as the discretized material properties. In addition to making the inverse solution more flexible, this choice of parameter vector makes the implementation of the gradient method, namely the RTV scheme, very efficient. Instead of working with the sensitivity coefficients, we work with the gradient matrix G, which can be derived analytically with basic rules of calculus. The method for computing the gradients resembles the type 2 method of Li et al. (1986), but the G matrix is formulated directly, and hence requires only one simulation.

At first glance, it might appear that the function g, defined by (3.20) and (3.40), particularly the latter, is rather difficult to differentiate, but the differentiation can be done at the elemental level. In the conduction problem,

$$\mathbf{g} = \mathbf{K}\cdot\mathbf{T} - \mathbf{W} = (\sum_e \mathbf{K}^e)\cdot\mathbf{T} - \sum_e \mathbf{W}^e = \sum_e (\mathbf{K}^e\cdot\mathbf{T} - \mathbf{W}^e) \tag{4.28}$$

and in the coupled problem,

$$\mathbf{g} = \mathbf{K}\cdot\mathbf{U} = (\sum_e \mathbf{K}^e)\cdot\mathbf{U} = \sum_e (\mathbf{K}^e\cdot\mathbf{U}) \tag{4.29}$$

Therefore in both problems

$$\mathbf{g} = \sum_e \mathbf{g}^e \tag{4.30}$$

and hence

$$G_{lm} = \frac{\partial^i g_l}{\partial p_m} = \sum_e \frac{\partial^i g_l^e}{\partial p_m} = \sum_e G_{lm}^e \tag{4.31}$$

where G^e is the elemental gradient matrix. Since the differentiation is of the first order, the placement of the left superscript i of g right after ∂ should not create any confusion. The same comment applies to the following derivations.

With (4.30) and (4.31), the function g and matrix G can be derived for individual elements, and assembled at the global level for each iteration. The number of nonzero rows in G^e is the number of equations in g^e, and the number of nonzero columns in G^e is the number of parameters related to the element, i.e., the

number of nodal values of field variables plus the number of material properties of the element. With the material properties assumed to be isotropic, the entries of the elemental G^e matrix are derived as follows. In the following equations, N_e is the number of nodal points in element e, and l, m, n, k = 1, 2, ..., N_e.

4.3.2 The gradient matrix for the conduction problem

For the conduction problem, from equations (3.20) and (3.7)

$$\frac{\partial g_l^e}{\partial T_m} = K_{lm}^e = \int_{\Omega^e} \lambda \frac{\partial H_l}{\partial x_i} \frac{\partial H_m}{\partial x_i} d\Omega \tag{4.32}$$

$$\frac{\partial g_l^e}{\partial \gamma} = \frac{\partial K_{lk}^e}{\partial \gamma} T_k = \frac{\partial}{\partial \gamma} \int_{\Omega^e} \exp(\gamma \ln 10) \frac{\partial H_l}{\partial x_i} \frac{\partial H_k}{\partial x_i} d\Omega \, T_k$$

$$= \ln 10 \int_{\Omega^e} \lambda \frac{\partial H_l}{\partial x_i} \frac{\partial H_k}{\partial x_i} d\Omega \, T_k \tag{4.33}$$

$$\frac{\partial g_l^e}{\partial \epsilon} = -\frac{\partial W_l^e}{\partial \epsilon} = -\frac{\partial}{\partial \epsilon} \int_{\Omega^e} \exp(\epsilon \ln 10) H_l \, d\Omega = -\ln 10 \int_{\Omega^e} R H_l \, d\Omega \tag{4.34}$$

The elemental G^e has N_e nonzero rows and N_e+2 nonzero columns, since there are N_e nodal temperatures and 2 material property values (one thermal conductivity and one heat source).

4.3.3 The gradient matrix for the coupled problem

For the coupled problem, from equations (3.40), (3.34) and (3.30),

$$\frac{\partial^1 g_l^e}{\partial T_m} = {}^{11}K_{lm}^e + \frac{\partial {}^{11}K_{lk}^e}{\partial T_m} T_k$$

$$= {}^{11}K_{lm}^e - \int_{\Omega^e} \rho c \kappa H_l H_m (\eta v_i^1 - \beta g \mu^{-1} \delta_{2i}) \frac{\partial H_k}{\partial x_i} d\Omega \, T_k \tag{4.35}$$

where $v_i^1 = \rho_o g \left(\frac{\partial H_n}{\partial x_i} h_n + \rho_r \delta_{2i}\right)$

$$\mu^{-1} = \mu_o^{-1} + \eta (H_n T_n - T_o)$$

$$\frac{\partial^1 g_l^e}{\partial h_m} = \frac{\partial {}^{11}K_{lk}^e}{\partial h_m} T_k = -\int_{\Omega^e} \rho c \mu^{-1} \kappa \rho_o g H_l \frac{\partial H_m}{\partial x_i} \frac{\partial H_k}{\partial x_i} d\Omega \, T_k \tag{4.36}$$

$$\frac{\partial^1 g_l^e}{\partial \gamma} = \frac{\partial^{1\,1} K_{lk}^e}{\partial \gamma} T_k = \ln 10 \int_{\Omega^e} \lambda \frac{\partial H_l}{\partial x_i} \frac{\partial H_k}{\partial x_i} d\Omega \, T_k \tag{4.37}$$

$$\frac{\partial^1 g_l^e}{\partial \kappa} = \frac{\partial^{1\,1} K_{lk}^e}{\partial \kappa} T_k = -\ln 10 \int_{\Omega^e} \rho c \kappa \, \mu^{-1} v_i \, H_l \frac{\partial H_k}{\partial x_i} d\Omega \, T_k \tag{4.38}$$

$$\frac{\partial^2 g_l^e}{\partial T_m} = {}^{21}K_{lm}^e + \frac{\partial^{2\,1} K_{lk}^e}{\partial T_m} T_k + \frac{\partial^{2\,2} K_{lk}^e}{\partial T_m} h_k$$

$$= {}^{21}K_{lm}^e - \int_{\Omega^e} \kappa g \phi_{2i} \eta \beta H_m \frac{\partial H_l}{\partial x_i} H_k d\Omega \, T_k + \int_{\Omega^e} \kappa \eta \rho_o g H_m \frac{\partial H_l}{\partial x_i} \frac{\partial H_k}{\partial x_i} d\Omega \, h_k \tag{4.39}$$

$$\frac{\partial^2 g_l^e}{\partial h_m} = {}^{22}K_{lm}^e \tag{4.40}$$

$$\frac{\partial^2 g_l^e}{\partial \gamma} = 0 \tag{4.41}$$

$$\frac{\partial^2 g_l^e}{\partial \kappa} = \ln 10 \, ({}^{21}K_{lm}^e T_k + {}^{22}K_{lm}^e h_k) = \ln 10 \, {}^2g_l^e \tag{4.42}$$

The total number of equations in $\mathbf{g}^e$ is $2N_e$, since each node has two degrees of freedom (equation 3.25), temperature, indicated by the left superscript 1, and reference hydraulic head, indicated by the left superscript 2. The number of parameters is $2N_e+2$, the number of nodal values of field variables plus the number of material properties. Therefore $\mathbf{G}^e$ has $2N_e$ nonzero rows and $(2N_e+2)$ nonzero columns. In actual computer implementation, numerical schemes are used to perform the integrations in equations (4.32) through (4.42) (Appendix A).

4.4 A priori information

4.4.1 The nature of the a priori information

Because of the Gaussian assumption for the a priori probability distributions of both **p** and **q**, the a priori information is entered in terms of the first two moments of the PDF's, namely, the expectations and the variances (and covariances). When the information is of objective origin, the a priori variances

reflect the experimental uncertainties in the given a priori values. When the information is of subjective origin, the variances reflect the researcher's personal confidence in the values. With a constrained optimization interpretation, the variances serve as the "soft" bounds (Jackson, 1977) on the parameters; with a weighted least squares interpretation, they are the weights. For a value that one regards as the most reliable, a small variance is given that tightly constrains the parameter; for a value that one has little confidence in, a large variance is given, leaving the parameter virtually unconstrained and easily adjusted in the parameter estimation procedure to accommodate the tightly constrained parameters; for a value in which one has modest confidence, an appropriate variance is given so that the parameter is allowed to be adjusted relatively easily but without violating one's knowledge. The input of boundary conditions will be discussed in the next chapter, here only the input of $\mathbf{p}_0$ and C_{pp} is considered.

4.4.2 Methods for specifying a priori values

To specify the a priori information on $\mathbf{p}$, all the discretized material property values and all the nodal values of the field variables, together with their variances, must be given. The value of a material property for a zone may be given as the average of observed values, or inferred from a limited quantity of data together with other geological and geophysical information on the subsurface materials. The a priori values of field variables must be specified at every finite element node. Very often, a crude estimate of the values using some less sophisticated methods is possible. When such methods are not available, to specify directly the nodal values may pose certain difficulty. Technically, in dealing with a field problem, the a priori expectation and variances of the field variables can be directly specified in the following five possible ways, listed in decreasing order of sufficiency of data:

1) Actual measurements. The nodal values of the field variables are determined by field measurements, and the variances are given by the observational uncertainties. This would be the ideal situation, but is almost impossible for obvious practical reasons.

2) Deterministic interpolation. When there is a sufficient number of field variable data, the value at a nodal point can be interpolated from neighboring (randomly spaced) points using various deterministic interpolation methods, such as spline and other piecewise polynomial interpolation schemes. Sometimes, interpolation may be performed by piecewisely fitting a curve or surface to the data. The variances of the interpolated values are either calculated in accordance with the interpolation technique or specified intuitively.

3) Intuitive interpolation. When the field variable data are not sufficient to allow a point by point deterministic interpolation, the values at some points may have to be interpolated intuitively. Correspondingly, the variances are specified in the same manner. The so–called intuitive interpolation is actually the interpretation of the researcher's own understanding of the relevant physical laws in terms of numbers, and the variances depict his confidence in the numbers. Normally, an intuitively interpolated value is necessarily accompanied by a large variance. When the measured data contain large experimental errors, the intuitive interpolation may make more sense than the deterministic approach.

4) Probabilistic interpolation. When the data are really scarce, a probabilistic interpolation may be a practical approach. One probabilistic interpolation technique well known in the mining industry, hydrosciences and physical geography is "kriging". The mathematical foundation of the kriging method is given in Matheron (1973). Many recent versions of kriging method under various names can be seen in the literature, such as universal kriging (Hughes and Lettenmaier, 1981), co–kriging (Freund, 1986), disjunctive kriging

(Yates et al., 1986), Bayesian kriging (Omre, 1987), etc., but as an interpolation technique, the conventional (or simple) kriging technique, e.g., that described in the early work of Delfiner (1976) and Delhomme (1978), is appropriate. In the conventional kriging method, the material properties and hence the field variables are not described as deterministic functions of space, but are regarded as the realizations of spatial stochastic processes or random fields. The spatial relation of the physical quantities at different points is defined by statistical moments, such as the mean and the autocorrelations. The kriging method makes no effort to recover the exact numerical value of a physical quantity at a location where measurement is not made, it only tells what value the quantity is likely to take at this point with certain probability. The principal advantage of the kriging method is that covariances due to interpolation uncertainties are rigorously developed, although with an arbitrary scaling factor. However, simple kriging methods do not take the relevant physical laws explicitly into consideration; the governing rules are certain stationarity assumptions on the random fields introduced by the generalized covariance functions (Delhomme, 1978). Other kriging methods that do make use of the physical laws in some ways may be used to perform the probabilistic interpolation, but the laws are usually invoked in an intuitive manner (Woodbury et al., 1987). Kriging interpolation was used as a data input technique in the finite element inversion of hydrological data by Neuman and Yakowitz (1979).

A method proposed by Willett and Chapman (1987) for analyzing large data sets of bottom hole temperatures can also be used as a probabilistic interpolation technique for temperature data. In their method, the temperature distribution is governed by the Fourier's law of heat conduction in the vertical direction and by statistical laws in the horizontal direction. Because physical laws are partially invoked, this approach is expected to give better results than the

kriging method.

5) Forward simulation. A forward simulation using the same grid may be used to provide data for an inversion. This may sound absurd, for an inversion is needed just because a forward simulation is not as good. However, when the measured values of field variables are virtually nonexistent in large portions of the spatial domain considered, such as temperature at depths in the problem of downward continuation of heat flow data, this method may be the only choice. Since there are many uncertain factors when doing such a forward simulation, one has to follow a route similar to the trial–and–error method to let the simulated results as close to the available data and one's own judgment as possible. Therefore, the values provided by the forward simulation method are largely intuitive, so must be the variances. It is important to note that the inverse method can be formally used as a variance analysis technique for a trial–and–error approach to an inverse problem.

4.4.3 On the structure of the covariance matrix C_{pp}

If the a priori information is based on a statistical study or a probabilistic interpolation technique, such as kriging or the method of Willett and Chapman, the structure of C_{pp} is given. Without any statistical study, C_{pp} is conveniently assumed to be diagonal, meaning that the uncertainties in the components of p are considered mutually uncorrelated a priori. This is a conservative choice for the correlations (Tarantola, 1987, p.48). It should be remembered that the a priori PDF of p is only a summary of the available information defined in an arbitrary manner to describe one's knowledge or ignorance of the parameters. Usually, all one knows about the parameters are their approximate values with variances, and in such a case, the covariance matrix C_{pp} has to be diagonal. If one does have knowledge about the covariances but still assumes a diagonal C_{pp} , maybe for

computational convenience, there is a waste of information because fully use is not being made of the knowledge. In this method, however, physical laws such as Fourier's law and Darcy's law represented by the partial differential equations are explicitly introduced by the likelihood function to control the (deterministic) spatial relation of the physical quantities. Based on careful numerical experiments using the RTV scheme applied to a problem of downward continuation of heat flow data, parameterized with a finite difference model, Shen (1988, personal communication) has concluded that if the boundary conditions and the thermal conductivities were somewhat constrained, the a priori covariances of the grid temperatures brought little improvement to the results compared to those obtained with a diagonal covariance matrix. After all, it is very important to realize that an intuitively specified covariance may violate the applied physical laws.

CHAPTER 5: APPLYING AND UPDATING BOUNDARY CONDITIONS

5.1 Preface

Two types of boundary conditions for steady state partial differential equation systems are considered: the Dirichlet condition, or specified field variable value, and the Neumann condition, or specified boundary flux.

In forward finite element formulations with the field variables as unknowns, an algebraic equation is established for each degree of freedom at a nodal point. In the global algebraic system, the left–hand side is the product of the conductivity matrix and the nodal field variables, and the right–hand side is the combination of the source–equivalent nodal flow vector and the flux–equivalent nodal flow vector. The physical interpretation for a Neumann boundary condition is that it provides the flux–equivalent nodal flow to balance the equation for each degree of freedom at a boundary node. At an inner node, the flux–equivalent nodal flow is always zero and one could follow the Neumann condition interpretation and imagine that fluxes were specified at every elemental boundary (which is not a global boundary) but, when transformed into the flux–equivalent nodal flows, the flows that went into and out of the node canceled each other. Therefore, implicitly, a "Neumann condition" is needed wherever an equation is to be established. In contrast, Dirichlet conditions do not help establish equations. When the value of a field variable is specified at a nodal point, a degree of freedom is lost and the corresponding equation is removed from the algebraic system, thus keeping the numbers of unknowns and equations equal; corresponding adjustment is made to

the other equations related to this degree of freedom. Alternatively, for computational convenience, numerical techniques can be used to transform a Dirichlet condition into a Neumann type.

In the current inverse finite element formulation, information on the Neumann boundary conditions is always given in terms of a PDF, and the nodal boundary fluxes are formulated into the parameter vector P. Prior field variable values are specified for every nodal points, including those at the global boundaries with Neumann boundary conditions. We use the term "Dirichlet condition" at a boundary to describe the situation that the Neumann condition is not given and not to be estimated at that boundary. When a nodal boundary flux is not included in P, no equation can be established for the associated degree of freedom, but, different from the forward method, the corresponding parameters still exist. When the nodal field variables are updated, the Dirichlet boundary conditions are updated.

5.2 Updating Neumann boundary conditions

At some boundaries, flux distribution can be reasonably well specified through actual field measurements and they will help constrain the inversion; for example, the HFD pattern at the ground surface can be found from field measurements of temperature gradient and thermal conductivity. At some other boundaries, the flux distribution is poorly known a priori and is to be determined by the inversion, for example, the deep seated or background HFD. The latter situation is the major concern of this section.

The nodal values of boundary flux, **q**, have been formulated into the total parameter vector P, and separated as the linear part of P, in Chapter 3. The

spatial correlation of the components of the nonlinear part of **P**, **p**, is incorporated into the solution by the physical laws upon which the mathematical models are based. The a priori covariance matrix of **p**, C_{pp}, is conveniently constructed as a diagonal matrix (see section 4.4.3). However, the smoothness of the field variable fields depends on the smoothness of the boundary fluxes, and vice versa. If the uncertainties in the components of both **p** and **q** are uncorrelated a priori, oscillations in the solution may occur, unless many components are tightly constrained; to stabilize the solution, the spatial correlation of the uncertainties of **q** can be specified as part of the a priori information.

The diagonal entries of C_{qq}, the variances, represent the uncertainties in the nodal boundary fluxes; the off-diagonal entries, the covariances, define the spatial correlations between the uncertainties in different components of **q**. If the covariances in C_{qq} are governed by physical or statistical theories, they should be obtained rigorously using the theories. If the covariances are used just to define the degree of smoothness of the flux distribution at a boundary, an extensively used exponential correlation function

$$\sigma_{lk}^2 = \sigma^2 \exp\left(-\frac{1}{2}\frac{S_{lk}^2}{L^2}\right) \tag{5.1}$$

can be applied; here σ_{lk}^2 is the covariance between the two components of **q**, q_l and q_k, separated by a distance S_{lk}, σ^2 the uniform variance of the components of **q** at this boundary, and L the correlation length. If the a priori flux distribution is smooth (for example, a uniform value), the correlation length determines the degree of smoothness of the a posteriori flux distribution at this boundary. When $L = 0$, no correlation exists, and the boundary flux at any node is allowed to take a value regardless of the values at adjacent nodes. When L is much larger than the scale of the length of the boundary, there is very strong correlation between the uncertainties in the flux values at different nodes, and the flux distribution tends

to be a very smooth function at the boundary. Note that C_{qq} becomes generally a full matrix.

The updated flux–equivalent nodal flow vector $\dot{\mathbf{f}}$ is given by equation (4.22). A linear inversion of the components of the updated $\dot{\mathbf{f}}$ using equation (3.19) or (3.41) will give the updated boundary flux vector $\dot{\mathbf{q}}$:

$$\dot{\mathbf{q}} = \mathbf{V}^{-1} \cdot \dot{\mathbf{f}} \tag{5.2}$$

From (5.2), the covariance matrix of $\dot{\mathbf{q}}$, $\dot{C}_{qq}$, is

$$\dot{C}_{qq} = \mathbf{V}^{-1} \cdot \dot{C}_{ff} \cdot \mathbf{V}^{-1} \tag{5.3}$$

$\dot{C}_{ff}$ is related to $\dot{C}_{pp}$ (as a linear approximation) by

$$\dot{C}_{ff} = E[(\mathbf{f} - \dot{\mathbf{f}})(\mathbf{f} - \dot{\mathbf{f}})^t] = G\{E[(\mathbf{p} - \dot{\mathbf{p}})(\mathbf{p} - \dot{\mathbf{p}})]\}G^t = G \cdot \dot{C}_{pp} \cdot G^t \tag{5.4}$$

where G is evaluated at point $\dot{\mathbf{p}}$. Equation (5.4) leads to

$$\dot{C}_{qq} = \mathbf{V}^{-1} \cdot G \cdot \dot{C}_{pp} \cdot G^t \cdot \mathbf{V}^{-1} \tag{5.5}$$

Because updating $\dot{\mathbf{q}}$ from $\dot{\mathbf{f}}$ is a well determined linear inverse problem ($\mathbf{V}$ is square), any method will lead to the same Kramer solution (5.2) and the covariance matrix (5.3).

To show that (5.5) is equivalent to (4.27), we denote $G \cdot C_{pp} \cdot G^t$ by R', and substitute (4.26) into (5.4), thus,

$$\begin{aligned}
\dot{C}_{ff} &= R' - R' \cdot (R' + C_{ff})^{-1} \cdot R' \\
&= R' - R' \cdot (R' + C_{ff})^{-1} \cdot (R' + C_{ff} - C_{ff}) \\
&= R' - R' \cdot [I - (R' + C_{ff})^{-1} \cdot C_{ff}] \\
&= R' \cdot (R' + C_{ff})^{-1} \cdot C_{ff} \\
&= (R' + C_{ff} - C_{ff}) \cdot (R' + C_{ff})^{-1} \cdot C_{ff} \\
&= C_{ff} - C_{ff} \cdot (R' + C_{ff})^{-1} \cdot C_{ff}
\end{aligned} \tag{5.6}$$

Using (5.3) after substituting (4.16) into (5.6), we obtain equation (4.27).

Equation (4.27) makes the computation of $\dot{C}_{qq}$ much more efficient than (5.5), because we can 1) choose to compute only those entries of C_{qq} that are

related to the boundary fluxes that interest us, such as the background HFD, 2) avoid the time consuming computation of $\dot{C}_{pf}$ and $\dot{C}_{ff}$, and 3) directly use the factorized form of R (Appendix B) from the last iteration of the nonlinear part of the system.

The updated boundary flux **q** at any boundary point of an element is interpolated with the updated nodal values of boundary flux of the element using (3.2) and (3.21), i.e., in matrix form,

$$\dot{q} = \mathbf{H}^t \cdot \dot{\mathbf{q}} \tag{5.7}$$

The variance of $\dot{q}$ is then

$$\dot{\sigma}_q^2 = \mathbf{H}^t \cdot \dot{C}_{qq} \cdot \mathbf{H} \tag{5.8}$$

5.3 An alternative approach to dealing with heat sources

Heat source $\aleph$ is formulated into the nonlinear part of the system (3.11),

$$h \cdot \mathbf{T} - \mathbf{W} - \mathbf{f} = 0 \tag{5.9}$$

because its logarithmic transform ϵ is used in order to constrain the heat sources to be positive.

If the heat sources are well known a priori and hence well constrained to stay positive, $\aleph$, instead of ϵ, can be formulated as parameters. If formulated as such, $\aleph$ will be a linear part of the parameter vector **P** (see equation 3.9) together with **q**, and the nonlinear part of the parameter estimation will have a smaller dimension and the computation will be more efficient. Again, it is assumed that the uncertainties of the nonlinear and linear parts of **P** are uncorrelated. The problem with this approach is that the updated source–equivalent and flux-equivalent nodal flows are given by one vector **W** + **f**, as can be seen from (5.9). Separating these two contributions poses problems. However, this

procedure can be simplified if **W** and **f** can be separated in the first place in the parameterization of the problem (i.e., for any non–zero component of one vector, the corresponding component of the other is zero).

It is easily observed from equation (3.9) and (3.10) that non zero components of **f** are associated with global boundary nodal points only, while non–zero components of **W** with non–zero heat source elements only. The mixing of the two effects occurs only at those global boundary nodal points where the finite elements related to these points have non–zero heat sources. Therefore, the two effects can be separated if the elements related to the boundary nodal points do not have heat sources. Some auxiliary elements with constant thermal conductivity and zero heat source can be added to the boundary. If the geometry of the boundary is smooth, the shape of the new boundary is simply duplicated from that of the old one; and if the auxiliary elements are "slim" enough, the heat fluxes of the new boundaries will very closely approximate those of the old ones.

Once **W** and **f** are separated, updating **R** from **W** and **q** from **f** become two independent, but similar, problems. The former differs from the latter in that it is an over determined problem, i.e. there are more independent equations than heat source values.

CHAPTER 6: CONDUCTIVE HEAT FLOW PROBLEMS

6.1 Preface

Inverse methods were applied to heat conduction problems in mechanical engineering as early as 1960 (Stolz, 1960). The inverse problems considered there form a specific class, "where the temperature history is known at some interior point in the body and the transient surface temperature and surface heat flux are to be determined" (Bass, 1980). One should notice the analogy between this type of inverse problems and the problem studied by Wang and Beck (1987) and Shen and Beck (1988), where probe measurements are taken in lake sediments a few times over a time period, and the data are used to determine the water bottom temperature history and the steady state local HFD. A major advantage one has in the engineering study is that the thermal conductivity of the material considered is usually accurately known. If the conductivity is not temperature dependent, the inverse problem is linear; if it is temperature dependent, the problem is nonlinear. Inverse methods were developed for both linear and nonlinear problems (Beck, 1970). The first inverse finite element solution, to the 1–D linear inverse heat conduction problem was obtained by Hore et al. (1977), and to the 1–D nonlinear problem by Bass (1980). A 2–D inverse finite element method was developed by Macqueene (1981) for dealing with problems related to welding processes. Further studies on the inverse finite element methods for such heat conduction problems can be seen in Kratz and Akau (1983).

The inverse problems of conductive terrestrial heat flow bear more

production rate of $\aleph = 0.1$ W m^{-3}. The upper and lower boundaries are insulators. The left end of the body ($x = 0$ m) is kept at a constant temperature of 30 °C, and the right end ($x = 3$ m) has a constant in flowing HFD of 2.0 W m^{-2}. With these values of material properties and boundary conditions, the nodal temperature values are computed for all the 23 nodes with a forward calculation. The continuous temperature distribution in the x direction is shown in Fig.6.1b. This temperature distribution appears almost linear because the contribution from the internal heat sources is very small, compared with that of the boundary HFD.

To illustrate the general inverse method using this model, we assume that we know the structure of the body to such an extent that we can assign a uniform λ to element 1 and 2, another uniform λ to element 3 and 4, and two distinct $\aleph$ values for element 2 and 3, respectively. The three boundary HFD nodal values at the right end (nodes 21, 22 and 23) are also taken as parameters. The two λ values, two $\aleph$ values, three boundary nodal HFDs, and the 23 nodal temperatures compose the 30 component parameter vector **P**, in which the nonlinear part **p** has 27 components and the linear part **q** has 3. The left end boundary has the Dirichlet boundary condition, therefore the three finite element algebraic equations associated with nodes 1, 2 and 3 are crossed out, leaving **g** and **f** in equation (3.22) with 20 components. Some of the parameters are assumed to be better known than others in the following case studies, but every parameter is assigned a non-vanishing value of STD. Sometimes, an incorrect value is used as the a priori value for a parameter, with the intention to see whether, or how well, the correct value can be recovered by the inversion.

The actual (full) G matrix would have 20 x 27 entries, but the parameters in **p** are numbered in such a way that the G matrix is somewhat banded (Fig.6.2), and the zero entries beyond the skylines (shown in the figure) are not stored during the computation. Similarly, only the upper part of the symmetric matrix R

(equation 4.14) is stored. Proper numbering of parameters may easily reduce by two thirds the computer memory required, which is a significant amount for very large problems. As can be reasoned from Fig.6.2, using a larger number of material property zones will increase the dimension of the G matrix, and leave the dimension of the R matrix unchanged, but it may significantly reduce the dimensions of the actual storage arrays for the G and R matrices if parameters are properly numbered. The G and R matrices for the coupled problem are stored using the same scheme.

6.2.2 A "forward" problem

When the values of the material properties and the boundary conditions are perfectly known, but the temperature distribution in the body is unknown, we have a forward problem. To use this current inverse method to solve the forward problem, we approximate "perfectly known" with "accurately known", and "unknown" with "extremely poorly known". The correct values of the material properties and boundary conditions are thus tightly constrained with very small STDs of 0.0001 (SI units), and the randomly guessed temperature values (30 °C) are assigned a large STD of 5 K. The inverse solution gives the correct temperature values, i.e., those given by the forward calculation, with the STDs in the order of 10^{-4} K. If the temperature values thus obtained are plotted, they will be indistinguishable from those shown in Fig.6.1b.

6.2.3 A "system identification" problem

When good knowledge of temperatures and boundary conditions is used to determine all or some of the much more poorly known material properties, we have a typical system identification problem. In this case, the correct nodal temperatures are perturbed with Gaussian noise of STD = 0.01 K, and then used

as the a priori values with the same STD. At the right boundary the correct HFD values are used as the a priori values with STDs of 0.01 W m^{-2}. A priori values that differ significantly from the correct values are assigned to the material properties with large STDs. As shown in Table 6.1, two conductivity values are well resolved, but the heat source values are not. This is because the heat source values are very small, and their contribution to the temperature distribution, i.e., causing a slight curvature, is hardly detectable in the noisy temperature data. If the noise in the a priori temperatures is reduced to STD = 0.001 K, the solution is much improved (Table 6.2).

6.2.4 Updating boundary HFD

In this case, information on the nodal temperatures and material properties are used to update our knowledge of boundary HFD. The nodal temperatures contain Gaussian noise of STD = 0.01 K, except that those of nodes 1, 2 and 3, where accurate Dirichlet boundary condition is applied, have STDs of 0.0001 K. The boundary HFD at the right boundary is assigned an incorrect a priori value of 2.2 ± 0.2 W m^{-2}; our knowledge that the HFD across this boundary should be uniform is expressed by a large correlation length (see section 5.2) L = 5 m.

When the material properties are accurately known, with log STD = 0.0001 (SI units), the boundary HFD is well resolved to be 2.00 ± 0.02 W m^{-2}.

When the heat sources are accurately known, with log STD = 0.0001 (SI units), but the thermal conductivities are poorly known as in the examples of "system identification", the a posteriori boundary HFD is 2.14 ± 0.19 W m^{-2}. The a posteriori STD is almost the same as the a priori one, meaning that the HFD is very poorly resolved. This is an example of non–identifiability (section 1.3). In the case of small internal heat sources, the temperature data can only resolve the ratio of the HFD and conductivity, i.e., the temperature gradient. When the

conductivities are accurately known, but the heat sources are poorly known, it may be difficult to distinguish the contributions to the temperature distribution from the sources and from the boundary HFD, depending on the noise level of the temperature data and the intensity of the heat sources.

6.3 Heat flow in the presence of topography

6.3.1 Introduction

"Terrain disturbances" are the differences between the observed geothermal field and that of an ideal solid earth medium with a flat isothermal surface. Terrain effects may be steady state or transient, and may involve groundwater flow; topographic effects are the small scale (usually a few km) terrain disturbances due purely to the presence of a real topographic surface. Corrections for the topographic effects can be performed by subtracting the computed disturbance field from the observed field to find the undisturbed field, or equivalently, modeling the actual field to find the undisturbed values away from the disturbing sources. Analytical techniques are often used with the former approach, and numerical methods are frequently used with the latter. A comprehensive review of topographic correction methods was given by Powell et al. (1988).

Analytical methods, such as the widely used solid angle method (Birch, 1950), the spectrum method (Blackwell et al, 1980) and the source function method (Brott et al., 1981), usually require the assumption of a homogeneous thermal conductivity. For some methods, a particular functional form of the surface temperature distribution, such as a linear function of elevation with an elevation intercept and a lapse rate, is used. Unless favorable conditions exist, the

errors introduced by the simplifications may overshadow the merits of the methods, such as being easy to apply and interpret. Numerical methods allow heterogeneous and anisotropic thermal conductivity and arbitrary surface temperature distributions to be modeled, and are superior to the analytical methods in many applications.

When numerical methods are applied to a problem of topographic correction, a direct modeling approach can be stated as follows. Given the thermal conductivity structure and values, the measured borehole temperature data and the temperature distribution at the upper boundary and symmetry condition at the vertical boundaries, estimate the constant HFD at the lower boundary. This is an inverse problem, and trial–and–error approaches that adjust the background HFD value to fit the computed temperature field to the measured temperature data are often used. Henry and Pollack (1985) used a least squares criterion in the fitting procedure and allowed some parameters in the surface temperature distribution, assumed to be a linear function of elevation, to be adjustable.

In this work, the problem is posed in a general sense described in section 4.1: we know the symmetry condition at the vertical boundaries and the thermal conductivity structure, we have certain knowledge of the thermal conductivity values, the temperature distribution at the upper boundary and the subsurface temperature field, in which some borehole temperatures have very small uncertainties, we also have some idea, through some kind of analysis and reasoning, about the constant background HFD value; what are the most probable values and uncertainties of the thermal conductivities, the temperature field, as well as the HFD at the lower boundary, according to the available information. All the three types of physical quantities are the parameters to be estimated. Our final state of knowledge is determined by the relative quality of the a priori information on the parameters: the parameters poorly known a priori are adjusted

to a larger extent in the inversion while those well known a priori to a lesser extent. The uncertainty in the estimated HFD value reflects our uncertainties in all the parameters: all uncertainties are reduced by the combination and reorganization of our a priori knowledge and the relevant physical laws described by equation (2.2).

Many methods for topographic corrections can be used as data preprocessors to provide, for our inverse formulation, the a priori values of the parameters, especially the background HFD. The uncertainties in these a priori values depend on our confidence in the particular methods. Even in less complex situations, where the HFD values given by some existing methods are quite accurate, it is still worthwhile to apply the current inverse method for a formal variance analysis.

6.3.2 A synthetic example

The synthetic example used by Henry and Pollack (1985) is used here to illustrate the current inverse method. With the isoparametric finite element model, it is possible to construct a structure model that has a smooth ground surface with a small number of nodal points (Fig.6.3a). The temperature at the ground surface decreases with increasing elevation with a lapse rate of 0.066 K m^{-1} to a minimum value of 6 °C at the highest elevation. The HFD across the lower boundary is a uniform 60 mW m^{-2}, and there is zero horizontal HFD at the two vertical boundaries. The conductivity of the medium is 4 W $m^{-1}K^{-1}$. Using these boundary conditions and the thermal conductivity values, the "true" temperature field was obtained with a forward calculation.

Henry and Pollack used synthetic data from four boreholes, presumably drilled at different locations along the topographic profile, and the known surface temperature lapse rate to estimate the background HFD. With a strong constraint

that the background HFD is uniform and with reasonable knowledge of the surface temperatures, a data set from one borehole is in fact adequate. The borehole is assumed to have been drilled in the valley, and the solid circles in Fig.6.3a indicate where accurate temperature data has been obtained. For the inversion, all the "true" nodal temperatures are perturbed with Gaussian random noise, then used as the a priori values; the STDs of the noise added are used as the a priori STDs of these values. The best known temperature values are the borehole measurements, and Gaussian noise with small STD of 0.01 K is used to simulate experimental errors. The surface temperature values, as uncertain Dirichlet boundary conditions, contain Gaussian noise with an STD = 0.5 K. The rest of the a priori nodal temperature values contain Gaussian random noise with an STD as large as 4 K and therefore are extremely poorly known. A background HFD is guessed to be 70 ± 70 mW m^{-2} to show our uncertainty, and a correlation length of 5 km is used to make the HFD essentially uniform. There is only one conductivity zone, that is the whole spatial domain, and there is no heat source present. Clearly, in such a problem, the HFD and the conductivity cannot be estimated separately, but only their ratio, i.e., the temperature gradient, can be determined. Therefore, the uncertainties in the thermal conductivity are not formally considered in the inversion. This makes the problem linear, and only one iteration is needed to obtain the a posteriori values. If there is any uncertainty in the thermal conductivity value, the same percentage uncertainty should be added to the HFD estimate.

The background HFD estimates and the one STD uncertainty range are shown in Fig.6.3b. The estimated HFD distribution is always better resolved in the center part of the profile than at the two ends. This is true even if there is no assumed borehole and all the a priori nodal temperatures have the same uncertainties (necessarily smaller than the 4 K used in the above example for a

physically reasonable solution). The pattern of the resolution of the HFD reflects the pattern of the resolution of the a posteriori subsurface temperature values. Compared to a nodal temperature on a vertical boundary, a nodal temperature in the center part of the domain is constrained by, among other factors, more neighboring temperatures, and hence is better resolved. The borehole located near the center has amplified the effects. It should be noted that the HFD being uniform at such a shallow depth as in this example does not represent real situations; the topographic perturbations affect much deeper regions.

6.3.3 An example from Bolivian Andes

This example was used by Henry and Pollack (1985) to illustrate a method to obtain local HFD values in the presence of topography. The data were collected from the Bolivar mine in Bolivia, where the structurally controlled topography was developed along axial anticlines and synclines in folded Devonian shales, so that a 2–D model is a good representation of the topography and structure. Fig.6.4a shows the topography of the cross section considered by Henry and Pollack, together with the locations of the four boreholes drilled at the lowest level of a mine into the undisturbed rock. Henry and Pollack have also shown that it is reasonable to apply the symmetry boundary condition at the two vertical boundaries of the cross section. Details of the local and regional geology and the data acquisition procedure can be found in Henry's Ph.D. thesis (1981). In applying the inverse finite element method to this example, the assumptions of 2–D, steady state and pure conduction made by Henry and Pollack (1985) are assumed to be valid.

The measured temperatures from the four boreholes are shown as crosses in Fig.6.4b where temperatures from inclined boreholes 78-21 and 78-10 have been projected onto vertical lines extending from the collars of the holes. Two

conspicuous features of the plotted data cannot be explained as topographic effects. First, the temperatures in hole 78–10 are abnormally high compared to those in the other holes; for example, below 50 m, the temperatures are higher than those in the adjacent 78–25 by more than 1.5 K. The existence of an isolated "warm hole" is hard to explain by any steady state conduction mechanism. The sudden temperature rise at about 20 meters depth might suggest water flow, yet there might be some other unknown local effects. To accept the assumption of steady state pure conduction for the purpose of comparing results, the data from this hole are discarded in the following calculation. Henry and Pollack (1985) also had problems fitting a model to the data from this borehole. Second, there appear to be some very local warming effects in the top 20 meters of 78–25; if the curvature in that portion were to be explained by the variation of thermal conductivities, the conductivity values would be too low to be acceptable. Therefore, temperatures between 20 to 50 meter depth were extrapolated upwards to the mine bottom, and the extrapolated values used as the data.

The rocks in the area are reported to be rather homogeneous, and a uniform thermal conductivity of 4.9 W m^{-1} K^{-1} was used in Henry and Pollack's model fitting. By examining the measured temperature profiles, however, it is felt that some spatial variations in conductivity must exist. Therefore, in applying the finite element inverse method, the domain is arbitrarily divided into 23 conductivity zones (Fig.6.4a). All the zones are assigned the same a priori value of λ = 4.9 W $m^{-1}K^{-1}$, and the STD of $\log(\lambda)$ is identically 0.1 (Fig.6.4c).

The ground surface temperature distribution is essential in topographic correction of HFD data. The usual approach is to assume a temperature distribution that is a linear function of descending elevation with a given lapse rate and an elevation-intercept. The assumed function form may introduce large errors in the corrected HFD value. Henry and Pollack (1985) made use

approach slightly more flexible by allowing the intercept to be adjustable during model fitting. In the case of a single borehole without independent information on the surface temperature distribution, to assume a function form might be the only choice, but when there are a few boreholes such as in the current case, it is possible to construct a temperature distribution from data. Before doing this, we can take another advantage of the Bolivar Mine data set as follows.

All the boreholes were drilled from the same level, defined as 0 depth in Fig.6.4a. This level, instead of the ground surface, is used as the upper boundary of the spatial domain for the calculation, and a temperature distribution is constructed by hand using the measured data. If the horizontal temperature variations at this level are caused by the temperature variations at the ground surface only, specifying the Dirichlet condition at this level is equivalent to specifying the corresponding Dirichlet condition at the surface. Since the 0 depth temperatures are less influenced than ground surface temperatures by the climatic temperature perturbation, there is no reason to believe that any assumed surface temperature distribution would be better than the one constructed at this level. The temperature nodal values specified here still have uncertainties because of the paucity of data and the extrapolation made for 78–25, although these uncertainties are probably smaller than those of an assumed surface temperature function; an a priori STD of 0.5 K is assigned to each value. The temperature distribution constructed at 0 depth, now the upper boundary of the model, is shown in Fig.6.4d.

The two vertical boundaries have the symmetry condition, i.e., zero horizontal heat flux. At the lower boundary, a very uncertain Neumann condition is applied; nodal HFD values on this boundary are the parameters of our interest. A large a priori correlation length, L = 10 km, for the nodal HFDs is used, making the HFD essentially uniform along the lower boundary. To provide the a priori

approach slightly more flexible by allowing the intercept to be adjustable during model fitting. In the case of a single borehole without independent information on the surface temperature distribution, to assume a function form might be the only choice, but when there are a few boreholes such as in the current case, it is possible to construct a temperature distribution from data. Before doing this, we can take another advantage of the Bolivar Mine data set as follows.

All the boreholes were drilled from the same level, defined as 0 depth in Fig.6.4a. This level, instead of the ground surface, is used as the upper boundary of the spatial domain for the calculation, and a temperature distribution is constructed by hand using the measured data. If the horizontal temperature variations at this level are caused by the temperature variations at the ground surface only, specifying the Dirichlet condition at this level is equivalent to specifying the corresponding Dirichlet condition at the surface. Since the 0 depth temperatures are less influenced than ground surface temperatures by the climatic temperature perturbation, there is no reason to believe that any assumed surface temperature distribution would be better than the one constructed at this level. The temperature nodal values specified here still have uncertainties because of the paucity of data and the extrapolation made for 78–25, although these uncertainties are probably smaller than those of an assumed surface temperature function; an a priori STD of 0.5 K is assigned to each value. The temperature distribution constructed at 0 depth, now the upper boundary of the model, is shown in Fig.6.4d.

The two vertical boundaries have the symmetry condition, i.e., zero horizontal heat flux. At the lower boundary, a very uncertain Neumann condition is applied; nodal HFD values on this boundary are the parameters of our interest. A large a priori correlation length, L = 10 km, for the nodal HFDs is used, making

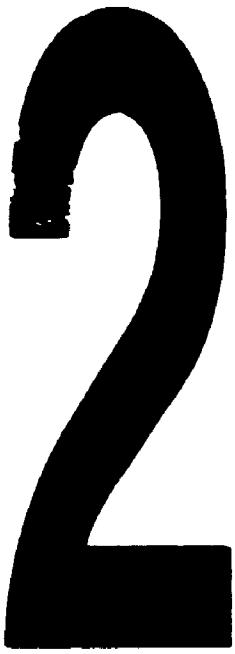

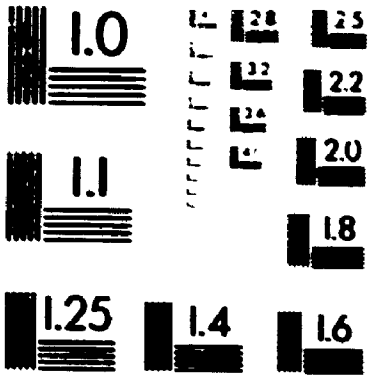
1.0
1.1
1.25
1.4
1.6
1.8
2.0
2.2

HFD value, a trial and error method is used, in which the a priori upper boundary condition and thermal conductivity values are used, and the HFD value is adjusted to let the computed temperatures at the borehole locations approach, by naked eye, the measured values. A crucial estimate of 120 mW m^{-2} is obtained with a couple of trial runs, and the value is used as the a priori HFD value, with an STD of 100 mW m^{-2} representing our uncertainties.

The finite element mesh of this example extends from the collars of the holes to a depth of 2400 m where, based on some simple numerical experiments, the topographic effects are believed to be negligible so that the HFD at the bottom boundary of the mesh can be safely taken to be uniform. The temperature nodal values obtained with the estimated HFD of 120 mW m^{-2} are used as the a priori values. In the inverse calculation, these values, excluding those at the data points, are assigned a priori STDs which increase with depth from a value of 0.5 K at the upper boundary to 24 K at the lower boundary, because our uncertainties in the nodal temperature values are likely to increase with depth. All the borehole temperature data below 0 m depth are assumed to have STDs of 0.02 K to account for experimental errors.

The a posteriori values of the parameters obtained in the finite element inversion are shown in Fig.6.4, together with the a priori values. The estimated background local HFD is about 131 ± 10 mW m^{-2} (Fig.6.4e). The value 128 mW m^{-2} obtained by Henry and Pollack is well within one STD of this estimate.

6.3.4 Conclusions

The general inverse finite element method has been applied to a synthetic example and a field example. The problem of topographic correction of HFD data is stable, because, based on the small spatial scale of the problem, the background HFD is assumed to be a constant in the horizontal direction. Given knowledge of

the upper boundary temperature distribution and some borehole temperatures, a unique solution can be obtained. From the examples, we can draw the following conclusions.

1) The solutions are comparable to those by other methods. The HFD value obtained by Henry and Pollack (1985) for the Bolivar Mine is within one STD of the current solution.

2) By allowing uncertainties in the upper boundary nodal temperatures, our uncertainties in this boundary condition are taken into account in the estimate of the HFD value.

3) The knowledge of the thermal conductivities of the subsurface medium can also be updated. In more general cases, the distortion of the observed surface HFD due to subsurface conductivity contrasts can be corrected together with the topographic effects.

4) An uncertainty range is rigorously given, for example, by a one STD error bar, for the HFD estimate and each of the other estimated parameters.

6.4 Downward continuation of HFD data

6.4.1 Introduction

For interpretation of HFD data, one important need is to infer, by downward continuation, the HFD and temperature fields at a depth of interest, for example, the Moho–discontinuity. "Extrapolating" surface HFD data on such a scale is a complicated problem; the thermal effects of many geophysical, geochemical and geodynamical processes, such as geotectonical movements, phase changes of rock minerals and mantle convection, may contribute to the near surface HFD pattern. Downward continuation, at the current level of HFD

research, however, usually implies the assumption of steady state and purely conductive heat flow in a solid earth medium, which is probably reasonable at temperatures less than 1200 °C.

A classical downward continuation problem is formulated as: given HFD (or temperature gradient) and temperature distribution (usually conveniently taken as 0 °C) at the ground surface (depth = 0), given distribution of thermal conductivities in the subsurface medium free of heat production, the temperature and HFD fields at a greater depth are to be determined. It is called "downward" in the potential theory because the continuation is toward the source of heat flow. A unique formal solution to such an inverse problem may exist, but is notoriously unstable, in the sense that a slight variation (say, due to an experimental error) in the surface boundary conditions may result in a drastic change in the solution at depth. The instability of the problem puts into considerable doubt the validity of using the HFD data, which are known to contain many experimental errors, as the surface boundary conditions. In more realistic earth models, heat production (distributed heat sources) of significant quantity may exist in the medium into which the temperature field is continued, and the values of the heat production rates and thermal conductivities are known with large uncertainties; the solution to such a problem is unstable and non–unique.

The instability results in physically unreasonable oscillations of the continued field in the horizontal direction. Methods for numerical downward continuation all focus on minimizing such oscillations. It is well known, as shown by the Fourier transform solution by Bodvarsson (1973) and Mareschal et al (1985), that large oscillations at depths are related to short wavelength variations of the surface boundary conditions; as the wave number tends to infinity, the solution diverges. To stabilize the solution, the quoted authors chose to set up a cutoff wave number, and discarded higher wave number terms (Bodvarsson, 1973)

or regarded them as the effects of shallow heat sources (Mareschel, 1985). Huestis and Parker (1979) stated the downward continuation problem as a Backus–Gilbert inverse problem. The Backus and Gilbert solution (1968) seeks the local average of the continued field and hence provides a smoothed version of the solution, i.e., increases stability by decreasing resolution (Backus–Gilbert concept of resolution is different from that used in the rest of the thesis, as explained in section 4.2.3). The weighted least squares method used by Stromeyer (1984) with a finite difference formulation smoothed the continued HFD by introducing a regularizing factor that bounded the magnitude of the first derivatives of the downward continued HFD with respect to the horizontal coordinate. Beck and Shen (1989) used the RTV scheme (section 4.2) with a finite difference formulation, and stabilized the HFD solution using the appropriate smoothly distributed a priori HFD values and variances; the latter tends to keep the estimated HFD values within a reasonable neighborhood of the a priori values in the parameter space. It is not difficult to relate the referred inverse methods to the low wave number solution of Bodvarsson (1973), because all the smoothing or regularizing methods are effectively some kinds of "low pass filter". An extreme case of the smoothed field is in the topographic correction discussed in the previous section, where the continued HFD is kept essentially uniform in the horizontal direction, and hence stability is not a problem. In the less rigorous trial-and-error approach to the inverse problem of downward continuation of HFD, smoothness and boundedness are already implicitly assumed by the researcher in the Neumann condition specified at the lower boundary (Cermak and Bodri, 1986).

The existence of heat production by the decay of natural radioactive isotopes in the earth's crustal material further complicates the downward continuation problem. To make things worse, direct measurements can so far be made only on a very limited number of specimens of the near surface rocks, and

our understanding of the heat production distribution with depth is limited to a very small depth range and is based upon an empirical linear relation between the surface HFD and near surface heat production (Birch et al., 1968; Lachenbruch, 1968; Jaupart, 1983; Nielsen, 1987). Our knowledge of the heat production distribution in the deeper parts of the lithosphere has been largely speculative and qualitative. The most pervasive geophysical survey of the earth's lithosphere is performed by seismological methods, and hence efforts are being made to relate other geophysical quantities to the seismic velocities. On the basis of laboratory experiments, Rybach and Buntebarth (1984) proposed a general empirical linear relation between P–wave velocities and logarithmic heat production rates for rocks of different ages and types. Cermak and Bodri (1986) used the relation, with further corrections, to obtain heat source distributions in the lithosphere. Unfortunately, the data set on which the relation is based is small and there is not a convincing theoretical explanation so that the relation has not been widely accepted. In any case, it can be seen that no matter how a heat source distribution is obtained, the uncertainties are likely to be large, perhaps orders of magnitude. Such large uncertainties should be considered in any scheme of downward continuation of HFD data. In Huestis (1980), the heat sources were assigned rather narrow bounds. In Stromeyer (1984), the contributions to the observed surface HFD from the heat sources in the crustal rocks and from the background HFD were investigated separately. In the BTV approach of Beck and Shen (1989), both the heat sources and background HFD were formulated as parameters and estimated simultaneously by the inversion.

The method proposed in this work is very similar to that of Beck and Shen (1989). The main differences are in the finite element parameterization approach, in invoking the auto–covariances of the boundary HFD as part of our a priori information, and in using logarithmic heat production rates as parameters (see

Chapter 3). The use of log(A) is convenient because the values of heat production rates are very small (compared to other parameters, in consistent units), and could otherwise be easily assigned negative values by the automatic inverse procedure, unless tightly constrained by small a priori STDs. As mentioned above, a small STD will not reflect our large uncertainties in the heat production rates, no matter how the values are obtained. Using logarithmic transforms allows the a priori STDs to be given in orders of magnitude if observed on the original linear scale and never result in negative a posteriori A values. When our uncertainties in a small, positive physical quantity is of orders of magnitude, a log–normal probability distribution is much more reasonable than a linear normal distribution.

In the following text, the proposed method is applied to three European geotraverses. In each of the three examples, the cross section extends to a depth of 60 km, the two vertical boundaries are assumed to have symmetry condition (horizontal HFD = 0), and the surface temperature is conveniently taken as 0 °C.

6.4.2 A central Europe geotraverse

Hurtig and Oelsner (1977) constructed three transcontinental profiles across central Europe with known surface HFD values, and computed the temperature field in each cross section using a 2–D forward finite difference method. The first of the three geotraverses (CEGT1), extending almost north–south from South Sweden to Italy, was later used by Stromeyer (1984) and Beck and Shen (1989) to demonstrate their inverse methods. The data, upon which the construction of the 2–D model was based, have since been updated by other work, but for "calibrating" the method by comparing results with that of Stromeyer (1984) and Beck and Shen (1989), the same geotraverse is chosen in this work. More detailed geological information is given in Hurtig and Oelsner (1977).

In this example, each finite element is taken as a thermal conductivity and

heat production zone, and the zone numbers are given in Fig.6.5. The thermal conductivity and heat production values given by Hurtig and Oelsner are used as the a priori material property values. An STD of 0.1 (SI units) is assigned to each a priori log(λ) value. A constant HFD of 33.9 mW m^{-2} suggested by Stromeyer (1984) is used as the a priori value of the HFD at the lower boundary. The observed surface HFD given by Hurtig and Oelsner is applied to the upper boundary with an STD of 10 mW m^{-2} for each node. Following Beck and Shen's example, the a priori temperature field is computed using the a priori material property and HFD values. Six cases involving different a priori information are investigated as follows.

Case 1. Unknown values of background HFD *and temperature field.* For a set of parameter values, the approximate expression of "we do not know" is represented by very large a priori STDs, and zero covariances. Here the STDs of the nodal HFD values are given as 10^5 mW m^{-2}. The STD of the temperature at every node is 4000% of the nodal value. The STDs of the log(δ) values are the same as those of the log(λ) values, i.e., identically 0.1 (SI units). As is mentioned in section 4.2.1, as far as the iteration for the parameter values is concerned, the magnitudes of the variances have only relative meanings, a looser constraint on the HFD and temperature means a tighter constraint on other parameters. If we reduce the STD of all parameters by, say a factor of 100, which means a very small STD of 0.1 mW m^{-2} for the surface HFD, the parameter estimates would be exactly the same, except that the a posteriori STDs of all the parameters would be smaller by a factor of 100. Therefore, this case approximates a direct downward continuation (without regularization) with known surface boundary conditions and subsurface material properties. The instability of the solution is illustrated by the oscillations of the continued background HFD in Fig.6.6.

Case 2. The STD of *the background* HFD *in case 1 is reduced to 50 mW*

m^{-2}. In this case, our a priori information on the background HFD is in the form a smaller STD of 50 mW m^{-2}, but no covariances. As shown in Fig.6.7a, the stability of the solution is greatly improved, and the a posteriori uncertainties represented by the error bars are much smaller.

Case 3. The a priori HFD *values in case 1 are assigned positive covariances.* The a priori STD of the nodal HFDs is still 10^5 mW m^{-2} (virtually unknown), but a correlation length L = 200 km is used that indicate our belief that the HFD should be somewhat smooth. This, in a sense, corresponds to the low wave number deterministic solution of Bodvarsson (1973), but is stated in a probabilistic manner. The results (Fig.6.7b) illustrate the increased stability and decreased uncertainty compared to the solution of case 1.

Case 4. Unknown HFD, *better known temperature field.* Our knowledge of the HFD, as well as other parameters, is the same as in case 1, but the STDs of nodal temperatures are reduced from 4000% to 40%. This case corresponds to the first example of Beck and Shen (1989). The constraints on the temperature field have stabilized the solution to some extent as shown by Fig.6.7c.

Case 5. "Reasonable" a priori information on all parameters. The following constraints are used: the STDs of the nodal temperature are 40%, the STDs of the log(k) values are 0.3 (SI units), and the nodal values of the background HFD have an STD of 100 mW m^{-2} and a correlation length L = 100 km. The contour maps of the a posteriori temperature field and STDs, the a priori and a posteriori background HFD, the values of thermal conductivities and heat production rates with their uncertainty ranges are shown in Fig.6.8.

Case 6. Large uncertainties in heat production rates. In this case, we investigate the possibility that the background HFD is very smooth and the variations of the surface HFD are due mainly to the spatial variations in the heat production rates. Our poor knowledge of the log(k) values is represented by an

STD of 1.0 (SI units), corresponding to one order of magnitude on the linear scale. The correlation length of the background HFD is increased to 200 km from the 100 km in case 5. All the other constraints to the parameters remain the same as in case 4. The results in Fig.6.9b show that the a posteriori background HFD is fairly constant (within an uncertainty range), therefore the spatial variations of the surface HFD are due to the variations of the heat sources. From the estimated heat source values shown in Fig.6.9c, it can be seen that the spatial variations of the heat sources are well within our a priori uncertainties in the values.

6.4.3 Two eastern Europe geotraverses

Cermak and Bodri (1986) performed 2–D forward numerical modeling of the temperature field along five eastern Europe geotraverses (Fig.6.10). The typical values for the thermal conductivities of lithospheric rock categories, slightly dependent on temperature, were used. The rock heat production rates were estimated using, with some modifications, the heat production – P wave velocity relation proposed by Rybach and Buntebarth (1984). The "observed" surface HFD values were sampled from the HFD map of Europe compiled by Cermak and Hurtig (1979), and these are necessarily "smoothed" values. The background HFD values (as a Neumann boundary condition at the lower boundary of the model) were adjusted by comparing the computed surface HFD distribution with the observed one, until a "best" fit was reached. Two of the five geotraverses are used in this work to demonstrate the inverse finite element method: EEGT1, oriented approximately north–south, going through the Alpine geosyncline, Bohemian Massif and East European platform; and EEGT5, oriented roughly east–west, through the Bohemian Massif, Pannonian Basin and East Carpathians. Further geological and geophysical description of the models are given in Cermak and Bodri (1986).

The thermal conductivity as a function of temperature used by Cermak and Bodri is $\lambda = \lambda_o/(1 + \nu T)$, where ν is a constant of the order of 10^{-4}–10^{-3} K^{-1}. At temperatures below 300 °C, conductivity generally decreases with increasing temperature, and therefore $\nu > 0$; at temperatures above 500 °C, the radiative conductivity, which increases with temperature, becomes more important, and $\nu < 0$. According to the ν values Cermak and Bodri gave for rocks at different depths, the maximum variation of the conductivity values would be about 0.3 $W\ m^{-1}K^{-1}$. Adopting the zeroth order approximation $\lambda = \lambda_o$, we obtain temperature fields (results not shown) almost identical to that of Cermak and Bodri, using the same boundary conditions. This is partly because ν is small, partly because different λ_o values were assigned by Cermak and Bodri to rocks at different depth ranges, which already accounts for the temperature dependence of the conductivities to some extent. More importantly, the actual variations of the thermal conductivities due to structure and our uncertainties in the λ–T relation and the λ_o values chosen really make the slight temperature dependence a secondary problem. In the following inverse modeling, the zeroth order approximation of conductivity is used, and the λ_o values given by Cermak and Bodri are used as the a priori values for the conductivity of appropriate rock types, with our uncertainties represented by log–normal probability distributions.

The heat production rates of Cermak and Bodri, averaged over each zone, are used to give the a priori log(A) values. Due to our large uncertainties in these values, as explained in section 6.4.1, STDs that are of orders of magnitude on the linear scale are assigned to them.

Geotraverse EEGT1. The finite element mesh of the model, and the thermal conductivity and heat source structures, based on Cermak and Bodri (1986), are shown in Fig.6.11. The a priori nodal temperatures are given by forward modeling using the same finite element mesh, the a priori material

property values, and a background HFD obtained by reducing the observed surface HFD by 30 mW m^{-2} (a value that very roughly reflects the magnitude of the contribution of the heat production of the crustal rocks to the observed surface HFD). An STD that is 40% of the temperature value is assigned to each of these nodal values. In the inverse modeling, a constant a priori background HFD of 40 mW m^{-2} is used. Two cases are considered.

First, we consider this situation (EEGT1 case 1): we have much confidence that the background HFD is unlikely to be negative or higher than 80 mW m^{-2}, therefore an STD of 40 mW m^{-2} is assigned to every lower boundary HFD nodal value; we also feel that the HFD at that depth is unlikely to change rapidly over short distances, and hence a correlation length L = 100 km is used to generate the covariances between the HFD nodal values. The heat source values obtained from the empirical relation between heat production rate and P–wave velocity is assumed to be reliable to an order of magnitude, so that an STD of 1.0 (SI units) is assigned to each of the a priori log(R) values; a fairly small STD of 0.1 (SI units) is assigned to each of the log(λ) values. The results of the inversion are presented in Fig.6.12. The temperature field thus obtained (Fig.6.12a) is similar to that of Cermak and Bodri. The main contribution here is that our uncertainties in the numerically modeled field are explicitly shown by the contour map of the a posteriori STDs. The high temperatures in the lower left corner of the cross section are accompanied by larger uncertainties. The a posteriori surface HFD (Fig.6.12b) matches the observed HFD pattern more closely than the trial–and–error results of Cermak and Bodri, especially from –100 km to 500 km on the profile; in the less well–fitted sections (e.g., –400 km to –150 km), the observed values are generally within one STD of the calculated values. The updated background HFD is smoother than the surface HFD, which agrees with the common belief that long wavelength variations of the observed surface HFD

have deep origins and the short wave length ones are likely due to the variations of the nearsurface heat source distribution and experimental errors. It is interesting to notice in Fig.6.12c that the heat sources of deeper zones are almost unresolved but those of the shallower zones are better resolved by the relatively good surface HFD data; this is also because the a priori STDs for the values of the deeper zones, observed on the linear scale, are already very small, little more information has been gained in the inversion.

The second situation (EEGT1 case 2) we consider is different from the first in that it is assumed that we have less confidence in the a priori values of log heat production rate values (STD = 2.0) and of log conductivity (STD = 0.2) but a stronger belief that the background HFD is smooth and close to the a priori value of 40 mW m^{-2} (L = 200 km, STD = 30 mW m^{-2}). The results of inversion are shown in Fig.6.13. Compared to the results for EEGT1 case 1 (Fig.6.12), we see that the pattern of the observed surface HFD is equally well followed by the a posteriori surface HFD, but the background HFD is so smooth that only the general trend agrees with the surface pattern (Fig.13b). This means that the background HFD pattern contributes even less to the small variations of the surface HFD than in the previous case, and correspondingly, that the variations of the heat sources and conductivities make more contribution. Some of the heat production and conductivity values are adjusted accordingly by the inversion to fit the observed HFD pattern, with the resolution decreasing with increasing depth in general (Fig.13c).

Geotraverse EEGT5. The finite element mesh for the model and the thermal conductivity and heat source structures, based on Cermak and Bodri (1986) are shown in Fig.6.14. Fewer conductivity zones are needed for this model due to the simpler geological structure. The a priori nodal temperatures are generated with the method used for EEGT1, but the lower boundary HFD used in

the forward calculation was obtained by subtracting 25 mW m^{-2} from the observed surface HFD values. In the inverse modeling, the a priori STD for a nodal temperature is also 40% of the temperature value, and again 40 mW m^{-2} is used as the a priori background HFD value. Two situations, EEGT5 case 1 and EEGT5 case 2, corresponding to the two cases for EEGT1 are investigated.

In EEGT5 case 1, our a priori knowledge of the parameters is assumed to be in the same state as for EEGT1 case 1, that is, an STD of 40 mW m^{-2} and a correlation length L = 100 km for the background HFD, an STD of 0.1 for the $\log(\lambda)$ values and 1.0 for the $\log(R)$ values, and an STD of 10 mW m^{-2} for the observed surface HFD values. The resolved temperature field, similar to that of Cermak and Bodri, and the STDs are shown by the contour maps in Fig.6.15a. As expected, and as seen in Fig.6.15b, the comments on the a posteriori surface and background HFDs for EEGT1 case 1 also apply to this case. The a priori and a posteriori material property values are shown in Fig.6.15c.

In EEGT5 case 2, a priori knowledge of the parameters similar to that of EEGT1 case 2 is assumed. A correlation length of 200 km ensures a smooth background HFD distribution. Again 2.0 is used as the STD of the $\log(R)$ values, but our uncertainties in these values are more emphasized than in EEGT1 case 2 by relatively tight constraints on the $\log(\lambda)$ values, STD = 0.1. Results are presented in Fig.6.16. The solution further confirms the observations made on the results of EEGT1 case 2. In Cermak and Bodri (1986), a background HFD that "echoed" the details of the observed surface HFD in details had to be postulated to let the calculated surface HFD match the observed one. In the current solution obtained with very loose constraints on the heat production values, however, the calculated and observed surface HFD is a better match than that of Cermak and Bodri, but the background HFD (Fig.16b) is smoother, and perhaps more reasonable; the short wave length variations of the surface HFD are due mainly to

the spatial variations of the heat production rates. It is not meaningful to describe one solution as more "accurate" than the other (in fact, Cermak and Bodri's background HFD values mostly fall into one STD of the current solution); the comparison between the two only tells us that an "accurate" solution is not possible if we admit large uncertainties in the heat production values. The current solution confirms, in spite of the large uncertainties, the general trend (long wave length variations) of the background HFD obtained by Cermak and Bodri.

6.4.4 Conclusions and discussions

The general inverse finite element method developed in the previous chapters has been applied to the problem of downward continuation of HFD data. Three examples, one central Europe and two eastern Europe geotraverses, were used. By comparing the inverse solutions using the current method with other published results, the following conclusions can be drawn.

1) The observations and conclusions of Stromeyer (1984) and Beck and Shen (1989) on the stabilization or regularization of numerical downward continuation of HFD data are reasonable.

2) The general shape of the background HFDs obtained by Cermak and Bodri (1986) for two investigated east Europe geotraverses are reasonable, even if the uncertainties in the heat production values are of one or two orders of magnitude.

3) If viewed as a numerical modeling technique, this method, as that of Beck and Shen (1989), provides uncertainty estimates at all depths for all the physical quantities involved. This allows us to judge better the significance of the results. It is natural that these uncertainties depend on our a priori knowledge, particularly the researchers' personal beliefs in the methods to collect data and infer parameter values.

4) The use of logarithmic heat production rates allows us to take account of uncertainties as large as orders of magnitude in the values. When these large uncertainties are considered, only the very long wavelength variations of the background HFD can be resolved; in some cases (e.g., case 6 of the central Europe geotraverse) we may not detect any significant variations in the background HFD.

5) This method does not solve the problem of obtaining accurate values of downward continued HFD; it does provide a flexible method for solving the problem of assigning reliable error bounds on the extrapolated fields. An accurate solution calls for better knowledge of the subsurface structure, thermal conductivity, heat source distributions, etc..

In all the three examples, the temperature gradient is very smooth, especially in the horizontal direction. This allows very large finite elements to be used, and the discretization errors thus arising are insignificant. However, the zonation of the material properties always introduces errors, and as discussed in section 4.1.3, these errors are not evaluated rigorously. In all the three examples, the zones are defined in accordance with the structure inferred by seismic surveys. All these zonations are obviously too coarse to account for the actual spatial variations of the properties. However, considering the scale of the problem and our poor knowledge of the physical quantities involved at the current stage, a finer zonation is not necessary, although it may result in even better fit to the observed surface HFD.

Other disturbing factors, such as hydrological and climatic disturbances to the near surface temperature field, the effects of material phase changes at temperatures higher than 1200 °C, and the theoretical inconsistencies due to simplifying the problem into the purely conductive and steady state case, have been discussed by Cermak and Bodri (1986) and Beck and Shen (1989).

Table 6.1. Simple example: a "system identification problem", nodal temperatures containing Gaussian noise with STD = 0.01 K. The thermal conductivity λ is in W $m^{-1}K^{-1}$, and the heat production R in W m^{-3}.

Parameter	True Value	A priori Value	A priori Log STD	A posteriori Value	A posteriori Log STD
λ_1	2.0	3.000	0.300	2.037	0.016
λ_2	2.0	1.500	0.200	2.027	0.005
R_1	0.1	0.200	1.000	0.096	0.314
R_2	0.1	0.050	0.300	0.144	0.168

Table 6.2. Simple example: a "system identification problem", nodal temperatures containing Gaussian noise with STD = 0.001 K. The thermal conductivity λ is in W $m^{-1}K^{-1}$, and the heat production R in W m^{-3}.

Parameter	True Value	A priori Value	A priori Log STD	A posteriori Value	A posteriori Log STD
λ_1	2.0	3.000	0.300	2.010	0.002
λ_2	2.0	1.500	0.200	2.005	0.001
R_1	0.1	0.200	1.000	0.101	0.032
R_2	0.1	0.050	0.300	0.110	0.026

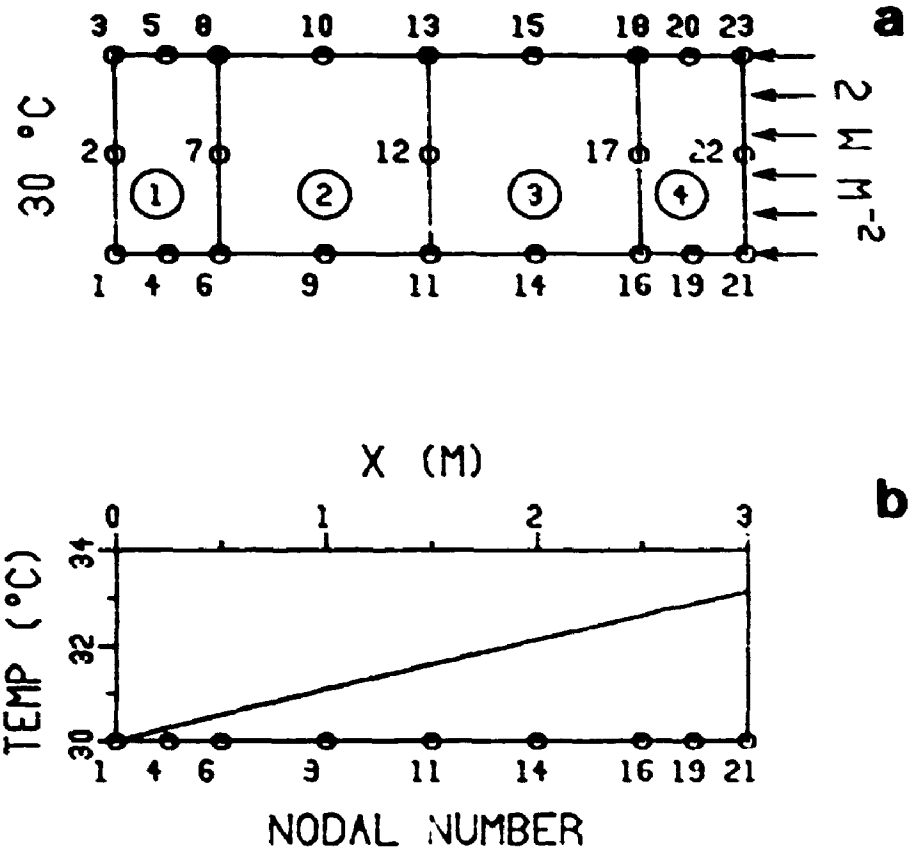

Fig.6.1. The 2–D finite element formulation of a 1–D problem. (a) The finite element mesh, nodal numbers, elemental numbers (in circles) and boundary conditions. (b) The actual temperature distribution in the x direction.

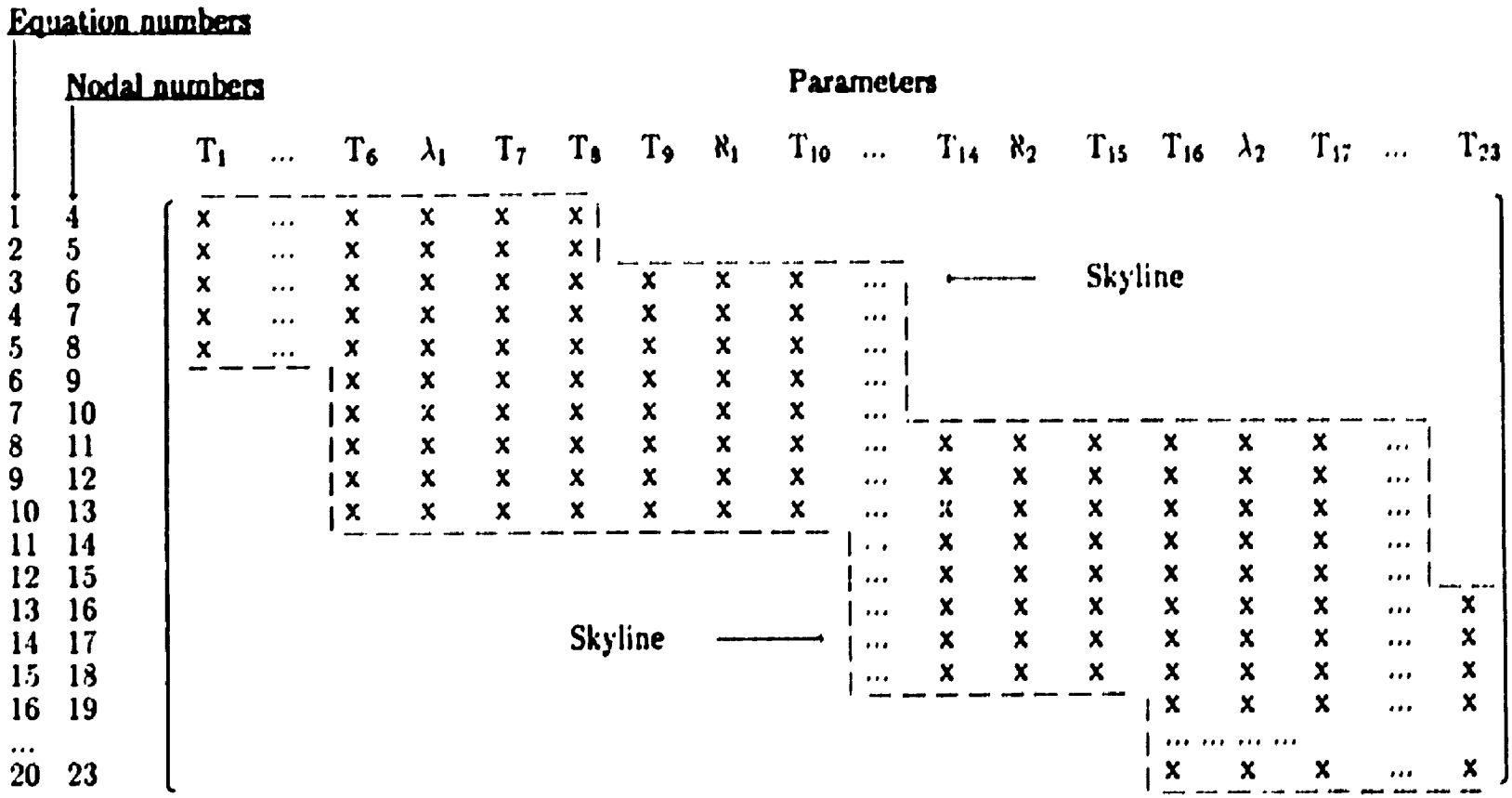

Fig.6.2. A schematic of the structure of the G matrix for the simple example in section 6.2. The equation numbers correspond to the indices of the components of g (see equation 3.20). Non-zero entries are represented by "x". The zeros beyond the skylines are not stored during computation.

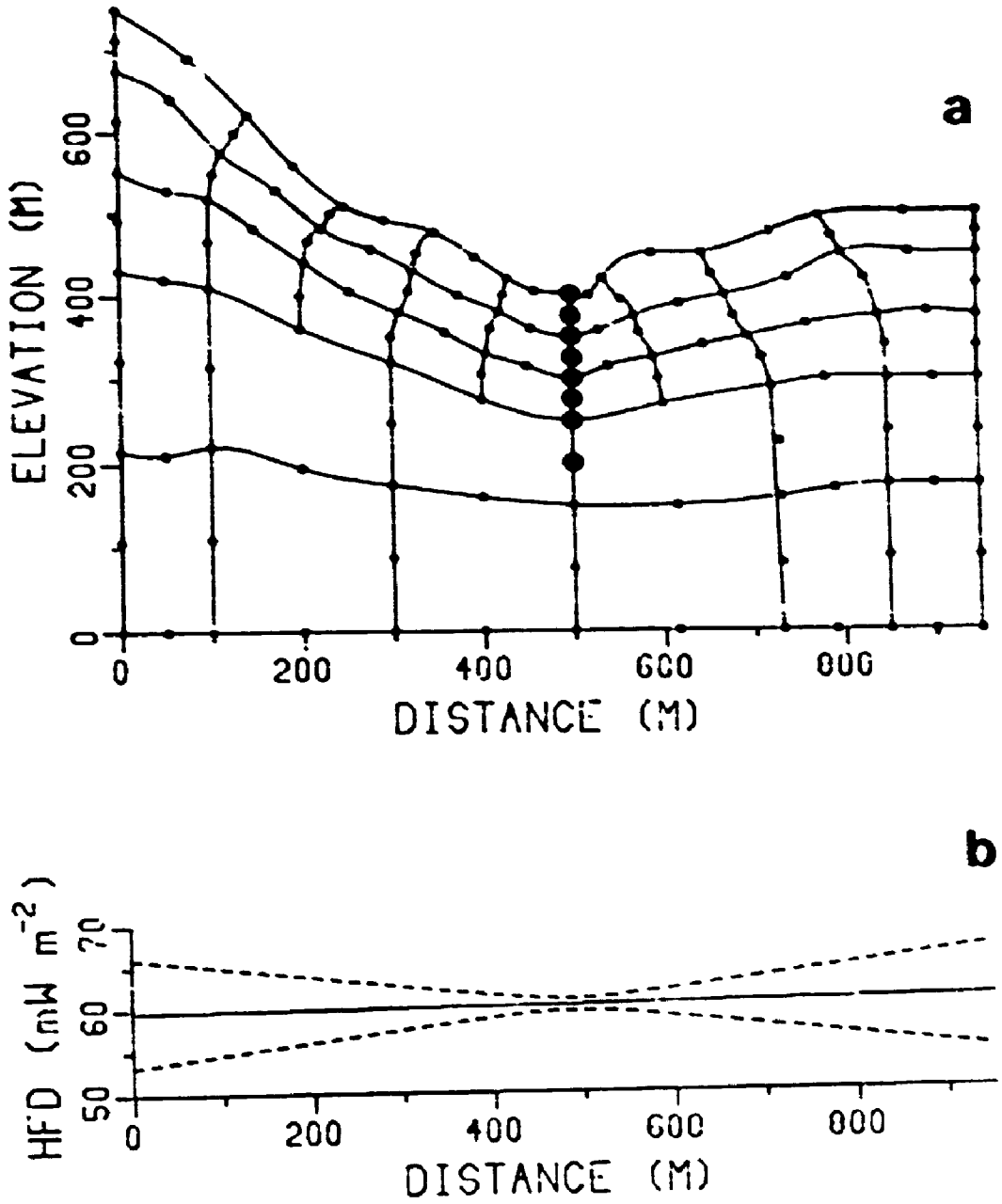

Fig.6.3. A synthetic example of topographic correction. (a) The finite element mesh. The small circles are nodal points. The large solid circles represent borehole data points. (b) The estimated HFD, with the dashed lines representing the one STD uncertainty range. The HFD has been well resolved (from the a priori value of 70 ± 70 mW m^{-2}).

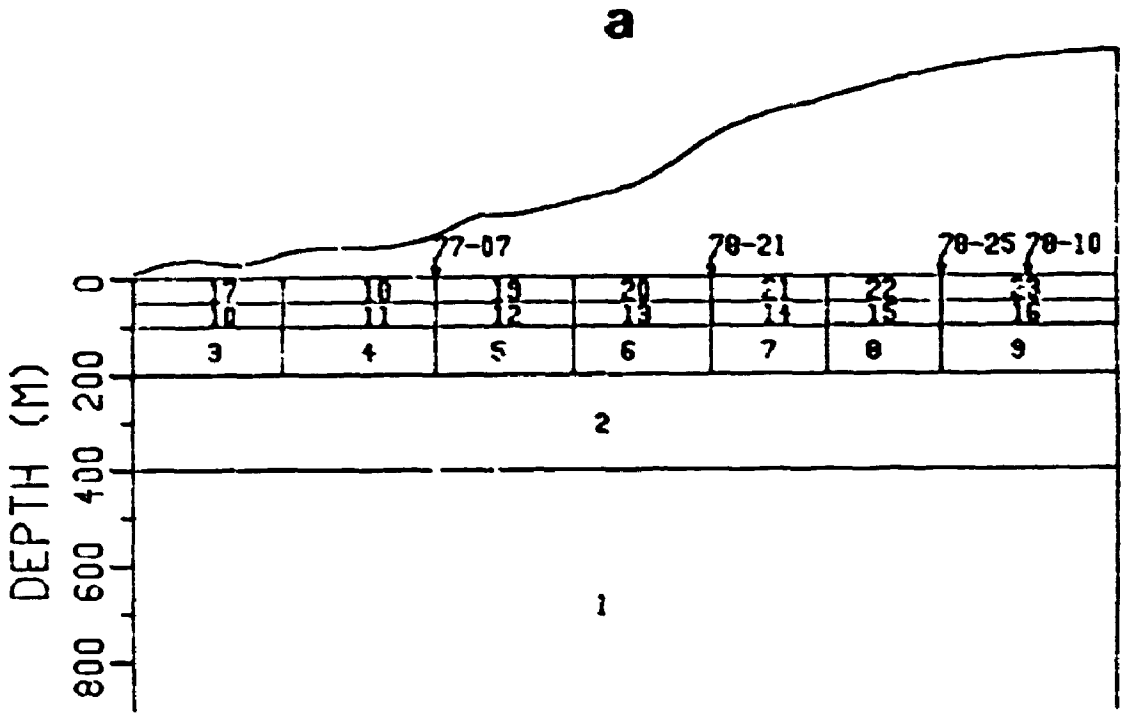

Fig.6.4. The Bolivar Mine example of topographic correction. (a) The topography and thermal conductivity zones. The locations of the boreholes are indicated by the arrows. The finite element mesh used (not shown) extends to 2400 m depth from the collars of the holes (0 m). (b) The measured borehole temperatures (crosses), and their a posteriori values (solid lines). The problematic data from hole 78–10 were not used in the inversion; the a posteriori temperature for this hole is shown by the dashed line. (c) The thermal conductivity values. The uniform a priori value is shown by the solid line, and the one STD uncertainty range by the dashed lines. The a posteriori values (open circles) are shown with one STD error bars. For zone numbers, refer to (a). (d) Dirichlet condition at the upper boundary (the 0 depth). The solid line is the a priori temperature distribution, with one STD uncertainty range (dashed lines). The a posteriori nodal temperatures are shown by pluses, with the one STD uncertainty range represented by the length of the vertical bar. (e) The a posteriori HFD at the lower boundary (2400 m from the collars of the boreholes) with one STD uncertainty range (dashed lines).

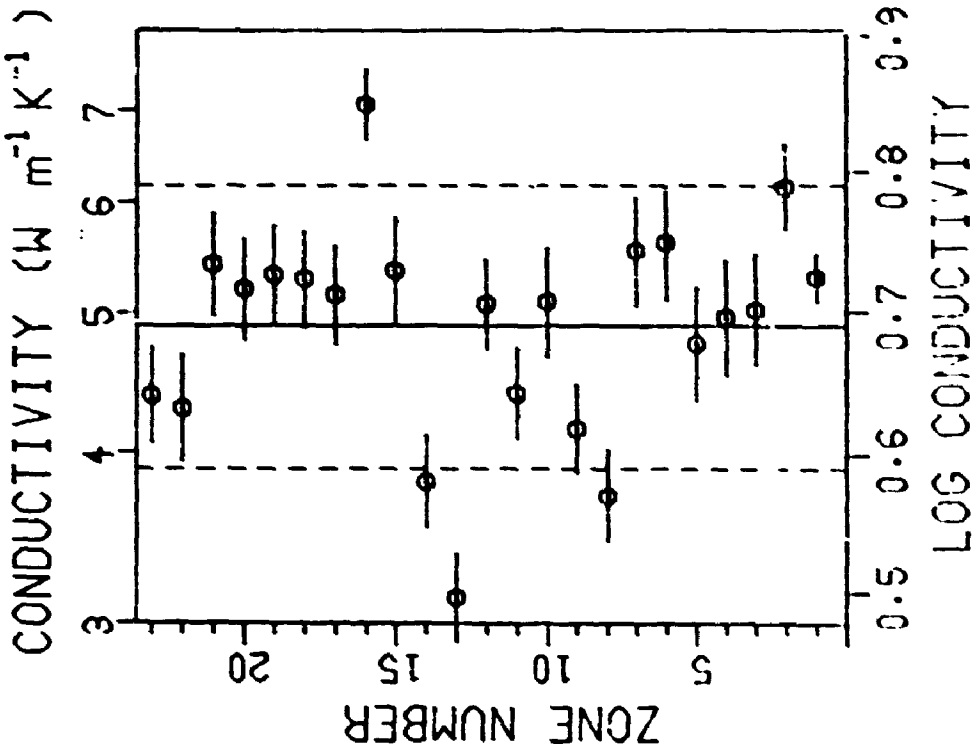

Fig.6.4c. Continued.

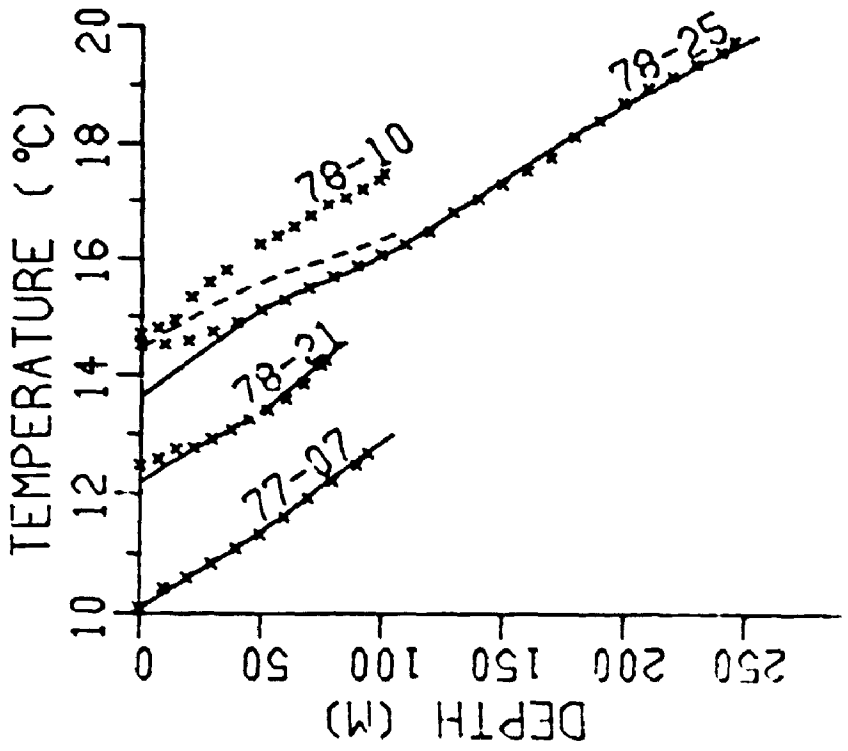

Fig.6.4b. Continued.

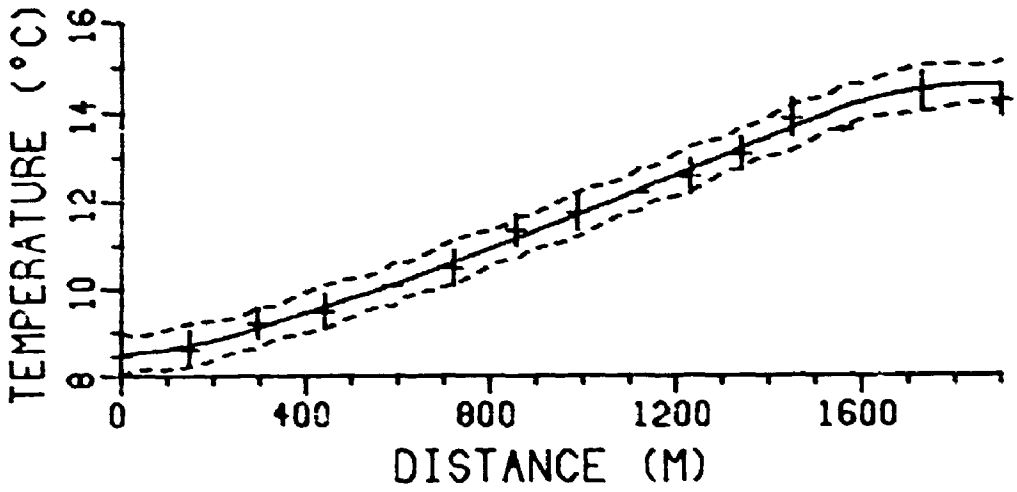

Fig.6.4d. Continued.

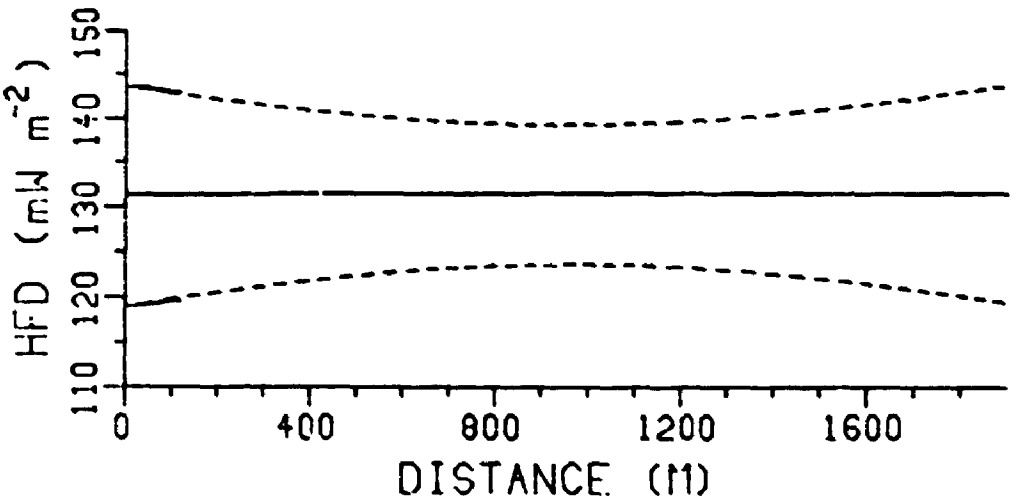

Fig.6.4e. Continued.

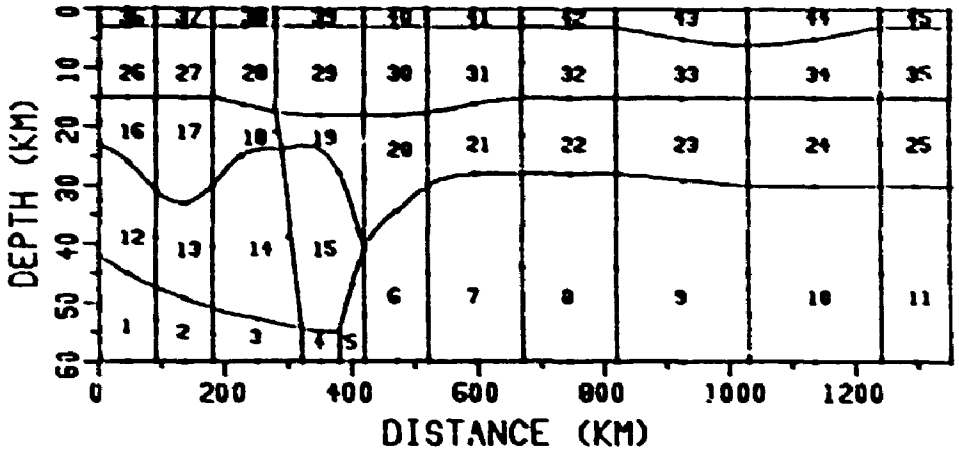

Fig.6.5. The finite element mesh and the material property zones for CEGT1. Nodal points in the finite element mesh are indicated by dots. The zone numbers are for both the conductivity and the heat production rate.

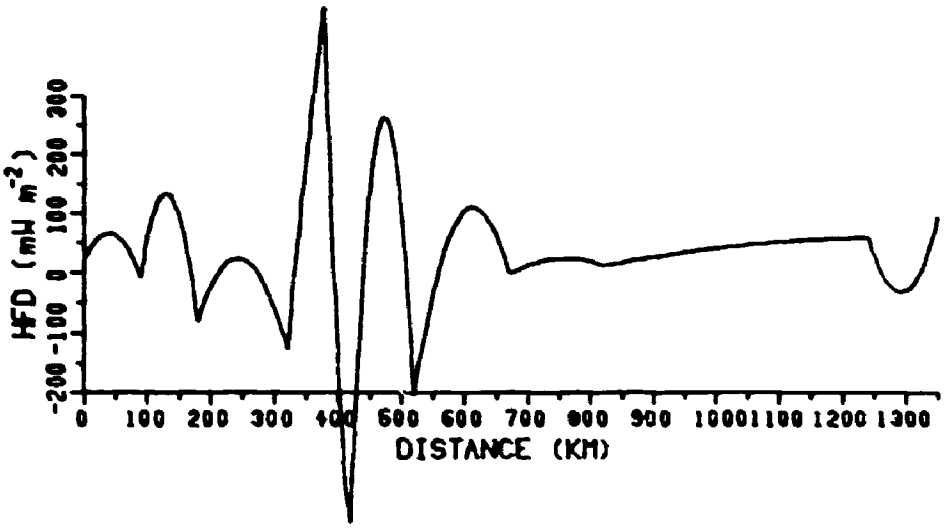

Fig.6.6. The a posteriori background HFD of CEGT1 case 1. The large amplitude oscillations illustrate the instability of the problem when the background HFD and the temperature field are not constrained. The one STD uncertainty range of the HFD is too large to be plotted on this scale.

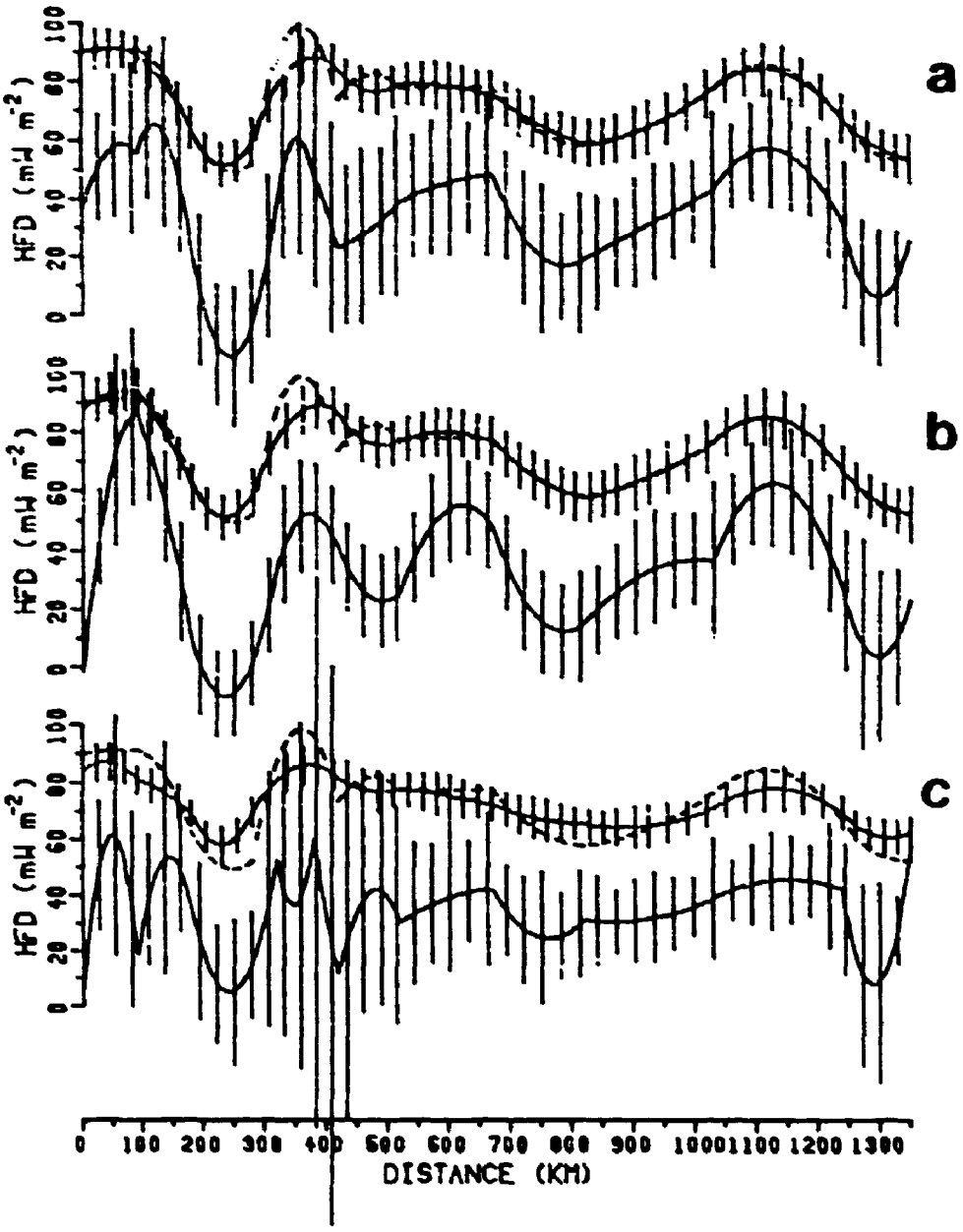

Fig.6.7. The a posteriori background HFDs of CEGT1 case 2, 3 and 4, using the same data as in case 1 but with improved a priori information: (a) Case 2, with smaller STD for the a priori background HFD; (b) Case 3, with nonzero correlation length; (c) Case 4, with a better known temperature field. In each case, the upper and lower solid lines are the a posteriori ground surface HFD and background HFD, respectively, with the one STD uncertainty range represented by the vertical bars, and the dashed line is the observed surface HFD.

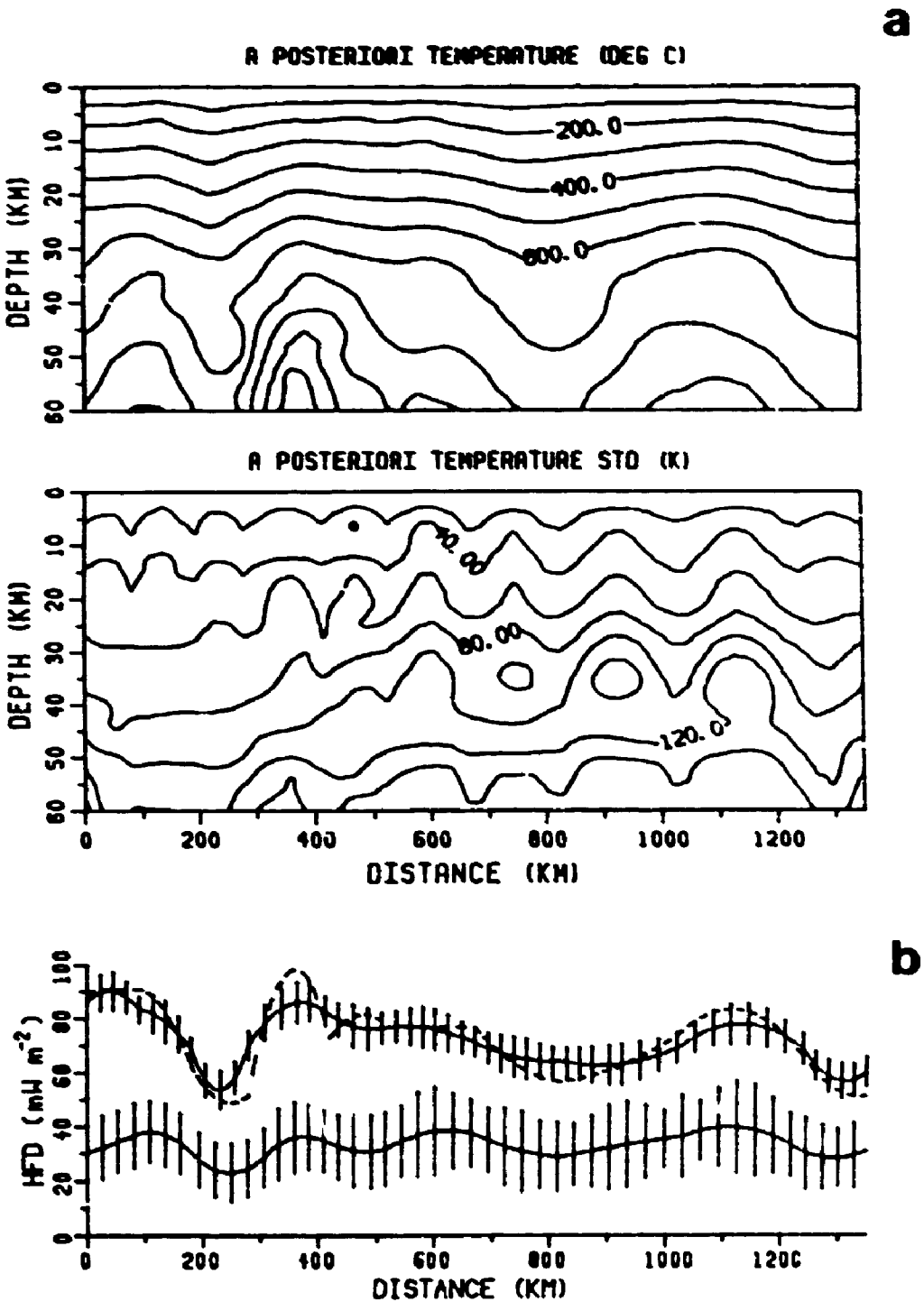

Fig.6.8. The results for CEGT1 case 5. (a) Contour maps of the a posteriori temperature field and STD. (b) The a posteriori background HFD (lower solid line) and ground surface HFD (upper solid line) and the one STD uncertainty range (vertical bars). The dashed line is the observed surface HFD. (c) The a priori and a posteriori values of the material properties. For zone numbers, refer to Fig.6.5.

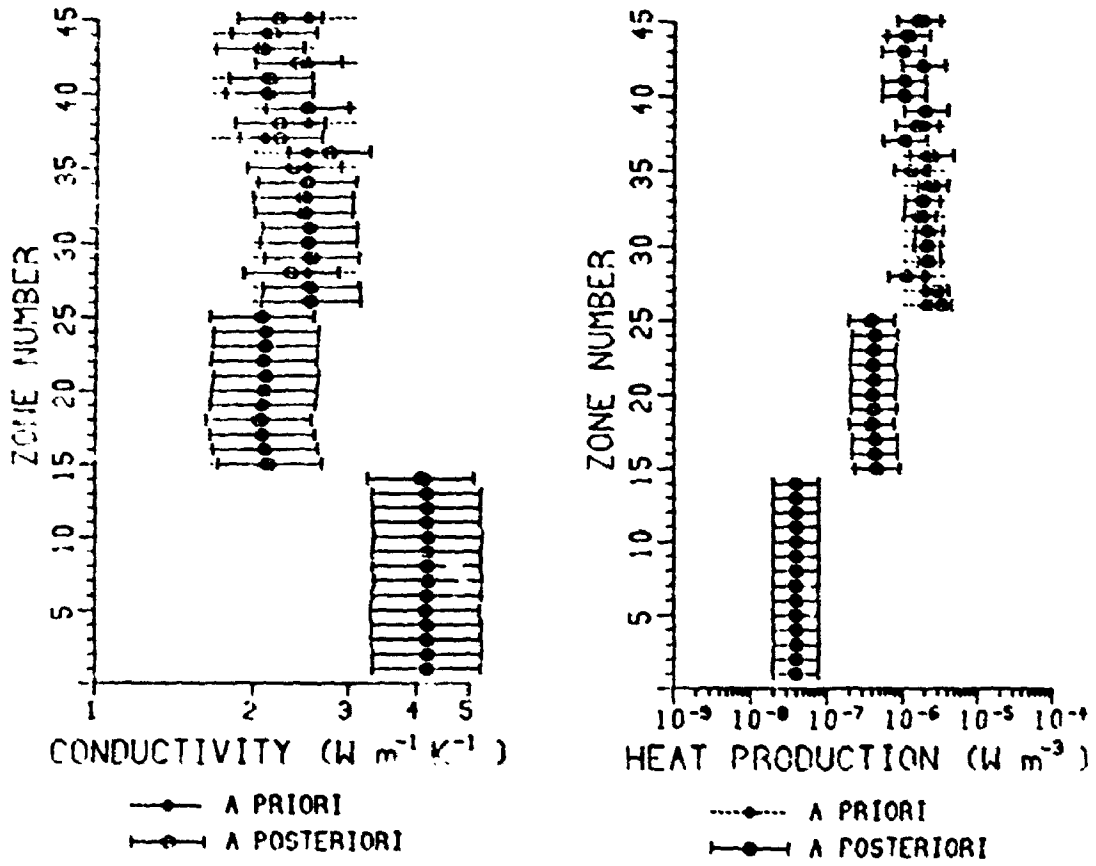

Fig.6.8c. Continued.

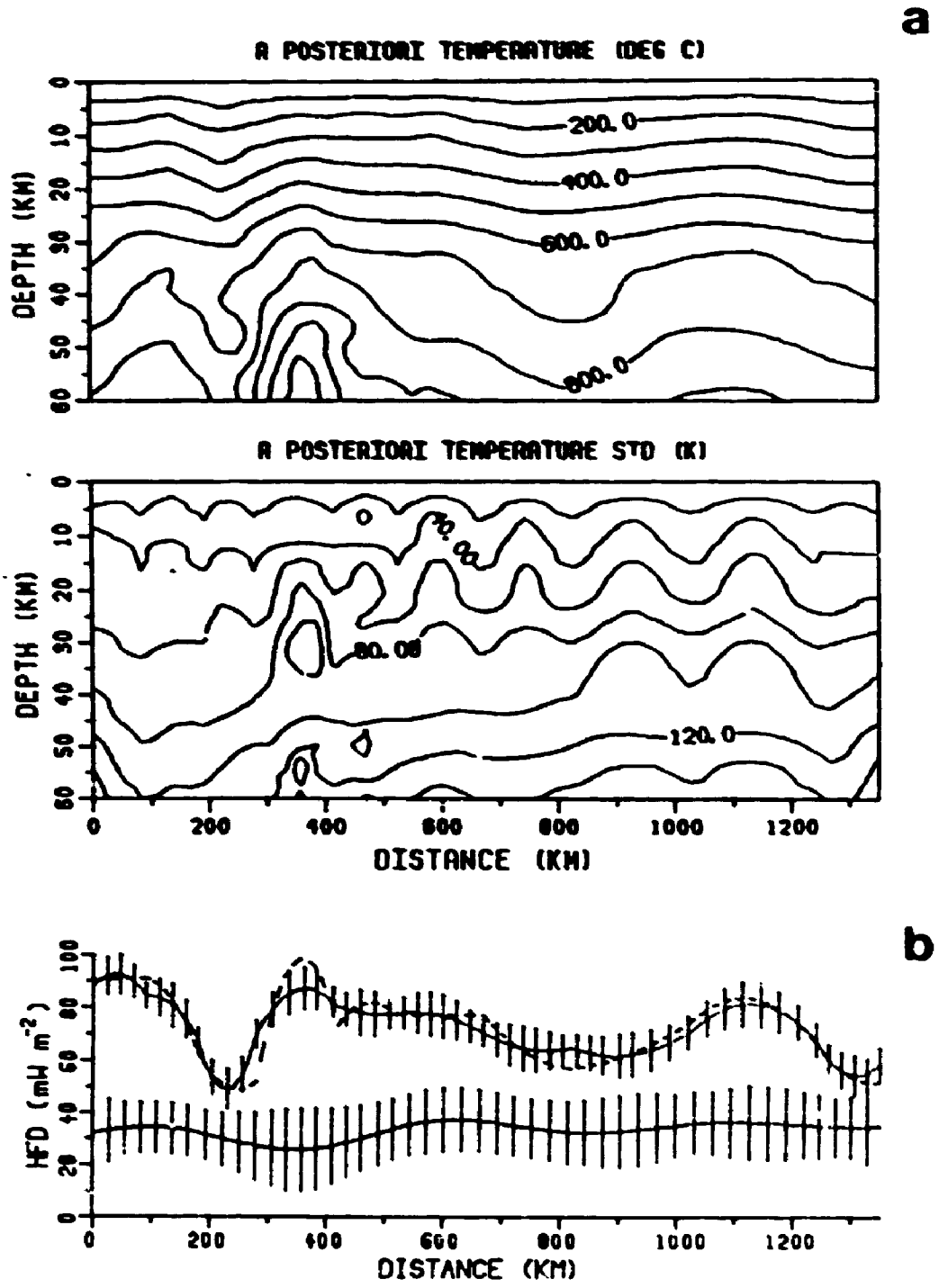

Fig.6.9. The results for CEGT1 case 6. The input is different from case 5 in: a longer correlation length and a smaller STD for the a priori HFD and larger uncertainties in the a priori heat source values. (a) Contour maps of the a posteriori temperature field and STD. (b) The a posteriori background HFD (lower solid line) and ground surface HFD (upper solid line) and the one STD uncertainty range (vertical bars). The dashed line is the observed surface HFD. (c) The a priori and a posteriori values of the material properties. For zone numbers, refer to Fig.6.5.

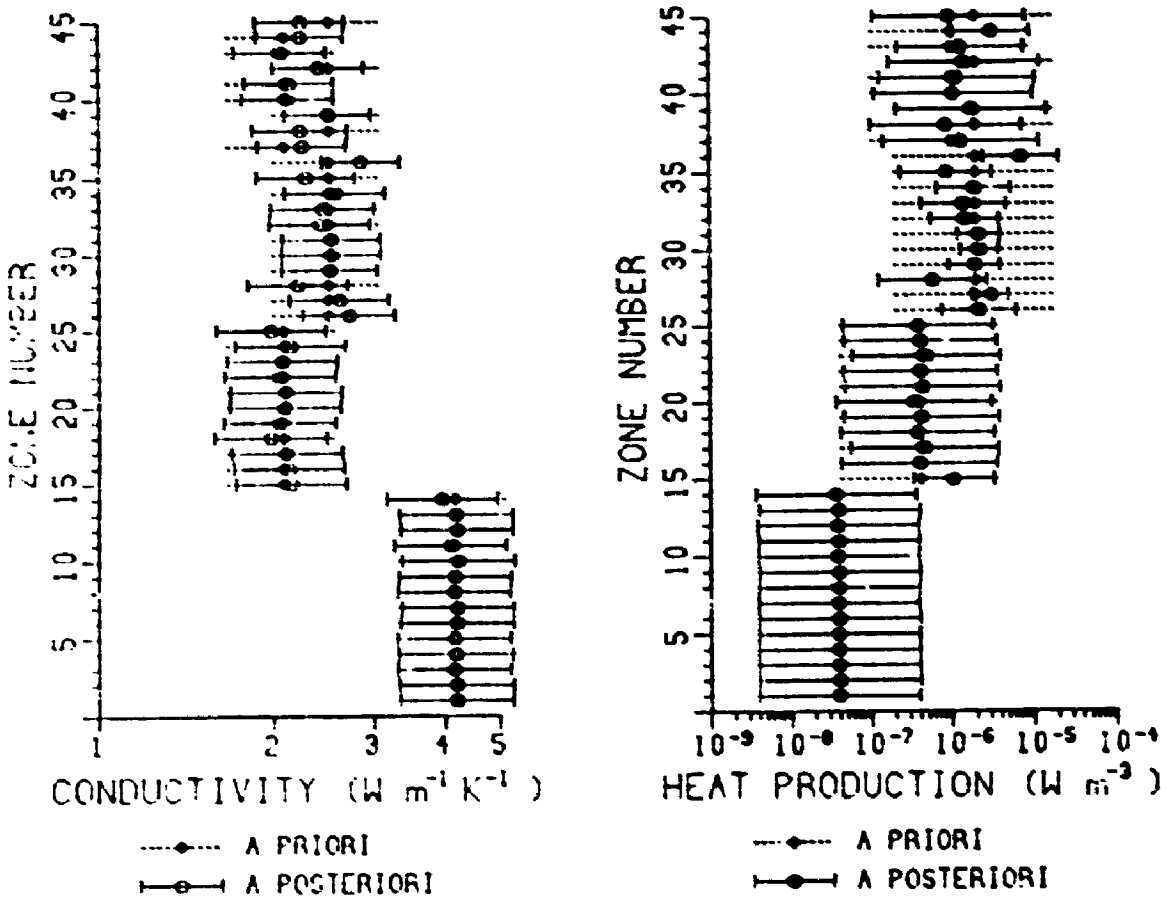

Fig.6.9c. Continued.

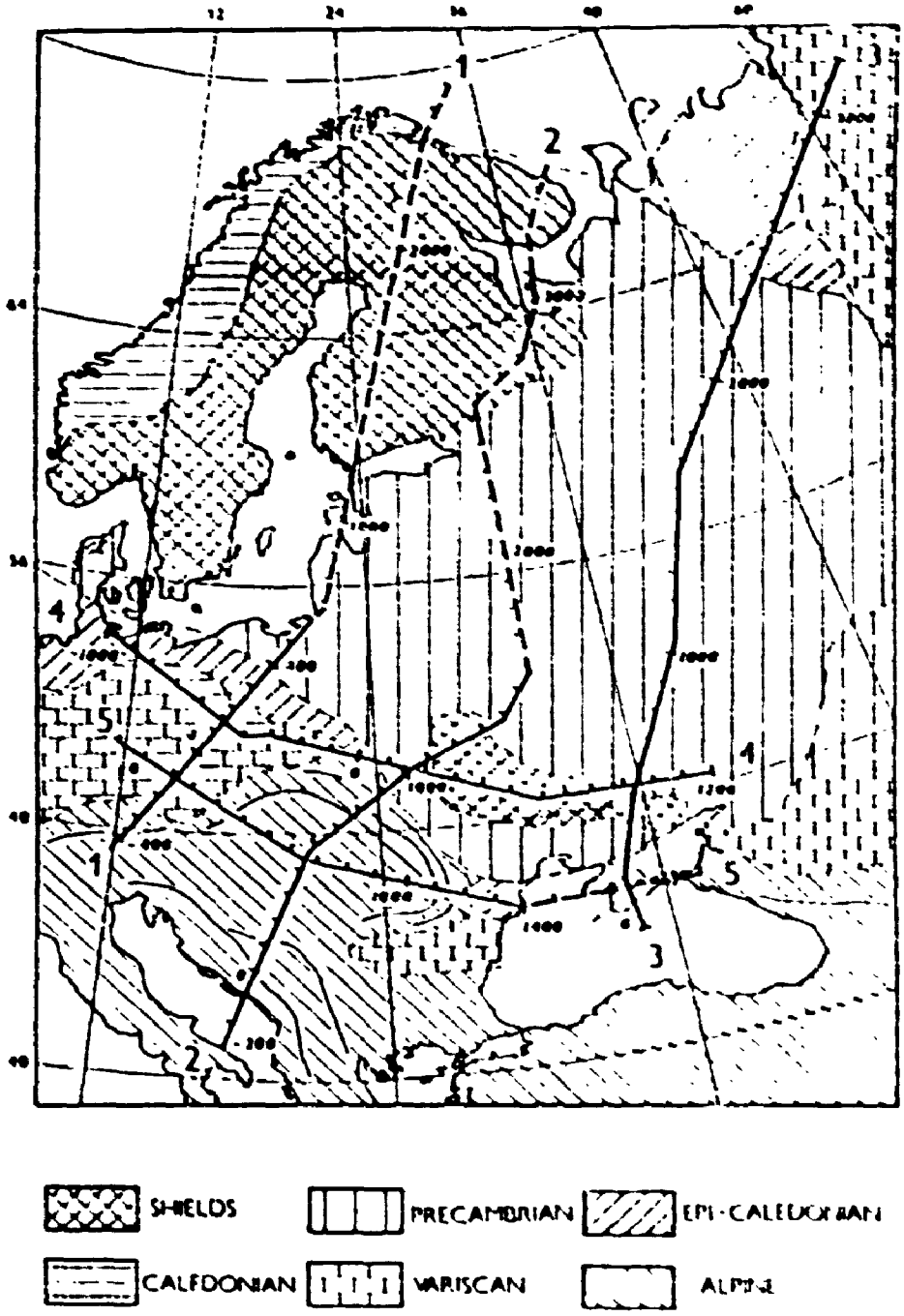

Fig.6.10. Simplified tectonic map for Central and Eastern Europe, with the five geotraverses constructed by Cermak and Bodri (1986) indicated. The broken lines represent proposed but not yet used portions of the geotraverses. After Cermak and Bodri (1986).

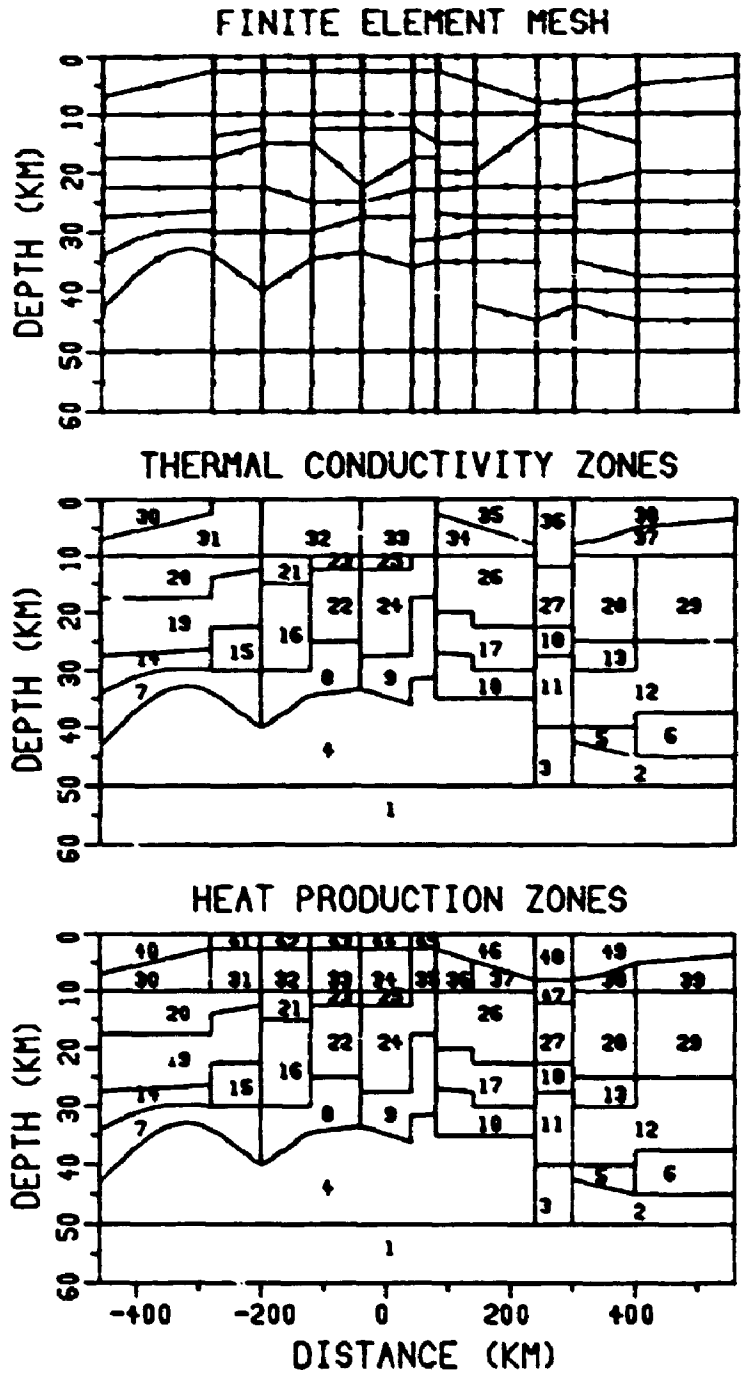

Fig.6.11. The finite element mesh and the material property zones for EEGT1. Nodal points in the finite element mesh are indicated by dots.

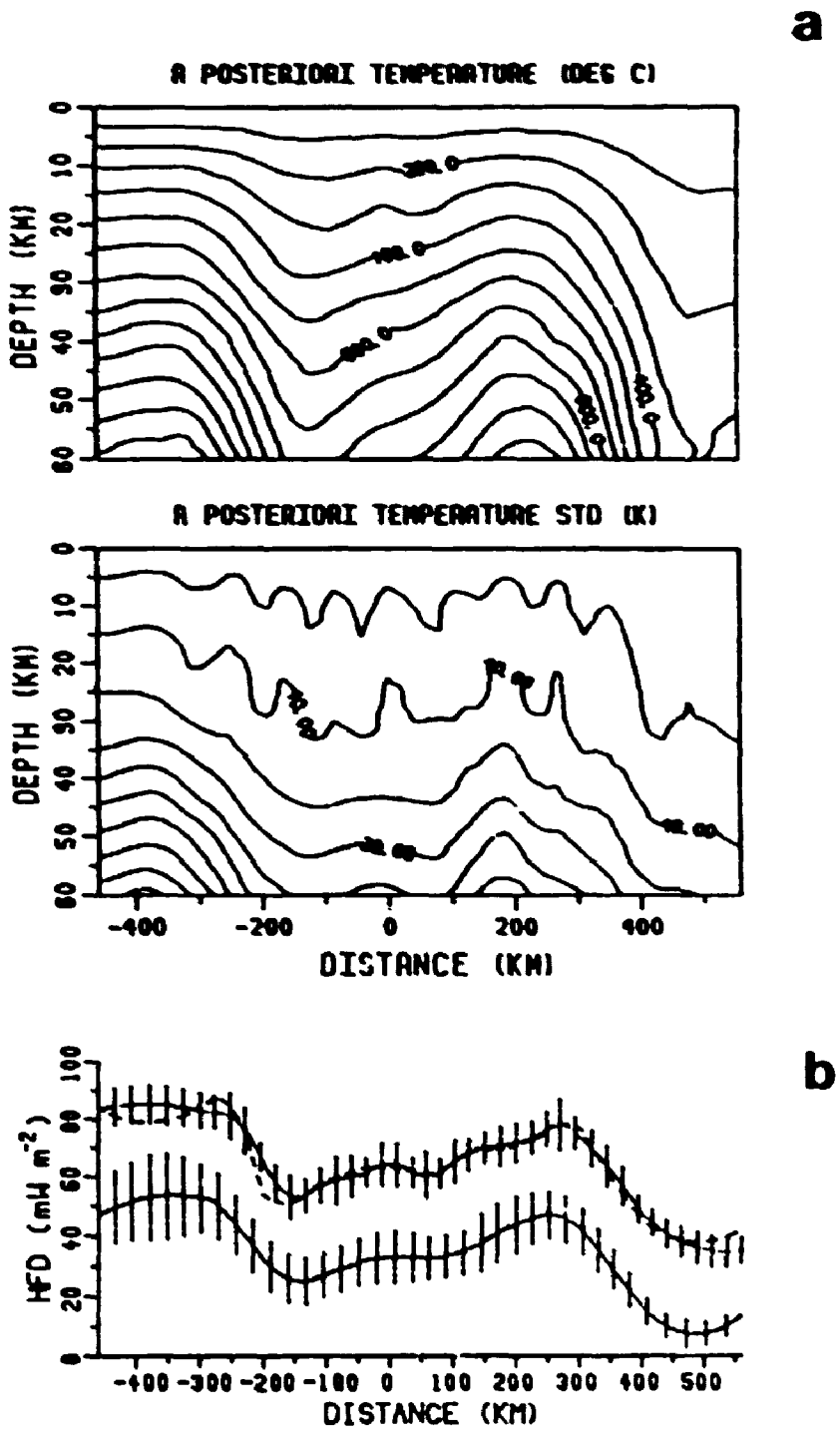

Fig.6.12. The results for EEGT1 case 1. (a) Contour maps of the a posteriori temperature field and STD. (b) The a posteriori background HFD (lower solid line) and ground surface HFD (upper solid line) and the one STD uncertainty range (vertical bars). The dashed line is the observed surface HFD. (c) The a priori and a posteriori values of the material properties. For zone numbers, refer to Fig.6.11.

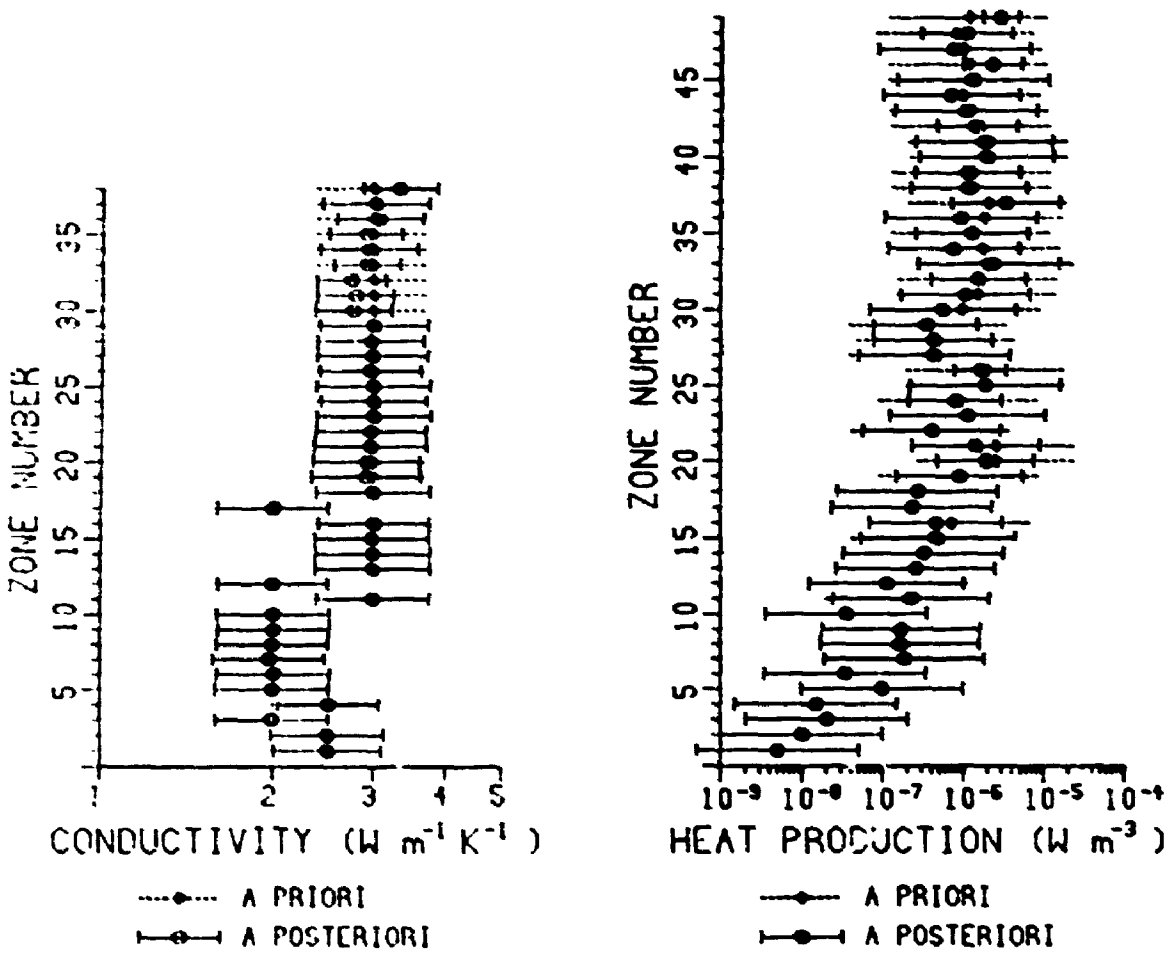

Fig.6.12c. Continued.

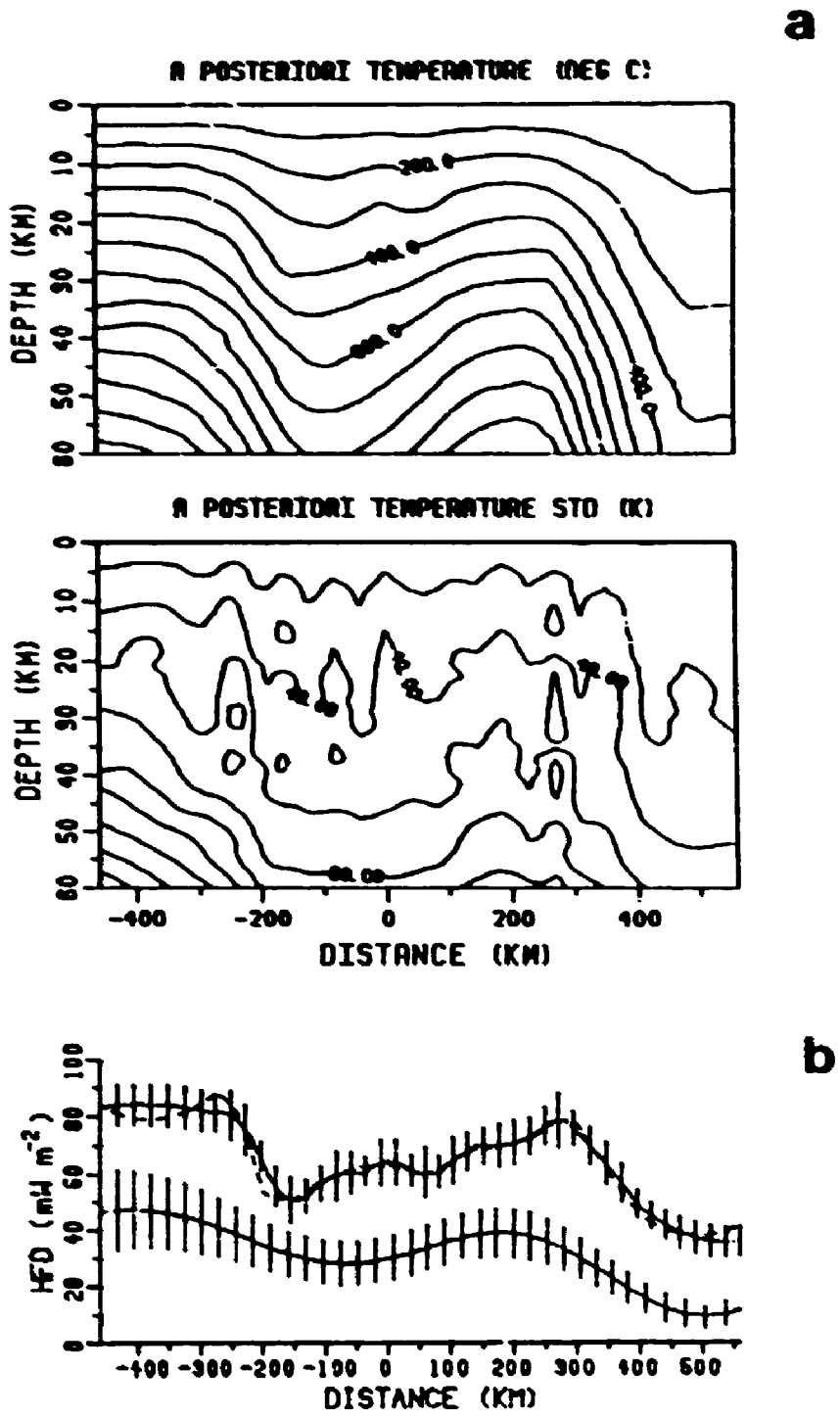

Fig.6.13. The results for EEGT1 case 2. The input is different from case 1 in: a longer correlation length and a smaller STD for the a priori HFD and larger uncertainties in the a priori heat source values. (a) Contour maps of the a posteriori temperature field and STD. (b) The a posteriori background HFD (lower solid line) and ground surface HFD (upper solid line) and the one STD uncertainty range (vertical bars). The dashed line is the observed surface HFD. (c) The a priori and a posteriori values of the material properties. For zone numbers, refer to Fig.6.11.

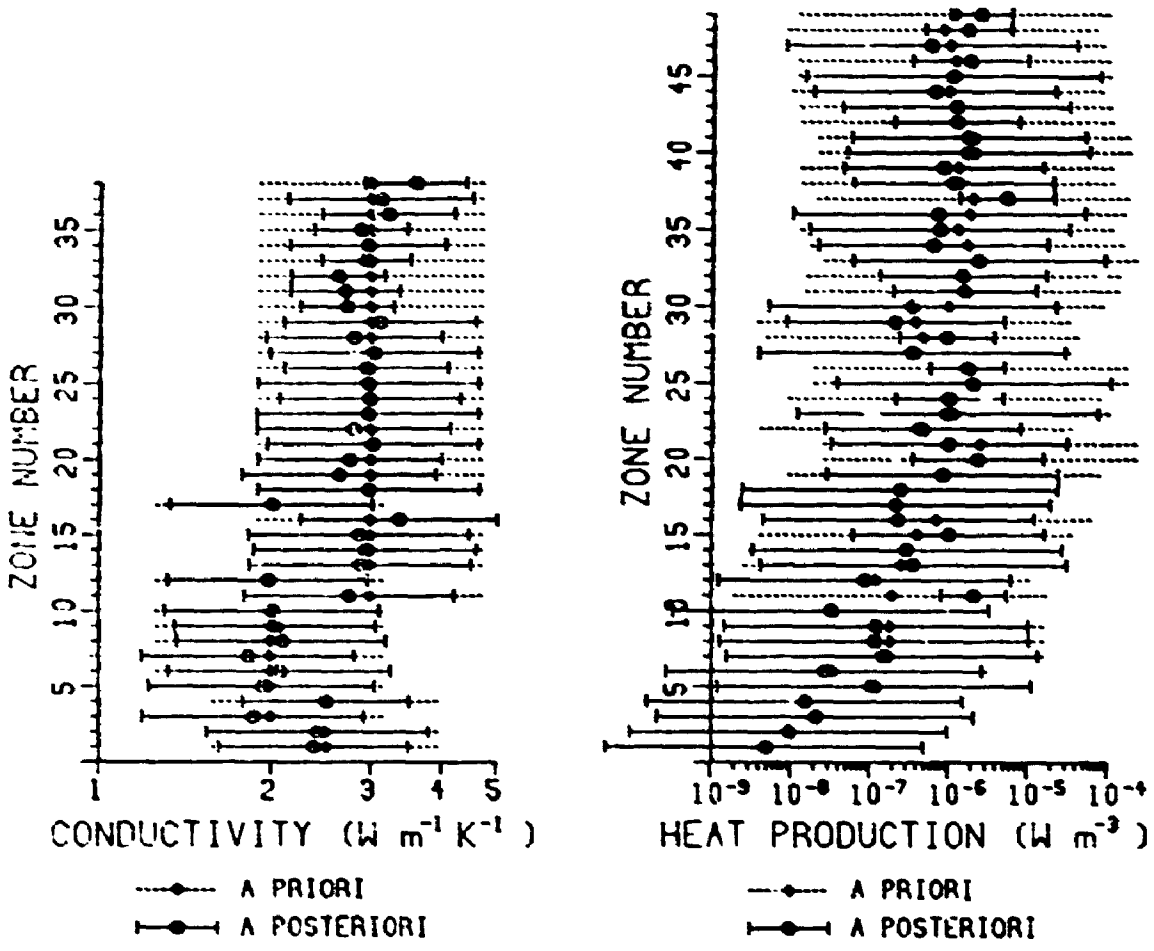

Fig.6.13c. Continued.

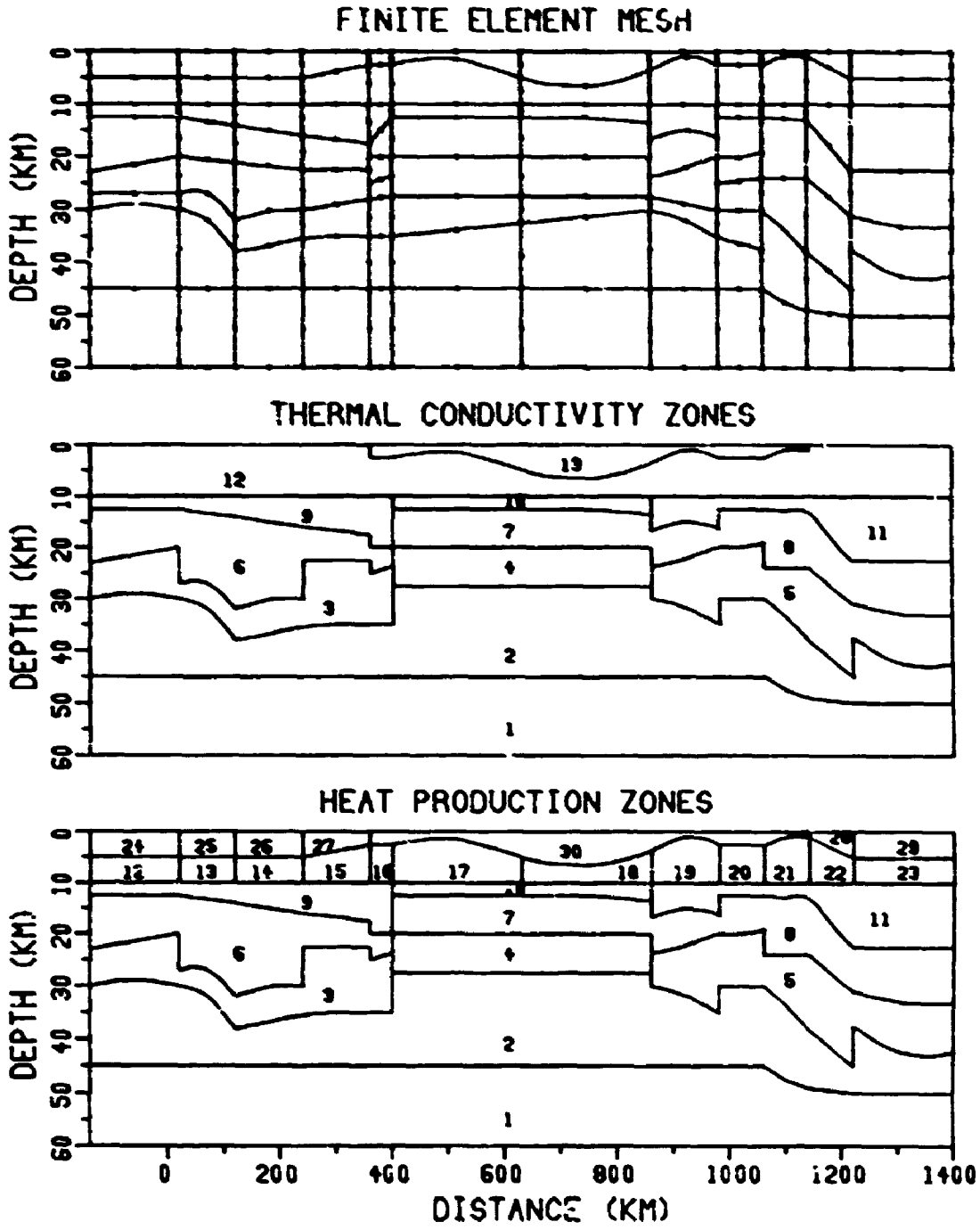

Fig.6.14. The finite element mesh and the material property zones for EEGT5. Nodal points in the finite element mesh are indicated by dots.

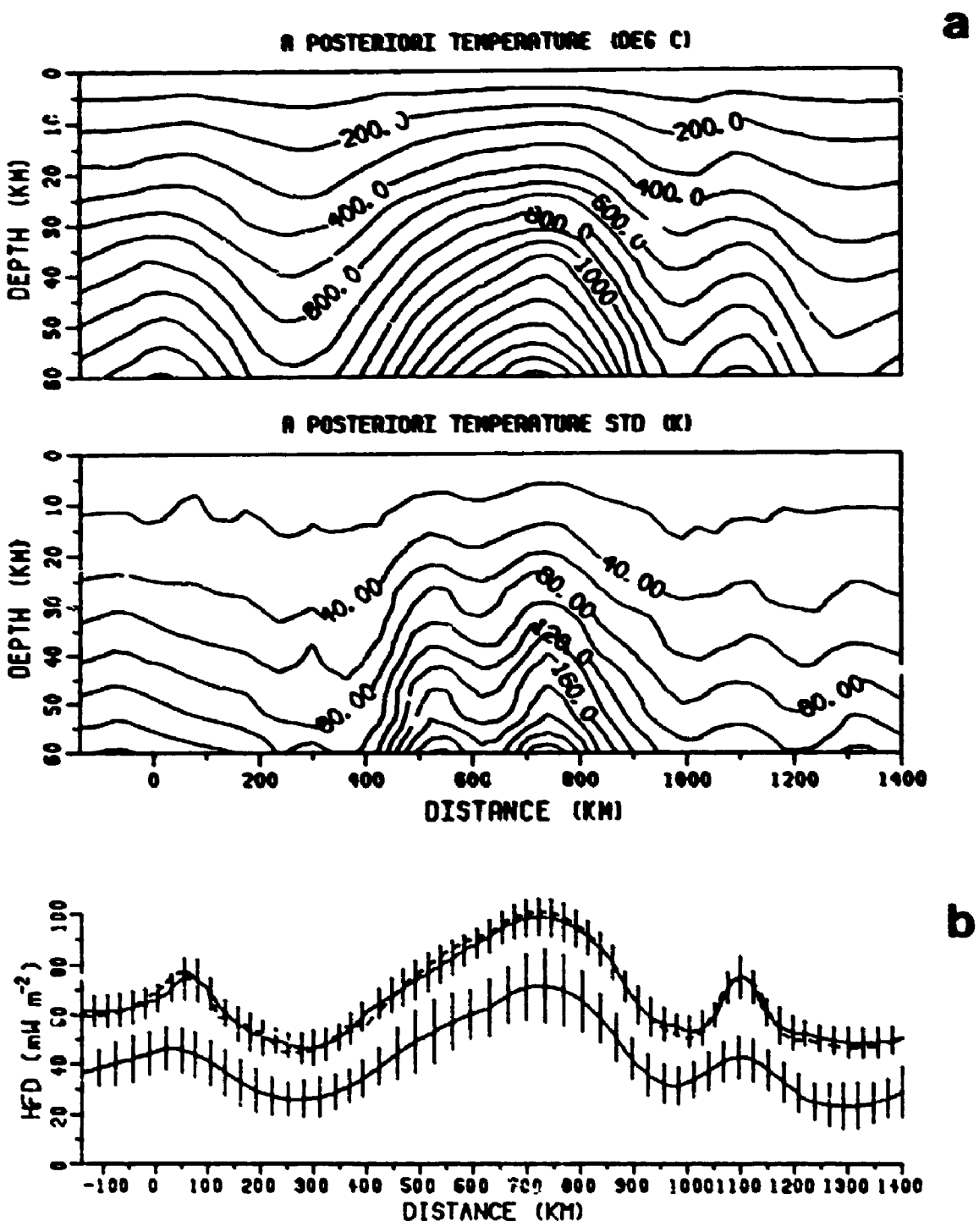

Fig.6.15. The results for EEGT5 case 1. (a) Contour maps of the a posteriori temperature field and STD. (b) The a posteriori background HFD (lower solid line) and ground surface HFD (upper solid line) and the one STD uncertainty range (vertical bars). The dashed line is the observed surface HFD. (c) The a priori and a posteriori values of the material properties. For zone numbers, refer to Fig.6.14.

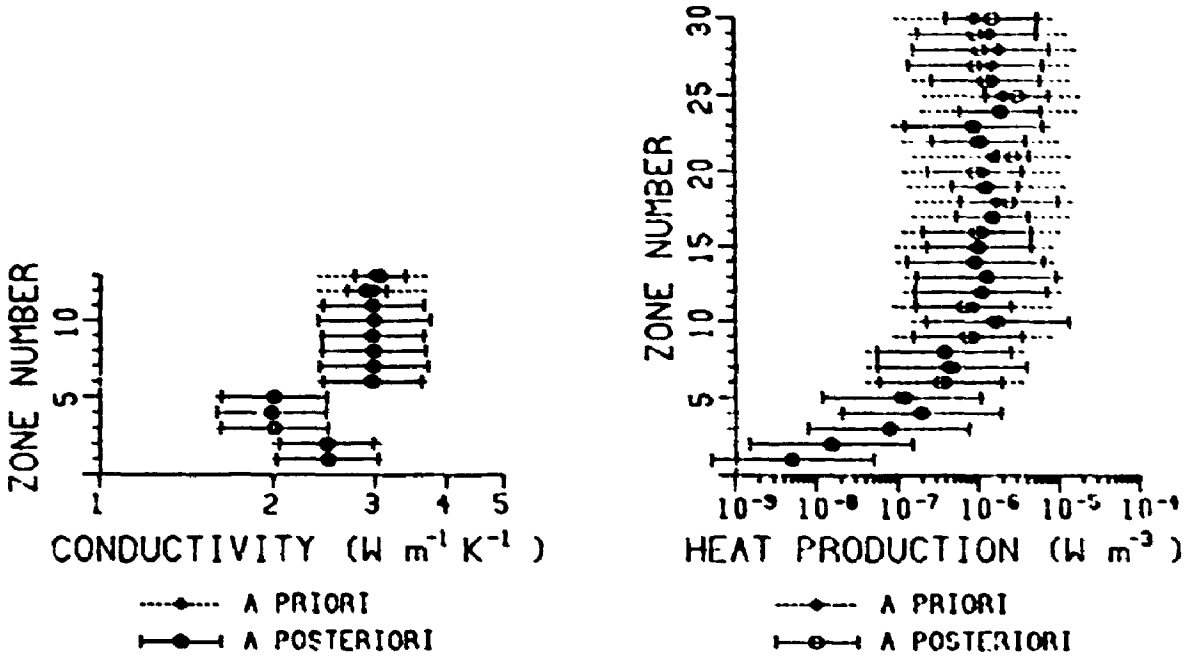

Fig.6.15c. Continued.

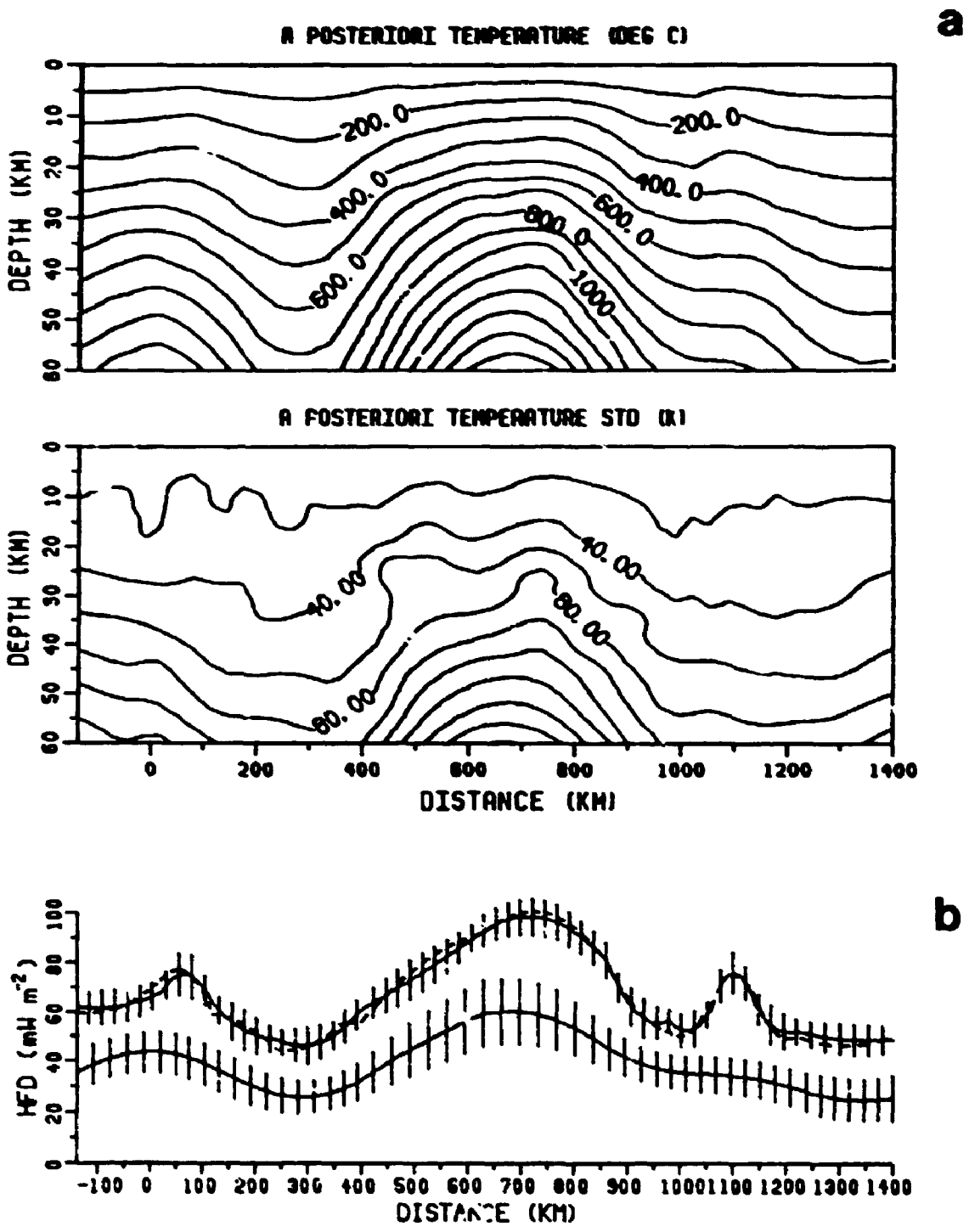

Fig.6.16. The results for EEGT5 case 2. The input is different from case 1 in: a longer correlation length and a smaller STD for the a priori HFD and larger uncertainties in the a priori heat source values. (a) Contour maps of the a posteriori temperature field and STD. (b) The a posteriori background HFD (lower solid line) and ground surface HFD (upper solid line) and the one STD uncertainty range (vertical bars). The dashed line is the observed surface HFD. (c) The a priori and a posteriori values of the material properties. For zone numbers, refer to Fig.6.14.

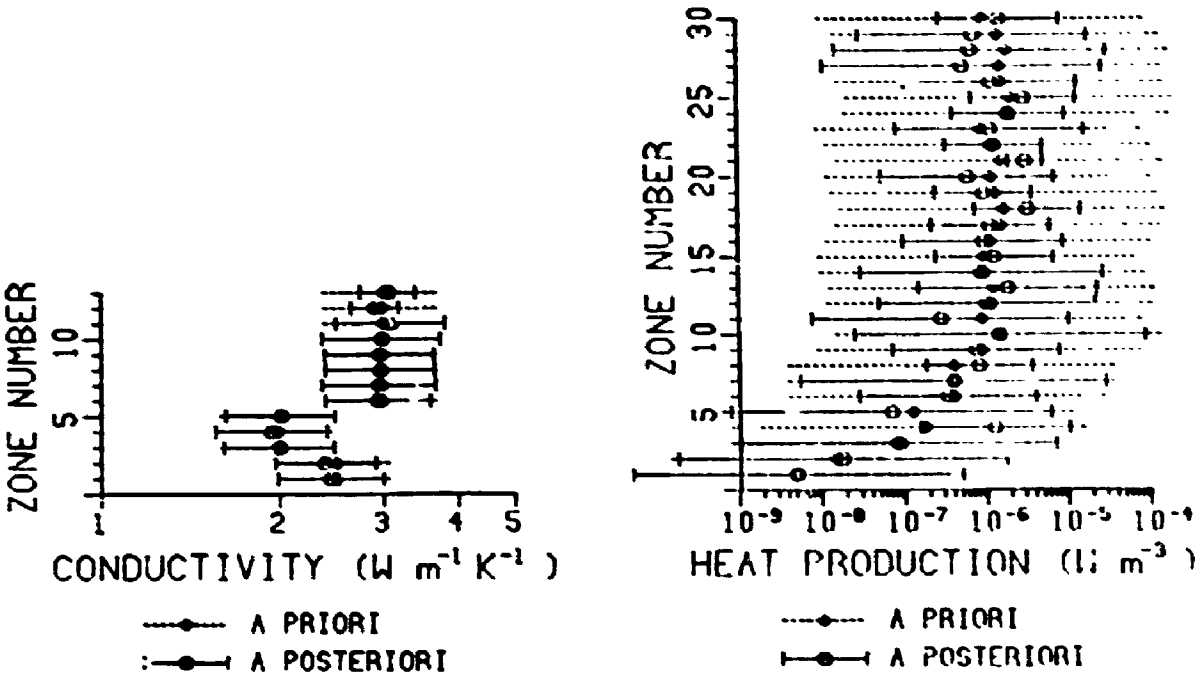

Fig.6.16c. Continued.

CHAPTER 7: COUPLED THERMAL AND HYDROLOGICAL REGIMES

7.1 Introduction

Groundwater movement often provides a much more efficient means of subsurface heat transfer than pure heat conduction; the hydrological and thermal regimes have therefore been studied as coupled systems on various scales for different purposes. Groundwater is often used as part of a cooling system to "dump" waste heat, but thermal pollution could be a potential hazard to the environment and ecology; various aspects of this have been investigated by, e.g., Andrews and Anderson (1978, 1979), Sauty *et al.* (1982a, b), using numerical modeling techniques. In the petroleum industry, heat transport by flowing water is believed to have played an important role in the maturation and migration of oil (e.g., Hitchon, 1984; Gosnold and Fischer, 1986; Jones et al., 1985) and numerical modeling techniques have again been used in various studies (e.g., Garven and Freeze, 1984a,b; Garven, 1985, 1986; Doligez et al., 1986; Burrus and Bessis, 1986).

Hydrodynamic contributions to the geothermal regime have long been of concern to terrestrial heat flow researchers, but it was usual to assume that the effects on the conductive thermal regime were not significant if there were no obvious warning signatures in the temperature – depth plots. However, in recent years it has become more evident that this criterion is not valid and that gravitationally driven groundwater movements may give rise to regional scale advective heat transfer to disturb substantially, and perhaps control, the subsurface temperature field; therefore the HFD determined from near surface

measurements may not be representative of the background (deep seated) values. For example, Majorowicz and Jessop (1981) and Jones et al. (1985) analyzed bottom hole temperature (BHT) data, thermal conductivity and Precambrian basement rock heat generation of the Western Canada sedimentary basin and concluded that groundwater flow is the most plausible reason for the observed uneven surface HFD pattern of low values in the southwest, where groundwater recharge takes place, and high values in the northeast, where groundwater discharge takes place. Their conclusion was supported by the study of the overall groundwater flow pattern of the basin (Hitchon, 1984). A number of other similar cases can be found in the literature, e.g., Chapman et al. (1984), Cermak and Jetel (1985), Wang et al. (1985), Gosnold and Fischer (1986), Willett and Chapman (1987) and Cermak (1989), although some of the interpretations are largely qualitative and some conclusions subject to debate (Bachu, 1985). Numerical modeling of the interaction between the thermal and hydrological regimes of basin scale has been performed by, for example, Mercer et al. (1975), Smith and Chapman (1983), Bethke (1985), Wang et al. (1985), Luheshi and Jackson (1986) and Willett and Chapman (1987) using 2–D models and Woodbury and Smith (1985) using a 3–D model.

The forward numerical simulations of the interaction between the hydrological and thermal regimes have led to much insight into the mechanism of the phenomena. However, because precise knowledge of the parameters and data is usually lacking in numerical modeling, inverse approaches have been gaining attention in this field. When there are sufficient data on the field variables, the very poorly known material properties may be estimated from the data. In hydrologically active regions, that is, in regions where groundwater flow is strong enough to give significant thermal effects, the basal HFD (a Neumann boundary condition), must be estimated from the thermal and hydrological data and

whatever other information that is available. Pioneer work on the simultaneous inversion of thermal and hydrological data to estimate aquifer parameters (system identification) has been done by Kasameyer et al. (1985) with an analytical model and Woodbury and Smith (1988) with a numerical model.

The inverse finite element method for the coupled problem developed in this research can be viewed as a continuation of the work of Woodbury and Smith (1988). The major differences are: 1) a larger depth scale, and hence a wider temperature range, is considered, so that the temperature dependence of water density and dynamic viscosity must be taken into account, with the consequence that equations (2.6) and (2.7) are coupled, and not only the inverse but also the forward problem is nonlinear: 2) in this work, the field variables, material properties and boundary fluxes are all formulated as parameters; and 3) at the parameter estimation stage, a gradient method (the RTV scheme) is used.

In this chapter, the feasibility of applying the inverse finite element method to the coupled problem at a basin scale is investigated using synthetic examples, with particular attention paid to the determination of the basal HFD. Some of the results have already been given in Wang et.al (1989) and Wang and Beck (1989), where the base e logarithmic transform of λ and κ was used. They are recomputed here using base 10 logarithmic transform (section 3.3), which is easier to be visualized in terms of orders of magnitude.

7.2 Model I: a simple synthetic model of basin scale

7.2.1 Description of the model

The model used here is based on an idealized small trough–type sedimentary basin, with the cross–section shown in Fig.7.1. Three sedimentary

formations, each having a distinct thermal conductivity and permeability value (Table 7.1), overlie an impermeable crystalline basement. The first (top) geological unit is an aquitard, the second unit is the major aquifer in the system, and the third unit is a less permeable aquifer. The upper part of the basement is included in the model as the fourth layer. The conductive HFD across the lower boundary of the cross–section is assumed to be unperturbed by the water movement in the overlaying permeable units. The geometrical and structural simplicity of the geological model removes the need to take into account perturbing factors such as the effects of topographic relief and 3–D structure and makes it relatively easy to demonstrate the salient features of the inverse solutions to the coupled problem.

Synthetic data of field variables T and h, are generated from given material property values (Table 7.1) and appropriate boundary conditions, using a forward finite element calculation, which employed a sequential procedure similar to that of Smith and Chapman (1983). The nodal values of the temperature and head fields obtained by the forward calculation are shown in Fig.7.2. These values, together with the logarithmic transform of λ and κ values, are taken as the true values of the components of p, the nonlinear part of the parameter vector P. The true basal HFD across the bottom of the cross–section is taken to be a constant at a typical value of 60 mW m^{-2}. The "measured" ground surface HFD, as well as its noise level, is a function of position (Fig.7.3), and the water table is assumed to coincide with the ground surface; these surface boundary conditions are used in all numerical experiments pertaining to this example. The nodal values of these functions and those of the basal HFD (which may be guessed) constitute the non–zero components of the nodal boundary flux vector q. The two vertical boundaries are assumed to be impermeable and perfectly insulated. For our inverse problem, the "field data" are the values of the parameters together with

their STDs. Our major interest is to determine the basal HFD using data of different quality, but we start with a system identification problem with well known basal HFD.

7.2.2 Case 0, a system identification problem

Because this case is not one of the examples of basal HFD determination, it is called case 0. Other cases using the same geological model are devoted to the problem of basal HFD determination.

With reasonably well known boundary heat fluxes, the inverse method can resolve the field variables and material properties even with noisy data. For example, consider a situation where the basal HFD is accurately known to be 60 mW m^{-2} with a standard deviation (STD) of only 1 mW m^{-2}, but the values of the material properties are unknown. To indicate our lack of knowledge of the material properties ($\log(\lambda)$ and $\log(\kappa)$), we assign to them a priori normal PDFs with erroneous a priori expectations and large STDs (loose constraints) (Table 7.2). To simulate noisy data, the nodal values of T and h obtained from the forward solution are perturbed with Gaussian random noise (Fig.7.4a,b), and then used as the field variable data. Because the availability of accurate measurements and the certainty in the data usually decrease with increasing depth, the noise added to the nodal values of T and h has been given as increasing with depth, as shown in the contour maps of the STDs of T and h (Fig.7.4a,b). The inverse solution shows that the estimates of most of the parameters are close to their true values, but the resolution decreases with increasing depth, as shown by the tabulated values in Table 7.2. There is not much gain in information on the permeability of the third layer and the thermal conductivity of the fourth layer, because of the high noise level in the field variable data at depths. Because the coupled problem is more nonlinear than the pure conduction problem considered in

Chapter 6, the power of the inverse method is more limited by the noise level in the input data. In the current system identification problem, for example, if the noise in the a priori nodal values of T and h is increased by 25%, an almost identical solution can be obtained; but if the noise is increased by 50%, the iteration will not converge, unless better information on the material properties or on the boundary conditions are given.

We now consider the problem of basal HFD determination. In each of the following cases the basal HFD is assumed to be very poorly known a priori, and a constant value of 70 mW m^{-2} is guessed at every lower boundary nodal point; a large STD of 40 mW m^{-2} is assigned to show our ignorance of the HFD value. The correlation length L for the basal HFD will be assigned different values for individual examples. We vary the noise level of other parts of the synthetic data set to examine the information requirement and the limitations of the technique in the problem of basal HFD determination.

7.2.3 Case 1, accurate field variable data

In this case, T and h data contain Gaussian random noise with very small STDs of 0.001 K and 0.1 m, respectively, but the material property values of all geological units are assumed to be unknown. Our objective is to estimate the thermal conductivities and permeabilities of all the geological units and the basal HFD. This is a system identification problem with one very uncertain boundary condition. Since it is assumed that little is known about the material property values, the same loosely constrained homogeneous a priori values of λ and of κ as were used for the previous case are taken (Table 7.3); the correlation length for the basal HFD is taken to be zero. It should be noted that, in this case, both the boundary heat flux and the thermal conductivities of the medium are poorly constrained, while the geothermal gradient is tightly constrained because the

temperature field is almost noise free. For a pure heat conduction problem, it is easy to see from Fourier's law that if the temperature gradient is the only physical quantity that is well constrained, an inverse method will tend to find a proper ratio of HFD and λ but not be able to resolve the HFD and λ separately, as noted by Wang and Beck (1987) and Shen and Beck (1988). The current case involves also convective heat transfer. The head field and its boundary conditions, that is, the water table and the water fluxes at other three impermeable boundaries, are well constrained or perfectly known. The hydrological data provide independent additional information, and thus help to resolve the basal HFD (Fig.7.5) as well as the material properties (Table 7.3).

We briefly examine the response of the solution to the assigned a priori values of the material properties. There can be an infinite number of combinations of different a priori λ and κ values, but the general behavior can be demonstrated by varying κ only. The results are given in Table 7.4. Convergence is defined, using equation (4.17), as when the L_∞ norm of the difference parameter vector at iteration step k, $\mathbf{p}_k - \mathbf{p}_{k-1}$, become less than 0.01 (SI units). Inasmuch as the iteration converged, it was found (results not shown) that all solutions were very similar to those shown in Table.7.3 and Fig.7.5. It is interesting to note that a smaller a priori κ may easily render the solution unstable, but a larger value only tends to cost more iteration steps.

7.2.4 Case 2, accurate material property data

In this case, the values of $\log(\lambda)$ and $\log(\kappa)$ are all accurately known, with STDs of 0.001. The noise levels of the T and h data are the same as in case 0 (Fig.7.4a,b). The objective is to estimate the temperature and head field and the basal HFD. Because the material property values are accurately known and therefore well constrained, this case is similar to a forward problem except that

one boundary condition, the basal HFD, is very uncertain. It is a downward continuation of HFD data in the presence of groundwater flow, and hence instability (as discussed in Chapter 6) is expected to pose problems, as illustrated in the following sub–case.

Case 2a, the above described data set, HFD *correlation length* L = 0. With this data set and the zero correlation for the basal HFD, the RTV iteration scheme converges to T values which are different from the true values in certain regions of the cross–section, as can be seen by comparing the contour maps of the a posteriori nodal values of the temperature field of Fig.7.6 with those of Fig.7.2; consistent with the incorrect temperature field, an incorrect basal HFD distribution is estimated (Fig.7.7a). The situation tends to be worse in the discharge and recharge regions where the vertical component of water movement is prominent, and since the flow of heat in this model is mainly vertical, the thermal and hydrological regimes are strongly coupled. It can be observed in equations (2.6) and (2.7) that, with given material property values, the more strongly coupled the two regimes are, the more nonlinear the problem becomes, and hence the more difficult it is for an iteration scheme to converge to a correct solution when data are noisy (see section 4.2.1 for a discussion on the RTV scheme). If we consider only the quality of the thermal data, there are three possible ways to improve the solution: pre–smoothing the data, assigning a suitable correlation length for the basal HFD, or constraining a few individual data points, as illustrated by the following three sub–cases.

Case 2b, smoother a priori T *and* h *values.* In case 2a, spatially uncorrelated noise was added to the true nodal values of T and h to form a noisy data set, so that there are some drastic, and possibly unrealistic, variations in the a priori T and h patterns as can be seen in Fig.7.6a,b. Since these T and h values were used as initial values for the iteration, the large magnitude errors in them had

an undue influence on the convergence, the problem being sufficiently nonlinear. If the noise in the a priori nodal values of T and h is reduced by 50% but the same variances are used, that is, the initial values are closer to the true solution although the uncertainties in these values remain the same, the results are improved (Fig.7.7b). In a real case, data would likely be processed, e.g., filtered, before being used and hence be smoother than in the synthetic case. Spatial correlations of the input nodal values, which are sometimes obtained by the data processing procedures, may also help to constrain the solution.

Case 2c, HFD *correlation length* L > 0. The assumption of zero correlation length in case 2a allows the basal HFD to have variations of short wave lengths. A correlation length L > 0 may smooth the results. The same case as shown in Fig.7.6 was recomputed with L = 20 km, and the results were obviously improved (Fig.7.7c). However, unless other information is available, either from theoretical or experimental studies, all we know about the spatial correlation of the HFD is that L is unlikely to be zero; the value of L is usually purely subjective information, as in the cases of downward continuation of HFD data considered in Chapter 6.

Case 2d, a few well constrained temperature values. Even without smoothing the data and without choosing L > 0, the solution may be greatly improved by tightly constraining a few temperature points in certain regions; in a real case this would mean that we have to obtain a few accurate borehole temperatures. For example, if the noise in the nodal temperatures at the seven circled points illustrated in Fig.7.6a are reduced to STD = 0.005 K, while those in the other nodal temperatures and the head values remain unchanged, the basal HFD is much better determined in the discharge region (Fig.7.7d); similar comments apply to the recharge region.

Case 2b, 2c and 2d show the possibilities of improving the solution for case

2a in different ways. Based on more numerical experiments, it was found that there are exceptions to the success of the methods in case 2c and 2d, when different realizations of the Gaussian random noise, with the same STDs, are used to "corrupt" the nodal values of temperature and head; i.e., the behavior of the method may depend not only on the probability distribution of the noise but also on the particular realizations. For some realizations, the iteration fails to converge. Such a behavior, which was not observed in the application of the same method to the conduction problems (Chapter 6), is apparently due to the stronger nonlinearity of the coupled problem, and it may be conjectured that the method may even be less robust if the problem is more nonlinear. This calls for further investigation in the future. However, it is interesting to note that many simulations of case 2c and 2d with different realizations of the Gaussian noise were performed, and it was observed that when the solution for case 2c failed, that for case 2d would succeed, and vice versa; no exception was found.

7.2.5 Case 3, field variable and material property data with varying quality

In a realistic situation, some information is often available for each of the physical quantities involved, but neither the field variables nor the material properties are perfectly known, and the data quality will vary from place to place in a study area. To test the inverse method for such a situation, the following case is considered.

The noise in the temperature and head data is the same as in case 0 and case 2a. Some of the material properties are better known than others, but only the thermal conductivity of the first layer (λ_1) is well constrained (Table 7.5). The a priori basal HFD is assumed to have a correlation length L = 20 km. Thus, the information on the field variables and boundary fluxes is the same as in case 2c. The inverse results show that the field variables (Fig.7.8a) and the basal HFD

(Fig.7.8b) are well resolved and that the resolution for the material properties (Table 7.5) decreases with increasing depth.

However, it should be noted that when the a priori information is not sufficient, a reasonable solution may not be obtained. For example, if $\log(\lambda_1)$ is also poorly constrained (STD = 0.1), the iteration does not converge, unless some other parameters are better constrained.

7.2.6 Case 4, accurate material property and h data, almost unknown T

This rather unrealistic but very interesting case is used to illustrate further the important feature of the inverse method, information compensation between different physical quantities.

The a priori information on the material properties is the same as in case 2a, and the head data are the same as in case 1, but the temperature is assumed to be essentially unknown. Ignorance of the temperature field is depicted by large noise in all the nodal temperatures with an identical STD as large as 30 K (Fig.7.9a), which makes the a priori values for this field variable very noisy and virtually unconstrained. Although the temperature data do not contribute to the inversion in a very positive way, the basal HFD is still well resolved (Fig.7.9b). This is because the lack of information on temperature is compensated by good knowledge (well constrained values) of head and material properties. A real situation is unlikely to be as extreme as in this case, but the principles of information compensation prevail. However, information compensation depends on the physical laws involved. Obviously, if the interaction between two physical quantities is weak, the information compensation link is also weak, as was observed by Woodbury and Smith (1988). For example, if the order of magnitude of the second term in equation (2.7) is not comparable to that of the first term, due either to a low Darcian velocity or to the orthogonality of the Darcian velocity

to the temperature gradient, little information on the temperature field can be extracted from the head values, even if they are perfectly known.

7.3 Model II, a more realistic example

Some general features of the solution to the problem of coupled thermal and hydrological regimes at basin scale have been demonstrated by the study of model I in the preceding section. A more realistic situation, i.e., a model that better approximates a real sedimentary basin, requires a finer finite element grid, more nodal points and more material property zones, but in principle, means only more computational cost. Such a model is briefly examined in this section.

The basin model considered here is based on the geological structure of the Rhine Graben as described by Clauser (1988). Rhine Graben is a trough type sedimentary basin in the central Europe which originated 60–45 Ma; and symmetrical normal faulting of the crust under horizontal tensile stress due to the upwelling of upper mantle materials is believed to be the mechanism of its formation. Clauser (1988) carried out a detailed analysis of the thermal and hydrological processes in the basin, and numerically modeled the interaction between the two regimes using a forward finite difference technique. At the present stage, the available data set is insufficient for an inverse modeling. To apply the inverse finite element method, the approach of the preceding section is used, that is, the nodal values of temperature and head are first generated by forward simulation using known geological structure, material property values and boundary conditions, these values are then perturbed with Gaussian random noise and used as the field variable data.

The NW–SE cross–section of the basin is divided into 15 material property

zones (Fig.7.10), each having distinct values of thermal conductivity and permeability. The division of the zones is based on the geological cross–section provided by Munch and Sauer (1979) as referenced by Clauser (1988), with some simplifications such as using highly permeable narrow vertical zones (zones 10, 11 and 12 in Fig.7.10) to represent fault zones (these "narrow" zones are probably still much too wide to be realistic). The spatial scale of the detailed structure of the simplified cross–section may not closely follow that of the real situation. The material property values for these zones, shown in Table 7.6 and 7.7 as the "true values", are based on the information provided by Clauser (1988). In Clauser (1988), seven rock types were identified, each of which was assigned a thermal conductivity value and a permeability value; for better flexibility, more zones are used in this inversion. For example, three zones (10, 11 and 12) are used for the highly permeable fault zone material, and five zones (1 through 5) are used for the very low permeability crystalline basement rocks.

Across the lower boundary of the cross–section, there is a constant vertical HFD of 80 mW m^{-2} but no water flux. Again, the two vertical boundaries are assumed to be impermeable insulators. The water table is approximated by the ground surface, which is assumed to be the 10 °C isotherm. With these boundary conditions and the "true" material property values, the "true" nodal values of the field variables are obtained by a forward simulation as described in section 7.2.1, and are shown in Fig.7.11.

In the inverse modeling, uncertainties in the physical quantities are simulated as follows. The basal HFD is assumed to be very poorly known, and a guessed constant value of 60 mW m^{-2} is used as the a priori value, with an STD of 40 mW m^{-2} and a correlation length L = 20 km. Some of the material properties are assumed better known than others (Table 7.6 and 7.7). The low permeability value (10^{-20} m^2) of the basement rocks (zones 1 through 5) is tightly constrained

because we know that the rocks are almost impermeable; the hydrological information of these zones will later be shown to be of little importance. The position of the water table is assumed to be accurately known (STD = 0.1 m). The ground surface HFD distribution is not used as a Neumann boundary condition, but instead, the nodal temperatures at and above the zero elevation are assumed to be accurately known (STD = 0.001 K). This is nearly equivalent to an uncertain surface HFD condition because some the a priori thermal conductivities above the zero elevation are poorly constrained. All the a priori nodal values of the temperature and head fields contain Gaussian random noise, with the STDs increasing with depth, as shown in Fig.7.12 and 7.13.

The temperature field has been well resolved (Fig.7.14). It is not surprising that the head field in the basement rocks is almost unresolved (see both the contour maps of the a posteriori nodal values and of the STDs in Fig.7.15). With a permeability as low as 10^{-20} m^2, the Darcian velocities in these rocks are so small that the contributions of the water flow in these regions to the whole flow system is insignificant. The thermal data cannot provide noticeable help because of the weak interaction between the heat and water flows at such low Darcian velocity (see discussion in section 7.2.6). Similar comments apply to the head values in zone 9, which also has a low permeability. In the other zones, the resolution of the head values is much better, as shown by the a posteriori STDs in Fig.7.15. The results for the material properties are tabulated in Table 7.6, for the thermal conductivities and Table 7.7, for the permeabilities. The resolution of the material property values depends on their a priori values and STDs, the quality of the field variable data, the magnitude of the Darcian velocity, the magnitude of the true permeability and therefore the interactions between the thermal and hydrological regimes in each particular zone. The accurately known and well constrained material property values of zone 15 obviously influence the resolution of the values

of the neighboring zones (5 and 12). The basal HFD is well resolved (Fig.7.16), with the best resolution occurring beneath zone 15.

7.4 Conclusions and discussions

The inverse finite element method has been applied to the problem of the coupled thermal and hydrological regimes of basin scale. Based on two synthetic models, the following conclusions can be drawn.

1) With reasonably sufficient data, the gradient method for the Bayesian parameter estimation (the RTV scheme) can be used to solved the inverse problem of the coupled thermal and hydrological regimes.

2) When the two regimes are closely coupled, they should be considered simultaneously and the coupling should be included in the mathematical model of the problem. The information on one regime may help to improve knowledge of the other, depending on the strength of the interaction between the two.

3) While the interaction between the heat flow and water flow provides the information link between the two regimes, the coupling also increases the nonlinearity of the problem. The performance of the inverse method for the coupled problem therefore depends more on the quality of data and a priori information than for the pure conduction problem.

4) Similar to the problem of downward continuation of HFD data discussed in Chapter 6, some knowledge about the correlation length for the a priori basal HFD may be essential for obtaining a solution.

In the presence of convective heat transfer, the element size is a major concern in forward numerical modeling using finite element techniques, because the convective term in the heat transfer equation (2.7) may result in large

off–diagonal entries in the conductivity matrix and cause numerical instabilities (Huyakorn and Pinder, 1983). With the quadratic isoparametric finite element model, it is possible to use quite large elements. The forward solution for the simple synthetic example in section 7.2 (Fig.7.2) was compared with the solution for the same problem but obtained using a much finer finite element mesh (483 nodal points and 144 elements), and the results were found to be nearly identical.

The maximum temperature in model II is nearly 200 °C. At such high temperatures the linear approximation for the density ρ and dynamic viscosity μ of water, equation (2.11) and (2.12) as functions of temperature will not be valid. However, the bottom part, about 2 km thickness, of the basin model in this example is mostly occupied by nearly impermeable basement rocks, and the significant thermal effects of water flow occur only in the overlaying aquifer formations and fault zones. For the temperature range in the upper part of the model, the linear approximations for ρ and μ are valid.

Table 7.1. Material property values for model I (refer to Fig.7.2 for the zone numbers).

zone number	λ Value ($W\ m^{-1}K^{-1}$)	κ value ($10^{-15}\ m^2$)
1	2.0	0.05
2	2.0	10.0
3	2.5	1.0
4	3.0	0.0

Table 7.2. A priori and a posteriori material property values for case 0 (model I): a system identification problem. The thermal conductivity λ is in W $m^{-1}K^{-1}$, the permeability κ in 10^{-15} m^{-2} (refer to Fig.7.1 for zone numbers).

Parameter	True Value	A priori Value	A priori Log STD	A posteriori Value	A posteriori Log STD
λ_1	2.0	2.5	0.1	1.992	0.011
λ_2	2.0	2.5	0.1	1.939	0.018
λ_3	2.5	2.5	0.1	2.516	0.031
λ_4	3.0	2.5	0.1	2.674	0.045
κ_1	0.05	1.0	1.0	0.050	0.053
κ_2	10.0	1.0	1.0	10.076	0.097
κ_3	1.0	1.0	1.0	0.675	0.413

Table 7.3. A priori and a posteriori material property values for case 1 (model I): accurate field variable data. The thermal conductivity λ is in W $m^{-1}K^{-1}$, the permeability κ in 10^{-15} m^{-2} (refer to Fig.7.1 for zone numbers).

Parameter	True Value	A priori Value	A priori Log STD	A posteriori Value	A posteriori Log STD
λ_1	2.0	2.5	0.1	1.988	0.017
λ_2	2.0	2.5	0.1	1.988	0.017
λ_3	2.5	2.5	0.1	2.486	0.017
λ_4	3.0	2.5	0.1	2.983	0.017
κ_1	0.05	1.0	1.0	0.050	0.017
κ_2	10.0	1.0	1.0	9.944	0.017
κ_3	1.0	1.0	1.0	0.991	0.017

Table 7.4. Convergence behaviour of the solution for case 1 (model I), responding to different a priori permeability κ values. The a priori values of λ and κ are uniformly constant (a priori thermal conductivity $\lambda = 2.5$ W m^{-1}K^{-1} in all cases). The true values are shown in Table 7.1.

κ value (m^2)	Log STD	Convergence Behaviour
10^{-6}	10.0	27 iterations
10^{-7}	9.0	25 iterations
10^{-8}	8.0	22 iterations
10^{-9}	7.0	20 iterations
10^{-10}	6.0	18 iterations
10^{-11}	5.0	15 iterations
10^{-12}	4.0	13 iterations
10^{-13}	3.0	11 iterations
10^{-14}	2.0	9 iterations
10^{-15}	1.0	6 iterations
10^{-16}	2.0	18 iterations
10^{-17}	3.0	27 iterations
10^{-18}	4.0	40 iterations
10^{-19}	5.0	non–convergent

Table 7.5. A priori and a posteriori material property values for case 3 (model 1): field variable and material property data vary in quality. The thermal conductivity λ is in $W\ m^{-1}K^{-1}$, the permeability κ in $10^{-15}\ m^2$ (refer to Fig.7.1 for zone numbers).

Parameter	True Value	A priori Value	A priori Log STD	A posteriori Value	A posteriori Log STD
λ_1	2.0	2.0	0.0005	2.000	0.0005
λ_2	2.0	1.9	0.05	1.911	0.021
λ_3	2.5	2.5	0.1	2.501	0.031
λ_4	3.0	3.3	0.1	2.838	0.048
κ_1	0.05	0.01	0.5	0.048	0.060
κ_2	10.0	1.0	1.0	9.961	0.095
κ_3	1.0	1.0	1.0	0.489	0.666

Table 7.6. A priori and a posteriori thermal conductivity values (W $m^{-1}K^{-1}$) for model II (refer to Fig.7.10 for zone numbers).

Zone number	true Value	A priori Value	A priori Log STD	A posteriori Value	A posteriori Log STD
1	3.4	3.4	0.1	3.467	0.020
2	3.4	3.3	0.1	3.235	0.025
3	3.4	3.4	0.1	3.379	0.015
4	3.4	3.4	0.1	3.589	0.038
5	3.4	3.4	0.1	3.333	0.008
6	3.4	3.4	0.1	3.340	0.034
7	2.8	3.0	0.2	2.834	0.030
8	2.1	2.0	0.1	2.059	0.017
9	2.1	2.1	0.1	2.078	0.009
10	2.5	2.4	0.1	2.206	0.033
11	2.5	2.3	0.1	2.328	0.063
12	2.5	2.5	0.1	2.441	0.011
13	2.8	2.8	0.1	2.772	0.013
14	2.5	2.5	0.05	2.466	0.010
15	2.8	2.8	0.0001	2.800	0.0001

Table 7.7. A priori and a posteriori logarithmic permeability values ($\log(\kappa)$) for model II (refer to Fig.7.10 for zone numbers). Example: −20.0 represents a permeability value of 10^{-20} m^2.

Zone number	true Value	A priori Value	STD	A posteriori Value	STD
1	−20.0	−20.0	0.0001	−20.0	0.0001
2	−20.0	−20.0	0.0001	−20.0	0.0001
3	−20.0	−20.0	0.0001	−20.0	0.0001
4	−20.0	−20.0	0.0001	−20.0	0.0001
5	−20.0	−20.0	0.0001	−20.0	0.0001
6	−16.0	−15.0	1.0	−18.0	0.430
7	−15.0	−15.0	1.0	−15.0	0.098
8	−16.0	−15.0	1.0	−15.3	0.407
9	−18.0	−17.0	1.0	−17.8	0.595
10	−14.0	−15.0	1.0	−15.8	0.258
11	−14.0	−12.0	1.0	−13.4	0.083
12	−14.0	−14.0	0.1	−14.0	0.010
13	−15.0	−15.0	0.1	−15.0	0.011
14	−14.0	−14.0	0.5	−13.7	0.450
15	−15.0	−15.0	0.05	−15.0	0.002

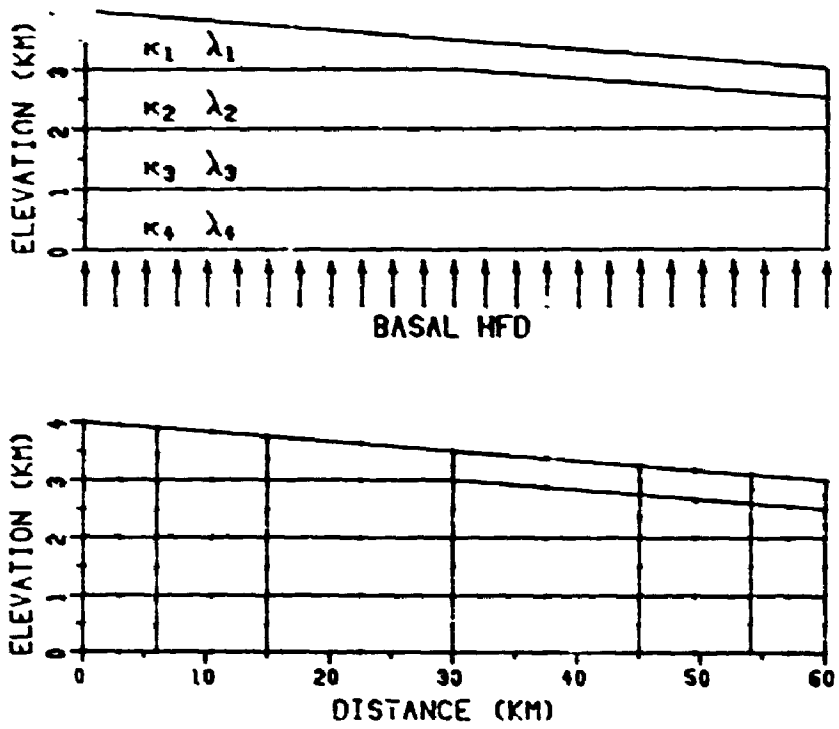

Fig.7.1. The material property zones and the finite element mesh for model I of the coupled problem. Nodal points in the finite element mesh are indicated by dots. The thermal conductivity and permeability values are listed in Table 7.1.

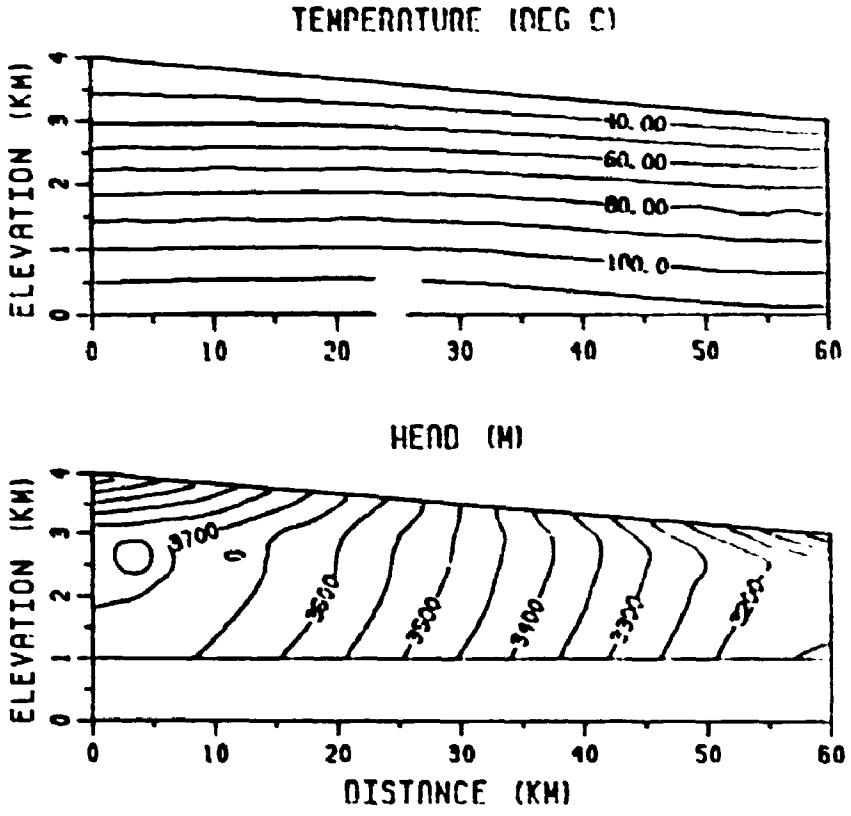

Fig.7.2. The "true" temperature and head fields of model I, obtained by forward calculation, for subsequent inversion; note that the reference hydraulic head as defined in the text is not a potential, and is therefore difficult to interpret visually. The results using a much finer mesh (483 nodal points and 144 elements) are essentially identical.

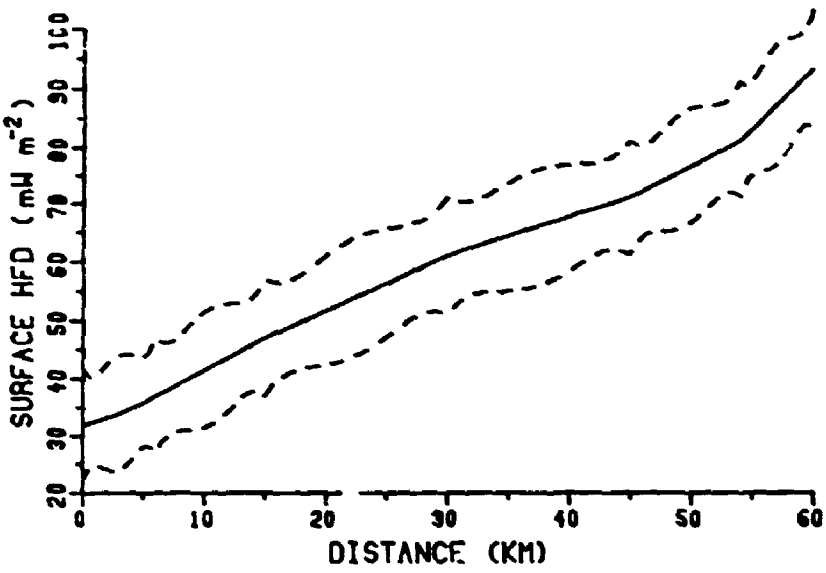

Fig.7.3. The nearsurface HFD distribution used as the upper thermal boundary conditio. for all the inverse solutions for model I. The dashed lines represent one STD uncertainty range.

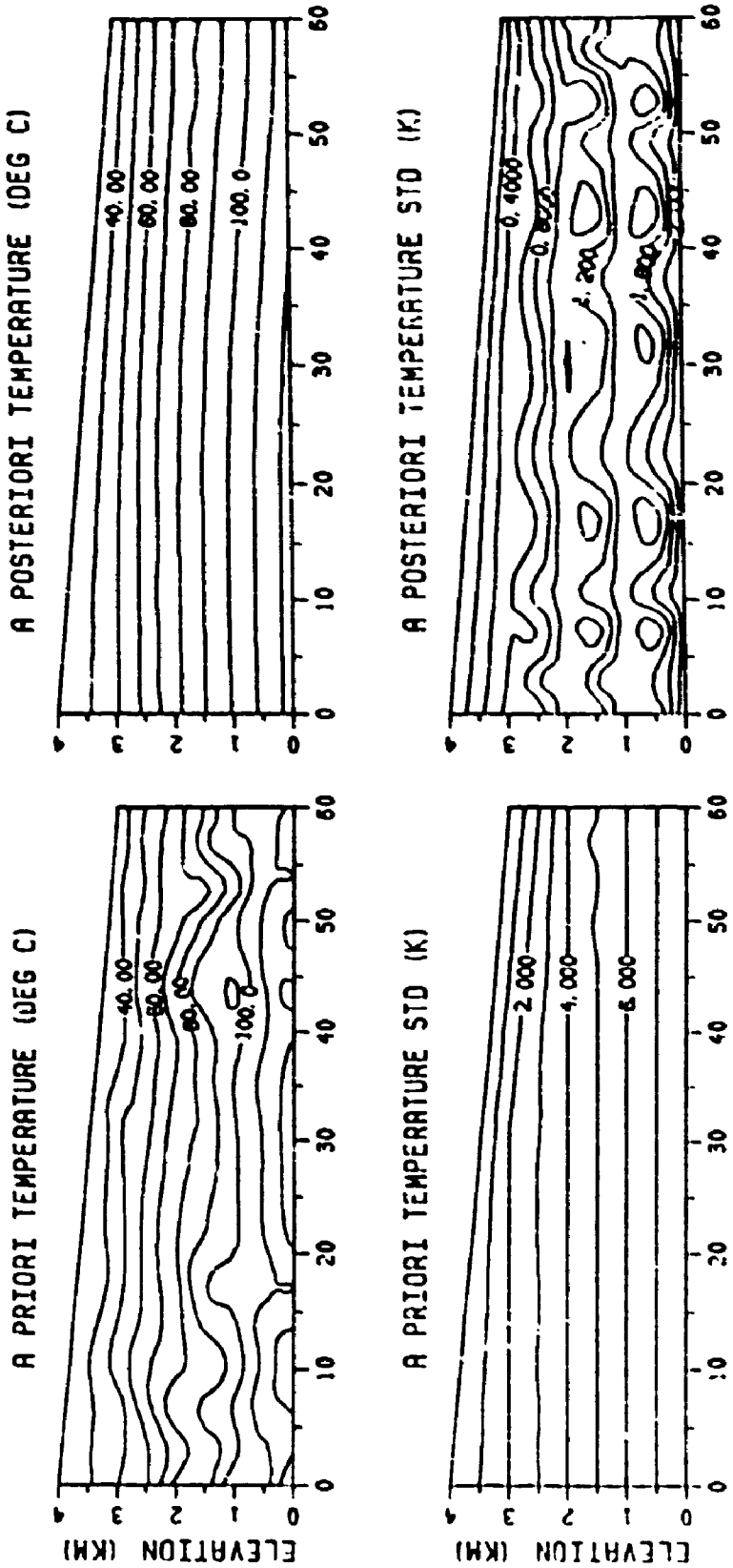

Fig.7.4. The results for case 0, model I: the material property values are poorly known (see Table7.2) and the STDs of noise in temperature and head data increase with depth. (a) Contour maps of nodal values and STDs for temperature. (b) Contour maps of nodal values and STDs for head.

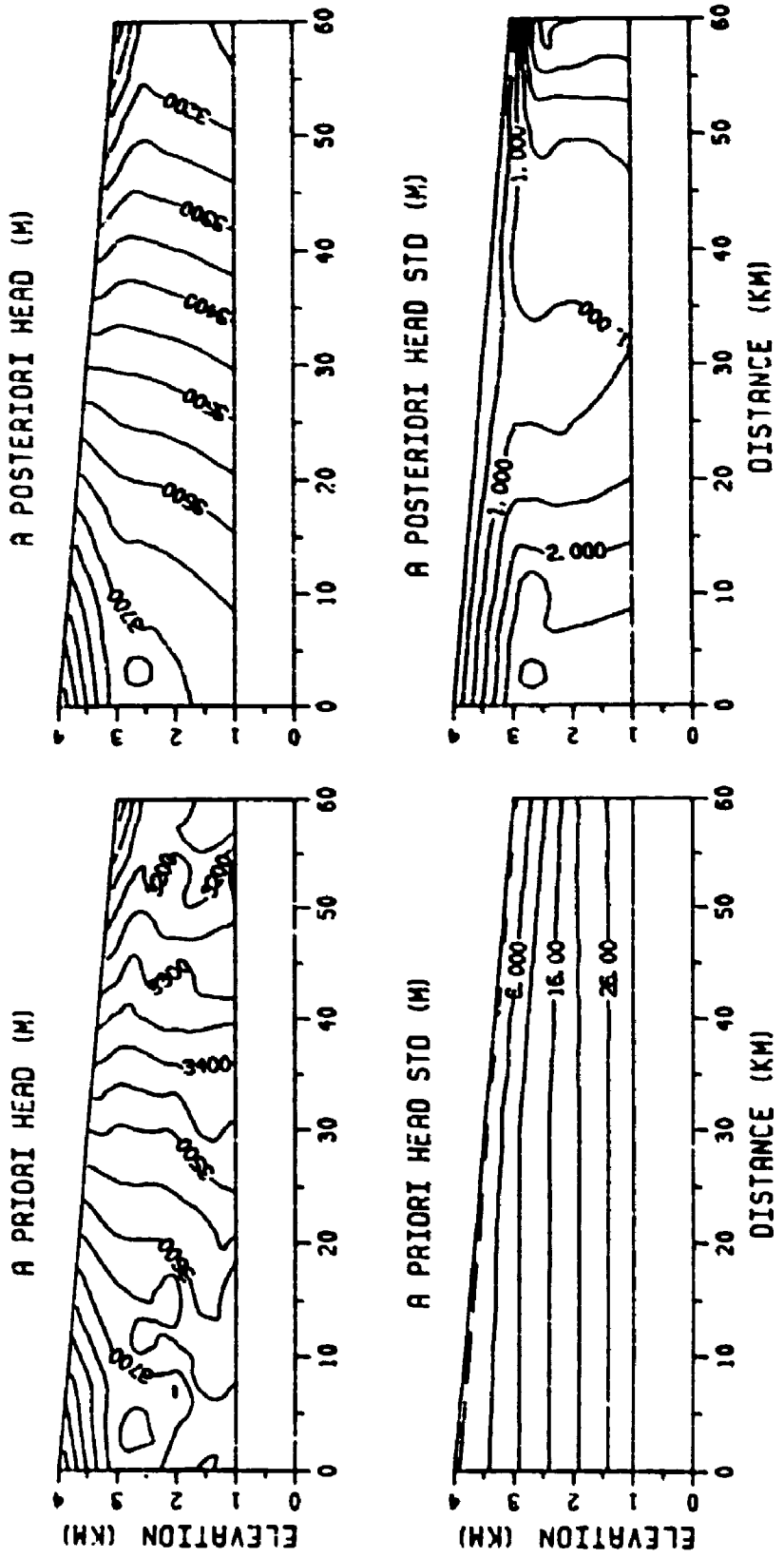

Fig.7.4b. Continued.

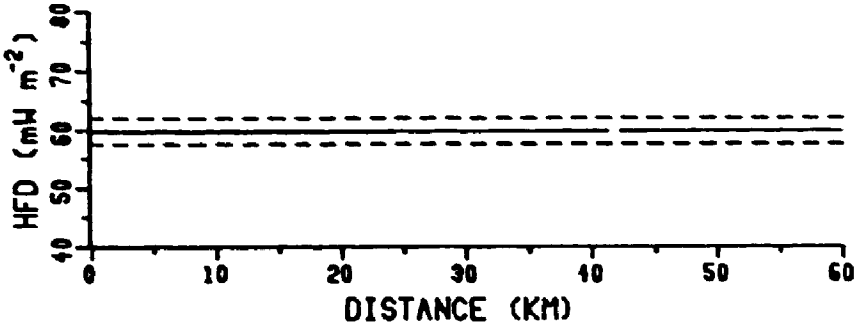

Fig.7.5. The updated basal HFD distribution for case 1 (model I), in which the T (STD = 0.001 K) and h (STD = 0.1 m) data are nearly noise free, λ and κ values are poorly known a priori (see Table 7.3).

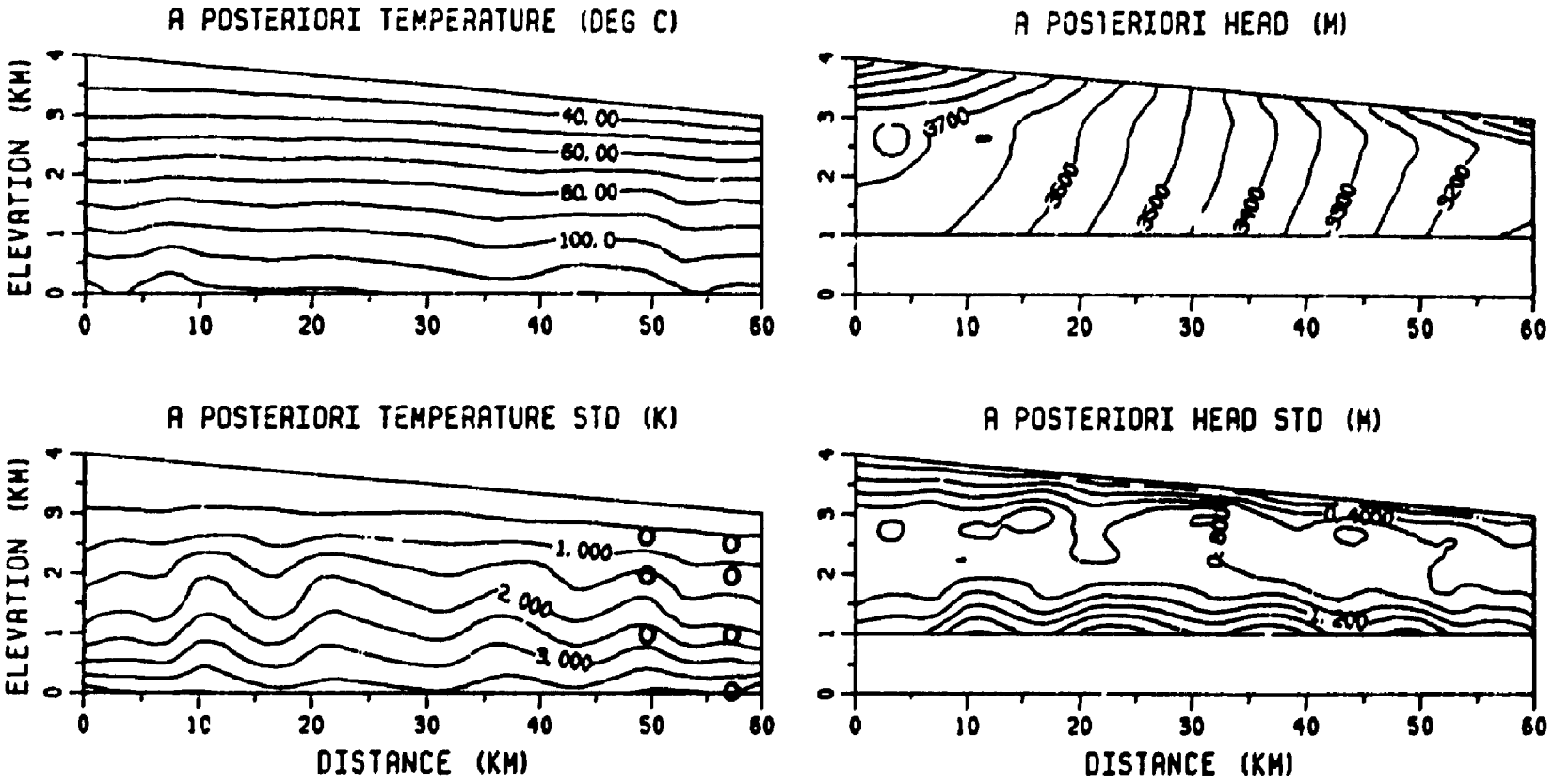

Fig.7.6. The contour maps of the a posteriori T and h and the STDs of the solution for case 2a (model I) in which the log(λ) and log(κ) values are all accurately known (STD = 0.001), and the a priori T and h are the same as in case 0 (Fig.7.4); HFD correlation length L = 0. The temperature contour map shows that the iteration has converged to some wrong values. See Fig.7.7 for explanation of the circled points.

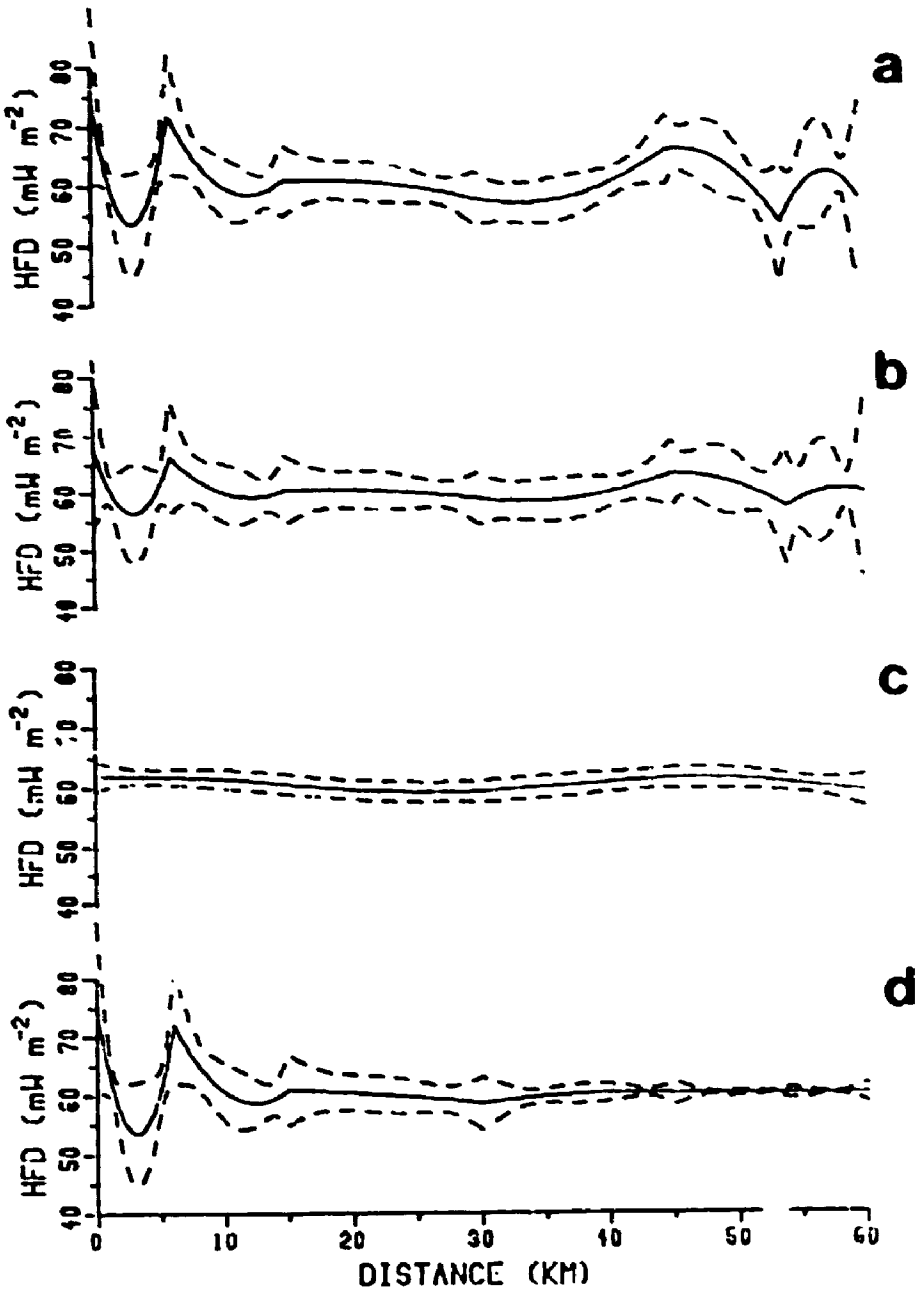

Fig.7.7. The updated basal HFD distributions of the solutions for case 2 (model I) with the one STD uncertainty range indicated by the dashed lines. (a) Case 2a. The unrealistic oscillations are due to the wrongly estimated temperature field shown in Fig.7.6. (b) Case 2b. The noise in the a priori values of T and h is reduced by 50%, although the same variances as in case 2a are used. (c) Case 2c. The correlation length for the basal HFD L = 20 km. (d) Case 2d. The seven nodal temperature values indicated by the circles in the discharge region in Fig.7.6 are tightly constrained with STD = 0.095 K.

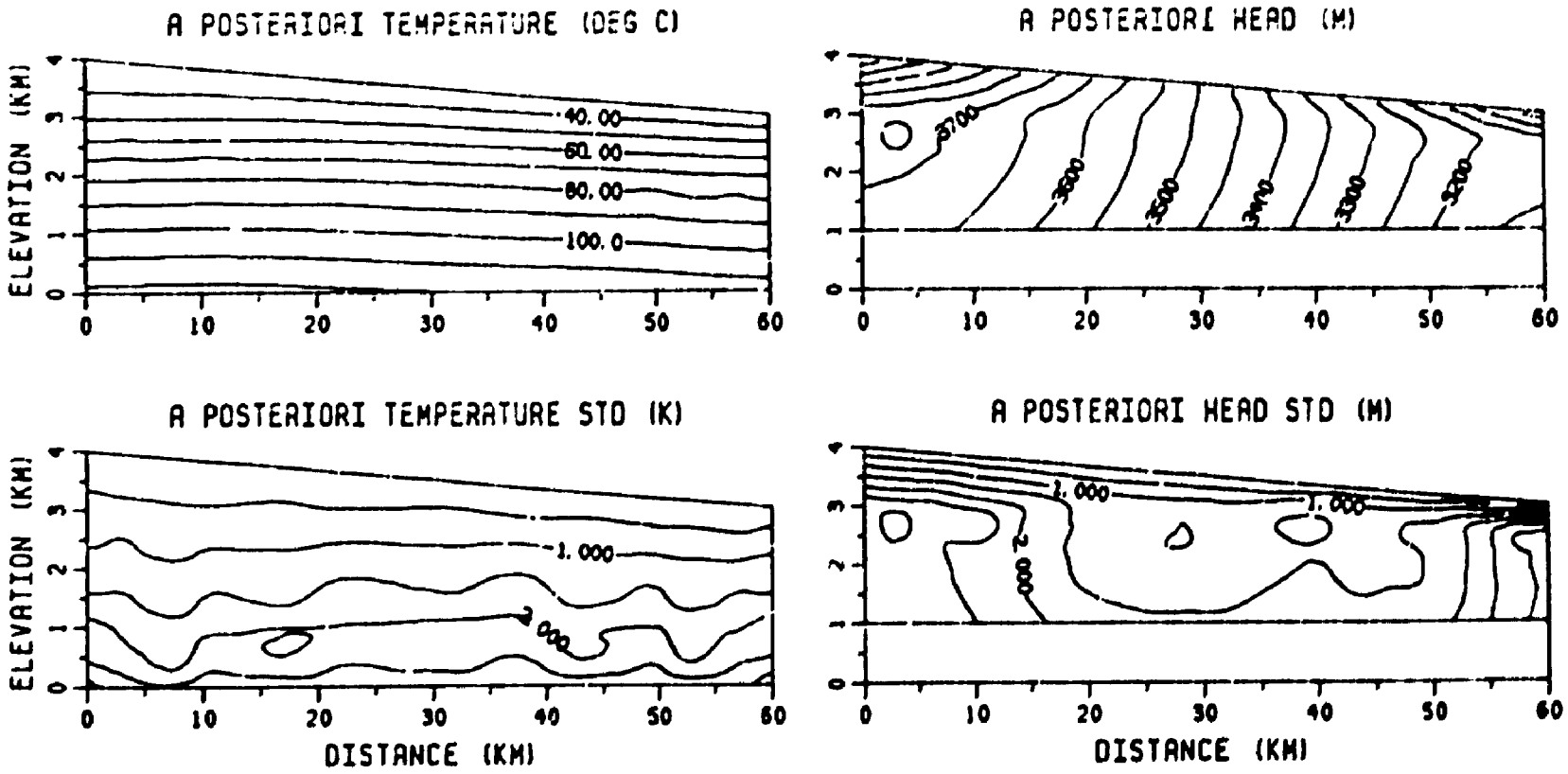

Fig.7.8. The solution for case 3 (model 1) in which the field variable data are the same as in case 0, the material property information is given in Table 7.5. (a) Contour maps of the a posteriori T and h and the STDs. (b) The updated basal HFD distribution, with the one STD uncertainty range indicated by the dashed lines.

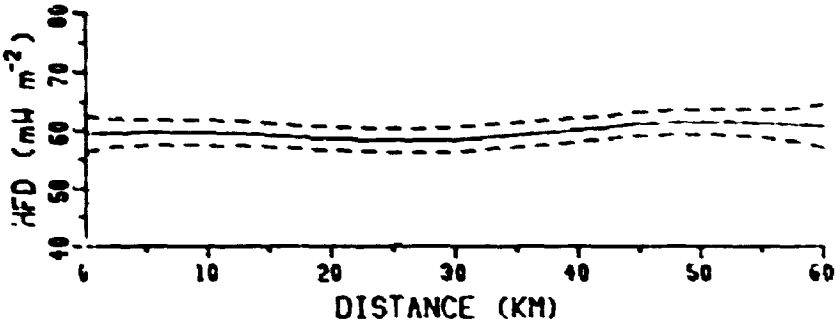

Fig.7.8b. Continued.

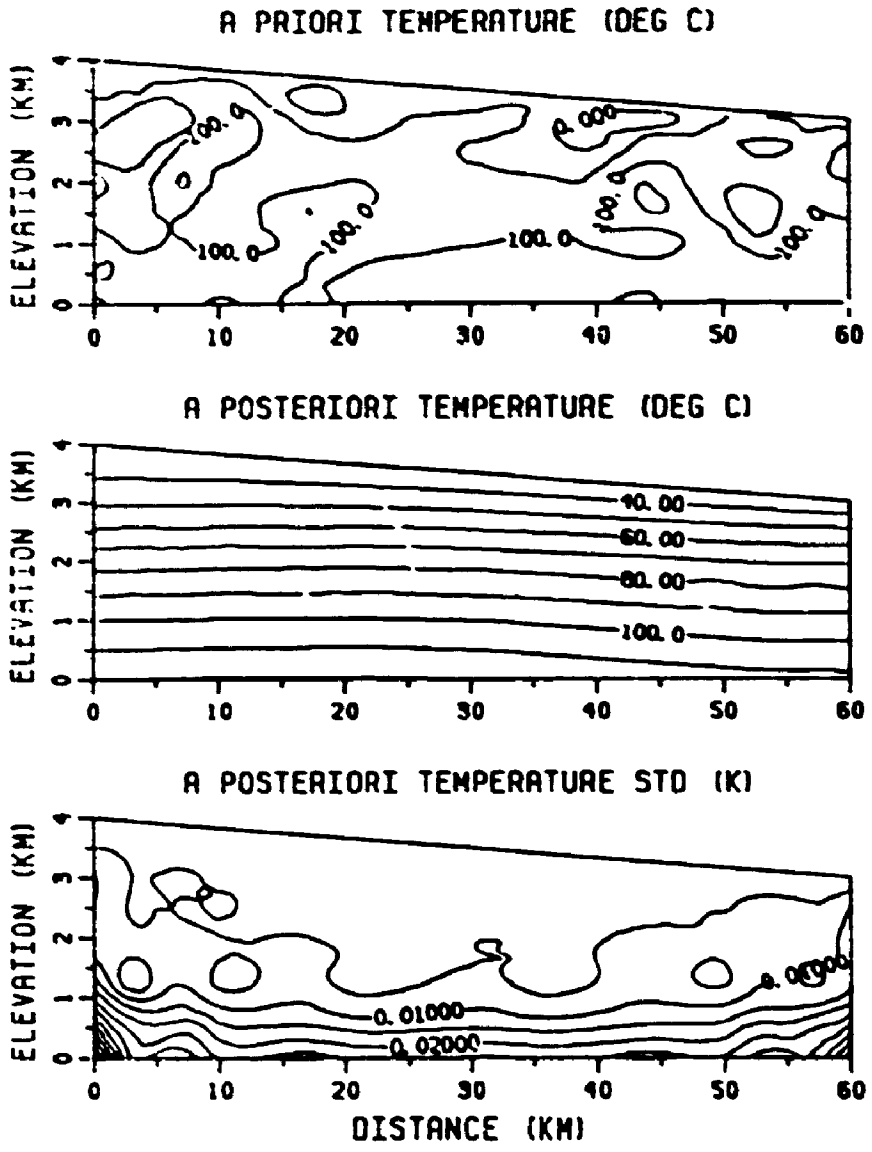

Fig.7.9. The solution for case 4 (model I), with nearly noise free head and material property data but very uncertain temperature data. The a priori STD for nodal temperatures is a uniform 30 K. (a) Contour maps of the a priori T and the a posteriori T and STD's. The contour interval for the a priori temperature is 50 K. (b) The updated basal HFD distribution; the one STD uncertainty range cannot be clearly seen because it is very small (< 0.18 mW m^{-2}).

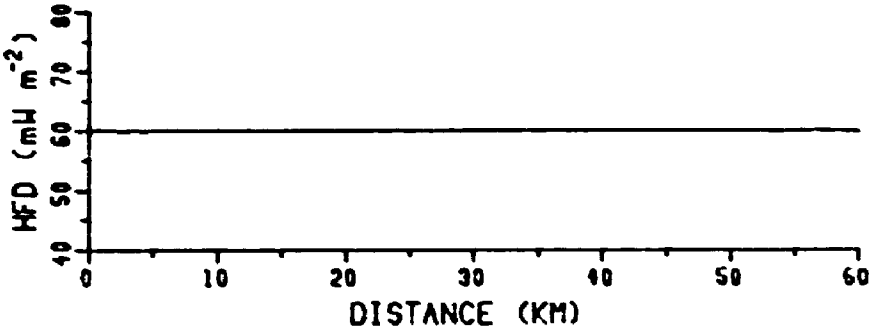

Fig.7.9b. Continued.

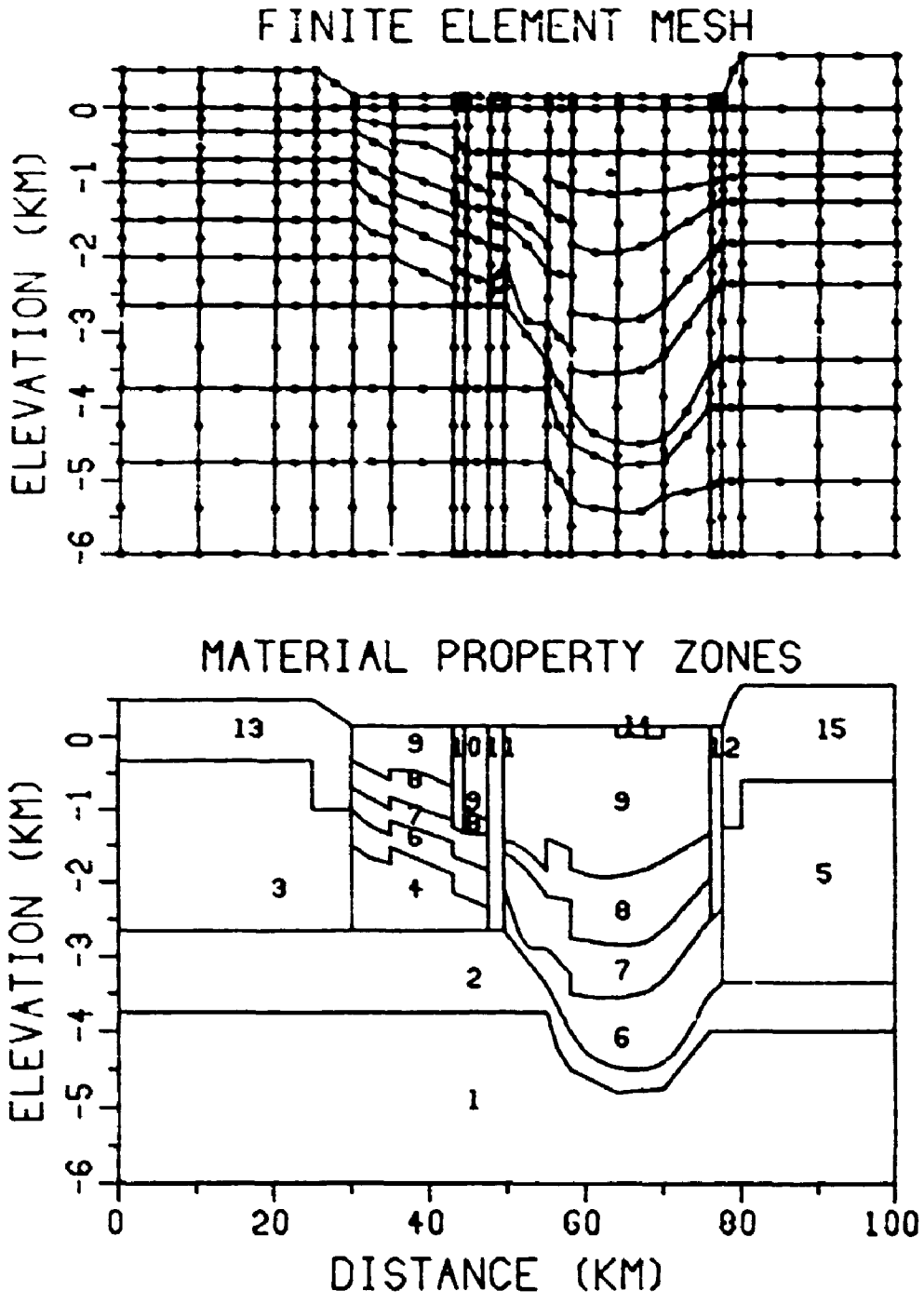

Fig.7.10. The finite element mesh and the material property zones (for both thermal conductivity and permeability) for model II. There are 593 nodal points, shown by circles, and 183 elements.

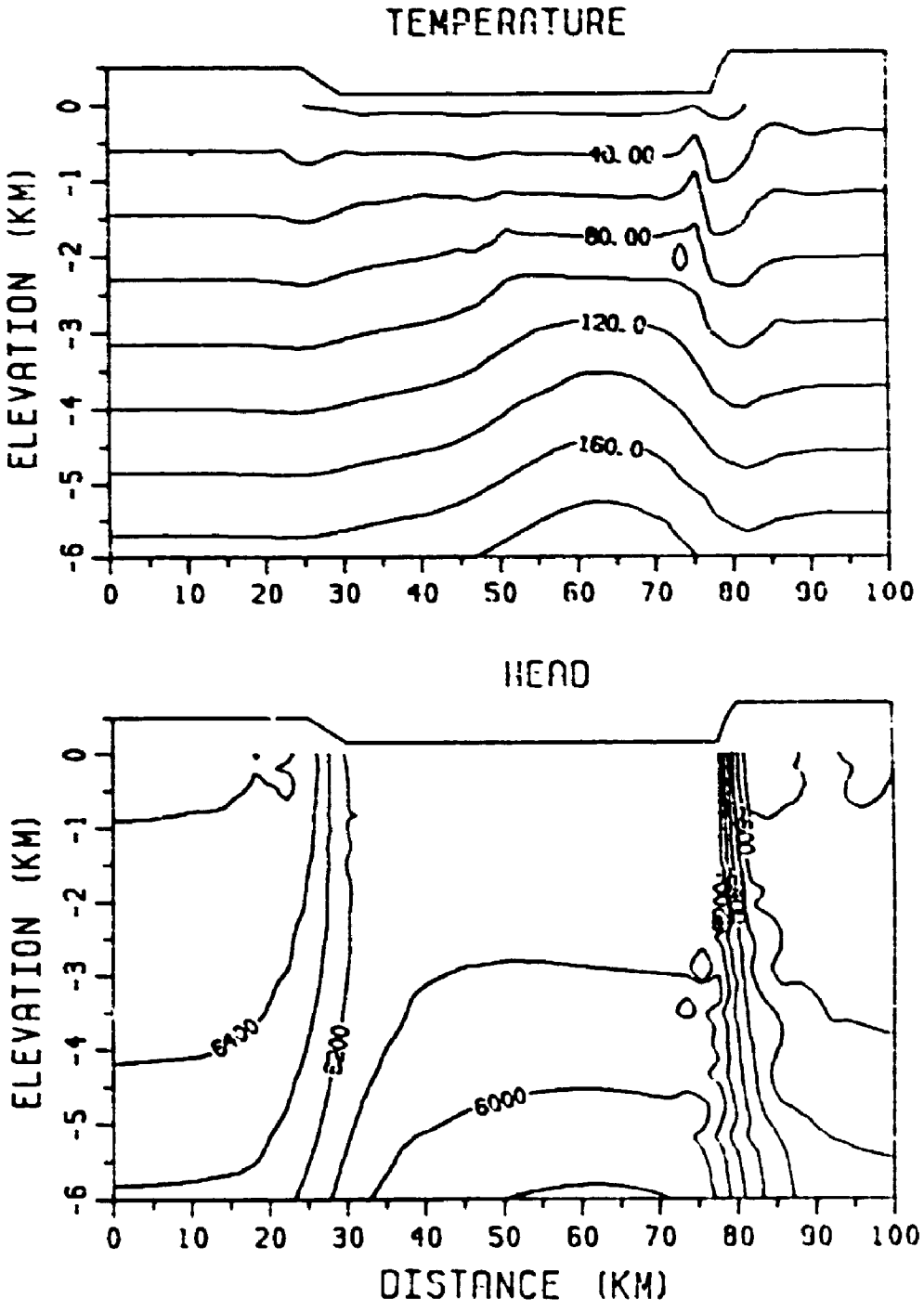

Fig.7.11. The "true" temperature (°C) and head (m) fields of model II, obtained by forward calculation, for the subsequent inversion.

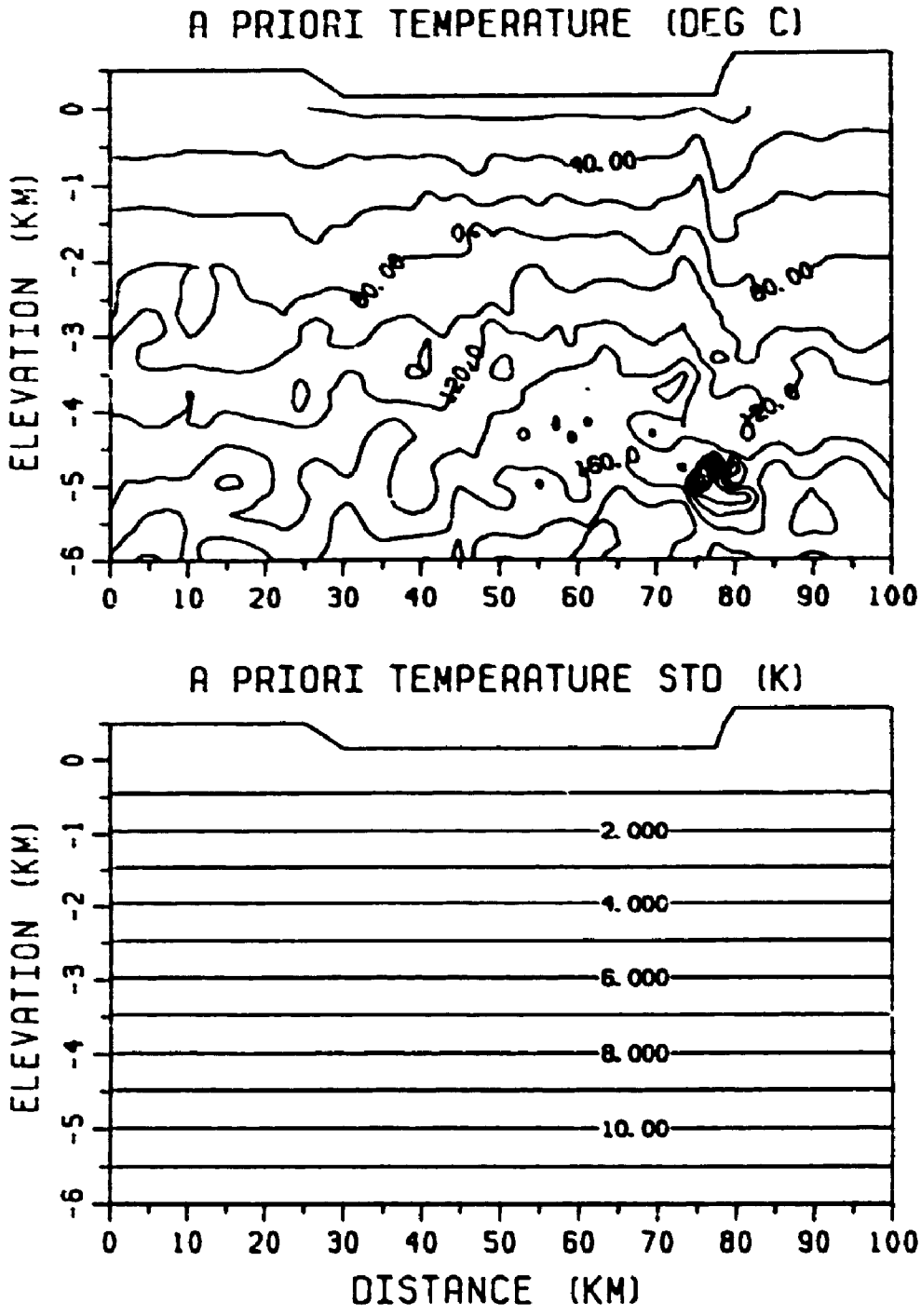

Fig.7.12. The contour maps of the a priori nodal temeprature values and the STDs for the inverse solution of model II.

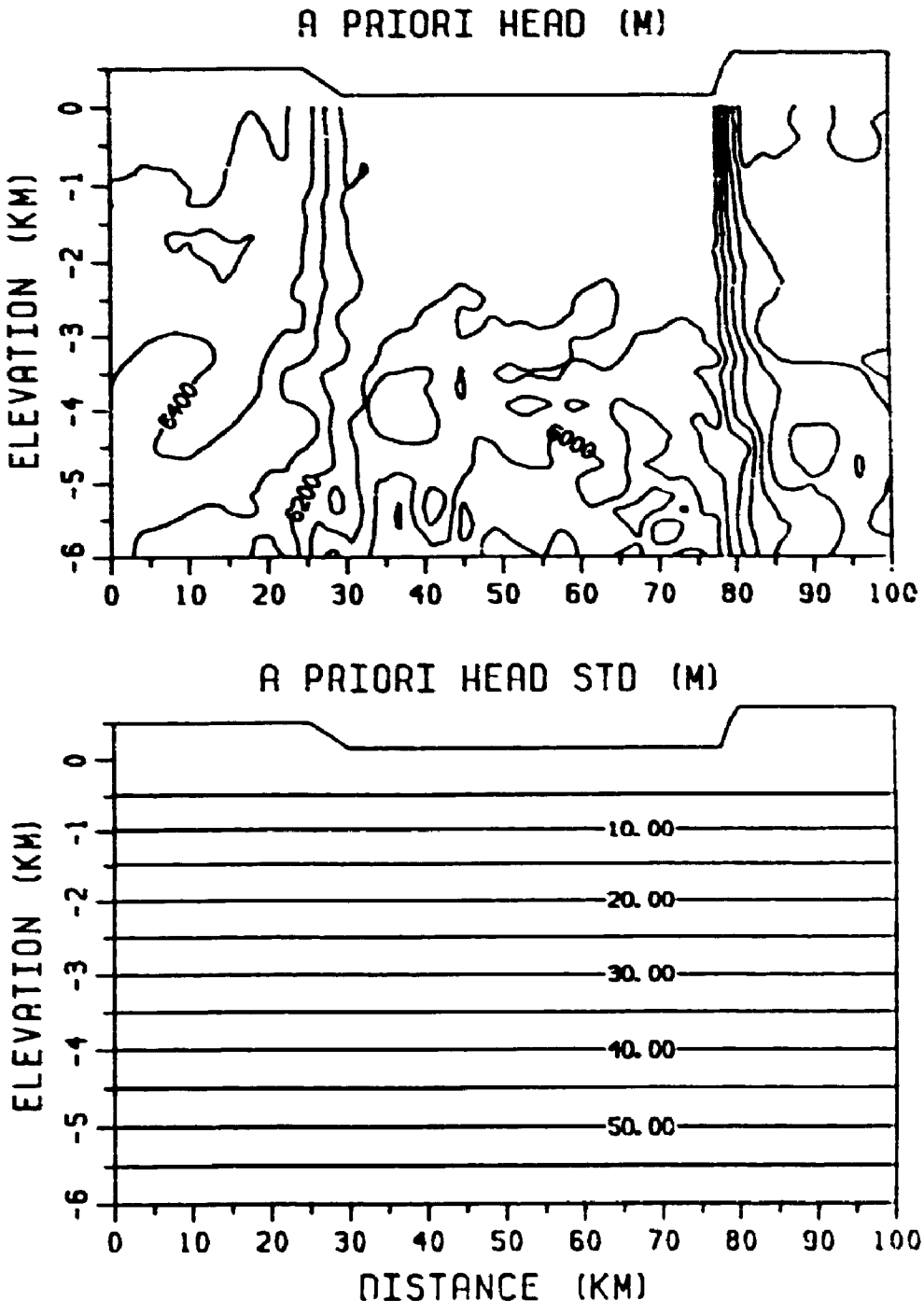

Fig.7.13. The contour maps of the a priori nodal head values and the STDs for the inverse solution of model II.

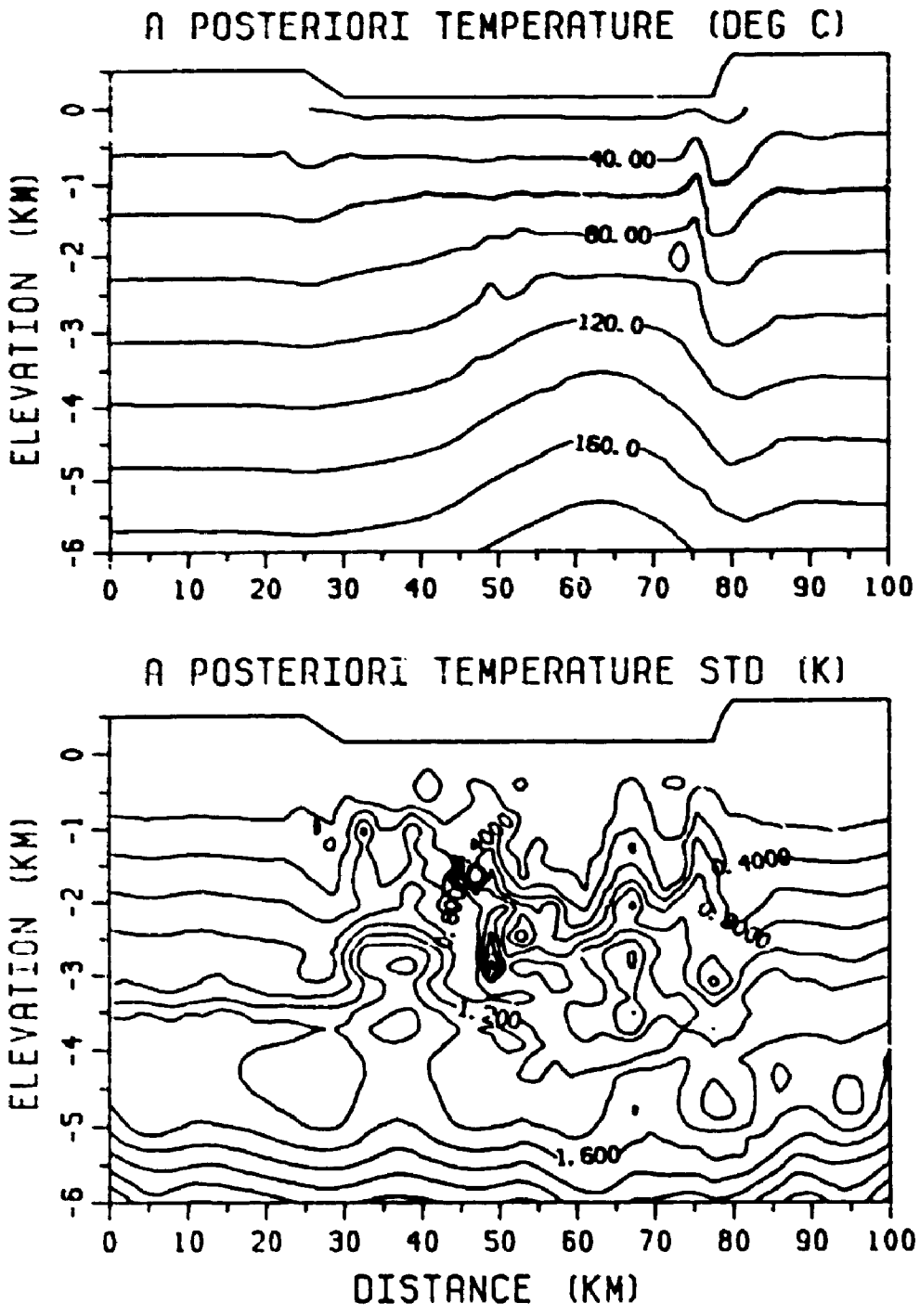

Fig.7.14. The contour maps of the a posteriori nodal temeprature values and the STDs for the inverse solution of model II.

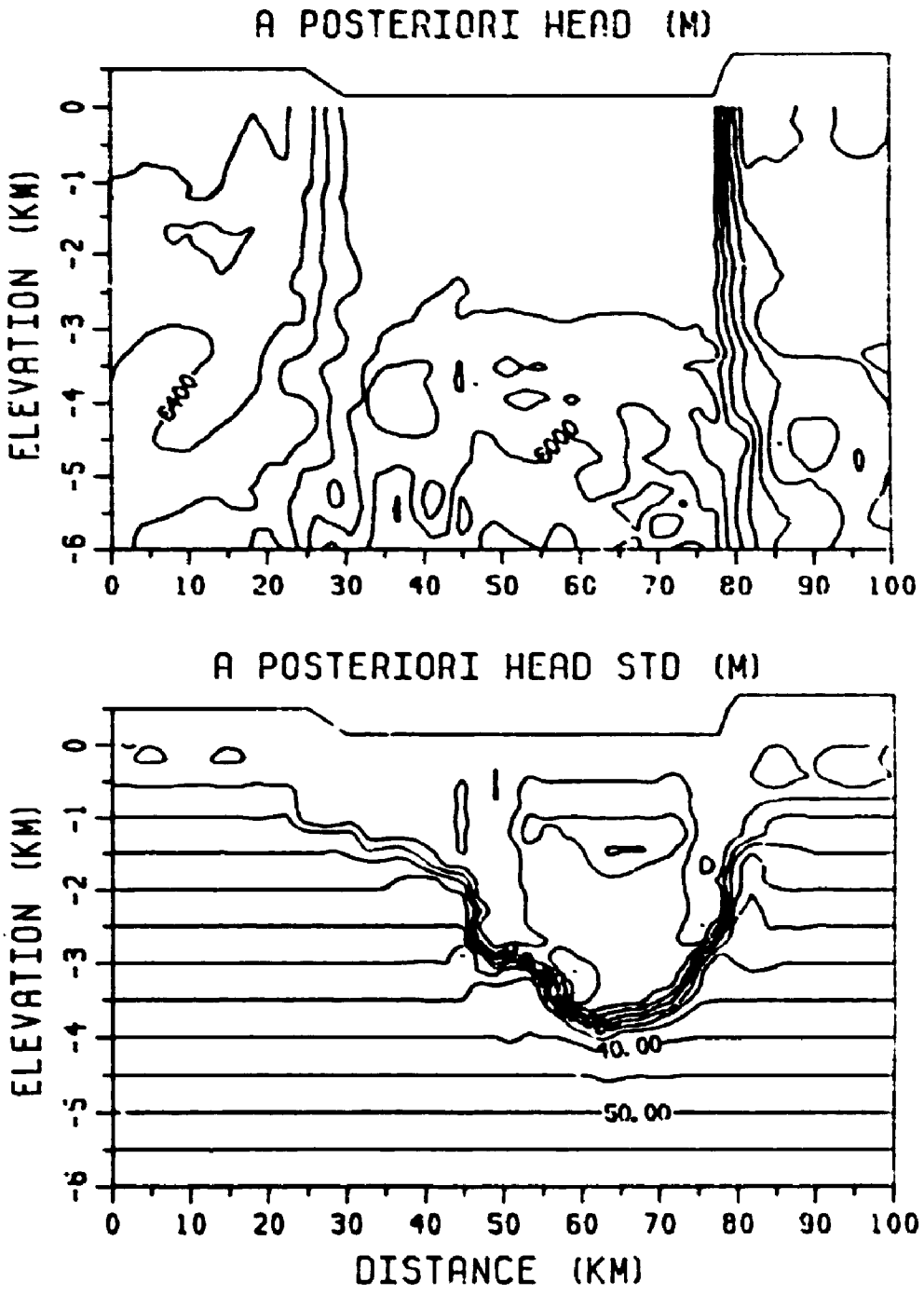

Fig.7.15. The contour maps of the a posteriori nodal head values and the STDs for the inverse solution of model II.

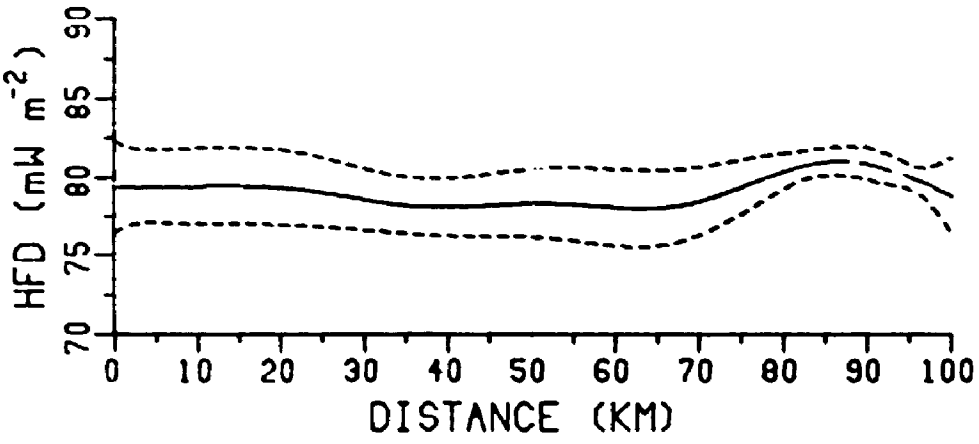

Fig.7.16. The updated basal HFD of model II, with the one STD uncertainty range indicated by the dashed lines. The a priori basal HFD is a uniform 60 ± 40 mW m^{-2}.

CHAPTER 8: CONCLUSIONS

8.1 Summary

An inverse finite element method has been developed in this research to solve the partial differential equations for 2–D, steady state terrestrial heat flow problems, namely, the problem of heat conduction and the problem of coupled thermal and hydrological regimes. The problems are first parameterized using an isoparametric finite element model, in which the field variables and boundary fluxes are represented by their nodal values and the material properties by zonal values assigned to elements or element groups. The nodal values of field variables and the zonal values of material properties constitute the components of a parameter vector, related by an algebraic system in each problem. A Bayesian type nonlinear inverse method is then applied to the statistical estimation of the parameters, in which the a priori information on the parameters are described by an a priori PDF, assumed to be jointly Gaussian. The most probable point estimate is obtained by maximizing the a posteriori PDF of the parameters, and a gradient method, namely the RTV scheme, is employed for the maximization.

Two types of heat conduction problem have been considered, the topographic correction of local HFD data and the downward continuation of surface HFD along geotraverses, the former being, mathematically, a special case of the latter. A synthetic example and a field example of the topographic correction were considered; in both cases, good estimates of the local HFD were obtained. Data from three European geotraverses were used to demonstrate the

use of an inverse approach to the downward continuation of HFD data. Positive spatial correlations of the a priori background HFD can be incorporated to ensure further the stability of the solution, and logarithmic transforms used to allow large uncertainties in the a priori heat production rates to be taken into account. Since the conduction problems are only weakly nonlinear, the RTV iteration scheme can be used in cases where data may contain relatively large noise, and convergence to the global maximum of the a posteriori PDF is generally not a problem.

The problem of coupled thermal and hydrological regimes of basin scale have been investigated using synthetic models. The forward problem is nonlinear in the field variables, and the inverse problem is nonlinear in the material properties as well. The stronger nonlinearity of the inverse coupled problem renders the solution based on the adopted gradient method more difficult than in the pure conduction problem, and the behavior of the solution is more complex. With a simple synthetic example (model I), the general features of the solutions have been illustrated, although the illustration is neither complete nor systematic at the current stage. With reasonable constraints, i.e, a priori information on the parameters, our knowledge about the whole system can be updated. The potential usefulness of applying the method to field problems was demonstrated in a "more realistic" model (model II) based on the Rhine Graben in Central Europe.

8.2 Advantages and disadvantages of the method

The finite element inverse method provides a, perhaps more flexible, way of optimally using the available information in solving heat flow problems. In common with other inverse methods incorporating statistical principles, this approach formally takes into account the uncertainties in the field variables,

material properties and the boundary conditions, and optimally utilizes the available a priori information. The ill–posedness of the problems is minimized by incorporating the a priori information. The solutions are given as the most probable point estimates, with uncertainty ranges. In addition to the specific advantages and disadvantages of applying the method to the conduction and coupled problems as discussed in section 6.3.4, 6.4.4 and 7.4, some general advantages and disadvantages of the method can be summarized. However, "advantages" and "disadvantages" must be appreciated in a relative sense; a gain in one thing is often accompanied by a loss in something else.

The advantages of the method:

1) The field variables, the material properties and the boundary fluxes are formulated equally as parameters, which introduces some practical flexibility in dealing with data of variable quality.

2) The use of a gradient method, namely the ItTV scheme, makes the computation very efficient. For example, in the inverse problem of section 7.3, there are a total of 1253 parameters in the parameter vector P; the total computation, including 50 iterations in the nonlinear parameter estimation, the linear boundary flux updating and the computation of the a posteriori variances, took 11 minutes on an ETA–10. Of course, more time would be needed if the a posteriori covariances were computed. The computer time required by each solution in Chapter 6, for the less nonlinear pure conduction problem, varied between 1 to 20 seconds.

3) The gradient matrix G is derived analytically at the elemental level and assembled at the global level, together with the conductivity matrix K. This is, by far, the most efficient way of computing the gradient matrix when a finite element model is used to parameterize the problems.

The principal disadvantages of the method:

2) Phase 2, iteration.

Gradient matrix G. Subroutine ELEMENT is called at each iteration to compute the elemental g and G for all elements and to assemble the global g and G. The subroutines needed to compute the elemental g and G are listed in Appendix C. The coordinate–related quantities for each element computed in the input phase are used in this phase. The G matrix for the coupled problem has a similar structure to that for the conduction problem (Fig.6.2). The entries between the sky lines are stored by rows in a one dimensional array, which is called the compact G matrix.

Iteration. Subroutine ITERAT is called to perform one iteration. The L_∞ norm of $(p_{k+1} - p_k)$ is represented by the argument AB. If AB is less than a prescribed criterion STP, or the total number of iteration steps has exceeded a specified limit MIT, the iteration is stopped. The first thing that subroutine ITERAT does is to form the R matrix using C_{ff}, C_{pp} and the G matrix evaluated at the current value of p. For each iteration, a linear algebraic equation system with R as the coefficient matrix must be solved (see equation 4.13). Since R is positive definite, the very efficient LDL^t factorization (or decompozation) method can be used, in which R is factorized into a diagonal matrix D, a lower triagular matrix L and its transpose L^t. Subroutine COLSOL, provi led by Bathe and Wilson (1976, p.257), is used with slight modification. COLSOL requires the R matrix to be stored in a compact form, that is, the upper triangle below a skyline (above which all entries are zeros) is stored by columns in a one dimensional array.

3) Phase 3, computing the a posteriori variances of p

Subroutine COVARE is called to compute the a posteriori variances of p. It can be seen from equation (4.26) that there are as many linear algebraic equation systems as the number of parameters in p to be solved. Since these systems all have R, evaluated at $\hat{p}$, as the coefficient matrix, the factorized form of

variable distributions along a boundary and consequently allow Dirichlet condition containing large uncertainties to be considered. This will result in some nonzero off–diagonal entries in the a priori covariance matrix C_{pp}. However, since Dirichlet conditions involve only a small number of nodal points, computation efficiency can be maintained.

3) Spatial correlations of the uncertainties in the a priori material property values can be modeled. This will help constrain the solution when a very large number of fine material property zones are used, especially in the case of large uncertainties. If the correlations are appropriately defined, zonation will be more closely related to the probabilistic parameterization approach. However, the off–diagonal entries of the a priori covariance matrix C_{pp} will make the computation less efficient.

4) The linear approximations for the density and dynamic viscosity of water as functions of temperature, equations (2.11) and (2.12), can be replaced by piecewise linear functions, so that the method can be applied to coupled problems involving wider temperature ranges.

The work for the longer term:

1) Monte–Carlo methods may be used to compute the a posteriori PDF. At the expense of probably hundred–fold computing cost, very nonlinear problems with very poor a priori information can be studied using such methods, but ways have to be found to present the results.

2) The inverse finite element method can be extended to 3–D cases. With the isoparametric finite element model, the extension is not difficult in principle.

3) The inverse formulation of the coupled problem can be applied to single phase solute transport problems. An advantage in dealing with such problems is that the equations for water flow and solute transport are usually decoupled; a disadvantage is that the effects of mechanical dispersion must be considered

APPENDIX A: GAUSS–LEGENDRE NUMERICAL INTEGRATION

The contents of this appendix are mainly from Burden et al. (1981) and Bathe and Wilson (1976).

The basic method of numerical integration of a function f(r),

$$\int_a^b f(r)\, dr \tag{A1}$$

involves the use of a Lagrange interpolating polynomial

$$\sum_{k=0}^{n} f(r_k)\, L_k(r) \tag{A2}$$

to approximate f(r) over [a, b], where r_k are (n + 1) sample points, and $L_k(r)$, polynomials of degree n, are defined as

$$L_k(r) = \prod_{m=0,\, m \neq k}^{n} \frac{(r - r_m)}{(r_k - r_m)} \tag{A3}$$

For almost all functions of practical interests, better accuracy of the interpolation (A2) is obtained with larger n. The approximation

$$\int_a^b f(r)\, dr \approx \sum_{k=0}^{n} w_k\, f(r_k) \tag{A4}$$

is called the quadrature formula, with the weights w_k obtained using (A2)

$$w_k = \int_a^b L_k(r)\, dr \tag{A5}$$

The degree of precision of a quadrature formula is a positive integer N such that the approximation (A4) is exact for any polynomial function f(r) of degree n when $n \leq N$, and may be inexact when $n > N$.

It can be shown that the possible maximum degree of precision of a quadrature formula using n sample points r_k is (2n − 1). It can also be shown that, if n is even, quadrature formulas that use n or (n + 1) equally spaced sample

points, such as the Newton–Cotes quadrature, can only have a degree of precision of n + 1. The idea of Gauss quadrature is to choose n unequally spaced sample points so that the degree of precision (2n − 1) can be reached.

Without loss of generality, we consider the case a = −1 and b = 1. It is well known that an arbitrary polynomial P(r) of order k, k ≤ (2n − 1), can be written into the form

$$P(r) = Q(r)P_n(r) + R(r) \tag{A6}$$

where Q and R are both some polynomials of degree less than n, and P_n is the Legendre polynomial of degree n, which can be shown to have n distinct roots r_k in [−1, 1]. Obviously, the second right–hand–side term can be exactly interpolated from these roots,

$$R(r) = \sum_{k=1}^{n} R(r_k)\, L_k(r) \tag{A7}$$

If a quadrature formula constructed using the points r_k

$$\int_{-1}^{1} f(r)\, dr \approx \sum_{k=1}^{n} w_k\, f(r_k) \tag{A8}$$

is applied to the integration of R(r), we have, exactly

$$\int_{-1}^{1} R(r)\, dr = \sum_{k=1}^{n} w_k\, R(r_k) \tag{A9}$$

becase the interpolation (A7) is exact. The first term on the right–hand–side of equation (A6) vanishes at all r_k, since the latter are the roots of P_n; therefore, as a consequence of (A9), the integration of P(r) using the same quadrature formula is also exact,

$$\int_{-1}^{1} P(r)\, dr = \sum_{k=1}^{n} w_k\, P(r_k) = \sum_{k=1}^{n} w_k\, [Q(r_k)P_n(r_k) + R(r_k)]$$

$$= 0 + \sum_{k=1}^{n} w_k\, R(r_k) \tag{A10}$$

Equation (A10) means that the quadrature formula (A8), constructed using the n roots of P_n as the sample points, has the degree of precision (2n − 1). Because of the use of Legendre polynomials to determine optimally the sample

points, the numerical method using Gauss quadrature (A8) is called the Gauss–Legendre numerical integration method. Once the sample points are determined, the weights can be calculated using (A3). The numerical values of the sample points and weights upto n = 6 are tabulated in Table A.1.

The Gauss–Legendre numerical integration method can be easily applied to the integration of a function of two independent variables $f(r_1, r_2)$, $r_i \in [-1, 1]$,

$$\int_{-1}^{1}\int_{-1}^{1} f(r_1,r_2)\, dr_1\, dr_2 \approx \sum_{k=1}^{n}\sum_{l=1}^{n} w_k\, w_l\, f(r_{1k},r_{2l}) \qquad \text{(A11)}$$

where r_{ik} is the k*th* sample point of coordinate r_i. The total number of sample points in the square domain is thus n^2. Simple extrapolation can be made for cases involving more independent variables.

The entries of the conductivity matrix K and the gradient matrix G have been given in Chapter 3 and 4, respectively, as integrations with the general form

$$\int_{\Omega^e} f(x)\, d\Omega \qquad \text{(A12)}$$

To apply the Gauss–Legendre numerical integration method, the domain Ω in the x coordinate system is mapped onto a square in the r system in the isoparametric finite element model using shape functions, thus

$$\int_{\Omega^e} f(x)\, d\Omega = \int_{-1}^{1}\int_{-1}^{1} \tilde{f}(r)\, \det\, dr \qquad \text{(A13)}$$

where $\tilde{f}$ is the transformed function; det is the Jacobian of the coordinate transformation, a function of r, and is a part of the integrand. In actual computer implementation, a subroutine is called to evaluate $[\tilde{f}(r)\ \det]$ for the entries of K and G at all Gauss–Legendre sample points in each element.

Table A.1. Sample points and weights in Gauss–Legendre numerical integration. n is the number of sample points, r_k are the sample points (the roots of Legendre polynomial of degree n in [−1, 1]), and w_k the corresponding weights.

n	r_k	w_k
1	0.00000 00000 00000	0.00000 00000 00000
2	±0.57735 02691 89626	1.00000 00000 00000
3	±0.77459 66692 41483	0.55555 55555 55556
	0.00000 00000 00000	0.88888 88888 88889
4	±0.86113 63115 94053	0.34785 48451 37454
	±0.33998 10435 84856	0.65214 51548 62546
5	±0.90617 98459 38664	0.23692 68850 56189
	±0.53846 93101 05683	0.47862 86704 99366
	0.00000 00000 00000	0.56888 88888 88889
6	±0.93246 95142 03152	0.17132 44923 79170
	±0.66120 93864 66265	0.36076 15730 46139
	±0.23861 91860 83197	0.46791 39345 72691

APPENDIX B: INTRODUCTION TO COMPUTER PROGRAM INVCUP

Program INVCUP, in standard FORTRAN V, is used to perform inverse finite element analysis of the problem of coupled thermal and hydrological regimes. INVCUP consists of a main program and 45 subroutines, with a total of about 2500 statements (including comment statements). A list of the names and principal functions of the subroutines is given in Table B.1. The main program and some of the subroutines are listed in Appendix C. The mathematics involved in the construction of the program is presented in Chapters 2, 3, 4 and 5 of this thesis. Another computer program INVCON, for the inverse finite element analysis of heat conduction problems, has a structure similar to that of INVCUP, and is not introduced here.

The basic array storage schemes and addressing procedures used in this program are developed from Bathe and Wilson (1976). All the matrices (including column and row matrices) are stored in a single array A. At different phases of computation, the addresses of the matrices in this array are re–organized in order to minimize the total length of the array at all times.

Seven files are used in the program. Four formatted files are for input of data and output of results, three unformatted files are for the temporary storage of intermediate results to minimize the central memory required.

The computation consists of 4 major phases: 1) input, 2) iteration for the estimate of **p**, 3) computing the a posteriori variances for **p**, and 4) computing the estimate of **q** and the variances. With reference to Fig.B.1 and the list of the main program in Appendix C, the procedure is outlined as follows.

1) Phase 1, input.

Nodal and material property information. After the control variables, such as the total numbers of nodal points, elements and boundary flux sections, are read in, subroutine NODEIN is called to input the coordinates of the finite element nodes, the a priori nodal values of T and h and their STDs. The argument IDUM in the calling statement for NODEIN is a Gaussian noise control parameter. When IDUM < 0, no noise is added to the a priori nodal values of T and h; when IDUM > 0, it is a seed for a Gaussian random number generator, taken from Press et al. (1986, p.202). The a priori material property values and STDs are then read in by calling subroutine PROPIN. Each material property value is assigned a property number, as a referring name, and a nodal number, for positioning the value in the parameter vector p. Subroutine PARAME re-organizes the field variable nodal values and the material property values to form the vector p, and the diagonal matrix C_{pp}.

Elemental information. Subroutine ELEMENT is called to input elemental information, such as the nodal numbers and the material property numbers for each element. Elements are grouped into a material property zone by having the same material property number. Some elemental quantities, related only to the coordinates of the elemental nodal points, will be repeatedly used in the subsequent iterations but need to be calculated only once, such as det, H(r), $\frac{\partial H}{\partial r}$, etc. at all Gauss–Legendre sample points. These quantities are computed in the input phase and written onto a file for later use.

Boundary flux information. After the control variables for the boundary fluxes, such as the numbers of nodes and the correlation length L for each boundary flux section, are read in, subroutine BOUNDRY is called to input the nodal values of the boundary fluxes and their variances. If L > 0, the covariance matrix C_{qq} is also computed. These nodal values and covariances are then used to form the global f vector and C_{ff} matrix.

2) Phase 2, iteration.

Gradient matrix G. Subroutine ELEMENT is called at each iteration to compute the elemental g and G for all elements and to assemble the global g and G. The subroutines needed to compute the elemental g and G are listed in Appendix C. The coordinate–related quantities for each element computed in the input phase are used in this phase. The G matrix for the coupled problem has a similar structure to that for the conduction problem (Fig.6.2). The entries between the sky lines are stored by rows in a one dimensional array, which is called the compact G matrix.

Iteration. Subroutine ITERAT is called to perform one iteration. The L_∞ norm of $(p_{k+1} - p_k)$ is represented by the argument AB. If AB is less than a prescribed criterion STP, or the total number of iteration steps has exceeded a specified limit MIT, the iteration is stopped. The first thing that subroutine ITERAT does is to form the R matrix using C_{ff}, C_{pp} and the G matrix evaluated at the current value of p. For each iteration, a linear algebraic equation system with R as the coefficient matrix must be solved (see equation 4.13). Since R is positive definite, the very efficient LDL^t factorization (or decompozation) method can be used, in which R is factorized into a diagonal matrix D, a lower triagular matrix L and its transpose L^t. Subroutine COLSOL, provided by Bathe and Wilson (1976, p.257), is used with slight modification. COLSOL requires the R matrix to be stored in a compact form, that is, the upper triangle below a skyline (above which all entries are zeros) is stored by columns in a one dimensional array.

3) Phase 3, computing the a posteriori variances of p

Subroutine COVARE is called to compute the a posteriori variances of p. It can be seen from equation (4.26) that there are as many linear algebraic equation systems as the number of parameters in p to be solved. Since these systems all have R, evaluated at $\hat{p}$, as the coefficient matrix, the factorized form of

R from the last iteration can be directly used.

Subroutine RESULT is used to transform the updated p vector back into the field variable nodal values and material propoerty values in their input order.

4) Phase 4, updating boundary fluxes

In subroutine ESFLOW, the g vector evaluated at $\hat{p}$ is used to give the updated value of q using equation (5.3). To compute the a posteriori variances of q using equation (4.27), the factorized form of R matrix from the last iteration is again used. The dimension of the V matrix for each boundary flux section is reduced to the number of boundary flux nodal values, and is stored in the same compact form as the R matrix.

Table B.1. List of subroutines in computer program INVCUP.

Subroutine	Description
ADDBAN*	Assemble the compact C_{ff} and V matrices
ADDCLM	An auxiliary subroutine for FORMCFF
ADDG	Assemble the compact global G matrix
ADDVCLM	An auxiliary subroutine for VCOLUMN
BOUNDRY	Input boundary fluxes and compute the V matrices, and the global f and C_{ff}
BOUQUAD	Perform Gauss–Legendre numerical integrations in the calculation of f
CGT	Compute the product of the diagonal C_{pp} and compact G^t
CLEAN	Set the values of an array to zeros
COLSOL*	Solve a linear algebraic equation system. The coefficient matrix is positive definite and in compact form
COVARE	Compute the a posteriori variances for p
CUPQUAD	Compute elemental g and G
DIRICH1	Input Dirichlet boundary conditions
DIRICH2	Modify f and C_{ff} for the Dirichlet conditions
ELEMENT	Call subroutines for elemental computation
ELPRIN	Input the elemental material property numbers
ESFLOW	Compute updated q and the a posteriori C_{qq}
FILMAN	Read (write) a real array from (onto) an unformatted file
FINEIN	Input elemental information
FSTLST	Determine the column numbers of the first and last nonzero entries in each row of the global G matrix (to define the skyline)
FORMCFF	Compute the global C_{ff} matrix

Table B.1. Continued.

Subroutine	Description
FORMFF	Compute the global f vector
FORMR	Form the R matrix at the current p value
GADDRES	Determine the addresses of the first nonzero entries in all the rows of the compact G matrix
GCOLUMN	Take a column from the compact G and put it into a 1–D array
GTIMEP	Compute the product of G (compact) and a column matrix
GTTIMP	Compute the product of G^t (compact) and a column matrix
HBDET	Evaluate the Jacobians, shape functions and their derivatives at all Gauss–Legendre sample points in one element
IFILMAN	Read (write) an integer array from (onto) an unformatted file
INTOUT	Write integer numbers to a formatted file
IRELOAD	Put the contents of an integer array into another integer array
ITERAT	Perform one iteration
MFSTINT	Set initial (large) values for array MFST
NBFFIN	Read in the global nodal numbers of all boundary flux nodes
NODEIN	Read in the coordinates of nodal points and call TOPO
PARAME	Re–organize the a priori values of field variables and material properties to form p and C_{pp}
PROPIN	Read in the a priori values of material properties
QUADS	Evaluate the elemental g and G at a Gauss–Legendre sample point in an element
RADDRES	Determine the diagonal addresses of the compact R matrix
RELOAD	Put the contents of a real array into another real array
RESULT	Re–organize and output the a posteriori values of p components

Table B.1. Continued.

Subroutine	Description
ROWLTH	Determine the length of each (nonzero) row of the global G matrix
STIFSS	An auxiliary subroutine for HBDET
TOPO	Read in the a priori nodal values of T and h and their STDs, and, if required, add Gaussian random noise to the nodal values
VADDRES	Determine the diagonal addresses of a V matrix in the compact form
VCOLUMN	An auxiliary subroutine for ESFLOW
GAUSSN*	Function, to generate Gaussian random numbers
RAN1*	Function, to generate uniform random numbers on [0, 1]

Notes: * Modified from Bathe and Wilson (1976).

* Modified from Press et al. (1986).

```
C                   =2, NO WATER FLOW; HEAT ONLY
C                   =3, BOTH HEAT AND WATER FLUX EXIST
C     CRL(I) --- CORRELATION LENGTH OF BF POINTS IN SECTION I,
C                POINTS IN DIFFERENT SECTIONS MUST BE UNCORRELATED
C     NBFT --- TOTAL NUMBER OF BF POINTS IN ALL SECTIONS
C     NBF  --- NUMNER OF BF POINTS IN THE LARGEST SECTION
C     NCQ  --- MAXIMUM LENGTH OF CQQ MATRIX, NBF*(NBF+1)/2
C
      REWIND NF3
      NEQ=NODE*2
      WRITE(NF3) (MAXV(I),I=1,NBF+1),(NBFF(I),I=1,NBFT)
      N1=0
      DO 200 LLL=1,NBL
      NBF1=NBFL(LLL,1)
      NN=N1+NBF1
      NCQ1=NBF1*(NBF1+1)/2
      CALL CLEAN(NCQ*2,CQQ)
      CALL CLEAN(NWV,V)
      IF(CRL(LLL).EQ.0.0) THEN
C
C     COMPUTE CQQ FOR UNCORRELATED BF POINTS
C
      READ(NF1,*) (QQ(I,1),CQQ(I,1),QQ(I,2),CQQ(I,2),I=1,NBF1)
      WRITE(NF2,2001) LLL,0.0,(I,NBFF(N1+I),QQ(I,1),CQQ(I,1),QQ(I,2),
     .           CQQ(I,2),I=1,NBF1)
      DO 11 LHW=1,2
        IF(NBFL(LLL,2).EQ.LHW) GOTO 11
      CQQ(1,LHW)=CQQ(1,LHW)*CQQ(1,LHW)
      CQQ(2,LHW)=CQQ(2,LHW)*CQQ(2,LHW)
      NNN=NCQ1-NBF1+1
      DO 10 I=NBF1,3,-1
      CQQ(NNN,LHW)=CQQ(I,LHW)*CQQ(I,LHW)
      CQQ(I,LHW)=0.0
      NNN=NNN-I+1
10    CONTINUE
11    CONTINUE
      ELSE
C
C     COMPUTE CQQ FOR CORRELATED BF POINTS
C
      READ(NF1,*) STD(1),STD(2)
      READ(NF1,*) (QQ(I,1),QQ(I,2),I=1,NBF1)
      WRITE(NF2,2001) LLL,CRL(LLL),(I,NBFF(N1+I),QQ(I,1),STD(1),
     .           QQ(I,2),STD(2),I=1,NBF1)
      CR=CRL(LLL)*CRL(LLL)
      DO 13 LHW=1,2
        IF(NBFL(LLL,2).EQ.LHW) GOTO 13
      VAR=STD(LHW)*STD(LHW)
      ICQ=0
      DO 12 J=1,NBF1
      NJ=NBFF(N1+J)
      XJ=X(NJ)
```

APPENDIX C: LIST OF PARTS OF INVCUP

The main program of INVCUP and the subroutines PARAME, BOUNDRY, ITERAT, COVARE, ESFLOW, ELEMENT, CUPQUAD and QUADS are listed in this appendix. A complete list of subroutine names with descriptions, and the relation between subroutines, is given in Appendix B.

```
      PROGRAM INVCUP
C
C*****************************************************************
C
C     PROGRAM FOR INVERSE FINITE ELEMENT ANALYSIS OF COUPLED
C                 THERMAL AND HYDROLOGICAL REGIMES
C
C                       KELIN WANG, 1989
C     DEPARTMENT OF GEOPHYSICS, UNIVERSITY OF WESTERN ONTARIO
C
C*****************************************************************
C
      COMMON/BLANK/A(1000000)
      COMMON/CONTRL/NODE,NELT,NLK,NWG,NWR,NWV,IPH,NPM
      COMMON/NOFILE/NF1,NF2,NF3,NF4,NF5,NF6,NF7
      COMMON/POSITN/N1,N2,N2X,N2Y,N2P,N3,N4,N5,N6,N7,N8,N9,N10,N11,
     .              N12,N13,N14,MTOT,NFIRST,NLAST,NIDST
      COMMON/MPRINT/NAPIT(11)
      COMMON/DIRI/NDR,IDR(50),IDE(50,2),ADR(50,2),TP(50,2),TPV(50,2)
      COMMON/BOUND/NBL,NBFL(10,2),CRL(10),NBFT,NBF,NCQ
      CHARACTER FNAME1*10,FNAME2*10,HEAD*80
      STIME=SECOND( )
      MTOT=1000000
      NF1=1
      NF2=2
      NF3=7
      NF4=8
      NF5=9
      NF6=10
      NF7=11
C
C   CONTROL VARIABLES:
```

```
C     NODE ---TOTAL NUMBER OF NODAL POINTS
C     NELT ---TOTAL NUMBER ELEMENTS
C     NLK  ---TOTAL NUMBER OF PHYSICAL PROPERTIES (THERMAL
C              CONDUCTIVITY AND PERMEABILITY)
C     NWG  ---LENGTH OF THE GLOBAL G (GRADIENT) MATRIX
C     NWR  ---LENGTH OF THE GLOBAL R MATRIX
C     NWV  ---MAXIMUM LENGTH OF THE V MATRICES
C     IPH  ---PHASE FLAG
C            =1, INPUT
C            =2, ITERATION
C            =3, COVARIANCE MATRIX COMPUTATION
C            =4, UPDATING BOUNDARY FLUXES
C     NPM  ---NUMBER OF PERMEABILITY ZONES
C
      PRINT*, ' PROGRAM OF FINITE ELEMENT INVERSION STARTS'
      PRINT*, ' '
      OPEN(NF1,FILE='CUPIN')
      REWIND NF1
      OPEN(NF2,FILE='CUPOUT')
      REWIND NF2
C
C     INTERMEDIATE RESULTS PRINT CODES (YES=1; NO=0)
C     H(B)  LME(P)  V  CFF  MADR  G  GP  MAXA  R  P  FF
C
      READ*, NAPIT
C
C   MIT  ---  MAXIMUM NUMBER OF ITERATIONS
C
      READ*, MIT
      OPEN(NF3,FILE='CFFF',FORM='UNFORMATTED')
      OPEN(NF4,FILE='CPPP',FORM='UNFORMATTED')
      OPEN(NF5,FILE='ELLL',FORM='UNFORMATTED')
      OPEN(NF6,FILE='OUUU')
      OPEN(NF7,FILE='MTTT')
      REWIND NF6
      REWIND NF7
C
CCCCCCCCCCCCCCCCCCCCCCCCCCCCCCCCCCCCCCCCCCCCCCCCCCCCCCCCCCCCCCCCCCCCCC
C     1. INPUT
CCCCCCCCCCCCCCCCCCCCCCCCCCCCCCCCCCCCCCCCCCCCCCCCCCCCCCCCCCCCCCCCCCCCCC
C
      IPH=1
      WRITE(NF2,2000) FNAME1,FNAME2
      READ(NF1,FMT='(A80)') HEAD
      READ(NF1,*) NODE,NELT,NLK1,NPM,STP,SDH,SDW,NBL,IDUM
      IF(NBL.GT.4) THEN
      PRINT*,'ARE THERE ',NBL,' BOUNDARY FLOW SECTIONS?'
      STOP
      END IF
      WRITE(NF2,2001) HEAD,NODE,NELT,NLK1,NPM,NBL,STP,IDUM
      NLK=NLK1+NPM
      NEQ=2*NODE
```

```
      NPARA=NEQ+NLK
C
C     A(N1) --- PARA(NPARA)    PARAMETERS
C     A(N2X)--- X(NODE)        X COORDINATES
C     A(N2Y)--- Y(NODE)        Y COORDINATES
C     A(N2P)--- PR(NLK)        PROPERTY VALUES
C     A(N3) --- ID(NLK)        PROPERTY NODAL NUMBERS
C     A(N4) --- IDP(NEQ)       PARAMETER NUMBERS OF NODAL T AND P
C     A(N5) --- PRV(NLK)       VARIANCE OF PR
C     A(N6) --- CPP(NPARA)     VARIANCE OF PARA
C     A(N7) --- T(NODE)        NODAL TEMPERATURE
C     A(N8) --- TV(NODE)       VARIANCE OF T
C     A(N9) --- P(NODE)        NODAL HEAD
C     A(N10)--- PV(NODE)       VARIANCE OF P
C
      N1=1
      N2X=N1+NPARA
      N2Y=N2X+NODE
      N2P=N2Y+NODE
      N3=N2P+NLK
      N4=N3+NLK
      N5=N4+NEQ+1
      N6=N5+NLK
      N7=N6+NPARA
      N8=N7+NODE
      N9=N8+NODE
      N10=N9+NODE
      N11=N10+NODE
      NFIRST=N11
      NLAST=NFIRST
      CALL NODEIN(NODE,A(N2X),A(N2Y),A(N7),A(N8),A(N9),A(N10),IDUM)
      CALL PROPIN(A(N2P),A(N3),A(N5))
      CALL PARAME(A(N1),A(N2P),A(N3),A(N4),A(N5),A(N6),A(N7),A(N8),
     .           A(N9),A(N10))
C
C     INPUT SPECIFIED TEMPERATURE AND HEAD INFORMATION
C
      READ(NF1,*) NDR
      IF(NDR.GT.0) CALL DIRICH1(A(N4),A(N1),A(N6))
C
C     A(N4) --- MADR(NEQ+1)    FIRST NON-ZERO COLUMN ADDRSSES OF G
C     A(N5) --- MFST(NEQ)      FIRST NON-ZERO COLUMNS OF G
C     A(N6) --- MLST(NEQ)      LAST NON-ZERO COLUMNS OF G
C               MLTH(NEQ)      ROW LENGTHS OF G
C               MAXA(NEQ+1)    DIAGONAL ADDRESSES OF R MATRIX
C     A(N7) --- FF(NEQ)        THE VECTOR OF EQUIVALENT NODAL FLOW
C     A(N8) ---                UNUSED, SET TO = A(N9)
C     A(N9) --- MAXV(NBF+1)    DIAGONAL ADDRESSES OF V MATRIX
C     A(N10)--- V(NWV)         CONDENSED BF TRANSFORMATION MATRIX
C     A(N11)--- NBFF(NBFT)     GLOBAL NODAL NUMBERS OF BF POINTS
C     A(N12)--- CQQ(NCQ,2)     VARIANCES OF QQ
C     A(N13)--- QQ(NBF,2)      BOUNDARY FLUX VALUES
```

```
C     A(N14)--- CFF(NWR)       THE COVARIANCE MATRIX OF FF
C
      N6=N5+NEQ
      N7=N6+NEQ+1
      N8=N7+NEQ
      NFIRST=N8
C
C     INPUT ELEMENTAL INFORMATION AND COMPUTE COORDINATE-DEPENDENT
C     ELEMENTAL QUANTITIES AND INPUT SOURCE INFORMATION
C
      CALL MESTINT(NEQ,A(N5))
      CALL CLEAN(NEQ+1,A(N6))
      CALL ELEMENT
C
C     CALL ROWLTH TO CHANGE MLST INTO MLTH, THEN CALL GADDRES TO USE
C     MLTH (A(N6)) TO COMPUTE MADR (A(N4))
C
      CALL ROWLTH(NEQ,A(N5),A(N6))
      CALL GADDRES(NEQ,NWG,MG,A(N6),A(N4))
        IF(NAPIT(5).LE.0) GOTO 20
        WRITE(NF2,FMT='(/4HMFST)')
        CALL INTOUT(NEQ,A(N5),NF2)
        WRITE(NF2,FMT='(/4HMADR)')
        CALL INTOUT(NEQ+1,A(N4),NF2)
20      CONTINUE
      READ(NF1,*) (NBFL(I,1),NBFL(I,2),CRL(I),I=1,NBL)
      NBF=0
      NBFT=0
      DO 35 I=1,NBL
      IF(NBF.LT.NBFL(I,1)) NBF=NBFL(I,1)
      NBFT=NBFT+NBFL(I,1)
35    CONTINUE
      N9=N8
      CALL VADDRES(NBF,NWV,A(N9))
      NCQ=NBF*(NBF+1)/2
      N10=N9+NBF+1
      N11=N10+NWV
      N12=N11+NBFT
      N13=N12+NCQ*2
      N14=N13+NBF*2
C
C     INPUT GLOBAL NODAL NUMBERS OF BF POINTS
C
      CALL CLEAN(NEQ+1,A(N6))
      CALL NBFFIN,A(N11),A(N6))
C
C     USE MADR AND MFST TO COMPUTE MAXA (A(N6))
C
      CALL RADDRES(NEQ,NWR,MR,A(N4),A(N5),A(N6))
        IF(NAPIT(8).LE.0) GOTO 30
        WRITE(NF2,FMT='(/4HMAXA)')
        CALL INTOUT(NEQ+1,A(N6),NF2)
```

```
30     CONTINUE
       WRITE(NF2,2005) MG,NWG,MR,NWR
       N15=N14+NWR
       NLAST=N15
       CALL CLEAN(NWR,A(N14))
       CALL CLEAN(NEQ,A(N7))
C
C      INPUT BOUNDARY CONDITIONS (NEUMANN) AND COMPUTE FF, CFF
C
       CALL BOUNDRY(SDH,SDW,A(N2X),A(N2Y),A(N6),A(N7),A(N11),A(N9),
      .             A(N10),A(N11),A(N12),A(N13))
       IF(NDR.GT.0) CALL DIRICH2(A(N6),A(N7),A(N14))
       CALL FILMAN(NF4,NWR,A(N14),-1)
       WRITE(NF2,2007) IPH,NLAST
C
CCCCCCCCCCCCCCCCCCCCCCCCCCCCCCCCCCCCCCCCCCCCCCCCCCCCCCCCCCCCCCCCCCCCC
C      2. ITERATION
CCCCCCCCCCCCCCCCCCCCCCCCCCCCCCCCCCCCCCCCCCCCCCCCCCCCCCCCCCCCCCCCCCCCC
C
       IPH=2
       N2=N1+NPARA
C
C      A(N1) --- P0(NPARA)      A PRIORI PARAMETER VALUES
C      A(N2) --- PARA(NPARA)    PARAMETERS
C      A(N8) --- G(NWG)         G MATRIX IN COMPACT FORM
C      A(N9) --- GP(NEQ)        GP VECTOR
C      A(N10)--- CP(NPARA)
C      A(N11)--- R(NWR)         R MATRIX IN COMPACT FORM
C      A(N12)--- WKF(NEQ)       WORK SPACE
C      A(N13)--- WKP(NPARA)     WORK SPACE
C
       N9=N8+NWG
       N10=N9+NEQ
       N11=N10+NPARA
       N12=N11+NWR
       N13=N12+NEQ
       N14=N13+NPARA
       NFIRST=N10
       NLAST=MAXO(N14,NFIRST+MIDST)
       IF(NLAST.GT.MTOT) THEN
       IERR=101
       PRINT*, 'PHASE',IPH,' ERROR',IERR,' MEMORY',N11,' EXCEEDS',MTOT
       STOP
       END IF
       WRITE(NF2,2003) IPH,NLAST
       CALL RELOAD(NPARA,A(N1),A(N2))
       ITER=0
50     ITER=ITER+1
C
C      FORM THE G MATRIX AND GP VECTOR FOR THE CURRENT STEP
C
       CALL CLEAN(NWG+NEQ,A(N8))
```

```
      CALL ELEMENT
C
C     COMPUTE FOR NEW PARAMETER VALUES
C
      CALL ITERAT(ITER,A(N1),A(N2),A(N4),A(N5),A(N6),A(N7),A(N8),
     .            A(N9),A(N10),A(N11),A(N12),A(N13),AB)
      PRINT*,'ITERATION ',ITER,'  DIFFERENCE=',AB
      WRITE(NFZ,2007) ITER,AB
      IF(AB.LE.STP) GOTO 200
      IF(ITER.LT.MIT) GOTO 50
200   CONTINUE
C
C
CCCCCCCCCCCCCCCCCCCCCCCCCCCCCCCCCCCCCCCCCCCCCCCCCCCCCCCCCCCCCCCCCCCC
C     3. COMPUTE A POSTERIORI VARIANCES
CCCCCCCCCCCCCCCCCCCCCCCCCCCCCCCCCCCCCCCCCCCCCCCCCCCCCCCCCCCCCCCCCCCC
C
      IV=1
      CALL COVARE(IV,A(N4),A(N5),A(N3),A(N6),A(N8),A(N12),A(N10),
     .            A(N13),A(N11))
C
C     A(N12)--- T(NODE)
C     A(N13)--- TV(NODE
C     A(N14)--- P(NODE)
C     A(N15)--- PV(NODE)
C
      N13=N12+NODE
      N14=N13+NODE
      N15=N14+NODE
      N16=N15+NODE
      CALL RESULT(A(N2),A(N3),A(N10),A(N12),A(N13),A(N14),A(N15))
C
CCCCCCCCCCCCCCCCCCCCCCCCCCCCCCCCCCCCCCCCCCCCCCCCCCCCCCCCCCCCCCCCCCCC
C     4. COMPUTE UPDATED BOUNDARY FLUXES
CCCCCCCCCCCCCCCCCCCCCCCCCCCCCCCCCCCCCCCCCCCCCCCCCCCCCCCCCCCCCCCCCCCC
C
      IFL=1
      IF(IFL.GT.0) THEN
C
C     A(N1) --- WK(NEQ,3)          WORK SPACE
C     A(N2) --- QQ(NBF,2)          UPDATED BOUNDARY FLUXES (NEW QQ)
C     A(N6)  -- MAXA(NEQ+1)
C     A(N7) --- CQQ(NCQ,2)
C     A(N7F)--- FF(NEQ)
C     A(N8) --- V(NWV)
C     A(N9) --- GP(NEQ)
C     A(N10)--- MAXV(NBF+1)
C     A(N11)--- R(NWR)
C     A(N12)--- NBFF(NPFT)
C     A(N13)--- CQN(NBF,3)         COVARIANCES OF THE NEW QQ
C
      N1=1
```

```
      N2=N1+NEQ*3
      N7F=N7+NCQ*2
      N8=N7F+NEQ
      N13=N12+NBFT
      N14=N13+NBF*3
      CALL ESFLOW(A(N1),A(N2),A(N6),A(N10),A(N8),A(N9),A(N7F),A(N7),
     .            A(N11),A(N12),A(N13))
      END IF
      RUNTIM=SECOND( )-STIME
      PRINT*,'RUNTIME IS ',RUNTIM,'.  OUTPUT FILE IS OUTPUT.'
      WRITE(NF2,*) '  RUNTIME = ',RUNTIM,' SECONDS.'
      STOP
2000  FORMAT(5X,'INPUT FILE IS ',A7,', OUTPUT FILE IS ',A7)
2001  FORMAT(////A80///
     .'      NUMBER OF NODES . . . . . (NODE) =',I6/
     .'      NUMBER OF ELEMENTS. . . . . (NELT) =',I6/
     .'      NUMNER OF THERMAL CONDUCTIVITY ZONES. (NLK) =',I6/
     .'      NUMNER OF PERMEABILITY ZONES. . . . .(NPM) =',I6/
     .'      NUMNER OF BOUNDARY FLOW SECTIONS. . . .(NBF) =',I6/
     .'      STOPPING CRITERION. . . . . .(STP) =',E8.3/
     .'      RANDOM NUMBER SEED. . . . . (IDUM) =',I6/
     .'          IF IDUM < 0, NO RANDOM NOISE IS ADDED.')
2003  FORMAT(////5X,'TOTAL CORE MEMORIES USED IN PHASE',I2,
     .    ' ------',I8)
2005  FORMAT(////5X,
     .    'MAXIMUM ROW LENGTH OF G      ----',I4,5X,
     .    'TOTAL LENGTH OF G   ----',I8//5X,
     .    'MAXIMUM COLUMN HEIGHT OF R   ----',I4,5X,
     .    'TOTAL LENGTH OF R   ----',I8)
2007  FORMAT(5X,'ITERATION',I5,'    DIFFERENCE=',E10.1)
      END


      SUBROUTINE PARAME(PARA,PR,ID,IDP,PRV,CPP,T,TV,P,PV)
C
C*****************************************************************
C     TO PUT NODAL TEMPERATURES, NODAL HEADS AND PHYSICAL PROPERTIES
C     INTO ARRAY PARA, ASSIGNING EACH PARAMETER A GLOBAL PARAMETER
C     NUMBER, AND PUT THEIR VARIANCES INTO ARRAY CPP
C*****************************************************************
C
      COMMON/CONTRL/NODE,NELT,NLK,NWG,NWR,NWV,IPH,NPM
      COMMON/NOFILE/NF1,NF2,NF3,NF4,NF5,NF6,NF7
      DIMENSION T(1),TV(1),P(1),PV(1),PARA(1),CPP(1),ID(1),
     .          PR(1),PRV(1),IDP(1)
      REWIND NF4
C
C     SET UP THE PARAMETER ARRAY PARA
C
      K1=NODE+1
      DO 100 K=NLK,0,-1
      K2=K1-1
```

```
      K1=1
      IF(K.GT.0) K1=IABS(ID(K))
      IF(K2.LT.K1) GOTO 95
      DO 90 I=K2,K1,-1
      II=2*I
      IK=II+K
      IDP(II)=IK
      PARA(IK)=P(I)
      CPP(IK)=PV(I)
      IK=IK-1
      IDP(II-1)=IK
      PARA(IK)=T(I)
      CPP(IK)=TV(I)
90    CONTINUE
95    IF(K.EQ.0) GOTO 100
      IK=IK-1
      PARA(IK)=PR(K)
      CPP(IK)=PRV(K)
C
C     CHANGE ID FROM PROPERTY NODAL NUMBERS TO PROPERTY PARA. NUMBERS
C
      IF(ID(K).LT.0) THEN
      ID(K)=-IK
      ELSE
      ID(K)=IK
      END IF
100   CONTINUE
      NPARA=NODE*2+NLK
      WRITE(NF4) (CPP(I),I=1,NPARA)
      RETURN
      END


      SUBROUTINE BOUNDRY(SDH,SDW,X,Y,MAXA,FF,CFF,MAXV,V,NBFF,CQQ,QQ)
C
C*********************************************************************
C     TO INPUT NEUMANN BOUNDARY CONDITIONS AND COMPUTE THE
C     FLUX-EQUIVALENT NODAL FLOW VECTOR FF, AND SET UP THE CFF MATRIX
C*********************************************************************
C
      COMMON/CONTRL/NODE,NELT,NLK,NWG,NWR,NWV,IFH,NPM
      COMMON/BOUND/NBL,NBFL(10,2),CRL(10),NBFT,NBF,NCQ
      COMMON/NOFILE/NF1,NF2,NF3,NF4,NF5,NF6,NF7
      COMMON/MPRINT/NAPIT(11)
      DIMENSION X(1),Y(1),MAXA(1),CFF(1),FF(1),V(1),MAXV(1),NBFF(1),
     .          CQQ(NCQ,2),QQ(NBF,2)
      DIMENSION NB(3),XY(2,3),SV(6),STD(2)
C
C     NBL  --- NUMBER OF BF SECTIONS
C     NBFL(I,1) --- NUMBER OF BF POINTS IN SECTION I,
C     NBFL(I,2) --- NULL FLUX CODE:
C                   =1, NO HEAT FLUX; WATER ONLY
```

```
C                   =2, NO WATER FLOW; HEAT ONLY
C                   =3, BOTH HEAT AND WATER FLUX EXIST
C     CRL(I) --- CORRELATION LENGTH OF BF POINTS IN SECTION I,
C                POINTS IN DIFFERENT SECTIONS MUST BE UNCORRELATED
C     NBFT --- TOTAL NUMBER OF BF POINTS IN ALL SECTIONS
C     NBF  --- NUMBER OF BF POINTS IN THE LARGEST SECTION
C     NCQ  --- MAXIMUM LENGTH OF CQQ MATRIX, NBF*(NBF+1)/2
C
      REWIND NF3
      NEQ=NODE*2
      WRITE(NF3) (MAXV(I),I=1,NBF+1),(NBFF(I),I=1,NBFT)
      N1=0
      DO 200 LLL=1,NBL
      NBF1=NBFL(LLL,1)
      NN=N1+NBF1
      NCQ1=NBF1*(NBF1+1)/2
      CALL CLEAN(NCQ*2,CQQ)
      CALL CLEAN(NWV,V)
      IF(CRL(LLL).EQ.0.0) THEN
C
C     COMPUTE CQQ FOR UNCORRELATED BF POINTS
C
      READ(NF1,*) (QQ(I,1),CQQ(I,1),QQ(I,2),CQQ(I,2),I=1,NBF1)
      WRITE(NF2,2001) LLL,0.0,(I,NBFF(N1+I),QQ(I,1),CQQ(I,1),QQ(I,2),
     .            CQQ(I,2),I=1,NBF1)
      DO 11 LHW=1,2
        IF(NBFL(LLL,2).EQ.LHW) GOTO 11
      CQQ(1,LHW)=CQQ(1,LHW)*CQQ(1,LHW)
      CQQ(2,LHW)=CQQ(2,LHW)*CQQ(2,LHW)
      NNN=NCQ1-NBF1+1
      DO 10 I=NBF1,3,-1
      CQQ(NNN,LHW)=CQQ(I,LHW)*CQQ(I,LHW)
      CQQ(I,LHW)=0.0
      NNN=NNN-I+1
10    CONTINUE
11    CONTINUE
      ELSE
C
C     COMPUTE CQQ FOR CORRELATED BF POINTS
C
      READ(NF1,*) STD(1),STD(2)
      READ(NF1,*) (QQ(I,1),QQ(I,2),I=1,NBF1)
      WRITE(NF2,2001) LLL,CRL(LLL),(I,NBFF(N1+I),QQ(I,1),STD(1),
     .            QQ(I,2),STD(2),I=1,NBF1)
      CR=CRL(LLL)*CRL(LLL)
      DO 13 LHW=1,2
        IF(NBFL(LLL,2).EQ.LHW) GOTO 13
      VAR=STD(LHW)*STD(LHW)
      ICQ=0
      DO 12 J=1,NBF1
      NJ=NBFF(N1+J)
      XJ=X(NJ)
```

```
      YJ=Y(NJ)
      DO 12 I=J,1,-1
      ICQ=ICQ+1
      NI=NBFF(N1+I)
      XX=X(NI)-XJ
      YY=Y(NI)-YJ
      DIS=(XX*XX+YY*YY)/CS
        IF(DIS.GT.200) GOTO 12
      CQQ(ICQ,LHW)=VAR*EXP(-0.5*DIS)
12    CONTINUE
13    CONTINUE
      END IF
      READ(NF1,*) NSUR
      WRITE(NF2,2002) NSUR
      IF(NBFL(LLL,2).NE.1) WRITE(NF3) NCQ1,((CQQ(I,J),I=1,NCQ1),J=1,2)
C
C     NB(3) --- BF NUMBERS OF THE BF POINTS, NOT NODAL NUMBERS, WHICH
C               ARE IN NBFF
C
      N=1
15    READ(NF1,*) NB,KK,KN
      WRITE(NF2,2003) N,NB,KK,KN
      NIP=3
      IF(NB(3).EQ.0) NIP=2
      DO 75 L=1,KN
      DO 20 J=1,NIP
      JJ=NB(J)
      NJ=NBFF(N1+JJ)
      XY(1,J)=X(NJ)
      XY(2,J)=Y(NJ)
20    CONTINUE
      CALL BOUQUAD(NIP,XY,SV)
      CALL ADDBAN(V,MAXV,SV,NB,NIP)
      DO 50 J=1,NIP
50    NB(J)=NB(J)+KK
75    N=N+1
      IF(N.LE.NSUR) GOTO 15
        IF(NAPIT(3).GT.0) THEN
        WRITE(NF2,'(5X,8HV MATRIX)')
        DO 100 I=1,NBF1
        J1=MAXV(I)
        J2=MAXV(I+1)-1
100     WRITE(NF2,'(I5/(5X,10E12.6))') I,(V(J),J=J1,J2)
        END IF
        IF(NBFL(LLL,2).NE.1) THEN
        WRITE(NF3) (V(I),I=1,NWV)
        WRITE(NF3) (V(I),I=1,NWV)
        END IF
      CALL FORMFF(NBF1,NBFF(N1+1),V,MAXV,QQ,FF,LLL)
      CALL FORMCFF(NBF1,NODE,SDH,SDW,NBFF(N1+1),V,MAXV,CQQ,CFF,MAXA,
     .             QQ,LLL)
200   N1=NN
```

```
      SDHH=SDH*SDH
      SDWW=SDW*SDW
      DO 230 I=1,NODE
      II=I+I
      IC1=MAXA(II-1)
      IC2=MAXA(II)
      CFF(IC1)=CFF(IC1)+SDHH
      CFF(IC2)=CFF(IC2)+SDWW
230   CONTINUE
      IF(NAPIT(11).GT.0) WRITE(NF2,'(/2HFF/(10E12.6))') (FF(I),I=1,NEQ)
      IF(NAPIT(4).GT.0) THEN
      WRITE(NF2,'(3HCFF)')
      DO 250 I=1,NEQ
      J1=MAXA(I)
      J2=MAXA(I+1)-1
250   WRITE(NF2,'(I5/(5X,10E12.6))') I,(CFF(J),J=J1,J2)
      END IF
      RETURN
2001  FORMAT(//5X,'GROUP ',I3,' BOUNDARY FLOW (BF) POINTS INFORMATION'//
     .    5X,'CORRELATION LENGTH = ',E10.4,' M'//
     .   6X,'BF    BF NODAL',12X,'H E A T',23X,'W A T E R'/
     .   4X,'NUMBER   NUMBER ',2(6X,'FLUX',8X,'   STD  ',4X)/
     .   (5X,I4,I9,2X,2(2E15.6,1X)))
2002  FORMAT(//5X,I5,' BOUNDARY FLOW LINES'//5X,
     .   'LINE',9X,'BF  POINT  NUMBER',11X,'GENERATION',5X,'LINES'//
     .   4X,'NUMBER',7X,'1',9X,'2',9X,'3',7X,'INCREMENT   GENERATED'/)
2003  FORMAT(5X,I3,2X,3I10,5X,I7,8X,I5)
      END


      SUBROUTINE ITERAT(IT,PO,PARA,MADR,MEST,MAXA,FF,G,GP,CP,R,
     .                  WKF,WKP,AB)
C
C*****************************************************************
C     TO PERFORM ONE ITERATION FOR THE ESTIMATE OF PARA
C*****************************************************************
C
      COMMON/CONTRL/NODE,NELT,NLK,NWG,NWR,NWV,IPH,NPM
      COMMON/NOFILE/NF1,NF2,NF3,NF4,NF5,NF6,NF7
      COMMON/MPRINT/NAPIT(11)
      DIMENSION PO(1),PARA(1),MADR(1),MEST(1),MAXA(1),FF(1),G(1),
     .        GP(1),CP(1),R(1),WKF(1),WKP(1)
      REWIND NF4
      NEQ=NODE*2
      NPARA=NEQ+NLK
      DO 20 I=1,NPARA
20    PARA(I)=PARA(I)-PO(I)
C
C     READ IN A PRIORI COVARIANCE MATRICES CPP AND CFF FROM FILE NF4
C
      READ(NF4) (CP(I),I=1,NPARA)
      READ(NF4) (R(I),I=1,NWR)
```

```
      CALL FORMR(NEQ,MFST,MADR,MAXA,G,CP,R)
        IF(NAPIT(6).GT.0) THEN
        WRITE(NF2,FMT='(8HG MATRIX)')
        DO 25 I=1,NEQ
        J1=MADR(I)
        J2=MADR(I+1)-1
25      WRITE(NF2,FMT='(I5/(5X,10E12.6))') I,(G(J),J=J1,J2)
        END IF
        IF(NAPIT(7).GT.0) WRITE(NF2,FMT='(2HGP/(10E12.6))')
     .           (GP(I),I=1,NEQ)
        IF(NAPIT(9).GT.0) THEN
        WRITE(NF2,FMT='(8HR MATRIX)')
        DO 30 I=1,NEQ
        J1=MAXA(I)
        J2=MAXA(I+1)-1
30      WRITE(NF2,FMT='(I5/(5X,10E12.6))') I,(R(J),J=J1,J2)
        END IF
      DO 50 I=1,NEQ
50    WKF(I)=FF(I)-GP(I)
      IF(IT.GT.1) THEN
      CALL GTIMEP(NEQ,MFST,MADR,G,PARA,WKP)
      DO 70 I=1,NEQ
70    WKF(I)=WKF(I)+WKP(I)
      END IF
      CALL COLSOL(R,WKF,MAXA,NEQ,2,NER)
      IF(NER.NE.0) THEN
      PRINT*,'ERROR ',NER,' IN PHASE 2, ITERATION ',IT
      PRINT*,'R MATRIX NOT POSITIVE DEFINITE.'
      STOP
      END IF
      CALL CLEAN(NPARA,WKP)
      CALL GTTIMP(NEQ,MFST,MADR,G,WKF,WKP)
C
C     OBTAIN THE SOLUTION P-P0
C
      DO 80 I=1,NPARA
80    WKP(I)=CP(I)*WKP(I)
      AB=0.0
      DO 100 I=1,NPARA
      AA=ABS(WKP(I)-PARA(I))
      IF(AB.LT.AA) AB=AA
100   CONTINUE
C
C     OBTAIN THE SOLUTION P BY ADDING P0 TO P-P0
C
      DO 120 I=1,NPARA
120   PARA(I)=WKP(I)+P0(I)
        IF(NAPIT(10).GT.0) WRITE(NF2,FMT='(1HP/(10E12.6))') (PARA(I),
     .           I=1,NPARA)
      RETURN
      END
```

```
      SUBROUTINE  OVARE(IV,MADR,MFST,ID,MAXA,G,F2,CP,F1,R)
C
C*****************************************************************
C     TO COMPUTE ASYMPTOTIC A POSTERIORI VARIANCES OF THE
C     PARAMETERS (DIAGONAL ELEMENTS OF THE COVARIANCE MATRIX).
C       IV  A POSTERIORI VARIANCES COMPUTATION FLAG
C           < 0, THE VARAINCES OF PHYSICAL PROPERTIES ONLY
C           = 0, NO VARIANCES COMPUTED
C           > 0, ALL VARIANCES COMPUTED
C*****************************************************************
C
      COMMON/CONTRL/NODE,NELT,NLK,NWG,NWR,NWV,IPH,NPM
      COMMON/NOFILE/NF1,NF2,NF3,NF4,NF5,NF6,NF7
      DIMENSION MADR(1),MFST(1),G(1),F2(1),CP(1),F1(1),MAXA(1),R(1),
     .          ID(1)
      REWIND NF4
      NEQ=2*NODE
      NPARA=NEQ+NLK
C
C     READ IN A PRIORI CPP FROM FILE NF4
C
      READ(NF4) (CP(I),I=1,NPARA)
      IF(IV) 20,10,30
10    RETURN
20    NN=NLK
      GOTO 40
30    NN=NPARA
40    CONTINUE
      CALL CGT(NEQ,MFST,MADR,G,CP)
      DO 100 II=1,NN
      IC=II
      IF(IV.LT.0) IC=IABS(ID(II))
      CALL GCOLUMN(IC,NEQ,MFST,MADR,G,F1)
      CALL RELOAD(NEQ,F1,F2)
      CALL COLSOL(R,F1,MAXA,NEQ,3,NER)
      FF=0.0
      DO 50 I=1,NEQ
50    FF=FF+F1(I)*F2(I)
      CP(IC)=CP(IC)-FF
100   CONTINUE
      RETURN
      END


      SUBROUTINE ESFLOW(WK,QQ,MAXA,MAXV,V,GP,FF,CQQ,R,NBFF,CQS)
C
C*****************************************************************
C     TO COMPUTE THE UPDATED BOUNDARY FLUXES AND THE VARIANCE
C*****************************************************************
C
      COMMON/CONTRL/NODE,NELT,NLK,NWG,NWR,NWV,IPH,NPM
      COMMON/BOUND/NBL,NBFL(10,2),CRL(10),NBFT,NBF,NCQ
```

```
      COMMON/NOFILE/NF1,NF2,NF3,NF4,NF5,NF6,NF7
      DIMENSION WK(NODE*2,3),QQ(NBF,2),MAXA(1),MAXV(1),V(1),GP(1),
     .          FF(1),CQQ(NCQ,2),R(1),NBFF(1),CQN(NBF,3)
      DIMENSION MINUS(2),Q(3)
      DATA MINUS/1,0/
      REWIND NF3
      WRITE(NF2,2001)
      NEQ=NODE*2
C
C     FILE NF3 CONTAINS THE V MATRIX, NODAL NUMBERS (NBFF), AND
C     A PRIORI CQQ MATRIX FOR EACH BF SECTION
C
      READ(NF3) (MAXV(I),I=1,NBF+1),(NBFF(I),I=1,NBFT)
      N1=0
      DO 200 LLL=1,NBL
      NBF1=NBF(LLL,1)
      NN=N1+NBF1
      IF(NBFL(LLL,2).EQ.1) GOTO 200
      READ(NF3) NCQ1,((CQQ(I,J),I=1,NCQ1),J=1,2)
      READ(NF3) (V(I),I=1,NWV)
      DO 20 I=1,NBF1
      II=NBFF(N1+1)*2
      QQ(I,1)=GP(II-1)
20    CONTINUE
      CALL COLSOL(V,QQ(1,1),MAXV,NBF1,2,NER)
      READ(NF3) (V(I),I=1,NWV)
      ICQ=1
      DO 80 IC=1,NBF1
      ICQ=ICQ+IC-1
      CALL CLEAN(NEQ,FF)
      CALL VCOLUM(IC,NBF1,MINUS(1),NBFF(N1+1),V,MAXV,CQQ(1,1),FF)
      CALL RELOAD(NEQ,WK(1,2),WK(1,3))
      CALL RELOAD(NEQ,WK(1,1),WK(1,2))
      CALL RELOAD(NEQ,FF,WK(1,1))
      CALL COLSOL(R,FF,MAXA,NEQ,3,NER)
      KC=3
      IF(IC.LT.3) KC=IC
      DO 50 KQ=1,KC
      Q(KQ)=0.0
      DO 50 K=1,NEQ
      Q(KQ)=Q(KQ)+FF(K)*WK(K,KQ)
50    CONTINUE
      CQN(IC,1)=CQQ(ICQ,1)-Q(1)
      IF(IC.EQ.1) GOTO 70
      CQN(IC-1,2)=CQQ(ICQ+1,1)-Q(2)
      IF(IC.EQ.2) GOTO 70
      CQN(IC-2,3)=CQQ(ICQ+2,1)-Q(3)
70    CQN(IC,1)=SQRT(CQN(IC,1))
80    CONTINUE
      WRITE(NF2,2002) (I,NBFF(N1+I),QQ(I,1),CQN(I,1),I=1,NBF1)
      WRITE(NF6,*) NBF1,(NBFF(N1+I),I=1,NBF1),(QQ(I,1),I=1,NBF1),
     .          ((CQN(I,J),I=1,NBF1),J=1,3)
```

```
200   N1=NX
      RETURN
2001  FORMAT(///5X,'UPDATED BOUNDARY HEAT FLOW'//
     .   6X,'BF    BF NODAL',12X,'H E A T',23X,'          '/
     .   4X,'NUMBER   NUMBER ',6X,'FLUX',8X,'   STD  ',4X)
2002  ORMAT((5X,I4,I9,2X,2E15.6))
      END


      SUBROUTINE ELEMENT
C
C*****************************************************************
C     THIS IS A SWITCH SUBROUTINE. ALL ELEMENTAL COMPUTATION
C     SOUBROUTINES HAS TO BE REACHED VIA THIS ONE.
C     NELE ---TOTAL NUMBER OF ELEMENTS
C             =1, PLANE ELEMENT
C             =2, AXI-SYMMETRIC ELEMENT
C     NPRS ---THE ORDER OF GAUSS INTEGRATION
C     NDM  ---MAXIMUN NUMBER OF NODES IN ONE ELEMENT
C     NPNP ---TOTAL NUMBER OF GAUSS POINTS (NPRS*NPRS)
C     NEG  ---TOTAL NUMBER OF CONGRUENT ELEMENT GROUPS
C     IEG  ---THE ELEMENTAL NUMBER OF THE LAST ELEMENT OF EACH GROUP
C*****************************************************************
C
      COMMON/CONTRL/NODE,NELT,NLK,NWG,NWR,NWV,IPH,NPM
      COMMON/NOFILE/NF1,NF2,NF3,NF4,NF5,NF6,NF7
      COMMON/ELECON/NELE,NPRS,NDM,NPNP,NEG,IEG(200)
      COMMON/POSITN/N1,N2,N2X,N2Y,N2P,N3,N4,N5,N6,N7,N8,N9,N10,N11,
     .              N12,N13,N14,MTOT,NFIRST,NLAST,MIDST
      COMMON/BLANK/A(1000000)
      REWIND NF5
      NEQ=2*NODE
C
C     IPH=1, INPUT PHASE. INPUT ELEMENTAL INFORMATION AND COMPUTE
C            SHAPE FUNCTIONS, DERIVATIVES, JOCOBIAN AND SOURCE TERM.
C       =2, ITERATION PHASE. COMPUTE G MATRIX AND GP VECTOR.
C
      IF(IPH.GT.1) GOTO 20
      NELE=NELT
      READ(NF1,*) NPRS,NDM,NEG
      WRITE(NF2,2001) NELE,1,NPRS,NDM,NEG
      NPNP=NPRS*NPRS
      READ(NF1,*) (IEG(I),I=1,NEG)
      WPITE(NF2,2002) (IEG(I),I=1,NEG)
20    CONTINUE
      N101=NFIRST
      N102=N101+NDM*2*NELE
      N103=N102+(NDM*2+2)*NELE
      N104=N103+NEG
      N105=N104+NEG*NPNP
      N106=N105+NEG*NPNP*NDM
      N107=N106+NEG*NPNP*NDM*2
```

```
      N108=N107+NEG*NPNP*NDM*NDM
      N109=N108+NELE*2
C
C     A(N101) --- LME(NDM2,NELE)  GLOBAL EQUATION NUMBERS
C     A(N102) --- LMP(NDM2+2,NELE) GLOBAL PARAMETER NUMBERS
C     A(N103) --- IELL(NEG)         NUMBER OF NODES IN EACH C.E. GROUP
C     A(N104) --- DET(NPNP,NEG)     JACOBIAN FOR EACH C.E. GROUP
C     A(N105) --- HH(NPNP*NDM,NEG)
C     A(N106) --- B(NPNP*NDM*2,NEG)
C     A(N107) --- SS(NPNP*NDM*NDM,NEG)
C     A(N108) --- LID(2,NELE)       GLOBAL PROPERTY NUMBERS
C
      IF(NLAST.LT.N109) NLAST=N109
      IF(NLAST.GT.MTOT) THEN
      IERR=203
      WRITE(NF2,*)'PHASE',IPH,' ERROR',IERR,' MEMORY',NLAST,
     .          ' EXCEEDS',MTOT
      STOP
      END IF
      MIDST=N108-NFIRST
      GOTO (60,100) IPH
60    CONTINUE
      CALL ELPRIN(NELE,A(N108))
      CALL FINEIN(A(N2X),A(N2Y),A(N3),A(N4),A(N5),A(N6),
     .          A(N101),A(N102),A(N103),A(N104),
     .          A(N105),A(N106),A(N107),A(N108))
      CALL FILMAN(NF5,MIDST,A(N101),-1)
      RETURN
100   CONTINUE
      CALL FILMAN(NF5,MIDST,A(N101),1)
      CALL CUPQUAD(A(N2),A(N4),A(N5),A(N8),A(N9),A(N101),A(N102),
     .            A(N103),A(N104),A(N105),A(N106),A(N107))
      RETURN
2001  FORMAT(////5X,'2-D FINITE ELEMENT INFORMATION'//
     . '      NUMBER OF ELEMENTS. . . . . . . . . . (NELE) =',I6/
     . '      ELEMENT TYPE. . . . . . . . . . . . . (ITYP) =',I6/
     . '              ITYP=1, PLANE ELEMENT'/
     . '              ITYP=2, AXISYMMETRIC ELEMENT'/
     . '      ORDER OF GAUSS INTEGRATION. . . . . . (NPRS) =',I6/
     . '      MAXIMUM NUMBER OF NODES IN ONE ELEMENT (NDM) =',I6/
     . '      NUMBER OF CONGRUENT ELEMENT GROUPS. . .(NEG) =',I6)
2002  FORMAT(///5X,'THE ELEMENTAL NUMBER OF THE LAST ELEMENT OF',
     . ' EACH CONGRUENT ELEMENT GROUP'//(5X,2015))
      END


      SUBROUTINE CUPQUAD(PARA,MADR,MFST,G,GP,LME,LMP,IELL,DET,HH,
     .                   B,SS)
C
C*********************************************************************
C     TO COMPUTE ELEMENTAL G MATRIX AND GP VECTOR AND ADD THEM TO
C     THE GLOBAL ONES
```

```
C*********************************************************************
C
      COMMON/ELECON/NELE,NPRS,NDM,NPNP,NEG,IEG(200)
      COMMON/NOFILE/NF1,NF2,NF3,NF4,NF5,NF6,NF7
      COMMON/DIR1/NDR,IDR(50),IDE(50,2),ADR(50,2),TP(50,2),TPV(50,2)
      DIMENSION PARA(1),MADR(1),MFST(1),G(1),GP(1),LME(NDM*2,1),
     .          LMP(NDM*2+2,1),IELL(1),DET(NPNP,1),HH(NPNP*NDM,1),
     .          B(NPNP*NDM*2,1),SS(NPNP*NDM*NDM,1)
      DIMENSION S(16,18),SP(16),T(8),P(8)
      AL10=ALOG(10.)
      NIEG=0
      IE=0
      DO 200 I=1,NELE
      IF(I.GT.NIEG) THEN
      IE=IE+1
      NIEG=IEG(IE)
      IEL=IELL(IE)
      ND=IEL*2
      ND2=16
      NS=IEL*IEL
      END IF
      DO 30 L=1,IEL
      L2=L+L
      LL=LMP(L2-1,I)
      T(L)=PARA(LL)
      LL=LMP(L2,I)
30    P(L)=PARA(LL)
      LL=LMP(ND+1,I)
      CD=EXP(PARA(LL)*AL10)
      IF(PARA(LL).EQ.0.) CD=0.0
      LL=LMP(ND+2,I)
      PM=EXP(PARA(LL)*AL10)
      IF(PARA(LL).EQ.0.) PM=0.0
      I1=1
      I2=1
      I3=1
      CALL CLEAN(288,S)
      CALL CLEAN(ND,SP)
C
C     LOOP FOR ALL GAUSS POINTS TO PERFORM NUMERICAL INTEGRATION
C     IN THE COMPUTATION OF G MATRIX
C
      DO 100 J=1,NPNP
      CALL QUADS(IEL,CD,PM,T,P,DET(J,IE),HH(I1,IE),B(I2,IE),S,
     .                 SP,SS(I3,IE),AL10)
      I1=I1+IEL
      I2=I2+ND
      I3=I3+NS
100   CONTINUE
C
C     CALL ADDG TO ADD THE ELEMENTAL G MATRIX S TO THE GLOBAL ONE
C
```

```
      CALL ADDG(ND,ND2,2,LME(1,I),LMP(1,I),MADR,MFST,S,G)
C
C     ADD THE ELEMENTAL GP VECTOR SP TO THE GLOBAL ONE
C
      DO 150 J=1,ND
      JJ=LME(J,I)
      GP(JJ)=GP(JJ)+SP(J)
150   CONTINUE
200   CONTINUE
C
C     DIRICHLET CONDITION TERM ADDED TO GP AND G
C
      IF(NDR.LE.0) RETURN
      KK=1
      DO 310 J=1,2
      DO 300 I=1,NDR
      IIE=IDR(I)*2-KK
      IIP=IDE(I,J)
      GP(IIE)=GP(IIE)+ADR(I,J)*TP(I,J)
      IIG=MADR(IIE)+IIP-MFST(IIE)
      G(IIG)=G(IIG)+ADR(I,J)
300   CONTINUE
310   KK=KK-1
      RETURN
      END


      SUBROUTINE QUADS(IEL,CD,PM,T,P,DET,H,B,S,SP,SS,AL10)
C
C*********************************************************************
C     TO COMPUTE THE ELEMENTAL G MATRIX AND GP VECTOR AT THE
C     CURRENT GAUSS POINT (R,S)
C*********************************************************************
C
      DIMENSION H(IEL),B(2,IEL),S(16,1),SP(16),T(IEL),P(IEL),SS(IEL,1)
      DIMENSION S11(8,8),S21(8,8),S22(8,8)
      DATA PC,PO,BATA,VO,ATA,TO,GR/4.18E+6,995.9125,.53625,1253.1,
     .            32.579,30.,9.8/
C
C     PC --- THERMAL CAPACITY [J/M**3/K] (CONSTANT)
C     PO --- REFRENCE WATER DENSITY [KG/M**3] (CONSTANT)
C     BATA-- SLOPE OF WATER DENSITY [KG/M**3] (CONSTANT)
C     VO --- REFERENCE RECIPEROCAL VISCOSITY
C     ATA--- SLOPE OF DYNAMIC VISCOSITY [M S/KG/K] (CONSTANT)
C     TO --- REFERENCE TEMPERATURE
C     GR --- GRAVITATIONAL ACCELERATION [M/S**2] (CONSTANT)
C     CD --- THERMAL CONDUCTIVITY [W/M/K] (PARAMETER)
C     PM --- PERMEABILITY [M**2] (PARAMATER)
C
      BT1=0.
      BT2=0.
      BP1=0.
```

```
      BP2=0.
      HT=0.
      ND=IEL*2
      DO 50 L=1,IEL
      PL=P(L)
      TL=T(L)
      BP1=BP1+B(1,L)*PL
      BP2=BP2+B(2,L)*PL
      BT1=BT1+B(1,L)*TL
      BT2=BT2+B(2,L)*TL
      HT=HT+H(L)*TL
50    CONTINUE
C
      POG=PO*GR
      VIS=VO+ATA*HT
      V1=POG*BP1
      V2=POG*(BP2-RATA*HT/PG)
      PMV=PM*VIS*DET
      CDT=CD*DET
      ALL=PC*PMV
      A21=PMV*GR*BATA
      A22=PMV*POG
C
C     THE FOLLOWING DO LOOP COMPUTES THE ELEMENTAL TRANSFER MATRIX
C
      DO 80 L=1,IEL
      FA11=ALL*H(L)
      FA21=A21*B(2,L)
      DO 80 K=1,IEL
      S11(L,K)=SS(L,K)*CDT-FA11*(V1*B(1,K)+V2*B(2,K))
      S21(L,K)=-FA21*H(K)
      S22(L,K)=A22*SS(L,K)
80    CONTINUE
C
      FAC=PC*PM*(ATA*V1*BT1+(ATA*V2-BATA*GR*VIS)*BT2)*DET
      A211=PM*GR*ATA*BATA*HT*DET
      A212=PM*ATA*POG*DET
      ALLPG=ALL*POG
      FAK=ALL*(V1*BT1+V2*BT2)
      DO 200 L=1,IEL
      L2=L+L
      L1=L2-1
      FACH=FAC*H(L)
      ALLPGH=ALLPG*H(L)
      FA211=A211*B(2,L)
      FA212=A212*(B(1,L)*BP1+B(2,L)*BP2)
      DO 180 M=1,IEL
      M2=M+M
      M1=M2-1
      S(L1,M1)=S(L1,M1)+S11(L,M)-FACH*H(M)
      S(L1,M2)=S(L1,M2)-ALLPGH*(B(1,M)*BT1+B(2,M)*BT2)
      S(L2,M1)=S(L2,M1)+S21(L,M)+H(M)*(FA212-FA211)
```

```
      S(L2,M2)=S(L2,M2)+S22(L,M)
180   CONTINUE
      S(L1,ND+1)=S(L1,ND+1)+CDT*(B(1,L)*BT1+B(2,L)*BT2)*AL10
      S(L1,ND+2)=S(L1,ND+2)-FAK*H(L)*AL10
      S(L2,ND+1)=0.0
200   CONTINUE
C
      DO 250 L=1,IEL
      G1=0.0
      G2=0.0
      L2=L+L
      L1=L2-1
      DO 240 K=1,IEL
      G1=G1+S11(L,K)*T(K)
      G2=G2+S21(L,K)*T(K)+S22(L,K)*P(K)
240   CONTINUE
      SP(L1)=SP(L1)+G1
      SP(L2)=SP(L2)+G2
      S(L2,ND+2)=S(L2,ND+2)+G2*AL10
250   CONTINUE
      RETURN
      END
```

REFERENCES

Andrews, C.B. and M.P. Anderson, Impact of a power plant on the groundwater system of a wetland, *Ground Water*, *16*(2), 105–111, 1978.

Andrews, C.B. and M.P. Anderson, Thermal alteration of groundwater by seepage from a cooling lake, *Water Resour. Res.*, *15*(3), 595–602, 1979.

Angeliar, J., A. Tarantola, S. Manoussis and B. Valette, Inversion of field data in fault tectonics to obtain the regional stress tensor, *Geophys. J. R. astr. Soc.*, *69*, 607–621, 1982.

Bachu, S., Influence of lithology and fluid flow on the temperature distribution in a sedimentary basin: a case study from the cold lake area, Alberta, Canada, *Tectonophysics*, *120*, 257–284, 1985.

Backus, G.E., Bayesian inference in geomagnetism, *Geophys. J.*, *92*, 125–142, 1988.

Backus, G.E. and F. Gilbert, The resolving power of gross Earth data, *Geophys. J. R. astr. Soc.*, *16*, 169–205, 1968.

Bakr, A.A., L.W. Gelhar, A.L. Gutjahr and J.R. MacMillan, Stochastic analysis of spatial variability in subsurface flows: 1. comparaisom of one– and three–dimensional flows, *Water Resour. Res.*, *14*(2), 263–271, 1978.

Ballard, S. and H.N. Pollack, Diversion of heat by Archean cratons: a model for southern Africa, *Earth Planet. Sci. Lett.*, *85*, 253–264, 1987.

Bass, B.R., Application of the finite element method to the nolinear inverse heat conduction problem using Beck's second method, *ASME, J. Eng. Industry*, *102*, 168–176, 1980.

Bathe, K.J. and E.L. Wilson, *Numerical Methods in Finite Element Analysis*, Prentice–Hall, Englewood Cliffs, 1976.

Bear, J., *Dynamics of Fluids in Porous Media*, American Elsevier, New York, 1972.

Beck, A.E., An improved method of computing the thermal conductivity of fluid–filled sedimentary rocks, *Geophysics*, *41*(1), 133–144, 1976.

Beck, A.E., Methods for determining thermal conductivity and thermal diffusivity, in *Handbook of Terrestrial Heat–Flow Density Determination*, edited by R. Haenel, L. Rybach and L. Stegena, Kluwer Academic Publishers, Dordrecht, 1988.

Beck, A.E. and P.Y. Shen, On a more rigorous approach to geothermic problems, *Tectonophysics*, in press, 1989.

Beck, A.E., K. Wang and P.Y. Shen, Sub–bottom temperature perturbations due to temperature variations at the boundary of inhomogeneous lake or oceanic sediments, *Tectonophysics*, *121*, 11–24, 1985.

Beck, J.V., Nonlinear estimation applied to the nonlinear inverse heat conduction problem, *Int. J. Heat Mass Transfer*, *13*, 703–716, 1970.

Bejan, A., *Convection Heat Transfer*, Wiley, New York, 1984.

Berger, J.O. and R.L. Wolpert, *The Likelihood Principle*, Institue of Mathematical Statistics, Hayward, Calif., 1984.

Bethke, C.M., A numerical model of compaction–driven groundwater flow and heat transfer and its application to the paleohydrology of intracratonic sedimentary basins, *J. Geophys. Res.*, *90*(*B*), 6817–6828, 1985.

Beveridge, G.S.G. and R.S. Schechter, *Optimization: Theory and Practice*, McGraw–Hill, New York, 1965.

Birch, F., Flow of heat in the Front Range, Colorado, *Bull. Geol. Soc. Amer.*, *61*, 567–620, 1950.

Birch, F., R.F. Roy and E.R., Decker, Heat flow and thermal history in New England and New York, in *Study of Appalachian Geology: Northern and Maritime*, edited by E. Zen, W.S. White and J.B. Hadley, John Wiley & Sons, New York, 1968.

Blackwell, D.D., J.L. Steel and C.A. Brott, The terrain effect on terrestrial heat flow, *J. Geophys. Res.*, *85*, 4757–4772.

Bodvarsson, C., Downward continuation of constrained potential fields, *J. Geophys. Res.*, *78*(*8*), 1288–1292, 1973.

Box, G.E.P. and G.C. Tiao, *Bayesian Inference in Statistical Analysis*, Addison–Wesley, Reading, Massachusetts, 1973.

Brailsford, A.D. and K.G. Major, The thermal conductivity of aggregates of several phases, including porous materials, *Brit. J. Appl. Phys.*, *15*, 313–319, 1964.

Brott, C.A., D.D. Blackwell and P. Morgan, Continuation of heat flow data: a method to construct isotherms in geothermal areas, *Geophysics*, *46*(*12*), 1732–1744, 1981.

Burden, R.L., J.D. Faires and A.C. Reynolds, *Numerical Analysis*, Prindle, Weber & Schmidt, Boston, 1981.

Burrus, J. and F. Bessis, Thermal modeling in the Provencal Basin (NW–Mediterranean), in *Thermal Modeling in Sedimentary Basins*, edited by J. Burrus Technip, Paris, 393–416, 1986.

Carrera, J. and S.P. Neuman, Estimation of aquifer parameters under transient and steady state conditions: 1. Maximum likelihood method incorporating priori information, *Water Resour. Res.*, *22*(*2*), 199–210, 1986a.

Carrera, J. and S.P. Neuman, Estimation of aquifer parameters under transient and steady state conditions: 2. uniqueness, stability and solution algorithms, *Water Resour. Res.*, *22*(2), 211–227, 1986b.

Carrera, J. and S.P. Neuman, Estimation of aquifer parameters under transient and steady state conditions: 3. application to synthetic and field data, *Water Resour. Res.*, *22*(2), 228–242, 1986c.

Carslaw, H.S. and J.C. Jaeger, *Conduction of Heat in Solids*, Oxford Univ. Press, London, 1959.

Cermak, V., Underground temperature and inferred climatic temperature of the past millienium, *Palaeogeogr. Palaeoclimatol. Palaeoecol.*, *10*, 1–10, 1971.

Cermak, V., Heat flow in a sedimentary basin in Czechoslovakia: evaluation of data with special attention to hydrology, in *Hydrological regimes and their subsurface thermal effects*, edited by A.E. Beck, L. Stegena and G. Garven, AGU monograph series, Washington, in press, 1989.

Cermak, V. and L. Bodri, Two–dimensional temperature modelling along five east–European geotransverses, *J. Geodynamics*, *5*, 133–163, 1986.

Cermak, V. and E. Hurtig, Heat flow map of Europe, 1:5,000,000, in *Terrestrial Heat Flow in Europe*, edited by V. Cermak and L. Rybach, Springer Verlag, Berlin and New York: enclosure, 1979.

Cermák, V. and J. Jetel, Heat flow and ground water movement in the Bohemian Cretaceous Basin (Czechoslovakia), *J. Geodynamics*, *4*, 285–303, 1985.

Chapman, D.S., T.H. Keho, M.S. Bauer and M.D. Picard, Heat flow in the Uinta Basin determined from bottom hole temperature (BHT) data, *Geophysics*, *49*, 453–466, 1984.

Cheremenski, G.A., *Applied Geothermics*, Publish House "Nedra", Leningrad, 1977 (Chinese translation of Russian original, by Y. Zhao and M. Chen, Geological Publishing House, Beijing, 1982).

Celia, M.A. and W.G. Gray, An improved isoparametric transformation for finite element analysis, *Int. J. Num. Meth. Eng.*, *20*, 1443–1459, 1984.

Chavent, G., M. Dupuy and P. Lemonnier, History matching by use of optimal control theory, *Soc. Pet. Eng. J.*, *15*(1), 74–86, 1975.

Clauser, C., A climatic correction on temperature gradients using surface temperature series of various periods, *Tectonophysics*, *103*, 33–46, 1984.

Clauser, C., Opacity – the concept of radiative thermal conductivity, in *Handbook of Terrestrial Heat–Flow Density Determination*, edited by R. Haenel, L. Rybach and L. Stegena, Kluwer Academic Publishers, Dordrecht, 1988.

Clauser, C., Undersuchungen zur Trennung der konduktiven und konvektiven Anteile im Wärmetransport in einem Sedimentbecken am Beispiel des

Oberrheintalgrabens, Ph.D. thesis, Technichen Universität Berlin, Berlin, 1983.

Constable, S.C., R.L. Parker and C.G. Constable, Occam's inversion: a practical algorithm for generating smooth models from electromagnetic sounding data, *Geophysics*, *52*(3),289–300, 1987.

Cooley, R.L., A method of estimating parameters and assessing reliability for models of steady state groundwater flow: 1. theory and numerical properties, *Water Resour. Res.*, *13*(2), 318–324, 1977.

Cooley, R.L., A method of estimating parameters and assessing reliability for models of steady state groundwater flow: 2. application of statistical analysis, *Water Resour. Res.*, *15*(3), 603–617, 1979.

Cooke, D.A. and W.A. Schneider, Generalized linear inversion of reflection seismic data, *Geophysics*, *48*(6), 665–676, 1983.

Dagan, G., Stochastic modeling of groundwater flow by unconditional and conditional probabilities, 1, confined simulation and the direct problem, *Water. Resour. Res.*, *18*(4), 813–833, 1982.

Dagan, G., Stochastic modeling of groundwater flow by unconditional and conditional probabilities: the inverse problem, *Water Resour. Res.*, *21*(1), 65–72, 1985.

Dagan, G., Statistical theory of groundwater flow and transport: pore to labarotory, laboratory to formation and formation to regional scale, *Water Resour. Res.*, *22*(9), 120S–134S, 1986.

Delfiner, P., Linear estimation of non–stationary spatial phenomena, in *Advanced Geostatistics in the Mining Industry*, 49–68. D. Reidel, Dordrecht, Holland, 1976.

Delhomme, J.P., Kriging in hydrosciences, *Adv. in Water Resour.*, *1*(5), 251–266, 1978.

Deming, D. and D. Chapman, Inversion of bottom–hole temperature data: the Pineview field, Utah–Wyoming thrust belt, *Geophysics*, *53*(5), 707–720, 1988.

Doligez, B., F. Bessis, J. Burrus, P. Ungerer and P.Y. Chénet, Integrated numerical simulation of the sedimentation, heat transfer, hydrocarbon formation and fluid migration in a sedimentary basin: the THEMIS model, in: *Thermal Modeling in Sedimentary Basins*, edited by J. Burrus, Technip, Paris, 173–195, 1986.

Finckh, P., Heat flow measurements in 17 perialpine lakes, *Geol. Soc. Ame. Bull.*, *92*(2), 452–514, 1981.

Finckh, P., On the calibration of lacustrine heat flow density measurements in a borehole in lake Zurich, Switzerland, *Zbl. Geol. Palaont. Teil I, H.1/2*, 102–117, 1983.

Fitterman, D.V. and R.F. Corwin, Inversion of self–potential data from the Cerro Prieto geothermal field, Mexico, *Geophysics*, *47*(6), 938–945, 1982.

Fradkin, L.J. and L.A. Dokter, Statistical identification of hydrological distributed–parameter systems: theory and applications, *Water Resour. Res.*, *23*(1), 15–31, 1987.

Franklin, J.N., Well–posed stochastic extensions of ill–posed linear problems, *J. Math. Analysis Appl.*, *31*, 682–716, 1970.

Freeze, R.A., A stochastic–conceptual analysis of one–dimensional groundwater flow in nonuniform homogeneous media, *Water Resour. Res.*, *11*(5), 725–741, 1975.

Freund, M.J., Cokriging: multivariable analysis in petroleum exploration. *Computers and Geosci.*, *12*(*4B*), 485–495, 1986.

Frind, E.O., Seawater intrusion in continuous coastal aquifer–aquitard systems, paper presented at the Third International Conference on Finite Elements in Water Resources, Univ. Miss., Oxford, May 1980.

Garven, G., The role of regional fluid flow in the genesis of the Pine Point deposit, Western Canada sedimentary basin, *Econ. Geol.*, *80*, 307–324, 1985.

Garven, G., The role of regional fluid flow in the genesis of the Pine Point deposit, Western Canada sedimentary basin – A reply, *Econ. Geol.*, *81*, 1015–1020, 1986.

Garven, G. and R.A. Freeze, Theoretical analysis of the role of groundwater flow in the genesis of stratabound ore deposits: 1. Mathematical and numerical model, *Am. J. Sci.*, *284*, 1085–1124, 1984a.

Garven, G. and R.A. Freeze, Theoretical analysis of the role of groundwater flow in the genesis of stratabound ore deposits: 2. Quantitative results, *Am. J. Sci.*, *284*, 1125–1174, 1984b.

Gavalas, G.R., P.C. Shah and J.H. Seinfeld, Reservoir history matching by bayesian estimation, *Soc. Pet. Eng. J.*, *16*, 337–350, 1976.

Gauthier, O., J. Virieux and A. Tarantola, Two–dimensional nonlinear inversion of seismic waveforms: numerical results, *Geophysics*, *51*(7), 1387–1403, 1986.

Gelhar, L.W., Stochastic subsurface hydrology from theory to applications, *Water Resour. Res.*, *22*(9), 135S–145S, 1986.

Good, I.J., *The Estimation of Probabilities: an Essay on Modern Bayesian Methods*, the M.I.T. Press, Camoridge, Massachusetts, 1965.

Gosnold, W.D. and D.W. Fischer, Heat flow studies in sedimentary basins, in: *Thermal Modeling in Sedimeniary Basins*, edited by J. Burrus, Technip, Paris, 199–217, 1986.

Gubbins, D. and J. Bloxnam, Geomagnetic field analysis–III: magnetic fields on the core–mantle boundary, *Geophys. J. R. astr. Soc.*, *80*, 695–714, 1985.

Haji–Sheikh, A. and E.M. Sparrow, The solution of heat conduction problems by probability methods, *J. Heat Transfer, Trans. Am. Soc. Mech. Eng.*, *89(C)*, 121–131, 1967.

Henry, S.G., Terrestrial heat flow overlying the Andean subduction zone, Ph.D. thesis, Univ. of Michigan, Ann Arbor, 1981.

Henry, S.G. and H.N. Pollack, Heat flow in the presence of topography: numerical analysis of data ensembles, *Geophysics*, *50*, 1335–1341, 1985.

Hitchon, B., Geothermal gradients, hydrodynamics, and hydrocarbon occurrences, Alberta, Canada, *AAPG*, *66*, 713–743, 1984.

Hoeksema, R.J. and P.K. Kitanidis, An application of the geostatistical approach to the inverse problem in two–dimensional groundwater modeling, *Water Resour. Res.*, *20(7)*, 1003–1020, 1984.

Hoeksema, R.J. and P.K. Kitanidis, Analysis of the spatial structure of properties of selected aquifers. *Water Resour. Res.*, 21(4), 563–572, 1985a.

Hoeksema, R.J. and P.K. Kitanidis, Comparison of Gaussian conditional mean and kriging estimation in the geostatistical solution of the inverse problem. *Water Resour. Res.*, 21(6), 825–836, 1985b.

Hoel, P.G., *Introduction to Mathematical Statistics*, John Wiley & Sons, New York, 1954.

Hore, P.S., G.W. Krutz and R.J. Schoenhals, Application of the finite element method to the inverse heat conduction problem, ASME paper No. 77–WA/TM–4, 1977.

Hubbert, M.K., The theory of ground–water motion, *J. Geol.*, *48*, 785–944, 1940.

Huestis, S.P., Extremal temperature bounds from surface gradient measurements, *Geophys. J. R. astr. Soc.*, *58*, 249–260, 1978.

Huestis, S.P., The inversion of heat flow data: a Backus–Gilbert formulation, *Geophys. J. R. astr. Soc.*, *62*, 649–660, 1980.

Huestis, S.P. and R.L. Parker, Upward and downward continuation as inverse problems, *Geophys. J. R. astr. Soc.*, *57*, 171–188, 1979.

Hughes, J.P. and D.P. Lettermaier, Data requirments for kriging: estimation and network design, *Water Resour. Res.*, *17(6)*, 1641–1650, 1981.

Hurtig, E. and Chr. Oelsner, Heat flow, temperature distribution and geothermal models in Europe: some tectonic implications, *Tectonophysics*, *41*, 147–156 1977.

Huyakorn, P.S. and G.F. Pinder, *Computational Methods in Subsurface Flow*. Academic Press, New York, 1983.

Jaeger, J.C., Application of the theory of heat conduction to geothermal measurements, in *Terrestrial Heat Flow*, edited by W.H.K. Lee, American

Geophysical Union, 1965.

Jackson, D.D., The use of a priori data to resolve non–uniqueness in linear inversion. *Geophys. J. R. astr. Soc.*, *57*, 137–157, 1979.

Jackson, D.D. and M. Matsu'ura, A Bayesian approach to nonlinear inversion, *J. Geophys. Res.*, *90(B1)*, 581–591, 1985.

Jaupart, C., Horizontal heat transfer due to radioactivity contrasts: causes and consequences of the linear heat flow relation, *Geophys. J. R. astr. Soc.*, *75*, 411–435, 1983.

Jaynes, E.T., Bayesian methods: general background, in *Maximum Entropy and Bayesian Methods in Applied Statistics*, edited by J.H. Justice, Cambridge Univ. Press, Cambridge, 1986.

Jeffrey, D.J., Conduction through a random suspension of spheres, *Proc. R. Soc. Lond. A.*, *335*, 355–367, 1973.

Jones, F.W., J.A. Majorowitz and H.L. Lam, The variation of heat flow density with depth in the Prairies Basin of western Canada, *Tectonophysics*, *121*, 35–44, 1985.

Kasameyer, P., L. Younker and J. Hanson, Inverse approach for thermal data from a convecting thermal system, *J. of Geodynamics*, *4*, 165–181, 1985.

Kitanidis, P.K. and R.W. Lane, Maximum likelihood parameter estimation of hydrologic spatial processes by the Gauss–Newton method, *J. Hydrology*, *79*, 53–71, 1985.

Kitanidis, P.K. and E.G. Vomvoris, A geostatistical approach to the inverse problem in groudwater modeling (steady state) and one–dimensional simulations, *Water Resour. Res.*, *19(3)*, 677–690, 1983.

Krutz, G.W. and R.L. Akau, Finite element with measurements: a predictive simulation. In *Numerical Methods in Heat Transfer*, V.II, edited by R.W. Lewis, K. Morgan and B.A. Schrefler, pp.53–71, John Wiley & Sons, Chichester, 1983.

Kuiper, L.K., A comparison of several methods for the solution of the inverse problem in two–dimensional steady state groundwater flow modeling, *Water Resour. Res.*, *22(5)*, 705–714, 1986.

Lachenbruch, A.H., Preliminary geothermal model of the Sierra Nevada, *J. Geophys. Res*, *73*, 6977–6989, 1968.

Langseth, M.G., S.J. Keihm and K. Peters, Revised lunar heat–flow values, *Proc. 7th Lunar Sci. Conf.*, 3143–3171, 1976.

Lee, T.C. and T.L. Henyey, Heat–flow refraction across dissimilar media, *Geophys. J. R. astr. Soc*, *39*, 319–333, 1974.

Lewis, T.J. and A.E. Beck, Analysis of heat flow data–detailed observations in many holes in a small area, *Tectonophysics*, *41*, 41–59, 1977.

Li, J., A. Lu, N.Z. Sun and W.W–G. Yeh, A comparative study of sensitivity coefficient calculation methods in groundwater flow, in *Finite Elements in Water Resources, Proceedings of the 6th International Conference, Lisboa, Portugal, June 1986*, edited by A. Sa da Costa, A. Melo Baptista, W.G. Gray, C.A., Brebbia and G.F. Pinder, 1986.

Liggett, J.A., P. L–F. Liu, *The Boundary Integral Equation Methods for Porous Media Flow*. George Allen & Unwin, London, 1983.

Lindley, D.V., *Bayesian Statistics, A Review*, Society for Industrial and Applied Mathematics, Philadelphia, 1972.

Lindqvist, J.G., Heat flow density measurements in the sediments of three lakes in Northern Sweden, *Tectonophysics, 103*, 121–140, 1984.

Loaiciga, H.A. and M.A. Marino. The inverse problem for confined Aquifer flow: identification and estimation with extensions, *Water Resour. Res., 23(1)*, 92–104, 1987.

Lu, A.H., F. Schmittroth and W.W-G. Yeh, Sequential estimation of aquifer parameters, *Water Resour. Res., 24(5)*, 670–682, 1988.

Luheshi, M.N. and D. Jackson, Conductive and convective heat transfer in sedimentary basins, in *Thermal Modeling in Sedimentary Basins*, edited by J. Burrus, Technip, Paris, 199–217, 1986.

Macqueene, J.W., Application of finite element methods to the inverse heat transfer problem. Master thesis, Purdue Univ., 1981.

Majorowicz, J. and A.M. Jessop, Regional heat flow patterns in the Western Canadian sedimentary basin, *Tectonophysics, 74*, 209–238, 1981.

Mareschal, J.–C., J.P. Cunningham and R.P. lowell, Downward continuation of heat flow data: method and examples from the western United States, *Geophysics, 50(5)*, 846–852, 1985.

Matheron, G., The intrinsic random functions and their applications, *Adv. Appl. Prob., 5*, 439–168, 1973.

Menke, W., *Geophysical Data Analysis: Discrete Inverse Theory*. Academic Press, New York, 1984.

Mercer, J.W. and C.R. Faust, Ground–water modeling: mathematical models, *Ground Water, 18(3)*, 212–227, 1980.

Mercer, J.W., G.F. Pinder and I.G. Donaldson, A Galerkin–finite element analysys of the hydrothermal system at Wairakei, New Zealand, *J. Geophys. Res., 80(17)*, 2608–2621, 1975.

Merriam, D.F. (editor), *Random Process in Geology*, Springer–Verlag, New York, 1976.

Munck, F and K. Sauer (editors), *Geothermische Synthese des Oberrheingrabens (Bestandsaufnahme)*, BRGM Service Geologique Regional Alsace/Geol.

Landesamt Baden–Wurttemberg, Strasbourg/Freiburg, 1979.

Nakamura, S., *Computational Methods in Engineering and Science, with Applications to Fluid Dynamics and Nuclear Systems*, John Wiley and Sons, New York, 1977.

Neuman, S.P. and S. Yakowitz, A statistical approach to the inverse problem of aquifer hydrology: 1. theory, *Water Resour. Res.*, *15*(4), 845–860, 1979.

Neuman, S.P., G.E. Fogg and E.A. Jacobson, Astatistical approach to the inverse problem of aquifer hydrology: 2. Case study, *Water Resour. Res.*, *16*(1), 33–58, 1980.

Nielsen, S.B., Continuous temperature log: theory and applications. PhD thesis, University of Western Ontario, 1986.

Nielsen, S.B., Steady state heat flow in a random medium and the linear heat flow – heat production relationship. *Geophys. Res. Letters*, 14(3), 318–321. 1987.

Nielsen, S.B. and N. Balling, Transient heat flow in a stratified medium, *Tectonophysics*, *121*, 1–10, 1985.

Oldenburg, D.W., An introduction to linear inverse theory, *IEEE Trans. Geosci. Remote Sensing*, *GE–22*(6), 665–674, 1984.

Omre, H., Bayesian kriging–merging observations and qualified guesses in kriging, *Math. Geol.*, *19*(1), 25–39, 1987.

Parker, R.L., Understanding inverse theory, *Ann. Rev. Earth. Planet Sci.*, *5*, 35–64, 1977.

Pina, H.L.G., Heat transfer application, in *Boundary Element Techniques in Computer–Aided Engineering*, edited by C.A. Brebbia. Martinus Nijhoff, Dordrecht, 1984.

Pinder, G.F. and W. Gray, *Finite Element Simulation in Surface and Subsurface Hydrology*, Academic Press, New York, 1977.

Powell, W.G., D.S. Chapman, N. Balling and A.E. Beck, Continental Heat–flow density, in *Handbook of Terrestrial Heat–Flow Density Determination*, edited by R. Haenel, L. Rybach and L. Stegena, Kluwer Academic Publishers, Dordrecht, 1988.

Press, W.H., B.P. Flannery, S.A. Teukolsky and W.T. Vetterling, *Numerical Recipes, the Art of Scientific Computing*, Cambridge University Press, Cambridge, 1986.

Rodgers, C.D., Retrieval of atmospheric temperature and composition from remote measurements of thermal radiation, *Rev. Geophys. Space Phys.*, *14*, 609–624, 1976.

Roy, R.F, A.E. Beck and Y.S. Touloukian, Thermophysical properties of rocks, in Physical properties of rocks and minerals, edited by Y.S. Touloukian,

W.R. Judd and R.F. Roy, Mcgraw–Hill, New York, 1981.

Rybach, L. and G. Buntebarth, The variation of heat generation, density and seimic velocity with rock types in the continental lithosphere, *Tectonophysics, 103*, 335–344, 1984.

Sabatier, P.C., On geophysical inverse problems and constraints, *J. Geophys., 43*, 115–137, 1977.

Sauty, J.P., A.C. Gringarten, A. Menjoz and P.A. Landel, Sensible Energy Storage in Aquifers: 1. theoretical study, *Water Resour. Res.*, 18(2), 245–252, 1982a.

Sauty, J.P., A.C. Gringarten, A. Menjoz and P.A. Landel, Sensible Energy Storage in Aquifers: 2. Field Experiments and comparisons with theoretical results, Water *Resour. Res., 18(2)*, 253–265, 1982b.

Scheidegger, A.E., Generai theory of dispersion in porous media, *J. Geophys. Res, 66(10)*, 3273–3278, 1961.

Schweppe, F.C., *Uncertain Dynamic Systems*, Prentice–Hall, New Jersey, 1973.

Shen, P.Y. and A.E. Beck, Determination of surface temperature history from borehole temperature gradients, *J. Geophys. Res., 88*, 7485–7493, 1983.

Shen, P.Y. and A.E. Beck, Stabilization of bottom hole temperature with finite circulation time and fluid flow, *Geophys. J. Roy. astr. Soc, 86*, 63–90, 1986.

Shen, P.Y. and A.E. Beck, Inversion of temperature measurements in lake sediment, *Geophys. J., 94*, 545–558, 1988.

Silva, J.B.C. and G.W. Hohmann, Nonlinear magnetic inversion using a ramdom search method, *Geophysics, 48(12)*, 1645–1658, 1983.

Smith, G.D., *Numerical Solution of Partial Differential Equations: Finite Difference Methods*, Clarendon Press, Oxford, 1978.

Smith, L. and D.S. Chapman, On the thermal effects of groundwater flow: 1. regional scale systems, *J. Geophys. Res., 88(B1)*, 593–608, 1983.

Smith, L. and R.A. Freeze, Stochastic analysis of steady state groundwater flow in a bounded domain: 1. one–dimensional simulations, *Water Resour. Res., 15(3)*, 521–528, 1979.

Soong, T.T., *Random Differential Equations in Sciences and Engineering*, Academic Press, New York, 1981.

Speece, M.A., T.D. Bowen, J.L. Folcik and H.N. Pollack, Analysis of temperatures in sedimentary basins: the Michigan basin, *Geophysics, 50(8)*, 1318–1334, 1985.

Stolz, G.Jr., Numerical solutions to an inverse problem of heat conduction for simple shapes, *ASME, J. Heat Transfer, 82C*, 20–26, 1960.

Straus, J.M. and G. Schubert, Thermal convection of water in a porous medium: effects of temperature– and pressure–dependent thermodynamic and transport properties, *J. Geophys. Res.*, *82*(2), 1977.

Stromeyer, D., Downward continuation of heat flow data by means of the least squares method, *Tectonophysics*, *103*, 55–66, 1984.

Sun, N.Z. and W.W.G. Yeh, Identification of parameter structure in groundwater inverse problem, *Water Resour. Res.*, *21*(6), 869–883, 1985.

Tarantola, A., *Inverse Problem Theory*, Elsevier, Amsterdam, 1987.

Tarantola, A. and B. Valette, Inverse problem = quest for information, *J.* Geophys, *50*, 159–170, 1982a.

Tarantola, A. and B. Valette, Generalized nonlinear inverse problems solved using the least squares criterion, *Rev. Geophys. Space Phys.*, *20*(2), 219–232, 1982b.

Vasseur, G., P.H. Bernard, J. Van de Meulebrouck, Y. Kast and J. Jolivet, Holocene palaeotemperatures deduced from geothermal measurements, *Palaeogeogr. Palaeoclimatol. Palaeoecol.*, *43*, 237–259, 1983.

Vasseur, G., F. Lucazeau and R. Bayer, The inverse problem of heat flow density determination from inaccurate data, *Tectonophysics*, *121*, 25–34, 1986.

Wang, J.Y, J.A. Wang, L.P. Xiong and J.M. Zhang, Analysis of factors affecting heat flow density determination in the Liaohe Basin, North China, *Tectonophysics*, *121*, 63–78, 1985.

Wang, K. and A.E. Beck, Heat flow measurement in lacustrine or oceanic sediments without recording water bottom temperature variations, *J. Geophys. Res*, *92*(*B12*), 12837–12845, 1987.

Wang, K. and A.E. Beck, An inverse approach to heat flow study in hydrologically active areas, *Geophys. J.*, *95*, in press, 1989.

Wang, K., P.Y. Shen and A.E. Beck, On the effects of thermal properties structure and water bottom temperature variation on temperature gradients in lake sediments, *Can. J. Earth Sci.*, *23*, 1257–1264, 1986.

Wang, K., P.Y. Shen and A.E. Beck, A solution to the inverse problem of the coupled hydrological and thermal regimes, in *Hydrological regimes and their subsurface thermal effects*, edited by A.E. Beck, L. Stegena and G. Garven, AGU monograph series, Washington, in press, 1989.

Wiggins, R.A., The general inverse problem: implication of surface waves and free oscillation for earth structure, *Rev. Geophys. Space Phys.*, *10*, 251–285, 1972.

Willett, S.D. and D.S Chapman, Analysis of temperatures and thermal processes in the Uinta basin, in *Sedimentary Basins and Basin–Forming Mechanisms*, edited by C. Beaumont and A.J. Tankard, Canadian Society of Petroleum Geologists, Memoir, 1987.

Woodbury, A.D. and L. Smith, On the thermal effects of three–dimensional groundwater flow, *J. Geophys. Res.*, *90*(*B1*), 759–767, 1985.

Woodbury, A.D. and L. Smith, Simultaneous inversion of hydrogeologic and thermal data: 2. incorporation of thermal data, *Water Resour. Res.*, *24*(*3*), 356–372, 1988.

Woodbury, A.D., L. Smith and W.S. Dunbar, Simultaneous inversion of hydrogeologic and thermal data: 1. theory and application using hydraulic head data, *Water Resour. Res.*, *23*(*8*), 1586–1606, 1988.

Xiong, L. and J. Zhang, Mathematical simulation of retract and redistribution of heat flow, *Scientia Geologica Sinica*, *4*, 445–454, 1984 (in Chinese with English title and abstract).

Yates, S.R., A.W. Warrick and D.E. Myers, A disjunctive kriging program for two dimensions, *Computer and Geosci.*, *12*(*3*), 281–313, 1986.

Yeh, W.W–G, Review of parameter identification procedures in groundwater hydrology: the inverse problem, *Water Resour. Res.*, *22*(*2*), 95–108, 1986.

Yeh, W.W–G and Y.S. Yoon, Aquifer parameter identification with optimum dimension in parameterization, *Water Resour. Res.*, *17*(*3*), 664–672, 1981.

Yeh, W.W–G, Y.S. Yoon and K.S. Lee, Aquifer parameter identification with kriging and optimum parameterization, *Water Resour. Res.*, *19*(*1*), 225–233, 1983.

Yoon, Y.S. and Yeh, W.W–G, Parameter identification in an inhomogeneous medium with the finite–element method, *Soc. Pet. Eng. J.*, 217–226, 1976.

Zhang, J. and L. Xiong, *Applications of the Finite Element Methods to Geothermal Research*, Scientific Publishing House, Beijing, 1986 (in Chinese).

Zhang, J., H. Sun and L. Xiong, Mathematical simulating of regional geothermal field and case analysis, *Scientia Geologica Sinica*, *3*, 315–321, 1982 (in Chinese with English title and abstract).

Zienkiewicz, O.C., *The Finite Element Method in Engineering Science*, McGraw–Hill, New York, 1972.

Wang, K., A.E. Beck and P.Y. Shen, Potential serious errors in heat flow determinations made in the sediments of continental lakes and shallow seas, at: Spring Meeting of the American Geophysical Union, Baltimore, Maryland, May 27–31, 1985.

Beck, A.E., P.Y. Shen and K. Wang, Sub–bottom perturbations due to climatic variations at the boundary of an inhomogeneous medium, at: the 1st Regional assembly of IASPEI, Hyderabad, India, November, 1984.